

Report No. UT-21.20

SIMPLIFIED CONE PENETRATION TEST PERFORMANCE-BASED ASSESSMENT OF LIQUEFACTION AND EFFECTS: PHASE 1, TASKS 1-4

Prepared For:

Utah Department of Transportation
Research & Innovation Division

Final Report – Phase 1 of 2

August 2021

DISCLAIMER

The authors alone are responsible for the preparation and accuracy of the information, data, analysis, discussions, recommendations, and conclusions presented herein. The contents do not necessarily reflect the views, opinions, endorsements, or policies of the Utah Department of Transportation or the U.S. Department of Transportation. The Utah Department of Transportation makes no representation or warranty of any kind, and assumes no liability therefore.

ACKNOWLEDGMENTS

The authors acknowledge the Utah, Oregon, South Carolina, and Connecticut Departments of Transportation for funding this research for pooled fund study TPF-5(338). The views and opinions presented in this report represent those of its authors, and may not represent those of the state agencies funding this research.

TECHNICAL REPORT ABSTRACT

1. Report No. UT-21.20		2. Government Accession No. NA		3. Recipient's Catalog No. NA	
4. Title and Subtitle SIMPLIFIED CONE PENETRATION TEST PERFORMANCE-BASED ASSESSMENT OF LIQUEFACTION AND EFFECTS: PHASE 1, TASKS 1-4				5. Report Date August 2021	
				6. Performing Organization Code NA	
7. Author(s) Kevin W. Franke, Tyler B. Coutu, Mikayla S. Hatch, Alex M. Arndt, Jingwen He, Jenny L. Blonquist				8. Performing Organization Report No. NA	
9. Performing Organization Name and Address Brigham Young University Department of Civil and Environmental Engineering 368 Clyde Building Provo, UT 84602-4009				10. Work Unit No. 42074 15D	
				11. Contract or Grant No. 16-9826	
12. Sponsoring Agency Name and Address Utah Department of Transportation 4501 South 2700 West P.O. Box 148410 Salt Lake City, UT 84114-8410				13. Type of Report & Period Covered Final Report May 2016 - June 2017	
				14. Sponsoring Agency Code PIC No. UT15.402	
15. Supplementary Notes Prepared in cooperation with the Utah Department of Transportation and the U.S. Department of Transportation, Federal Highway Administration					
16. Abstract <p>The purpose of the research presented is to provide the benefit of the full performance-based probabilistic earthquake hazard analysis using Cone Penetration Test (CPT) data, without requiring special software, training, and experience. To do this, simplified models of liquefaction triggering, post-liquefaction settlement, and lateral spread displacement that approximate the results of the full probabilistic analysis were developed. The full project scope consisted of two phases: Phase 1) the development of a research tool to run full performance-based probabilistic calculations (Tasks 1 through 4), and Phase 2) the development of simplified performance-based methods (Tasks 5 through 10). This final report volume addresses the results of Phase 1 of the pooled fund study TPF-5(338) research contract.</p> <p>The program, <i>CPTLiquefY</i>, is a research tool created to run full performance-based probabilistic calculations of liquefaction triggering, liquefaction-induced settlement, and lateral spread displacement. <i>CPTLiquefY</i> currently has the capabilities of reading in a CPT file, running soil parameter calculations, pseudo-probabilistic liquefaction analyses, and deterministic liquefaction analyses.</p> <p>Full-probabilistic methods are completely operational in the program, along with a connection to a new off-line USGS deaggregation tool that gives access to the 2014 USGS deaggregation models. This program, and the corresponding results, have been analyzed for 10 different cities and 20 CPT profiles. The results are compared to pseudo-probabilistic and semi-probabilistic methods.</p>					
17. Key Words Liquefaction Triggering, Performance-based Engineering, Seismic Hazards, Cone Penetration Test, USGS 2014 Deaggregation, Lateral Spread Displacement, Settlement, Probabilistic			18. Distribution Statement Not restricted. Available through: UDOT Research & Innovation Div. 4501 South 2700 West P.O. Box 148410 Salt Lake City, UT 84114-8410 www.udot.utah.gov/go/research		23. Registrant's Seal NA
19. Security Classification (of this report) Unclassified	20. Security Classification (of this page) Unclassified	21. No. of Pages 158	22. Price NA		

TABLE OF CONTENTS

LIST OF FIGURES	vi
LIST OF TABLES	xv
UNIT CONVERSION FACTORS	xvi
LIST OF ACRONYMS	xvii
LIST OF TERMS.....	xviii
EXECUTIVE SUMMARY	1
1.0 INTRODUCTION	3
1.1 Problem Statement.....	3
1.2 Objectives	3
1.3 Scope.....	4
2.0 LIQUEFACTION TRIGGERING EVALUATION USING THE CPT	5
2.1 Overview.....	5
2.2 Liquefaction Triggering Evaluation.....	5
2.2.1 Empirical Liquefaction Triggering Models	5
2.2.2 Robertson and Wride (1998, 2009) Procedure.....	7
2.2.3 Ku et al. (2012) Procedure [Probabilistic Version of Robertson and Wride Method].	12
2.2.4 Boulanger and Idriss (2014) Procedure	14
2.2.5 PBEE Liquefaction Triggering Procedures.....	18
2.3 Liquefaction-Induced Settlement Evaluation	20
2.3.1 Liquefaction-Induced Settlement Ishihara and Yoshimine (1992) Procedure.....	21
2.3.2 Liquefaction-Induced Settlement Juang et al. (2013) Procedure	23
2.3.3 Performance-Based Liquefaction-Induced Settlement Procedure	26
2.3.4 Correction Factor for Unrealistic Strain Values	28
2.4 Lateral Spread Displacement Evaluation.....	30
2.4.1 Lateral Spread Displacement Empirical Model	30
2.4.2 Performance-Based Lateral Spread Displacement Procedure	32
2.5 Pseudo-Probabilistic Liquefaction Hazard Analysis Method.....	35
2.6 Semi-Probabilistic Liquefaction Hazard Analysis Method	36
3.0 <i>CPTLiquefy</i>	37
3.1 Overview.....	37

3.2 Walk Through of <i>CPTLiquefY</i>	38
3.2.1 Soil Info Tab	38
3.2.2 Pseudo-Probabilistic Tab	42
3.2.3 Full Probabilistic User Inputs Tab	43
3.2.4 Liquefaction Triggering Results Tab	44
3.2.5 Settlement Results Tab.....	46
3.2.6 Lateral Spread Results Tab	48
3.3 Inclusion of New USGS Deaggregation Tool	49
3.3.1 USGS Offline Deaggregation tool (NSHMP-haz).....	49
4.0 METHODOLOGY AND RESULTS	54
4.1 Methodology.....	54
4.1.1 Soil Profiles.....	54
4.1.2 Site Locations.....	56
4.1.3 Return Periods.....	58
4.2 Liquefaction Triggering Results	58
4.2.1 Example of Results from <i>CPTLiquefY</i>	58
4.2.2 Comparison of Ku et al. and Boulanger and Idriss Full-Probabilistic Results.	60
4.2.3 Variation of FS_L between Sites	62
4.2.4 Variation of FS_L between Return Periods	64
4.2.5 Variation of FS with Soil Profile Stiffness	65
4.2.6 Comparison of Full-Probabilistic Methods with Pseudo-Probabilistic Methods.....	67
4.2.7 Robertson and Wride Pseudo-probabilistic vs. Ku et al. Full-Probabilistic Method...	68
4.2.8 Boulanger and Idriss Pseudo-probabilistic vs. Full-Probabilistic Methods.....	72
4.2.9 Summary of Comparisons.....	76
4.3 Settlement Results.....	81
4.3.1 Example of Results Calculated by <i>CPTLiquefY</i>	82
4.3.2 Comparison of Full-Probabilistic, Pseudo-Probabilistic, and Semi-Probabilistic	82
4.4 Lateral Spread Results	97
4.4.1 Example of Results Calculated by <i>CPTLiquefY</i>	97
4.4.2 Comparison of Full-Probabilistic, Pseudo-Probabilistic, and Semi-Probabilistic	98
5.0 SENSITIVITY ANALYSIS	113

5.1 Thin Layer Correction and Depth Weighting Factor	113
5.1.1 Depth Weighting Factor Correction.....	113
5.1.2 Thin Layer Correction.....	114
5.2 Sensitivity Analysis of Settlement.....	115
5.3 Sensitivity Analysis of Lateral Spread.....	118
6.0 CONCLUSIONS.....	123
6.1 Summary.....	123
REFERENCES	125
APPENDIX A: LATERAL SPREAD COMPARISONS.....	129

LIST OF FIGURES

Figure 2-1: Example development of the CRR line.....	6
Figure 2-2: Robertson and Wride (2009) liquefaction triggering curve with case history data points.	7
Figure 2-3: Normalized CPT soil behavior type chart (after Robertson, 1990). Soil types: 1, sensitive, fine grained; 2, peats; 3, silty clay to clay; 4, clayey silt to silty clay; 5, silty sand to sandy silt; 6, clean sand to silty sand; 7, gravelly sand to dense sand; 8, very stiff sand to clayey sand; 9, very stiff, fine grained.	8
Figure 2-4: Summary of the Robertson and Wride (2009) CRR procedure.	11
Figure 2-5: CRR liquefaction triggering curves based on P_L	13
Figure 2-6: Recommended correlation between I_c and FC with plus or minus one standard deviation against the dataset by Suzuki et al. (1998) (after Idriss and Boulanger, 2014).	15
Figure 2-7: CRR curves and liquefaction curves for the deterministic case history database (after Boulanger and Idriss, 2014).	17
Figure 2-8: Example FS_L curve from one soil layer at a depth of 6m of a CPT profile calculated at Eureka, CA.....	20
Figure 2-9 The relationship between FS_L , γ_{max} , and D_R as presented by Ishihara and Yoshimine (1992).	22
Figure 2-10: Example of a strain hazard curve from one specific soil layer.	27
Figure 2-11: Example of a total ground settlement hazard curve.	28
Figure 2-12: Maximum vertical strain levels inferred by deterministic vertical strain models and weighted average used to define mean value (after Huang, 2008).	29
Figure 2-13: The relationship between γ_{max} , D_R , and FS_L as presented by Zhang et al. (2004).	31
Figure 2-14: The three cases for site geometry when determining lateral displacement.....	32
Figure 2-15: Example of a shear strain hazard curve for a single soil layer.....	34
Figure 2-16 Example of a total lateral spread displacement hazard curve.	35
Figure 3-1: Opening view of <i>CPTLiquefy</i>	38
Figure 3-2: Initial view of <i>CPTLiquefy</i> , showing the Soil Info tab.....	39
Figure 3-3: View after running calculations on Soil Info tab in <i>CPTLiquefy</i>	40

Figure 3-4: Display of the Advanced Options dialog box in <i>CPTLiquefY</i> .	41
Figure 3-5: View of Pseudo Probabilistic tab once calculations are complete.	43
Figure 3-6: View of <i>CPTLiquefY</i> , showing the completed deaggregation analysis and development of amax hazard curves after selecting “Load Seismic Data”.	44
Figure 3-7: View of “Liquefaction Triggering Results” tab after analysis.	45
Figure 3-8: Example plot from “Liquefaction Triggering Results” tab.	45
Figure 3-9: View of “Settlement Results” tab after analysis is complete.	46
Figure 3-10: View of hazard curves for total ground surface settlement.	47
Figure 3-11: Strain hazard curve data for soil layer 94, corresponding to a depth of 4.6m.	48
Figure 3-12: View of “Lateral Spread Results” tab after analysis.	49
Figure 3-13: USGS NSHMP-haz code repository on GitHub.com.	50
Figure 3-14: Image of the old USGS online deaggregation tool.	51
Figure 3-15: Input options for new USGS tool on the “Pseudo Probabilistic” tab.	52
Figure 3-16: View of the window launched by NSHMP-haz.	52
Figure 3-17: Map showing the division in USGS between western, central, and eastern states.	53
Figure 4-1: Stiffness of CPT profiles plotted at depth.	55
Figure 4-2 Map of all ten cities in this study.	57
Figure 4-3: Example FS_L Hazard curve output from <i>CPTLiquefY</i> .	59
Figure 4-4: Comparison of results from the full-probabilistic liquefaction analysis of profile 6 at Butte, MT relating FS_L to depth in meters.	60
Figure 4-5: Comparison of FS_L for both full-probabilistic methods (Return Period = 1039 years).	61
Figure 4-6: FS_L results for profile 14 at a return period of 475 years.	62
Figure 4-7: FS_L results for profile 14 at a return period of 1039 years.	63
Figure 4-8: FS_L results for profile 14 at a return period of 2475 years.	63
Figure 4-9: Comparison of FS_L for 3 return periods (profile 14, Salt Lake City).	64
Figure 4-10: Comparison of FS_L results from different categories of profile stiffness.	66
Figure 4-11: Location of four quadrants on an example plot.	68

Figure 4-12: Comparison of FS_L from Robertson and Wride conventional (Mean) and Ku et al. full-probabilistic approaches, $T_r = 475$ years.	69
Figure 4-13: Comparison of FS_L from Robertson and Wride conventional (Modal) and Ku et al. full-probabilistic approaches, $T_r = 475$ years.	70
Figure 4-14: Comparison of FS_L from Robertson and Wride conventional (Mean) and Ku et al. full-probabilistic approaches, $T_r = 1039$ years.	70
Figure 4-15: Comparison of FS_L from Robertson and Wride conventional (Modal) and Ku et al. full-probabilistic approaches, $T_r = 1039$ years.	71
Figure 4-16: Comparison of FS_L from Robertson and Wride conventional (Mean) and Ku et al. full-probabilistic approaches, $T_r = 2475$ years.	71
Figure 4-17: Comparison of FS_L from Robertson and Wride conventional (Modal) and Ku et al. full-probabilistic approaches, $T_r = 2475$ years.	72
Figure 4-18: Comparison of FS_L for Boulanger and Idriss conventional (Mean) and full-probabilistic approaches, $T_r = 475$ years.	73
Figure 4-19: Comparison of FS_L for Boulanger and Idriss conventional (Modal) and full-probabilistic approaches, $T_r = 475$ years.	74
Figure 4-20: Comparison of FS_L for Boulanger and Idriss conventional (Mean) and full-probabilistic approaches, $T_r = 1039$ years.	74
Figure 4-21: Comparison of FS_L for Boulanger and Idriss conventional (Modal) and full-probabilistic approaches, $T_r = 1039$	75
Figure 4-22: Comparison of FS_L for Boulanger and Idriss conventional (Mean) and full-probabilistic approaches, $T_r = 2475$	75

Figure 4-23: Comparison of FS_L for Boulanger and Idriss conventional (Modal) and full-probabilistic approaches, $T_r = 2475$	76
Figure 4-24: Probability of liquefaction values from study (using Ku et al. equation) $T_r = 475$.	80
Figure 4-25: Probability of liquefaction values from study (using Boulanger and Idriss equation) $T_r = 475$	81
Figure 4-26: Example settlement hazard curve.	82
Figure 4-27: Mean magnitude pseudo-probabilistic versus fully-probabilistic for the 475 year return period using the Robertson and Wride liquefaction triggering procedure.	84
Figure 4-28: Mean magnitude pseudo-probabilistic versus fully-probabilistic for the 1039 year return period using the Robertson and Wride liquefaction triggering procedure.	84
Figure 4-29: Mean magnitude pseudo-probabilistic versus fully-probabilistic for the 2475 year return period using the Robertson and Wride liquefaction triggering procedure.	85
Figure 4-30: Modal magnitude pseudo-probabilistic versus fully-probabilistic for the 475 year return period using the Robertson and Wride liquefaction triggering procedure.	85
Figure 4-31: Modal magnitude pseudo-probabilistic versus fully-probabilistic for the 1039 year return period using the Robertson and Wride liquefaction triggering procedure.	86
Figure 4-32: Modal magnitude pseudo-probabilistic versus fully-probabilistic for the 2475 year return period using the Robertson and Wride liquefaction triggering procedure.	86
Figure 4-33: Semi-probabilistic versus fully-probabilistic for the 475 year return period using the Robertson and Wride liquefaction triggering procedure.	87
Figure 4-34: Semi-probabilistic versus fully-probabilistic for the 1039 year return period using the Robertson and Wride liquefaction triggering procedure.	87
Figure 4-35: Semi-probabilistic versus fully-probabilistic for the 2475 year return period using the Robertson and Wride liquefaction triggering procedure.	88
Figure 4-36: Mean magnitude pseudo-probabilistic versus fully-probabilistic for the 475 year return period using the Boulanger and Idriss liquefaction triggering procedure.	88
Figure 4-37: Mean magnitude pseudo-probabilistic versus fully-probabilistic for the 1039 year return period using the Boulanger and Idriss liquefaction triggering procedure.	89

Figure 4-38: Mean magnitude pseudo-probabilistic versus fully-probabilistic for the 2475 year return period using the Boulanger and Idriss liquefaction triggering procedure. ...	89
Figure 4-39: Modal magnitude pseudo-probabilistic versus fully-probabilistic for the 475 year return period using the Boulanger and Idriss liquefaction triggering procedure. ...	90
Figure 4-40: Modal magnitude pseudo-probabilistic versus fully-probabilistic for the 1039 year return period using the Boulanger and Idriss liquefaction triggering procedure. ...	90
Figure 4-41: Modal magnitude pseudo-probabilistic versus fully-probabilistic for the 2475 year return period using the Boulanger and Idriss liquefaction triggering procedure. ...	91
Figure 4-42: Semi-probabilistic versus fully-probabilistic for the 475 year return period using the Boulanger and Idriss liquefaction triggering procedure.	91
Figure 4-43: Semi-probabilistic versus fully-probabilistic for the 1039 year return period using the Boulanger and Idriss liquefaction triggering procedure.	92
Figure 4-44: Semi-probabilistic versus fully-probabilistic for the 2475 year return period using the Boulanger and Idriss liquefaction triggering procedure.	92
Figure 4-45: Box and whisker plots of actual return periods versus assumed 1039 year return period in the settlement analysis.	94
Figure 4-46: Box and whisker plots of actual return periods versus assumed 2475 year return period in the settlement analysis.	94
Figure 4-47: A heat map representing the number of CPT soundings, out of 20 soundings, in which the pseudo-probabilistic method under predicted settlement compared to the full-probabilistic procedure.....	95
Figure 4-48 Example of lateral spread hazard curve.	98
Figure 4-49: Mean magnitude pseudo-probabilistic versus fully-probabilistic for the 475 year return period using the Robertson and Wride liquefaction triggering procedure.	100
Figure 4-50: Mean magnitude pseudo-probabilistic versus fully-probabilistic for the 1039 year return period using the Robertson and Wride liquefaction triggering procedure.	100
Figure 4-51: Mean magnitude pseudo-probabilistic versus fully-probabilistic for the 2475 year return period using the Robertson and Wride liquefaction triggering procedure.	101

Figure 4-52: Modal magnitude pseudo-probabilistic versus fully-probabilistic for the 475 year return period using the Robertson and Wride liquefaction triggering procedure.	101
Figure 4-53: Modal magnitude pseudo-probabilistic versus fully-probabilistic for the 1039 year return period using the Robertson and Wride liquefaction triggering procedure.	102
Figure 4-54: Modal magnitude pseudo-probabilistic versus fully-probabilistic for the 2475 year return period using the Robertson and Wride liquefaction triggering procedure.	102
Figure 4-55: Semi-probabilistic versus fully-probabilistic for the 475 year return period using the Robertson and Wride liquefaction triggering procedure.	103
Figure 4-56: Semi-probabilistic versus fully-probabilistic for the 1039 year return period using the Robertson and Wride liquefaction triggering procedure.	103
Figure 4-57: Semi-probabilistic versus fully-probabilistic for the 2475 year return period using the Robertson and Wride liquefaction triggering procedure.	104
Figure 4-58: Mean magnitude pseudo-probabilistic versus fully-probabilistic for the 475 year return period using the Boulanger and Idriss liquefaction triggering procedure.	104
Figure 4-59: Mean magnitude pseudo-probabilistic versus fully-probabilistic for the 1039 year return period using the Boulanger and Idriss liquefaction triggering procedure.	105
Figure 4-60: Mean magnitude pseudo-probabilistic versus fully-probabilistic for the 2475 year return period using the Boulanger and Idriss liquefaction triggering procedure.	105
Figure 4-61: Modal magnitude pseudo-probabilistic versus fully-probabilistic for the 475 year return period using the Boulanger and Idriss liquefaction triggering procedure.	106
Figure 4-62: Modal magnitude pseudo-probabilistic versus fully-probabilistic for the 1039 year return period using the Boulanger and Idriss liquefaction triggering procedure.	106
Figure 4-63: Modal magnitude pseudo-probabilistic versus fully-probabilistic for the 2475 year return period using the Boulanger and Idriss liquefaction triggering procedure.	107
Figure 4-64: Semi-probabilistic versus fully-probabilistic for the 475 year return period using the Boulanger and Idriss liquefaction triggering procedure.	107
Figure 4-65: Semi-probabilistic versus fully-probabilistic for the 1039 year return period using the Boulanger and Idriss liquefaction triggering procedure.	108

Figure 4-66: Semi-probabilistic versus fully-probabilistic for the 2475 year return period using the Boulanger and Idriss liquefaction triggering procedure.	108
Figure 4-67: Box and whisker plots of actual return periods versus	110
Figure 4-68: Box and whisker plots of actual return periods versus	110
Figure 5-1: Tip resistance analysis for thin sand layer (deposit A) interbedded within soft clay layer (deposit B). (Ahmadi & Robertson, 2005).....	114
Figure 5-2: Box and whisker plots for R (settlement) at a return period of 475 years.	116
Figure 5-3: Box and whisker plots for R (settlement) at a return period of 1039 years.	117
Figure 5-4: Box and whisker plots for R (settlement) at a return period of 2475 years.	117
Figure 5-5: Box and whisker plots for R (lateral spread geometry 1) at a return period of 475 years.	118
Figure 5-6: Box and whisker plots for R (lateral spread geometry 1) at a return period of 1039 years.	119
Figure 5-7: Box and whisker plots for R (lateral spread geometry 1) at a return period of 2475 years.	119
Figure 5-8: Box and whisker plots for R (lateral spread geometry 3) at a return period of 475 years.	121
Figure 5-9: Box and whisker plots for R (lateral spread geometry 3) at a return period of 1039 years.	121
Figure 5-10: Box and whisker plots for R (lateral spread geometry 3) at a return period of 2475 years.	122
Figure A-1: Mean magnitude pseudo-probabilistic versus fully-probabilistic for the 475 year return period using the Robertson and Wride liquefaction triggering procedure.....	129
Figure A-2: Mean magnitude pseudo-probabilistic versus fully-probabilistic for the 1039 year return period using the Robertson and Wride liquefaction triggering procedure.	130
Figure A-3: Mean magnitude pseudo-probabilistic versus fully-probabilistic for the 2475 year return period using the Robertson and Wride liquefaction triggering procedure.	130

Figure A-4: Modal magnitude pseudo-probabilistic versus fully-probabilistic for the 475 year return period using the Robertson and Wride liquefaction triggering procedure.	131
Figure A-5: Modal magnitude pseudo-probabilistic versus fully-probabilistic for the 1039 year return period using the Robertson and Wride liquefaction triggering procedure.	131
Figure A-6: Modal magnitude pseudo-probabilistic versus fully-probabilistic for the 2475 year return period using the Robertson and Wride liquefaction triggering procedure.	132
Figure A-7: Semi-probabilistic versus fully-probabilistic for the 475 year return period using the Robertson and Wride liquefaction triggering procedure.	132
Figure A-8: Semi-probabilistic versus fully-probabilistic for the 1039 year return period using the Robertson and Wride liquefaction triggering procedure.	133
Figure A-9: Semi-probabilistic versus fully-probabilistic for the 2475 year return period using the Robertson and Wride liquefaction triggering procedure.	133
Figure A-10: Mean magnitude pseudo-probabilistic versus fully-probabilistic for the 475 year return period using the Boulanger and Idriss liquefaction triggering procedure.	134
Figure A-11: Mean magnitude pseudo-probabilistic versus fully-probabilistic for the 1039 year return period using the Boulanger and Idriss liquefaction triggering procedure.	134
Figure A-12: Mean magnitude pseudo-probabilistic versus fully-probabilistic for the 2475 year return period using the Boulanger and Idriss liquefaction triggering procedure.	135
Figure A-13: Modal magnitude pseudo-probabilistic versus fully-probabilistic for the 475 year return period using the Boulanger and Idriss liquefaction triggering procedure.	135
Figure A-14: Modal magnitude pseudo-probabilistic versus fully-probabilistic for the 1039 year return period using the Boulanger and Idriss liquefaction triggering procedure.	136
Figure A-15: Modal magnitude pseudo-probabilistic versus fully-probabilistic for the 2475 year return period using the Boulanger and Idriss liquefaction triggering procedure.	136
Figure A-16: Semi-probabilistic versus fully-probabilistic for the 475 year return period using the Boulanger and Idriss liquefaction triggering procedure.	137
Figure A-17: Semi-probabilistic versus fully-probabilistic for the 1039 year return period using the Boulanger and Idriss liquefaction triggering procedure.	137

Figure A-18: Semi-probabilistic versus fully-probabilistic for the 2475 year return period using the Boulanger and Idriss liquefaction triggering procedure.138

LIST OF TABLES

Table 4-1: Summary of Soil Profiles55

Table 4-2: Selected Cities Used in Study57

Table 4-3: Percentage Data in Each Quadrant: Robertson and Wride vs. Ku et al. $T_r = 475$ Years
.....77

Table 4-4: Percentage Data in Each Quadrant: Robertson and Wride vs. Ku et al. $T_r = 1039$ Years
.....77

Table 4-5: Percentage Data in Each Quadrant: Robertson and Wride vs. Ku et al. $T_r = 2475$ Years
.....78

Table 4-6: Percentage Data in Each Quadrant: Boulanger and Idriss (Conventional) vs. Boulanger
and Idriss (Full-Probabilistic) $T_r = 475$ Years.....78

Table 4-7: Percentage Data in Each Quadrant: Boulanger and Idriss (Conventional) vs. Boulanger
and Idriss (Full-Probabilistic) $T_r = 1039$ Years.....78

Table 4-8: Percentage Data in Each Quadrant: Boulanger and Idriss (Conventional) vs. Boulanger
and Idriss (Full-Probabilistic) $T_r = 2475$ Years.....79

UNIT CONVERSION FACTORS

Units used in this report and not conforming to the UDOT standard unit of measurement (U.S. Customary system) are given below with their U.S. Customary equivalents:

SI* (MODERN METRIC) CONVERSION FACTORS				
APPROXIMATE CONVERSIONS TO SI UNITS				
Symbol	When You Know	Multiply By	To Find	Symbol
LENGTH				
in	inches	25.4	millimeters	mm
ft	feet	0.305	meters	m
yd	yards	0.914	meters	m
mi	miles	1.61	kilometers	km
AREA				
in ²	square inches	645.2	square millimeters	mm ²
ft ²	square feet	0.093	square meters	m ²
yd ²	square yard	0.836	square meters	m ²
ac	acres	0.405	hectares	ha
mi ²	square miles	2.59	square kilometers	km ²
VOLUME				
fl oz	fluid ounces	29.57	milliliters	mL
gal	gallons	3.785	liters	L
ft ³	cubic feet	0.028	cubic meters	m ³
yd ³	cubic yards	0.765	cubic meters	m ³
NOTE: volumes greater than 1000 L shall be shown in m ³				
MASS				
oz	ounces	28.35	grams	g
lb	pounds	0.454	kilograms	kg
T	short tons (2000 lb)	0.907	megagrams (or "metric ton")	Mg (or "t")
TEMPERATURE (exact degrees)				
°F	Fahrenheit	5 (F-32)/9 or (F-32)/1.8	Celsius	°C
ILLUMINATION				
fc	foot-candles	10.76	lux	lx
fl	foot-Lamberts	3.426	candela/m ²	cd/m ²
FORCE and PRESSURE or STRESS				
lbf	poundforce	4.45	newtons	N
lbf/in ²	poundforce per square inch	6.89	kilopascals	kPa
APPROXIMATE CONVERSIONS FROM SI UNITS				
Symbol	When You Know	Multiply By	To Find	Symbol
LENGTH				
mm	millimeters	0.039	inches	in
m	meters	3.28	feet	ft
m	meters	1.09	yards	yd
km	kilometers	0.621	miles	mi
AREA				
mm ²	square millimeters	0.0016	square inches	in ²
m ²	square meters	10.764	square feet	ft ²
m ²	square meters	1.195	square yards	yd ²
ha	hectares	2.47	acres	ac
km ²	square kilometers	0.386	square miles	mi ²
VOLUME				
mL	milliliters	0.034	fluid ounces	fl oz
L	liters	0.264	gallons	gal
m ³	cubic meters	35.314	cubic feet	ft ³
m ³	cubic meters	1.307	cubic yards	yd ³
MASS				
g	grams	0.035	ounces	oz
kg	kilograms	2.202	pounds	lb
Mg (or "t")	megagrams (or "metric ton")	1.103	short tons (2000 lb)	T
TEMPERATURE (exact degrees)				
°C	Celsius	1.8C+32	Fahrenheit	°F
ILLUMINATION				
lx	lux	0.0929	foot-candles	fc
cd/m ²	candela/m ²	0.2919	foot-Lamberts	fl
FORCE and PRESSURE or STRESS				
N	newtons	0.225	poundforce	lbf
kPa	kilopascals	0.145	poundforce per square inch	lbf/in ²

*SI is the symbol for the International System of Units. (Adapted from FHWA report template, Revised March 2003)

LIST OF ACRONYMS

AASHTO	American Association of State Highway and Transportation Officials
ASCE	American Society of Civil Engineers
COV	Coefficient of Variation
CRR	Cyclic Resistance Ratio
CSR	Cyclic Stress Ratio
CPT	Cone Penetration Test
EDP	Engineering Demand Parameter
FHWA	Federal Highway Administration
FS	Factor of Safety
GUI	Graphical User Interface
IDE	Integrated Development Environment
IM	Intensity Measure
MSF	Magnitude Scaling Factor
NSHMP	National Seismic Hazard Model Project
NCEER	National Center for Earthquake Engineering Research
PBEE	Performance-Based Earthquake Engineering
PEER	Pacific Earthquake Engineering Research
PSHA	Probabilistic Seismic Hazard Analysis
SPT	Standard Penetration Test
TAC	Technical Advisory Committee
UDOT	Utah Department of Transportation
USGS	United States Geological Survey
VBA	Visual Basic for Applications

LIST OF TERMS

a	net area ratio
a_{max}	peak ground surface acceleration
C_{FC}	regression fitting parameter that can be used to minimize uncertainty
C_N	overburden correction factor (Robertson Method)
CRR	cyclic resistance ratio
CSR	cyclic stress ratio
DF	depth weighting factor
D_R	relative density
D_H	horizontal displacement
FC	finer content (%)
f_s	CPT sleeve friction
F_a	soil amplification factor
g	acceleration due to gravity
H	the free face height H
I_c	soil behavior type index
IND	indicator of the occurrence of liquefaction
K_c	soil behavior type correction factor
K_H	depth correction factor
K_α	initial shear stress correction factor
K_σ	overburden stress correction factor
λ	annual rate of exceedance or equal to 1/return period
LD	lateral displacement
LDI	lateral displacement index
L	the distance from toe of the free face
M	magnitude of earthquake event
M_w	moment magnitude of earthquake loading
MSF_{max}	the upper limit for MSF
N_{amax}	number of subdivided peak acceleration increments
N_M	number of subdivided Magnitude increments
N_{req}	required SPT/blow count resistance to resist liquefaction
ΔN_L	difference between $(N_1)_{60,cs}$ and N_{req} (Mayfield et al. 2010)
n	stress exponent (Robertson (2009))
P_a	atmospheric pressure (1 atm, 101.3 kPa, 0.2116 psf)
PGA	peak ground acceleration
P_L	probability of liquefaction
q_c	uncorrected CPT tip resistance

q_{c1N}	normalized CPT penetration resistance
q_{c1Ncs}	clean-sand equivalent normalized CPT tip resistance Robertson and Wride (1998) and Boulanger and Idriss
q_{req}	required cone tip resistance to resist liquefaction
q_t	corrected cone tip stress
R	ratio of baseline value to corrected value
λ_{ev}	mean annual rate of exceeding a specified strain
ε_v	volumetric strain
$\varepsilon_{v,max}$	maximum vertical strain
Q_{tn}	cone tip resistance corrected for overburden stress
Q_{mcs}	clean-sand equivalent normalized CPT tip resistance Robertson (2009)
r_d	shear stress reduction coefficient
S	the ground slope
S_a	actual settlement observed
δ_a	represents the coefficient of variation of S_a
S_p	vertical liquefaction-induced settlement
T_R	return period
u	CPT pore pressure
μ_a	mean of actual observed settlement
z	depth from ground surface to depth of interest
z_{max}	the deepest liquefiable layer
γ	unit weight of soil
γ_{max}	maximum cyclic shear strain
$\lambda_{\gamma_{max}}$	mean annual rate of exceeding the maximum cyclic shear strain
$\mathcal{E}_{ln(R)}$	total uncertainty
$\sigma_{ln(R)}$	model uncertainty
σ_{total}	total uncertainty
σ_{vo}	soil overburden pressure
σ'_{vo}	effective soil overburden pressure
σ_v	total vertical stress in the soil
σ'_v	effective vertical stress in the soil
Λ_{FSL}^*	mean annual rate of not exceeding some given value of FS_L
τ_{cyc}	equivalent uniform cyclic shear stress
$(N_1)_{60,cs}$	corrected SPT blow count
Φ	standard normal cumulative distribution function

EXECUTIVE SUMMARY

The purpose of the research presented is to provide the benefit of the full performance-based probabilistic earthquake hazard analysis using Cone Penetration Test (CPT) data, without requiring special software, training, and experience. To do this, full performance-based probabilistic procedures were created to calculate liquefaction triggering, liquefaction-induced settlements, and liquefaction-induced lateral spread based on CPT data. These new procedures were used in Phase 2 of this research. This final report volume provides a review of all work completed throughout Phase 1, addressing Tasks 1 through 4 of the pooled fund study TPF-5(338) research contract.

The focus of Tasks 1 through 4 was the development of a performance-based earthquake engineering (PBEE) liquefaction hazard analysis procedure for the CPT and an analysis tool, *CPTLiquefY*, to simplify extensive probabilistic calculations. Two PBEE liquefaction hazard analysis procedures were developed by using the Robertson and Wride (1998, 2009), and Idriss and Boulanger (2014) CPT liquefaction triggering models. The Ku et al. (2012) probabilistic version of the Robertson and Wride model was also used. Liquefaction-induced settlements and lateral spreading PBEE procedures were developed using the Juang et al. (2013) and Zhang et al. (2004) CPT methods, respectively.

These new PBEE procedures were tested and compared to conventional methods by performing liquefaction hazard analyses for 20 CPT profiles at 10 cities of varying levels of seismicity. The analysis of liquefaction triggering models appears to show that in general the new Boulanger and Idriss full-probabilistic procedure will give more conservative results than the Ku et al. full-probabilistic procedure. The results indicated similar trends between the liquefaction-induced settlements and lateral spreading. The data suggests for a low return period, the pseudo-probabilistic settlement and lateral spread values correlated fairly well with full-probabilistic values. However, at medium to high return periods, this correlation deteriorated and showed pseudo-probabilistic methods under-predicting settlements and lateral spreading significantly.

With all data collected and analyzed, Tasks 1 through 4 of the TPF-5(338) research contract have been completed. The second phase of this research project is the development of

simplified procedures and reference parameter maps, as presented in the Phase 2 final report volume.

1.0 INTRODUCTION

1.1 Problem Statement

The purpose of the research presented is to provide the benefit of the full performance-based probabilistic earthquake hazard analysis using Cone Penetration Test (CPT) data, without requiring special software, training, and experience. This research is comprised of two phases, with the results of Phase 1 being presented in this final report volume and Phase 2 being presented in a separate final report volume. The purpose of Phase 1 (Tasks 1-4) is to develop software that calculates a full performance-based probabilistic earthquake hazard analysis, to determine liquefaction triggering, lateral spread displacements, and post-liquefaction free-field settlements. To do this, equations and relationships derived from empirical models are used to determine the soil characteristics from a CPT as well as determine the behavior of the given soil during and after a seismic event. This is all accomplished using code written in Visual C++ to automate these procedures.

It is noted that a related study was performed previously for Standard Penetration Test (SPT) data by some of the same authors of this study. More information on the SPT-based study is available under the TPF-5(296) pooled fund study on the pooledfund.org website, from the Utah Department of Transportation Research & Innovation Division, or from the current study authors.

1.2 Objectives

The objective of this report is to detail the development of the research tool *CPTLiquefY*. The main research steps addressed in this report include:

- Develop the research tool, *CPTLiquefY*, to calculate full performance-based probabilistic earthquake hazard analyses
- Introduce the original models used to determine liquefaction hazards (i.e. liquefaction triggering, lateral spread displacement, and post-liquefaction settlement) and provide derivations of the simplified methods

- Present the results of a comparison between conventional and full-probabilistic procedures.

These steps specifically address Tasks 1 through 4 of the pooled fund study TPF-5(338) research contract.

1.3 Scope

This report is organized to include the following sections:

- Introduction
- Liquefaction Triggering Evaluation Using the CPT: Empirical Models Used for Liquefaction Hazards, and Integration of Models into Software
- *CPTLiquefY*: Development of *CPTLiquefY*, and Integration of New USGS Deaggregation Tool
- Methodology and Results: Methodology for Running Analyses; and Results of *CPTLiquefY* for Liquefaction Triggering, Settlement, and Lateral Spread
- Sensitivity Analysis: Thin Layer Correction and Depth Weighting Factor
- Conclusions
- References
- Appendix A: Lateral Spread Comparisons

2.0 LIQUEFACTION TRIGGERING EVALUATION USING THE CPT

2.1 Overview

This section describes the CPT-based procedure for evaluating liquefaction triggering, liquefaction-induced settlement, and lateral spread displacement. These procedures and models were used to develop *CPTLiquefY* and the simplified procedures.

2.2 Liquefaction Triggering Evaluation

This section will provide the necessary background to understand the liquefaction triggering procedure. A brief discussion regarding empirical liquefaction triggering models will be provided, followed by a discussion of performance-based implementation of those models.

2.2.1 Empirical Liquefaction Triggering Models

When dealing with liquefaction hazard evaluation, most professionals rely upon site-specific liquefaction triggering assessment for use in design. One of the most widely used methods of assessment in engineering practice today is the simplified empirical procedure (Seed (1979); Seed and Idriss (1971); Seed and Idriss (1982); Seed et al. (1985)). According to this simplified procedure, liquefaction triggering is evaluated by comparing the seismic loading of the soil to the soil's resistance to liquefaction triggering. Seismic loading is typically characterized using a cyclic stress ratio, *CSR*, which is computed as:

$$CSR = \frac{\tau_{cyc}}{\sigma'_v} = 0.65 \frac{a_{max}}{g} \frac{\sigma_v}{\sigma'_v} r_d \quad (1)$$

where τ_{cyc} is the equivalent uniform cyclic shear stress, σ'_v is the effective vertical stress in the soil, a_{max}/g is the peak ground surface acceleration as a fraction of gravity, σ_v is the total vertical stress in the soil, and r_d is a shear stress reduction coefficient.

Soil resistance to liquefaction triggering is characterized by performing some in-situ soil test (e.g., cone penetration resistance, standard penetration resistance, shear wave velocity, etc.) and comparing its results to those from documented case histories of liquefaction triggering. Based on observation and/or statistical regression, a function for the in-situ test can be delineated that separates the “liquefaction” case histories from the “non-liquefaction” case histories. This delineated boundary is referred to as the cyclic resistance ratio, *CRR*, and represents the unique combinations of *CSR* and in-situ soil resistance values at which liquefaction triggers (Figure 2-1).

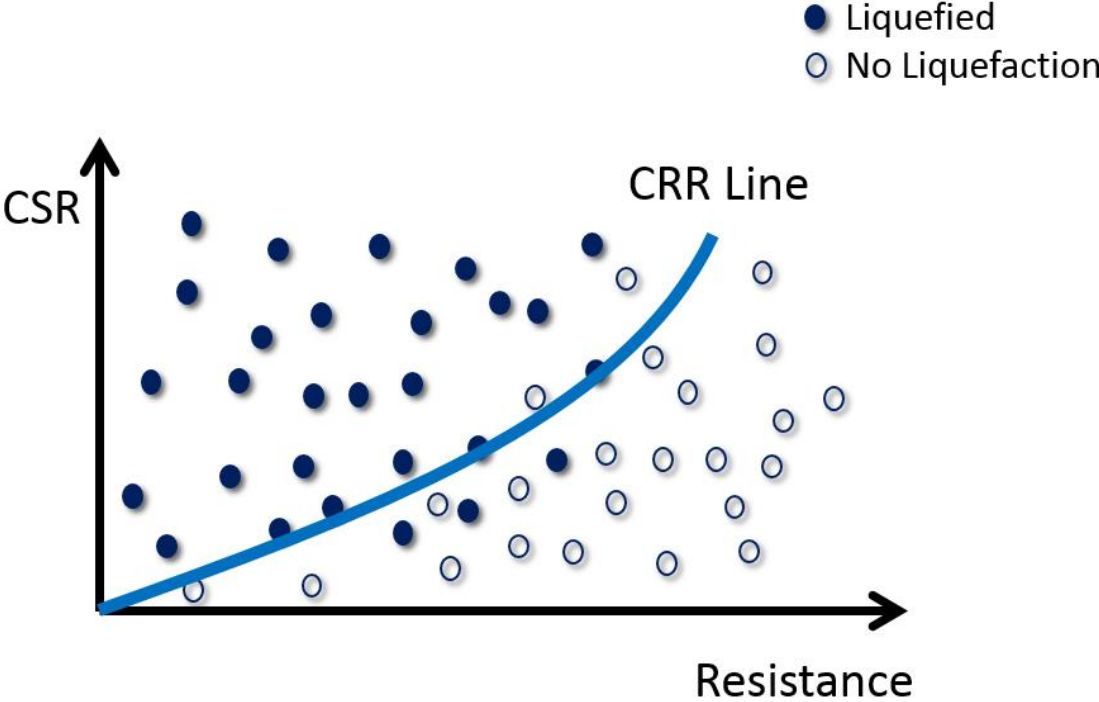


Figure 2-1: Example development of the CRR line.

Engineers and geologists commonly quantify liquefaction triggering using a factor of safety against liquefaction triggering, FS_L . This parameter is calculated as:

$$FS_L = \frac{\text{Resistance}}{\text{Loading}} = \frac{CRR}{CSR} \tag{2}$$

2.2.2 Robertson and Wride (1998, 2009) Procedure

Until recent years, most liquefaction assessments for the CPT were calculated based on CPT to SPT correlations, but the increased usage of the CPT initiated an increase of CPT assessment methods. One of the most widely used CPT liquefaction triggering procedures is Robertson and Wride (1998), which was updated to the Robertson and Wride (2009) procedure. This procedure uses all of the available CPT data variables [cone tip resistance (q_c), sleeve friction (f_s), pore pressure (u), and depth] to calculate a corrected normalized equivalent clean sand CPT penetration resistance, Q_{mcs} [e.g. $(q_{c1N})_{cs}$], based on correlations from case history data. Robertson and Wride used these Q_{mcs} values to develop a deterministic CRR curve, which represents a boundary between cases that are expected to liquefy and those which are not expected to liquefy (Figure 2-2).

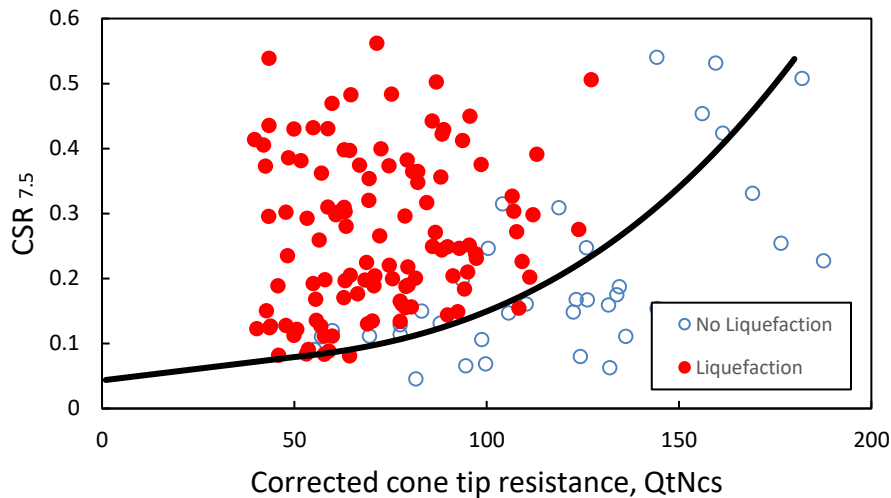


Figure 2-2: Robertson and Wride (2009) liquefaction triggering curve with case history data points.

Once the CRR is defined, it is then possible to make a prediction of liquefaction triggering by plotting the CPT resistance and the CSR calculated at a depth of interest for a certain earthquake event. If the point plots above the CRR curve it is expected that the factor of safety against liquefaction (FS_L) will be less than 1 and thus expected to liquefy. Conversely, if the point plots below the curve, FS_L will be greater than 1 and liquefaction will not be anticipated to occur.

To obtain a CRR , Q_{mcs} must be calculated. To calculate the Q_{mcs} , the Robertson and Wride method is an iterative process. To start an initial stress exponent, n , is calculated using:

$$n = 0.381(I_c) + 0.05 \left(\frac{\sigma'_{vo}}{P_o} \right) - 0.15 \quad (3)$$

where I_c is the soil behavior index. The soil behavior index is an indicator of how much a soil will behave like a fine-grained soil compared to a coarse-grained material. Robertson (1990) found a correlation for the I_c from the q_c and f_s . This relationship can be summarized with the soil behavior chart (Jefferies & Davies, 1993; Robertson, 1990) shown in Figure 2-3.

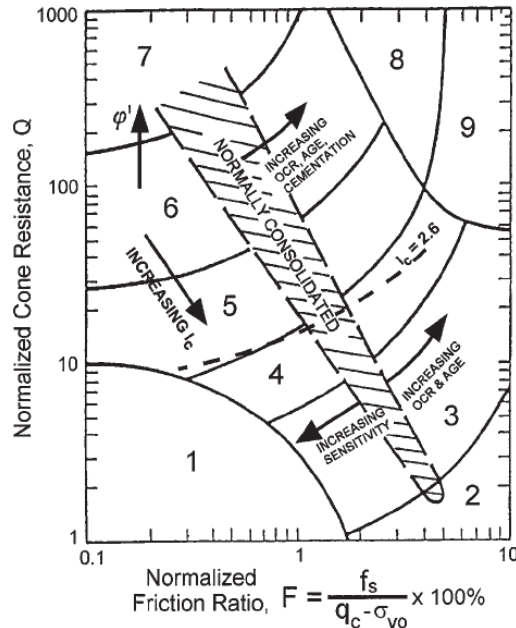


Figure 2-3: Normalized CPT soil behavior type chart (after Robertson, 1990). Soil types: 1, sensitive, fine grained; 2, peats; 3, silty clay to clay; 4, clayey silt to silty clay; 5, silty sand to sandy silt; 6, clean sand to silty sand; 7, gravelly sand to dense sand; 8, very stiff sand to clayey sand; 9, very stiff, fine grained.

I_c cannot be calculated directly, so an initial seed I_c value is used to start the iterative process. Using this seed value, n is calculated from Equation (3) and then used to calculate the overburden stress correction factor, C_N as:

$$C_N = \left(\frac{P_a}{\sigma_{vo}} \right)^n < 2.0 \quad (4)$$

The I_c value is then calculated as:

$$I_c = [(3.47 - \log(Q))^2 + (\log(F_r) + 1.22)^2]^{0.5} \quad (5)$$

where

$$Q = \left[\frac{q_t - \sigma_{vo}}{P_a} \right] * C_N \quad (6)$$

and

$$F_r = \frac{f_s}{(q_t - \sigma_{vo})} * 100 \quad (7)$$

Using the newly calculated I_c , from Equation (5), n is recalculated using Equation (3). This process is repeated until the change in n (Δn) is less than 0.01. Once $\Delta n < 0.01$, all current calculated values of Q , F_r , and I_c are used to calculate $Q_{m,cs}$, which is calculated using:

$$Q_{tn,cs} = K_c * Q_{tn} \quad (8)$$

where K_c is calculated using:

$$K_c = \begin{cases} K_c = 1.0 & \text{if } I_c \leq 1.64 \\ K_c = 5.58I_c^3 - 0.403I_c^4 - 21.63I_c^2 + 33.75I_c - 17.88 & \text{if } 1.64 < I_c < 2.60 \\ K_c = 6 * 10^{-7}(I_c)^{16.76} & \text{if } 2.50 < I_c < 2.70 \end{cases} \quad (9)$$

CRR is calculated using:

$$CRR_{7.5} = 93 \left[\frac{Q_{tn,cs}}{1000} \right]^3 + 0.08 \quad (10)$$

However, Equation (10) is only valid if $I_c < 2.70$. If $I_c \geq 2.70$, then K_c is not used and *CRR* is calculated as:

$$CRR_{7.5} = 0.053 * Q_{tn,cs} \quad (11)$$

This *CRR* value is then used to calculate the factor of safety against liquefaction. A summary flowchart of the Robertson and Wride (2009) procedure for computing *CRR* is presented in Figure 2-4.

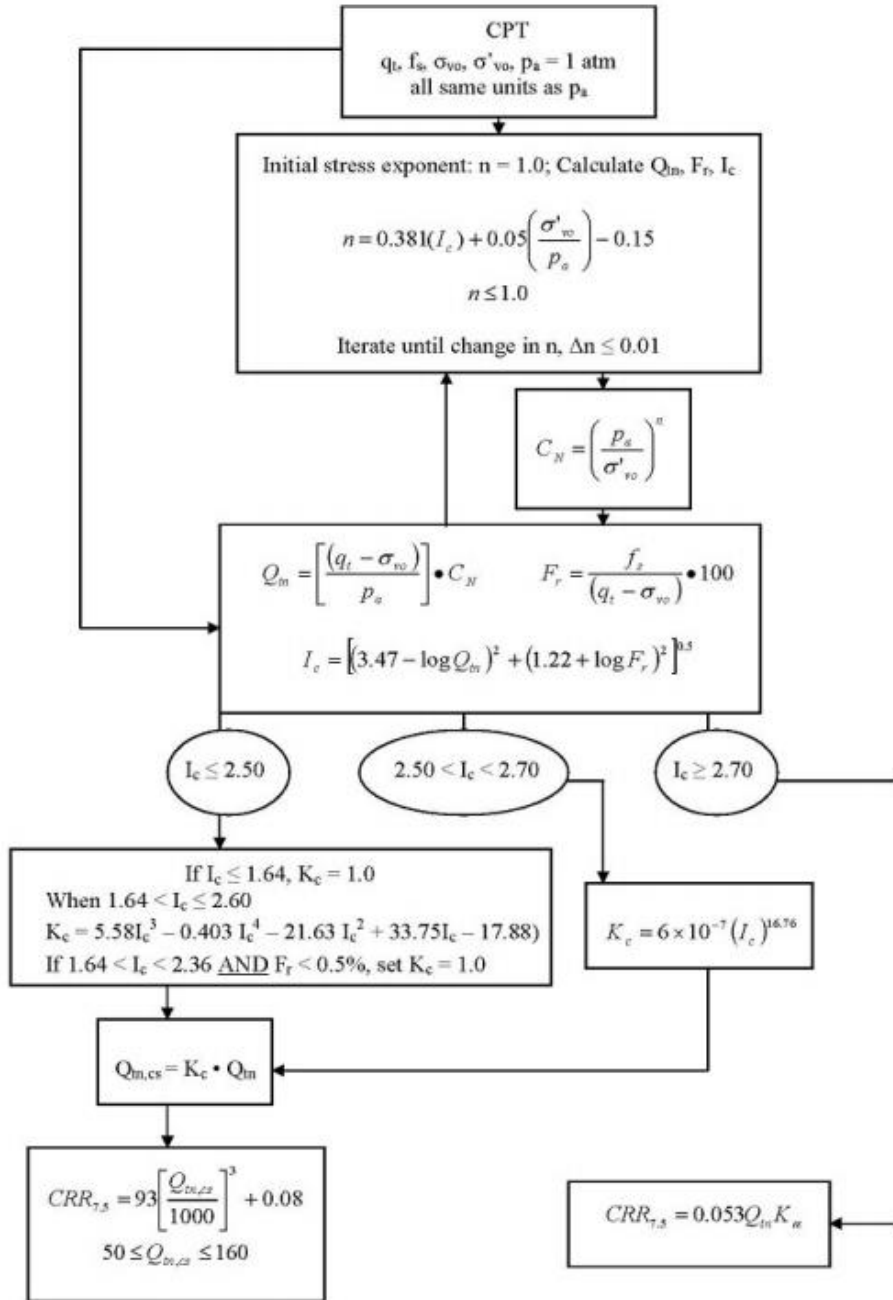


Figure 2-4: Summary of the Robertson and Wride (2009) CRR procedure.

Robertson and Wride presents a procedure to calculate the *CSR*. Robertson and Wride utilizes Equation (1) to calculate the *CSR*, but calculates the *MSF*, *rd*, and *K_σ* factors uniquely. Many values for *MSF* have been suggested by various researchers (Seed and Idriss, 1982;

Ambraseys, 1988), however, the Robertson and Wride method uses the lower-bound equation values suggested by Youd et al. (2001):

$$MSF = \frac{10^{2.24}}{M_w^{2.56}} \quad (12)$$

where M_w is the moment magnitude of the earthquake loading. The value r_d is a depth-dependent shear stress reduction factor. The Robertson and Wride procedure calculates the r_d , based on the work of Liao and Whitman (1986), Robertson and Wride (1998), and Seed and Idriss (1971), as:

$$r_d = \begin{cases} 1.0 - 0.00765z & \text{for } z \leq 9.15m \\ 1.174 - 0.0267z & \text{for } 9.15m < z \leq 23m \\ 0.744 - 0.008z & \text{for } 23m < z \leq 30m \\ 0.5 & \text{for } z > 30m \end{cases} \quad (13)$$

where z is the depth of interest in meters. Finally, to calculate the K_σ , Robertson and Wride utilizes the procedure from Idriss et al. (2001):

$$K_\sigma = \left(\frac{\sigma_{vo}'}{P_a} \right)^{(f-1)} \quad (14)$$

where σ_{vo}' is the effective overburden pressure, P_a is atmospheric pressure in the same units and f is an exponent that is a function of site conditions. After CRR and CSR are calculated FS_L can be computed using Equation (2).

2.2.3 Ku et al. (2012) Procedure [Probabilistic Version of Robertson and Wride Method]

Because of the increased usage and popularity of the Robertson and Wride (2009) liquefaction triggering procedure, the need for a probabilistic version of this method was needed. Ku et al. (2012) developed a probabilistic model of the Robertson and Wride (2009) method through statistical analysis of the liquefaction triggering case histories. The goal of this new model

was to create a probabilistic method that could be easily integrated into current reliability or performance-based design practices.

Ku et al. developed a function to relate FS_L (from the Robertson and Wride method) to a probability of liquefaction P_L . This function was intended to provide a smooth transition of integrating a probabilistic method into current design methods. By using the Bayesian statistical analysis of a case history database and the principle of maximum likelihood, Ku et al. developed the following relationship:

$$P_L = 1 - \Phi \left[\frac{0.102 + \ln(FS_L)}{\sigma_T} \right] \quad (15)$$

where Φ is the standard normal cumulative distribution function, and σ_T is the total uncertainty and is equal to 0.3537. This relationship between FS_L and P_L can be viewed visually in Figure 2-5. The curve indicated by the “RW” represents the Robertson and Wride (2009) deterministic triggering curve.

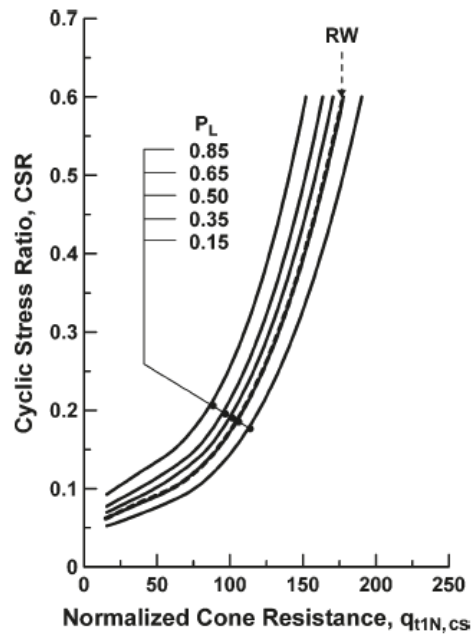


Figure 2-5: CRR liquefaction triggering curves based on P_L .

2.2.4 Boulanger and Idriss (2014) Procedure

The Boulanger and Idriss (2014) procedure calculates the q_{c1Ncs} differently than the Robertson and Wride (2009) procedure, which results in a different calculated CRR value. Boulanger and Idriss gathered together a database of old and recent (up through 2011) earthquake data. Using this database, Boulanger and Idriss created a new correlation between CPT data and the CRR for an earthquake.

Just like the Robertson and Wride method, the Boulanger and Idriss method requires an iterative calculation for q_{c1Ncs} . The method starts by correcting for overburden pressure as:

$$q_{c1N} = C_N \frac{q_c}{P_a} \quad (16)$$

where q_c is CPT cone tip resistance, P_a is atmospheric pressure, and C_N is the overburden correction factor calculated as:

$$C_N = \left(\frac{P_a}{\sigma'_v} \right)^m \leq 1.7 \quad (17)$$

where σ'_v is the vertical effective stress and m is calculated as:

$$m = 1.338 - 0.249(q_{c1Ncs})^{0.264} \quad (18)$$

and where q_{c1Ncs} is limited to values between 21 and 254. To start the iteration, an initial seed value of q_{c1Ncs} is specified, and Equations (16) through (18) are iteratively repeated until the change in q_{c1Ncs} is less than 0.5. Throughout the iterative process, the normalized clean-sand cone tip resistance (q_{c1Ncs}) value is calculated as:

$$q_{c1Ncs} = q_{c1N} + \Delta q_{c1N} \quad (19)$$

where Δq_{c1N} is the fines content adjustment factor, Δq_{c1N} is calculated as:

$$\Delta q_{c1N} = \left(11.9 + \frac{q_{c1N}}{14.6} \right) \exp \left(1.63 - \frac{9.7}{FC + 2} - \left(\frac{15.7}{FC + 0.01} \right)^2 \right) \quad (20)$$

where FC is the percentage of fines within the soil. To obtain FC from the CPT, Idriss and Boulanger suggest using the FC and I_c correlation from the Robertson and Wride (2009) procedure. However, Idriss and Boulanger suggest approaching this relationship with caution due to the data scatter. Idriss and Boulanger suggest calculating FC as:

$$FC = 80(I_c + C_{FC}) - 137 \quad (21)$$

$$0\% \leq FC \leq 100\%$$

where I_c is the soil behavior type index calculated from the Robertson and Wride procedure, and C_{FC} is a regression fitting parameter that can be used to minimize uncertainty when site-specific fines content data is available. Figure 2-6 is a plot of the relationship between FC and I_c along with the associated data scatter.

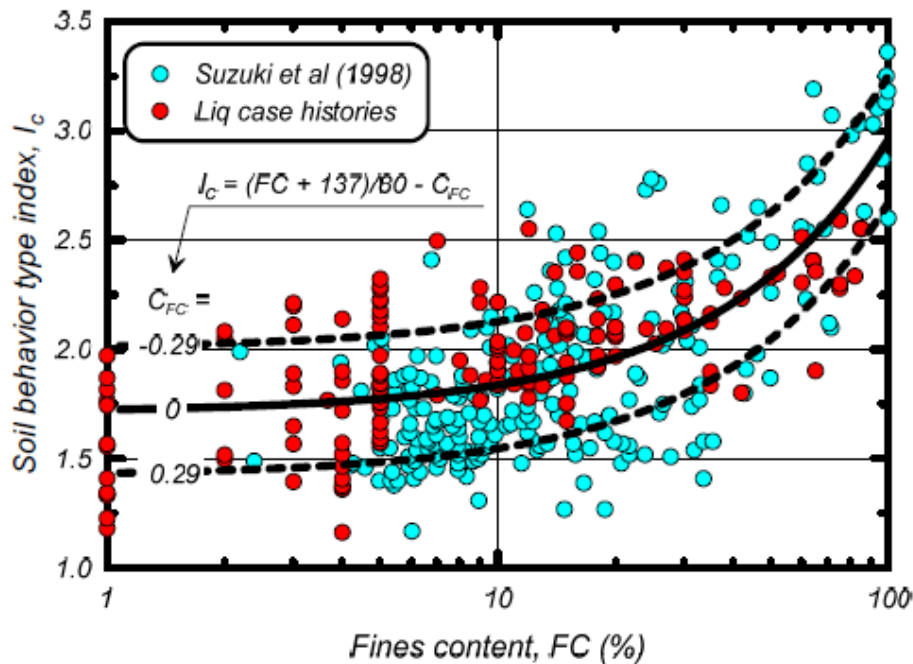


Figure 2-6: Recommended correlation between I_c and FC with plus or minus one standard deviation against the dataset by Suzuki et al. (1998) (after Idriss and Boulanger, 2014).

After the iteration has been completed to the desired level of accuracy, the *CRR* is then calculated. For the Boulanger and Idriss method, the *CRR* is calculated as:

$$CRR_{M=7.5, \sigma'_{vo}=1atm} = \exp\left(\frac{q_{c1Ncs}}{113} + \left(\frac{q_{c1Ncs}}{1000}\right)^2 - \left(\frac{q_{c1Ncs}}{140}\right)^3 + \left(\frac{q_{c1Ncs}}{137}\right)^4 - 2.8\right) \quad (22)$$

Boulanger and Idriss (2014) presents a procedure to calculate the *CSR*. Boulanger and Idriss (2014) utilizes Equation (2), just as the Robertson and Wride (2009) procedure, but implements different methods to calculate the *MSF*, r_d , and K_σ . Boulanger and Idriss (2014) developed a relationship to calculate the *MSF* by combining past *MSF* relationships (Idriss, 1999; Boulanger and Idriss, 2008). This new *MSF* relationship is calculated as:

$$MSF = 1 + (MSF_{max} - 1) \left(8.64 \exp\left(\frac{-M}{4}\right) - 1.325\right) \quad (23)$$

$$MSF_{max} = 1.09 + \left(\frac{q_{c1Ncs}}{180}\right)^3 \leq 2.2 \quad (24)$$

where M is the moment magnitude of the scenario earthquake and q_{c1Ncs} is the corrected cone tip resistance for the Boulanger and Idriss (2014) method. This new relationship allows for soil characteristics to be represented by CPT cone tip resistance and was found to improve the degree of fit between CPT-based liquefaction triggering correlation and their respective history databases (Boulanger and Idriss, 2014).

The Boulanger and Idriss (2014) procedure calculates r_d by using the equations of Golesorkhi (1989):

$$r_d = \exp[\alpha(z) + \beta(z) * M] \quad (25)$$

$$\alpha(z) = -1.012 - 1.126 \sin\left(\frac{z}{11.73} + 5.133\right) \quad (26)$$

$$\beta(z) = 0.106 + 0.118 \sin\left(\frac{z}{11.28} + 5.142\right) \quad (27)$$

where z is the depth below the ground surface in meters, M is the moment magnitude of the scenario earthquake, and the arguments within the trigonometric functions are in radians.

The K_σ factor in the Boulanger and Idriss method is calculated using the procedure developed by Boulanger (2003):

$$k_\sigma = 1 - C_\sigma \ln\left(\frac{\sigma'_v}{P_a}\right) \leq 1.1 \quad (28)$$

$$C_\sigma = \frac{1}{37.3 - 8.27(q_{c1Ncs})^{0.264}} \leq 0.3 \quad (29)$$

where σ'_v is the vertical overburden pressure, P_a is a reference pressure equal to 1 atm, and q_{c1Ncs} is the corrected cone tip resistance for the Idriss and Boulanger method.

Finally, with the calculated CSR and CRR values the liquefaction triggering model is applicable to wide ranges of CPT resistance values. The liquefaction triggering curve, for the Idriss and Boulanger deterministic model, is presented in Figure 2-7. The CRR lines for both Boulanger and Idriss studies (2008 and 2014) are shown.

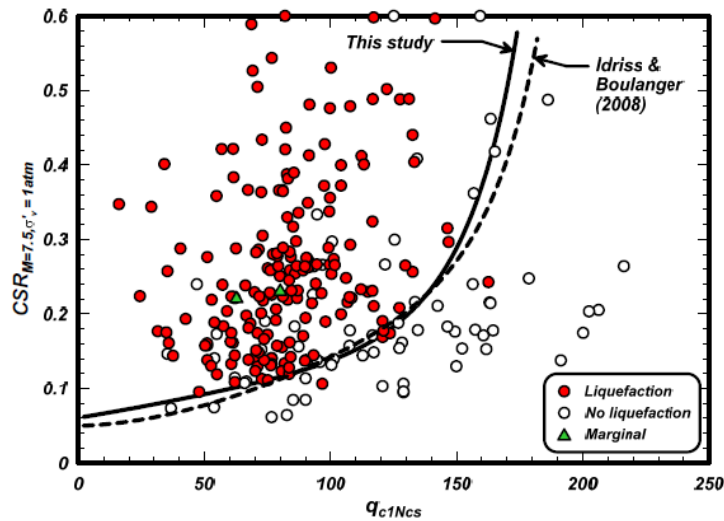


Figure 2-7: CRR curves and liquefaction curves for the deterministic case history database (after Boulanger and Idriss, 2014).

2.2.5 PBEE Liquefaction Triggering Procedures

The PBEE framework was used to develop a PBEE liquefaction triggering procedure for the CPT. To apply a performance-based procedure to the liquefaction triggering calculations, FS_L hazard curves are developed using the Kramer and Mayfield (2007) PBEE approach. This approach utilizes the PBEE framework by assigning the joint occurrence of M_w and a_{max} as an intensity measure and the FS_L as the engineering demand parameter. Engineers are more interested in when FS_L is expected to *not* exceed a certain value because FS_L , unlike other $EDPs$, is more favorable the larger it is. This equation of non-exceedance is presented as:

$$\Lambda_{FS^*_L} = \sum_{j=1}^{N_M} \sum_{i=1}^{N_{a_{max}}} P[FS_L < FS^*_L | a_{max,i}, m_j] \Delta\lambda_{a_{max,i},m_j} \quad (30)$$

where $\Lambda_{FS^*_L}$ is the mean annual rate of *not* exceeding some given value of factor of safety (FS^*_L), N_M and $N_{a_{max}}$ are the number of magnitude and a_{max} increments into which the hazard space is subdivided, and $\Delta\lambda_{a_{max,i},m_j}$ is the incremental mean annual rate of exceedance for intensity measures $a_{max,i}$ and m_j .

Kramer and Mayfield also related performance-based methodology with in-situ soil resistance by using the term N_{req} , which represents the SPT resistance required to prevent liquefaction. In other words, N_{req} is the number of blow counts required to prevent liquefaction or the condition of $FS_L = 1$. To apply this to the CPT q_{req} (i.e., the required tip resistance) can be used. Following the work of Kramer and Mayfield an expression for the mean annual rate of exceedance of the value q^*_{req} at a depth of interest can be defined as:

$$\lambda_{q^*_{req}} = \sum_{j=1}^{N_M} \sum_{i=1}^{N_{a_{max}}} P[q_{req} > q^*_{req} | a_{max,i}, m_j] \Delta\lambda_{a_{max,i},m_j} \quad (31)$$

where

$$P[q_{req} > q^*_{req} | a_{max,i}, m_j] = P_L(q^*_{req}) \quad (32)$$

Each of the two triggering procedures calculate Equation (32) differently. The Robertson and Wride (2009) P_L can be calculated as:

$$P_L = 1 - \Phi \left[\frac{0.102 + \ln \left(\frac{CRR}{CSR} \right)}{\sigma_{total}} \right] \quad (33)$$

where σ_{total} is the parameter of total uncertainty and is equal to 0.3537. The CRR and CSR are calculated according to Equations (3) through (14), but the input $Q_{m,cs}$ is replaced with q^*_{req} . For the Boulanger and Idriss (2014) procedure, the P_L is calculated as:

$$P_L = \Phi \left[- \frac{\left(\frac{q^*_{c1Ncs}}{113} \right) + \left(\frac{q^*_{c1Ncs}}{1000} \right)^2 - \left(\frac{q^*_{c1Ncs}}{140} \right)^3 + \left(\frac{q^*_{c1Ncs}}{137} \right)^4 - 2.60 - \ln(CSR_{M=7.5, \sigma'_v=1atm})}{\sigma_{total}} \right] \quad (34)$$

where σ_{total} is the parameter of total uncertainty and is equal to 0.506, q^*_{c1Ncs} is equal to q^*_{req} , and the $CSR_{M=7.5, \sigma'_v=1atm}$ is calculated using Equation (1).

Equation (31) is repeated for a range of q^*_{req} (1 to 250) for each triggering method and for every soil layer. These calculations result in a range of probabilities of exceedance (λ) corresponding to q_{req} values. This process develops a q_{req} hazard curve. Because FS_L and ΔN_L essentially provide the same information, Kramer and Mayfield (2007) provides a useful conversion between the two:

$$FS_L^{site} = \frac{CRR}{CSR} = \frac{CRR (N_{site})}{CRR (N_{req}^{site})} \quad (35)$$

This conversion may be applied to CPT data by using:

$$FS_L^{site} = \frac{CRR}{CSR} = \frac{CRR (q_{site})}{CRR (q_{req}^{site})} \quad (36)$$

where q_{site} is the measured corrected clean-sand equivalent CPT cone-tip resistance, and q_{req}^{site} is the computed corrected clean-sand equivalent CPT cone-tip resistance required to resist liquefaction at the site of interest. By using Equations (35) and (36), the q_{req} hazard curves are converted to FS_L hazard curves. When q_{req} is converted to FS_L the value $\lambda_{q_{req}^*}$ is automatically converted to an annual rate of non-exceedance of FS_L ($\lambda_{FS^*_L}$).

These calculations complete the process of creating an FS_L hazard curve for one soil layer. This process is repeated for each soil layer so that an FS_L hazard curve exists for each soil layer and for each triggering method. An example FS_L hazard curve for one soil layer is presented in (Figure 2-8).

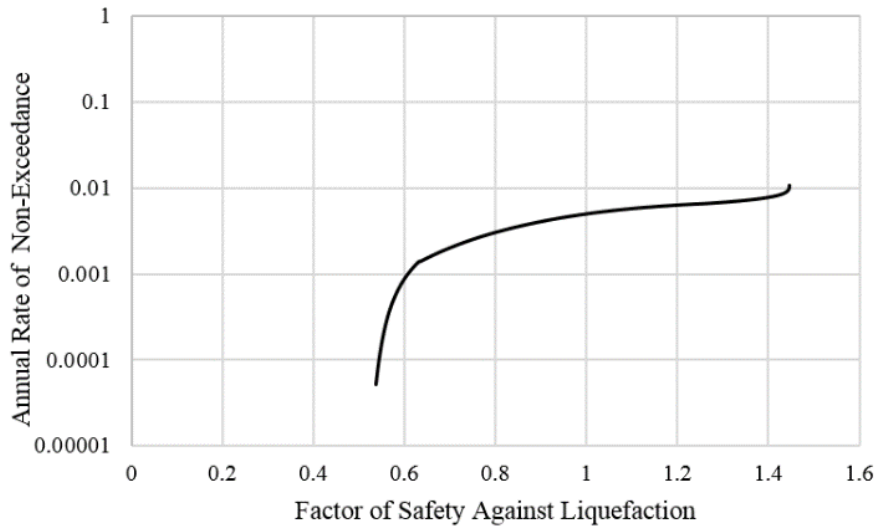


Figure 2-8: Example FS_L curve from one soil layer at a depth of 6m of a CPT profile calculated at Eureka, CA.

2.3 Liquefaction-Induced Settlement Evaluation

This section describes various methods and procedures to calculate liquefaction induced volumetric strains and subsequently vertical settlements in liquefied soils. To calculate a soil layer's vertical settlement, caused by liquefaction, volumetric strains are calculated and multiplied by soil layer thickness. The Ishihara and Yoshimine (1992) deterministic settlement calculation

method will be addressed, as well as the Juang et al. (2013) probabilistic method will be addressed. Finally, the performance-based approach will be discussed.

2.3.1 Liquefaction-Induced Settlement Ishihara and Yoshimine (1992) Procedure

Ishihara and Yoshimine (1992) produced a deterministic method to calculate the volumetric strains in liquefiable soils based on CPT input data. First, a factor of safety against liquefaction (FS_L) is obtained for each layer. A relative density is also calculated for each layer, using:

$$D_R = -85 + 76 \log \frac{q_c}{\sqrt{\sigma'_v}} \quad (37)$$

where q_c is the cone tip resistance and σ'_v is the vertical effective stress. Using FS_L , maximum shear strain (γ_{max}), and calculated D_R for each layer, Ishihara and Yoshimine (1992) developed a relationship between the calculated values and volumetric strain. Curves were developed to display this relationship, as seen in Figure 2-9.

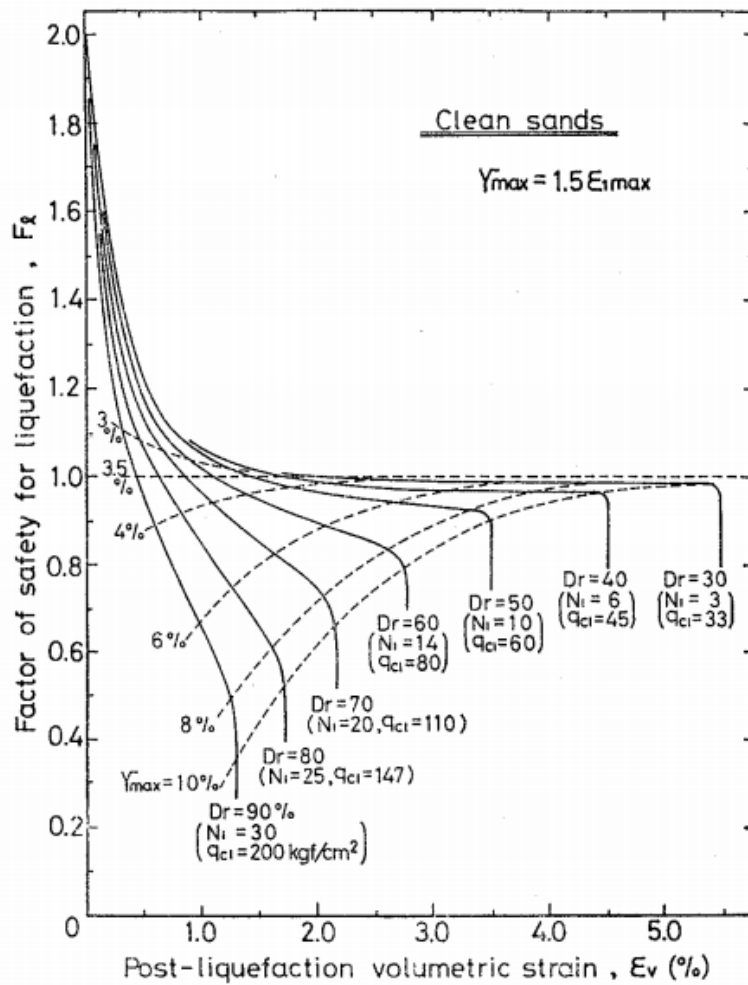


Figure 2-9 The relationship between F_{SL} , γ_{max} , and D_R as presented by Ishihara and Yoshimine (1992).

Using the developed curves, volumetric strain can be determined for each soil layer. Each layer's volumetric strain is multiplied by the layer's thickness, resulting in the vertical liquefaction-induced settlement (S_p) of each layer. Finally, each layer's settlement is summed together to calculate the predicted total ground surface settlement, using the following equation:

$$S_p = \sum_{i=1}^N \epsilon_v \Delta Z_i \quad (38)$$

Where ε_v is volumetric strain for the i^{th} layer, N is number of layers, and ΔZ_i is the i^{th} layer's thickness.

2.3.2 Liquefaction-Induced Settlement Juang et al. (2013) Procedure

The Juang et al. (2013) procedure calculates liquefaction-induced settlements by applying a probabilistic approach to the deterministic Ishihara and Yoshimine (1992) method. The procedure also uses Equation (38) to calculate predicted vertical settlements, but adds probabilistic parameters by using the following equation:

$$S_p = M \sum_{i=1}^N \varepsilon_v \Delta Z_i IND_i \quad (39)$$

where ε_v is volumetric strain for the i^{th} layer, N is the number of layers, M represents a multiplicative model bias, IND_i represents an indicator of liquefaction occurring, and ΔZ_i is layer thickness for the i^{th} layer. Volumetric strain is calculated by using a curve-fitted equation based on the Ishihara and Yoshimine (1992) curves (Figure 2-9), shown below:

$$\varepsilon_v (\%) = \begin{cases} 0 & \text{if } FS \geq 2 \\ \min \left\{ \frac{a_0 + a_1 \ln(q)}{\frac{1}{(2 - FS)} - [a_2 + a_3 \ln(q)]}, b_0 + b_1 \ln(q) + b_2 \ln(q)^2 \right\} & \text{if } 2 - \frac{1}{a_2 + a_3 \ln(q)} < FS < 2 \\ b_0 + b_1 \ln(q) + b_2 \ln(q)^2 & \text{if } FS \leq 2 - \frac{1}{a_2 + a_3 \ln(q)} \end{cases} \quad (40)$$

Where: $a_0 = 0.3773$, $a_1 = -0.0337$, $a_2 = 1.5672$, $a_3 = -0.1833$, $b_0 = 28.45$, $b_1 = -9.3372$, $b_2 = 0.7975$, $q = q_{t1Ncs}$

The multiplicative model bias is calculated by calibrating their model back to the case histories' data by matching means. Juang et al. (2013) presents the IND_i variable as probability of liquefaction (P_L) and is calculated by using Equation (41).

$$IND = P_L = 1 - \phi \left\{ \frac{0.102 + \ln(FS)}{0.276} \right\} \quad (41)$$

One significant disadvantage associated with the Juang et al. (2013) probabilistic model for CPT-based settlement prediction is that the model was based on the binomial assumption that liquefaction settlements can be caused by both liquefied and non-liquefied soils. Engineers commonly consider a soil layer susceptible to post-liquefaction settlement if the soil layer has a sufficiently low factor of safety against liquefaction (usually less than 1.2 to 2.0). Engineers rarely (if ever) consider non-liquefied soils to contribute to liquefaction settlements. However, the Juang et al. (2013) model includes the probability that non-liquefied soil layers contribute to the settlement, which may make sense mathematically, but not physically. While the possibility of non-liquefied soil layers contributing to post-liquefaction settlements is likely greater than zero, it is also likely sufficiently low that most engineers choose to neglect it. Furthermore, the consideration of this possibility greatly increases the mathematical difficulty of the Juang et al. model. Therefore, this study re-solved the maximum likelihood equation developed by Juang et al. (2013), but neglected the possibility that non-liquefied layers contribute to liquefaction so as to neglect the possible settlements. The resulting values of M and $\sigma_{\ln(s)}$ are 1.014 and 0.3313, respectively. Any potential error introduced by this simplification is accounted for in the larger value of $\sigma_{\ln(s)}$. Therefore, these re-regressed values of M and $\sigma_{\ln(s)}$ are used in this study.

These re-regressed values were calculated by altering the Juang et al. (2013) maximum likelihood equation. The original Juang et al. (2013) maximum likelihood equation for the database with $m + n$ case histories, where m is the number of cases with a fixed settlement observation and n is the number of case histories in which settlement is reported as a range, is given as:

$$\begin{aligned}
& \ln\{L[\theta|S_a(1), S_a(2), \dots, S_a(m), S_{a,low}(1), S_{a,up}(1), \dots, S_{a,low}(n), S_{a,up}(n)]\} \\
&= \sum_{k=1}^m \left\{ -\ln[\sqrt{2\pi}\xi(k)S_a(k)] - \frac{1}{2} \left(\frac{\ln[S_a(k)] - \lambda(k)}{\xi(k)} \right)^2 \right\} \\
&+ \sum_{l=1}^n \ln \left[\Phi \left(\frac{\ln[S_{a,up}(l)] - \lambda(l)}{\xi(l)} \right) - \Phi \left(\frac{\ln[S_{a,low}(l)] - \lambda(l)}{\xi(l)} \right) \right]
\end{aligned} \tag{42}$$

where S_a is the actual settlement observed, k represents the k th case history from the database with m case histories, and l is the l th case history from the database with n case histories. For the re-derivation, only the case histories containing actual recorded settlements were used. The case histories with ranges of settlement (n case histories) were removed. In Equation (42), the λ and ξ variables were represented as:

$$\lambda(k) = \ln \left\{ \frac{\mu_a(k)}{[1 + \delta_a^2(k)]^{0.5}} \right\} \quad (43)$$

and

$$\xi(k) = \ln \left\{ [1 + \delta_a^2(k)]^{0.5} \right\} \quad (44)$$

where $\mu_a(k)$ represents the mean of actual observed settlement for the k th case history and δ_a represents the coefficient of variation (COV) of S_a . This δ_a is given as:

$$\delta_a = \frac{(\mu_M^2 \sigma_p^2 + \mu_p^2 \sigma_M^2 + \sigma_M^2 \sigma_p^2)^{0.5}}{\mu_M^2 \mu_p^2} = (\delta_p^2 + \delta_M^2 + \delta_p^2 \delta_M^2)^{0.5} \quad (45)$$

where μ_M is the mean of M , σ_M is the standard deviation of M , μ_p is the mean of the predicted settlement, and σ_p is the standard deviation of the predicted settlement. For the re-regression, all of the variables with a ‘‘p’’ term were removed to remove the assumption of non-liquefied layers adding to settlement hazard. The δ_a term was simplified to:

$$\delta_a = \frac{\sigma_M}{\mu_M} = \delta_M \quad (46)$$

This simplified δ_a replaced equation (45). The new M and $\sigma_{\ln(S)}$ values were calculated by using Juang et al. (2013) maximum likelihood equation (42), but by replacing Equation (45) with Equation (46) and only using the m case histories.

2.3.3 Performance-Based Liquefaction-Induced Settlement Procedure

After the PBEE liquefaction triggering assessment is completed, a PBEE post-liquefaction analysis can be performed. PBEE liquefaction-induced settlements are calculated by using the developed FS_L hazard curves, described above. The intensity measure is FS_L , which is used to calculate mean annual rate of exceedance of volumetric strain, the engineering demand parameter. The modified equation is given as:

$$\lambda_{\varepsilon_v^*} = \sum_{j=1}^{N_{FS_L}} P[\bar{\varepsilon}_v > \varepsilon_v^* | q_{c1Ncsi}, FS_{Lj}] \Delta\lambda_{FS_{Lj}} \quad (47)$$

where $\lambda_{\varepsilon_v^*}$ is the mean annual rate of exceeding a specified level of strain (ε_v^*), N_{FS_L} is the number of FS_L increments within the current soil layer's FS_L hazard space, q_{c1Ncsi} is the current layer's corrected cone tip resistance, $\Delta\lambda_{FS_{Lj}}$ is the incremental mean annual rate of exceedance for intensity measure FS_L , and $P[\varepsilon_v > \varepsilon_v^* | q_{c1Ncsi}, FS_{Lj}]$ represents the probability the calculated strain will exceed a specified level of strain (ε_v^*) given a specific incremental value from the FS_L hazard curve. The equation to calculate $P[\bar{\varepsilon}_v > \varepsilon_v^* | q_{c1Ncsi}, FS_{Lj}]$ is given as:

$$P[\bar{\varepsilon}_v > \varepsilon_v^* | q_{c1Ncsi}, FS_{Lj}] = \Phi \left[\frac{\ln(\bar{\varepsilon}_v) - \ln(\varepsilon_v^*)}{\sigma_{\ln(\varepsilon_v)}} \right] \quad (48)$$

where $\bar{\varepsilon}_v$ is the calculated strain using the Juang et al. (2013) strain equation (Equation (40)) multiplied by P_L (Equation (41)), $\sigma_{\ln(\varepsilon_v)}$ is taken to equal $\sigma_{\ln(s)}$ from Equation (41). $\sigma_{\ln(\varepsilon_v)}$ can be assumed to equal $\sigma_{\ln(s)}$ because settlement is computed as a simple additive function of ε_v . The $P[\varepsilon_v > \varepsilon_v^* | q_{c1Ncsi}, FS_{Lj}]$ values are computed for all of the incremental FS_L values. These probabilities are then summed to calculate the total mean annual rate of exceedance of that specific ε_v^* value.

The calculated strain ($\bar{\varepsilon}_v$) is compared to the incremental ε_v^* value. Equation (47) is repeated for a range of ε_v^* values (0-20%), to account for all possible values of strain. All of the calculated $\lambda_{\varepsilon_v^*}$ values, with the corresponding ε_v^* values, develop a hazard curve for one soil layer (Figure 2-10). This process is repeated for each soil layer to develop a strain hazard curve for each individual soil layer.

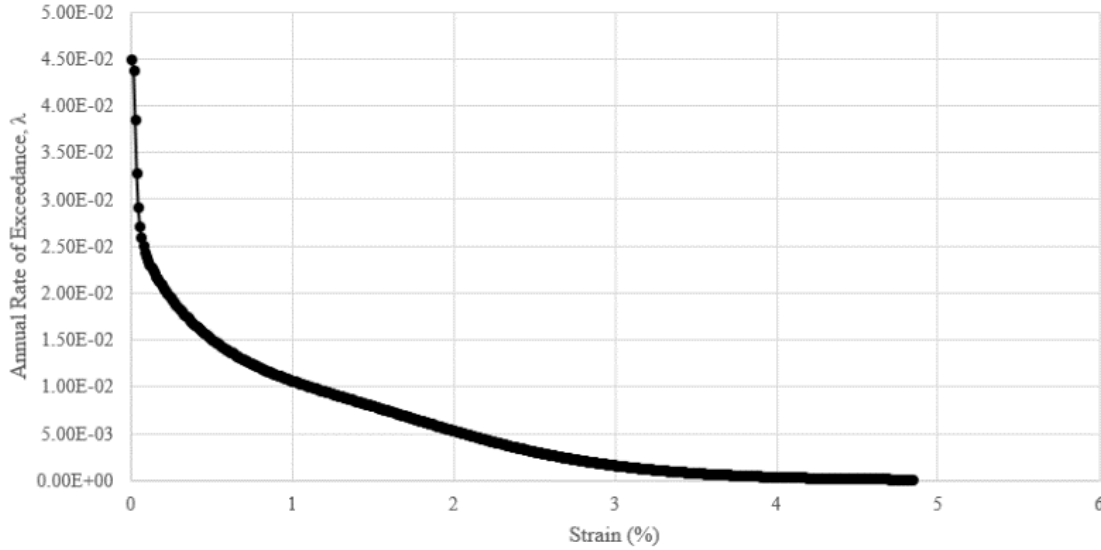


Figure 2-10: Example of a strain hazard curve from one specific soil layer.

After strain hazard curves are developed for each soil layer, settlement is calculated. A hazard curve of total ground surface settlement is developed, by using each strain hazard curve from each layer. This calculation is done by using Equation (39), from the Juang et al. (2013) procedure:

$$S_p = M \sum_{i=1}^N \varepsilon_v \Delta Z_i \quad (49)$$

where ε_v is a strain value obtained from each strain hazard curve at the return period of interest from every soil layer. The strains from each soil layer are summed together and multiplied by the layer thickness to calculate ground surface settlement. This process is repeated for a range of mean annual rate of exceedances, corresponding to return periods from 475 years to 10,000 years, to develop a total settlement hazard curve (Figure 2-11).

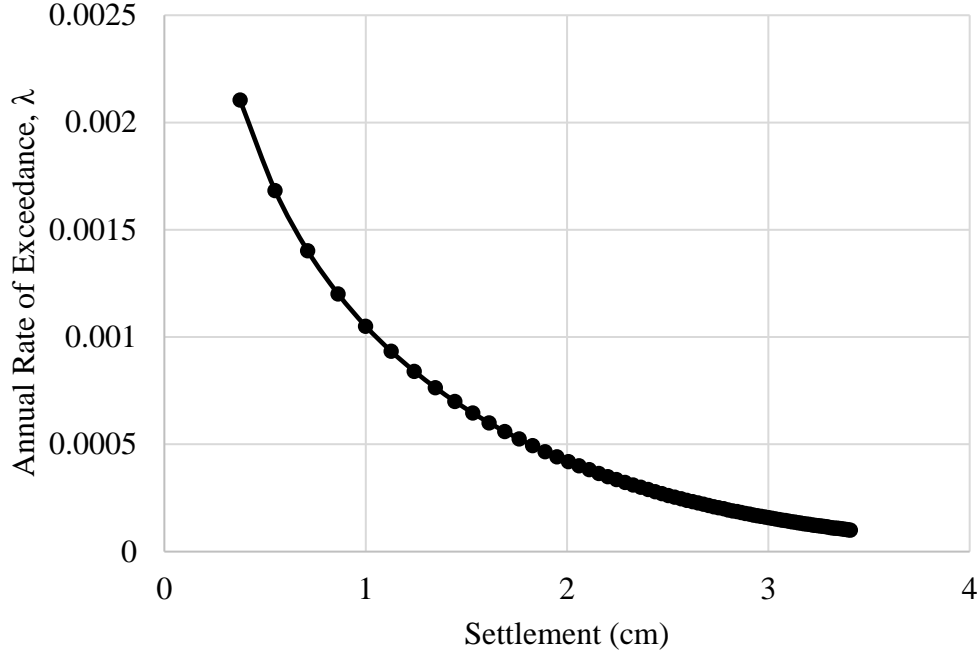


Figure 2-11: Example of a total ground settlement hazard curve.

2.3.4 Correction Factor for Unrealistic Strain Values

Huang (2008) developed a method to limit unrealistically high vertical strain values computed in probabilistic calculations. Kramer et al. (2008) explained that direct computation of probabilistic vertical strains has been found to produce significant unrealistically high probabilities of very large strain values. Kramer et al. (2008) explains these unrealistically high strain estimations are due to the assumption of lognormal probability distributions typically associated with the calculation of vertical strains. For low soil stiffness values, the slope of the lognormal probability density function increases infinitely, appropriately allowing large probabilities to be associated with large strains. Denser soils, however, can still predict large probabilities of vertical strain, even though both laboratory and field observations have shown that large vertical strains with such soils are very unlikely.

Huang (2008) performed a study to find the maximum limited strain for different types of soil. Huang evaluated theoretical, historical (i.e., field), and laboratory evidence of a maximum vertical strain experienced by a given soil layer. He relied heavily on the apparent limiting strain observed by four previous studies: Tokimatsu and Seed (1987), Ishihara and Yoshimine (1992), Shamoto et al.(1998), and Wu and Seed (2004), to develop estimates of the maximum or limiting vertical strain as a function of SPT blow counts. The Huang (2008) and Kramer et al. (2008) maximum vertical strain curves are shown in Figure 2-12.

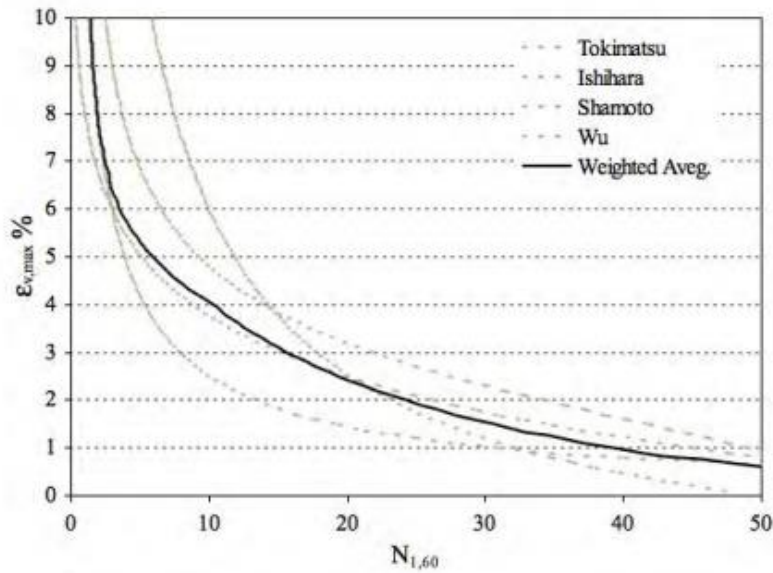


Figure 2-12: Maximum vertical strain levels inferred by deterministic vertical strain models and weighted average used to define mean value (after Huang, 2008).

Kramer et al. (2014) approximated the weighted average relationship by using the following equation.

$$\varepsilon_{v,max}(\%) = 9.765 - 2.427 \ln[(N_1)_{60,cs}] \quad (50)$$

Equation (50) was used to develop a limiting volumetric strain. Huang (2008) suggests using an $\varepsilon_{v,max}$ range of $0.5 \cdot \varepsilon_{v,max}$ to $1.5 \cdot \varepsilon_{v,max}$ with a uniform probability distribution to account for scatter in the data. Finally, to apply Equation (50) to CPT data, Jefferies and Davies (1993) was used to

convert between CPT tip resistance and SPT blow count values. Jefferies and Davies (1993) developed this CPT-SPT relationship as:

$$\frac{(q_t/p_a)}{(N_1)_{60,cs}} = 8.5 \left(1 - \frac{I_c}{4.6}\right) \quad (51)$$

where p_a is atmospheric pressure, I_c is the Soil Behavior Type Index, and q_t is the normalized CPT tip resistance. This approach has been implemented into *CPTLiquefY* to account for unrealistic strain values. Substituting Equation (51) into Equation (50), a CPT-based equation for the maximum volumetric strain is given as:

$$\varepsilon_{v,max} (\%) = 9.765 - 2.427 \ln \left[\frac{(q_t/p_a)}{8.5 \left(1 - \frac{I_c}{4.6}\right)} \right] \quad (52)$$

2.4 Lateral Spread Displacement Evaluation

This section will provide the necessary background to understand the lateral displacement procedure. A brief discussion regarding the Zhang et al. (2004) model will be provided, followed by a discussion of performance-based implementation of this model. The term lateral spread displacement describes the horizontal deformations of a site located on sloping ground or near a free-face due to seismically induced soil liquefaction. These deformations can range from a few millimeters to several meters. Structures near open bodies of water are particularly at risk to this seismic hazard.

2.4.1 Lateral Spread Displacement Empirical Model

The lateral spread displacement procedure presented by Zhang et al. (2004) demonstrates a calculation of the lateral displacement caused by each soil increment in a CPT sounding. In this procedure, $(q_{c1N})_{cs}$ from Robertson and Wride (1998, 2009) is used to calculate the relative density, D_R , following Tatsuoka et al. (1990). Lateral spread is directly related to the maximum horizontal

cyclic shear strain, γ_{max} , and the relationship between γ_{max} , D_R , and FS_L , as presented by Zhang et al. (2004) is displayed in Figure 2-13.

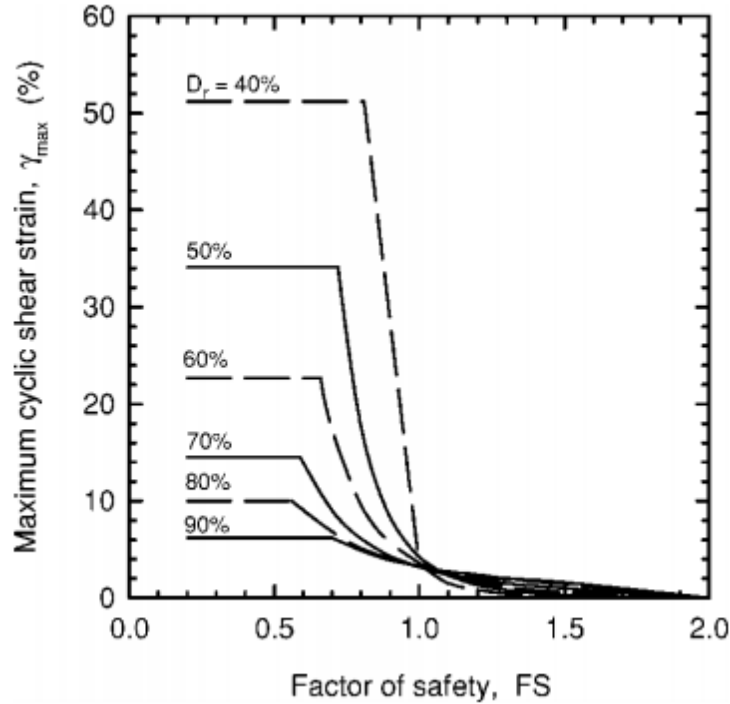


Figure 2-13: The relationship between γ_{max} , D_R , and FS_L as presented by Zhang et al. (2004).

With γ_{max} known for each increment of the CPT sounding, the lateral displacement index, LDI , can be determined using the following relationship:

$$LDI = \int_0^{z_{max}} \gamma_{max} dz \quad (53)$$

which shows LDI as the integral of γ_{max} , increasing from the smallest value at z_{max} (the deepest liquefiable layer) to the highest value at the ground surface. With a known LDI , the actual lateral displacement, LD (also known as the horizontal displacement, D_H) which is the amount of displacement or spread seen at the ground surface, can be calculated as a function of the site's geometry. LD is dependent upon three variables (other than LDI): the ground slope, S , the free

face height H , and the distance from toe of the free face, L . The three cases for site geometry are seen in Figure 2-14.

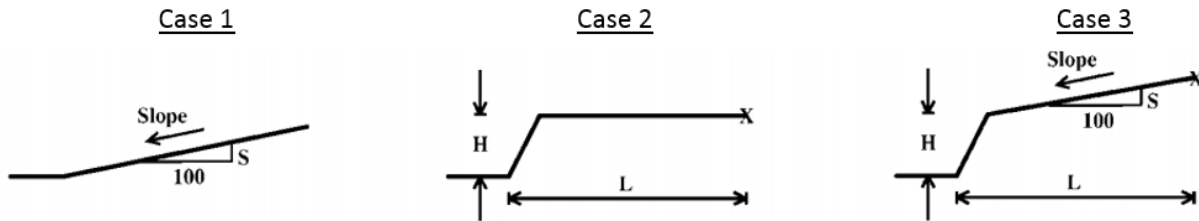


Figure 2-14: The three cases for site geometry when determining lateral displacement.

LD is then determined using one of two equations. Case 1 uses Equation (54) and Case 2 uses Equation (55). Referring to sites with a geometry as found in Case 3, Zhang et al. (2004) states that the data points for the case histories for a gently sloping ground with free face (Case 3) lie generally within the scatter of results for nearly level ground with a free face (Case 2). Therefore, sites with a geometry as found in Case 3 will also use Equation (55).

$$LD = (S + 0.2) \cdot LDI \quad (54)$$

$$LD = 6(L/H)^{-0.8} \cdot LDI \quad (55)$$

2.4.2 Performance-Based Lateral Spread Displacement Procedure

After the PBEE liquefaction triggering assessment is completed, a PBEE analysis of liquefaction-induced lateral spread displacement can be performed. The following steps are very similar to those demonstrated in the section on PBEE settlement, discussed previously. PBEE lateral spread displacements are calculated by using the FS_L hazard curves. The intensity measure is FS_L , which is used to calculate the mean annual rate of exceedance maximum cyclic shear strain, the engineering demand parameter. The modified equation is given as:

$$\lambda_{\gamma_{max}^*} = \sum_{j=1}^{N_{FSL}} P[\overline{\gamma_{max}} > \gamma_{max}^* | q_{c1Ncsi}, FS_{Lj}] \Delta\lambda_{FS_{Lj}} \quad (56)$$

where $\lambda_{\gamma_{max}^*}$ is the mean annual rate of exceeding a specified level of the maximum cyclic shear strain (γ_{max}^*), N_{FSL} is the number of FS_L increments in the soil layer's FS_L hazard space, q_{c1Ncsi} is the soil layer's corrected cone tip resistance, $\Delta\lambda_{FS_{Lj}}$ is the incremental mean annual rate of exceedance for FS_L , and $P[\overline{\gamma_{max}} > \gamma_{max}^* | q_{c1Ncsi}, FS_{Lj}]$ represents the probability the calculated maximum cyclic shear strain will exceed a specified level of that strain (γ_{max}^*) given a specific incremental value from the FS_L hazard curve. To then calculate $P[\overline{\gamma_{max}} > \gamma_{max}^* | q_{c1Ncsi}, FS_{Lj}]$ the following equation is used:

$$P[\overline{\gamma_{max}} > \gamma_{max}^* | q_{c1Ncsi}, FS_{Lj}] = \Phi \left[\frac{\ln(\overline{\gamma_{max}}) - \ln(\gamma_{max}^*)}{\sigma_{\ln(\gamma_{max})}} \right] \quad (57)$$

where $\overline{\gamma_{max}}$ is the calculated maximum cyclic shear strain (as determined by Zhang et al. (2004)) multiplied by P_L , and $\sigma_{\ln(\gamma_{max})}$ is the standard deviation derived from the case histories used to from the Zhang et al. (2004) semi-empirical model (with a single standard deviation for each of the three types of site geometry). While the standard deviation was derived using values of displacement, it is considered acceptable to apply this standard deviation to strain values as there is a direct correlation between strain and displacement.

Equation (56) is repeated for a wide range of γ_{max}^* , (0-60%) accounting for all possible values of maximum cyclic shear strain. With $P[\overline{\gamma_{max}} > \gamma_{max}^* | q_{c1Ncsi}, FS_{Lj}]$ calculated, $\lambda_{\gamma_{max}^*}$ can then be calculated for a corresponding γ_{max}^* , which then can be used to develop a hazard curve for each soil layer, as was done in the settlement analysis. An example of a hazard curve for a single soil layer is seen in Figure 2-15.

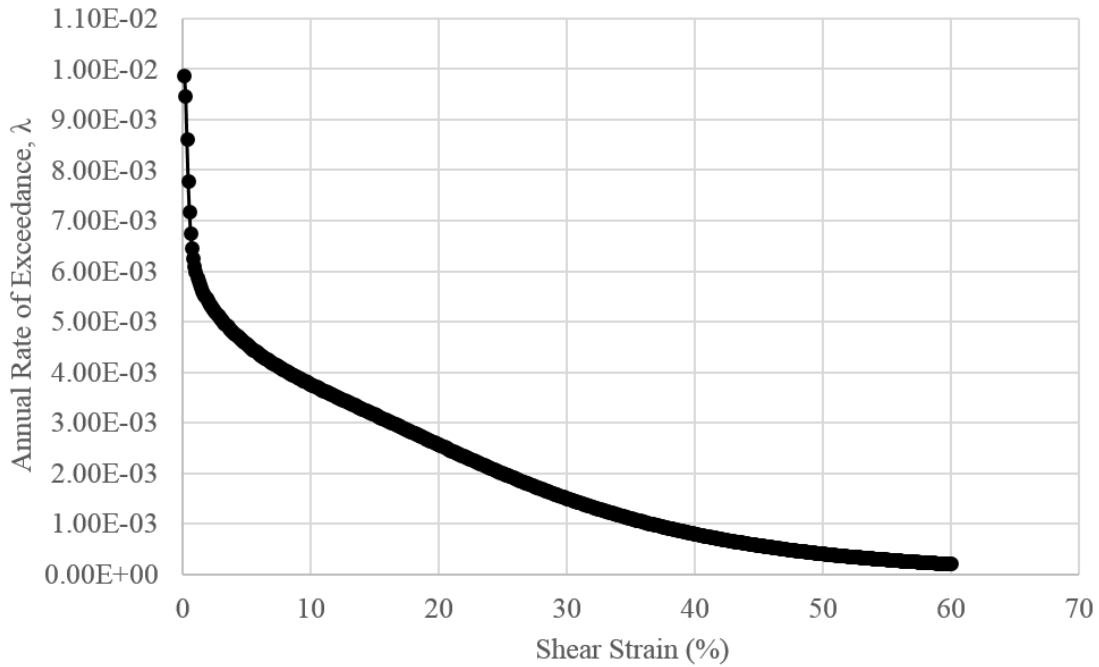


Figure 2-15: Example of a shear strain hazard curve for a single soil layer.

Once the hazard curves for each soil layer are made, a hazard curve for total lateral spread displacement can be created. The Zhang et al. (2004) procedure is used to calculate the lateral spread displacement. The input strain values for this procedure corresponding to a single annual rate of exceedance are taken from each individual layer hazard curves, and used to calculate the lateral spread displacement for that one annual rate of exceedance. This process is repeated for a range of mean annual rate of exceedances, corresponding to return periods from 475 years to 10,000 years, to develop a total lateral spread displacement hazard curve. An example of a hazard curve for total lateral spread displacement is seen in Figure 2-16.

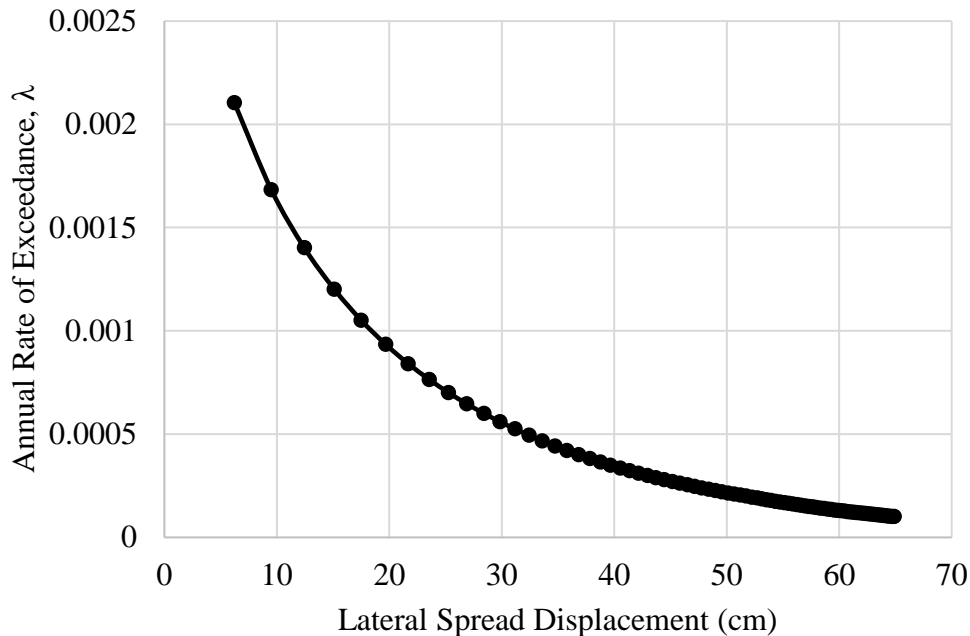


Figure 2-16 Example of a total lateral spread displacement hazard curve.

2.5 Pseudo-Probabilistic Liquefaction Hazard Analysis Method

The pseudo-probabilistic method is currently one of the most commonly used liquefaction hazard analysis methods. This approach involves selecting design ground motions through probabilistic methods and applying them to a deterministic calculation of earthquake effects. This procedure involves using a deterministic triggering procedure (sections 2.2.1, 2.2.2, and 2.2.4) to calculate FS_L , but by using a probabilistic seismic hazard analysis (PSHA) to select input ground motions. This PSHA selection of ground motions is performed by using the USGS deaggregation tool to select a design earthquake magnitude (the USGS tool is located at <https://earthquake.usgs.gov/hazards/interactive/>). This magnitude can be either the mean (i.e., average) or modal (i.e., occurring the most often) magnitude for the specific location. The FS_L and $Q_{m,cs}$, from the triggering procedures, are then applied to the deterministic post-liquefaction settlement and lateral spread procedures.

Even though the pseudo-probabilistic approach accounts for some uncertainty in ground motions, inherent uncertainty within the triggering of liquefaction and the calculation of its effects

are generally ignored. Furthermore, the approach assumes that all liquefaction hazard is caused by a single return period of ground motions. Therefore, a common misperception of the pseudo-probabilistic approach is that the return period of the computed post-liquefaction settlements is the same as the return period of the input ground motions. This perception would only be true if there was no uncertainty associated with the computation of settlements.

2.6 Semi-Probabilistic Liquefaction Hazard Analysis Method

The semi-probabilistic liquefaction hazard approach is fairly new and not yet commonly used. However, it is starting to gain popularity. Semi-probabilistic methods calculate FS_L using the fully-probabilistic methods (i.e., PBEE), described in section 2.2.5, and applies this FS_L to deterministic settlement calculations. This method accounts for the inherent uncertainty in predicting liquefaction triggering and correctly computes the return period of soil liquefaction. However, this method fails to account for the uncertainty in calculating liquefaction effects, such as settlement and lateral spread.

3.0 CPTLiquefY

3.1 Overview

CPTLiquefY has the ability to perform liquefaction hazard analyses based on CPT soundings. In the previous SPT work, *PBLiquefY* was built within the framework of Microsoft Excel, using its own functionality as well as programming in Visual Basic (VBA), however *CPTLiquefY* has been coded in Microsoft Visual Studio using C++. While VBA worked well for *PBLiquefY*, it would not work well for *CPTLiquefY* because of VBA's inability to effectively handle heavy amounts of data calculations. VBA worked well for *PBLiquefY* because a SPT data set is limited to about 15-25 depth measurements per location. CPT data sets, however, are several times larger with about 100-300 depth measurements per location, which leads to an exponential increase in the amount of required calculations. For this reason, it was decided that a more efficient program be developed for the CPT analysis. *CPTLiquefY* is built through Microsoft Visual Studio, an Integrated Development Environment (IDE) for various programming languages. Visual C++ was chosen as the programming language for the speed and rigor C++ provides, as well as the useful Graphical User Interface (GUI) Visual C++ contributes to C++. The opening view of *CPTLiquefY* can be viewed in Figure 3-1.

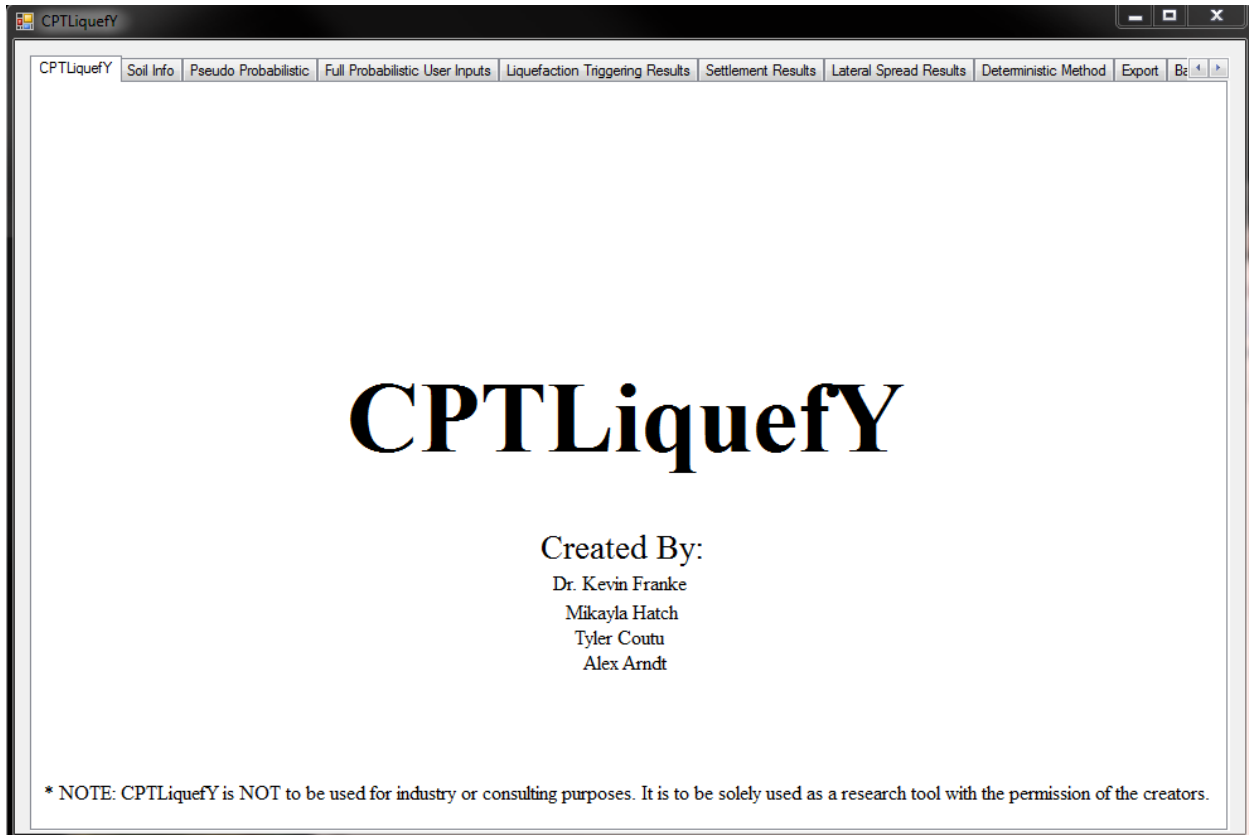


Figure 3-1: Opening view of *CPTLiquefY*.

3.2 Walk Through of *CPTLiquefY*

3.2.1 Soil Info Tab

When *CPTLiquefY* is launched, the view in Figure 3-1 is visible to the user. As seen, there are tabs for Soil Info, Pseudo-Probabilistic, Full-Probabilistic User Inputs, Liquefaction Triggering Results, Settlement Results, Lateral Spread Results, Export, and Batch Run. To start a liquefaction hazard analysis the user will select the “Soil Info” tab, as shown in Figure 3-2.

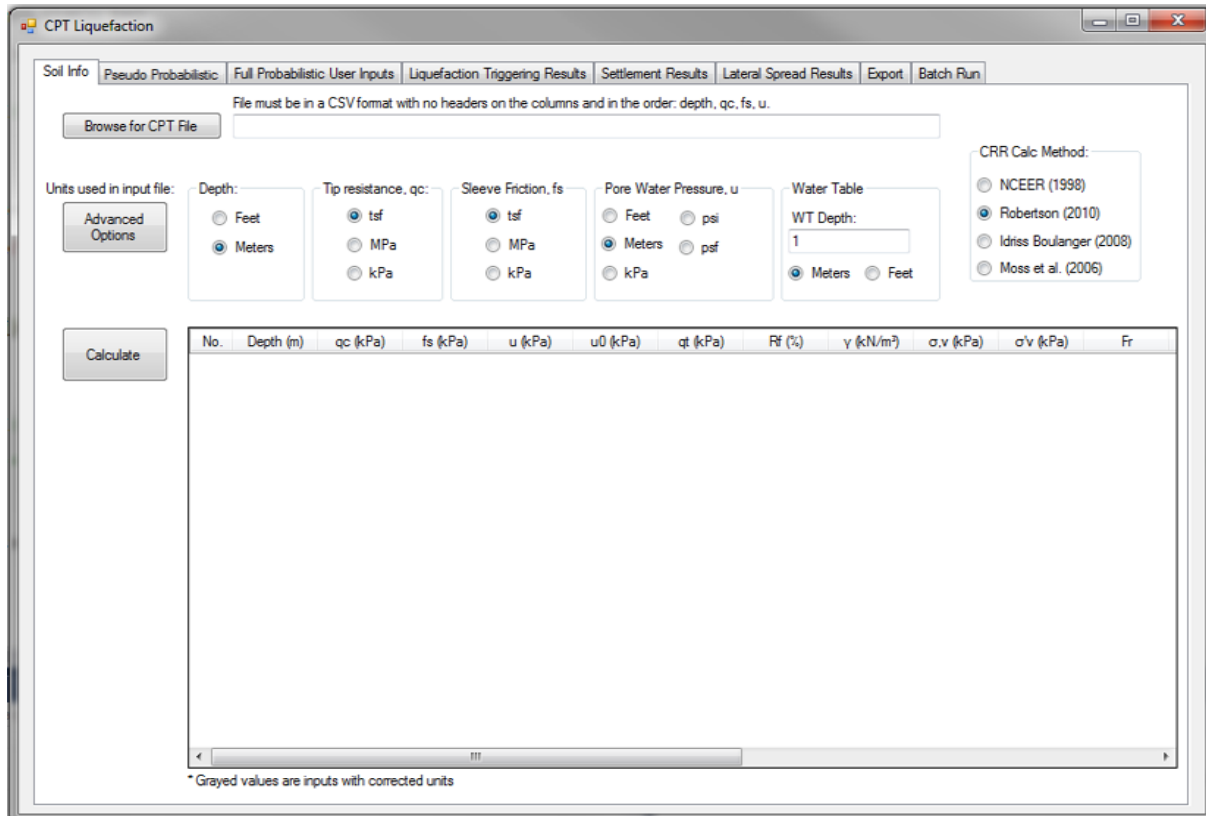


Figure 3-2: Initial view of *CPTLiquefy*, showing the Soil Info tab.

Once the user starts the program, the program will open to Soil Info tab as shown above (Figure 3-2). To upload a specific CPT sounding, the “Browse for CPT File” button is clicked and users are able to browse for a CSV file with CPT data (depth, q_c , f_s , and u). The user can then select the input units, which will then be converted into uniform metric units for ease of calculation. An estimate of the depth of the water table is also needed from the user to be used in the calculation of effective stress, σ'_v and each layer’s susceptibility to liquefaction. Once all user inputs are complete, the calculation of the CRR can be performed. Once the user has selected the “Calculate” button calculations will be performed through the CRR calculation. When the CRR calculation is complete, the table is populated and the preliminary calculations are seen, up to the CRR. This can be seen in Figure 3-3.

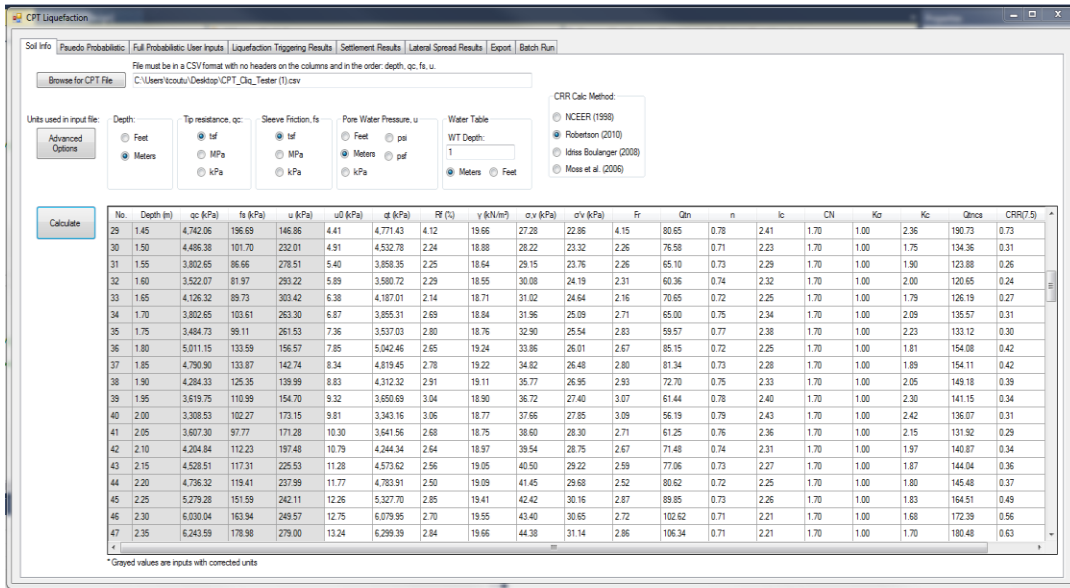


Figure 3-3: View after running calculations on Soil Info tab in *CPTLiquefy*.

To be able to run unique analyses, an Advanced Option section was created to allow for adjustments to the default values. To access the Advanced Options section, the user clicks the “Advanced Options” button on the Soil Info tab. When the Advanced Options window is opened, the user will see the dialog box shown in Figure 3-4, which currently displays the default values.

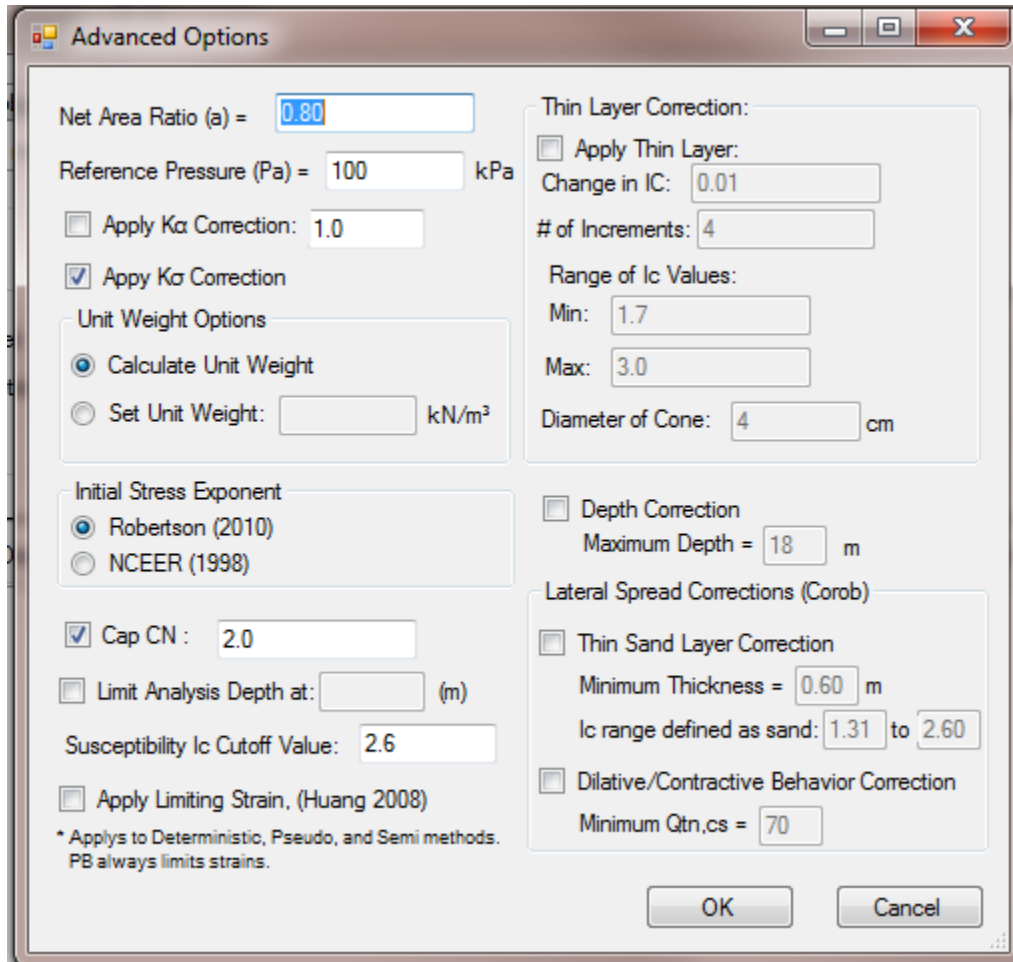


Figure 3-4: Display of the Advanced Options dialog box in CPTLiquefy.

There are many variables, methods, and options that can be adjusted in the Advanced Options window. The net area ratio (a) is a function of the geometry of the probe itself, and is used in determining the corrected cone tip resistance (q_t). The reference pressure (P_a) is used in the Robertson (2009) procedure in correcting the cone tip resistance for overburden stress (Q_m). K_a is the initial shear stress correction factor and K_σ is the overburden stress correction factor. Since the unit weight is unknown, it is either set at a constant unit weight, or it can be estimated using a correlation from the cone time resistance and sleeve friction Robertson and Cabal (2010). C_N , the overburden correction factor can be seen in the procedure for Robertson (2009), it is recommended to be limited to either 2.0 or 1.7, depending on which procedure is being run. Similarly, it is recommended that the soil behavior type index, I_c , be limited to approximately 2.6 (after an I_c

value of 2.6 the soil is classified as a clay and is much less likely to experience liquefaction). Also, an option is available to limit the depth at which the liquefaction analysis calculations are made. Ahmadi and Robertson (2005) discusses the need to account for thin-layer and transition zone effects on CPT q_c measurement. Following Robertson (2011), *CPTLiquefY* is able to make adjustments for these thin layers which can affect the accuracy of the CPT data.

3.2.2 Pseudo-Probabilistic Tab

CPTLiquefY has the ability to run a pseudo-probabilistic analysis by navigating to the “Pseudo-Probabilistic” tab. By inputting the location (latitude and longitude), the probability of exceedance, the USGS year, and whether to use the mean or modal magnitude, the deaggregation can be run. The user can then select to run either or both models to calculate a pseudo-probabilistic FS_L . The models include the Robertson and Wride (1998, 2009) and the Boulanger and Idriss (2014) methods. A description of each model can be found previously in Section 2.

An amplification factor (Fa) must also be calculated to convert the peak ground acceleration (PGA) value, from USGS, into an a_{max} value for calculations. This can be done by entering a specific Fa , using the AASHTO/ASCE 7-10 method and selecting a site class, using the Stewart et al. (2003) method and selecting a site class, or it can be done using Stewart et al. (2003) with site specific values. A display of the Pseudo Probabilistic tab can be seen in Figure 3-5.

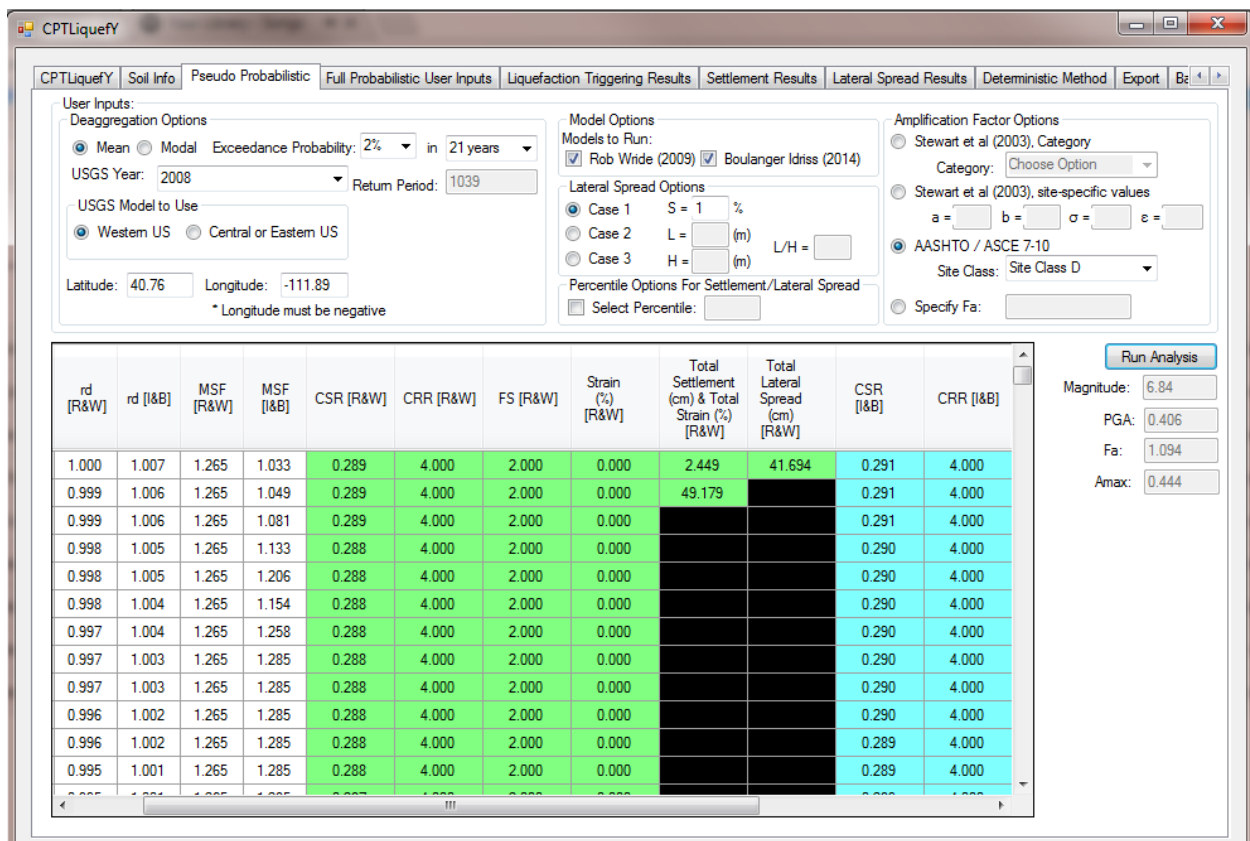


Figure 3-5: View of Pseudo Probabilistic tab once calculations are complete.

3.2.3 Full Probabilistic User Inputs Tab

CPTLiquefy contains the ability to perform full-probabilistic analysis of liquefaction triggering. This allows the user to do a PBEE liquefaction hazard analysis while considering data from a CPT. To perform this analysis the user must complete the inputs on both the “Soil Info” and “Pseudo-Probabilistic” tabs. The user can then go to the “Full Probabilistic User Inputs” tab and select “Load Seismic Data”. This will load information from the new USGS uniform hazard deaggregation tool that will allow the user to perform a full-probabilistic analysis by developing a_{max} hazard curves for the site (Figure 3-6). Once the green bar above the “Load Seismic Data” button is full, then the user can press the “Run Analysis” to begin this process. Once the lower green loading bar is full, the analysis is complete and the results are plotted in the “Liquefaction Triggering Results” tab.

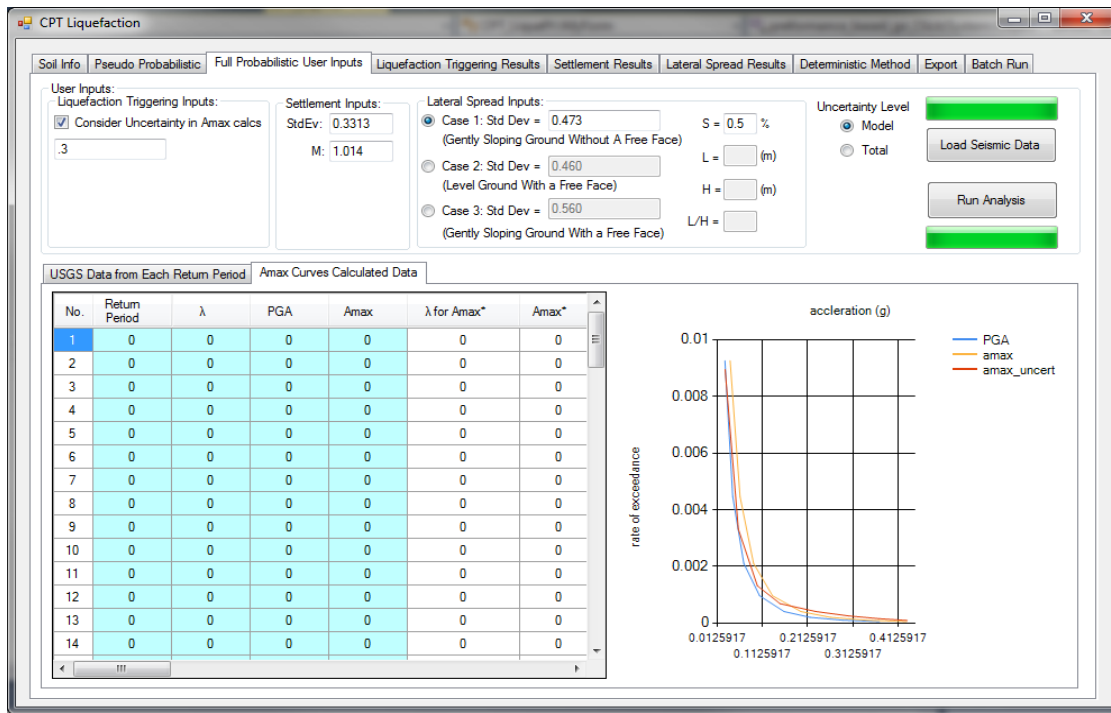


Figure 3-6: View of *CPTLiquefy*, showing the completed deaggregation analysis and development of amax hazard curves after selecting “Load Seismic Data”.

3.2.4 Liquefaction Triggering Results Tab

At the completion of the analysis, the user may navigate to the “Liquefaction Triggering Results” tab, as shown in Figure 3-7. Each layer of the CPT profile that has been analyzed will have a distinct liquefaction triggering hazard curve calculated using both Boulanger and Idriss (2014) and Ku et al. (2012) (i.e., Robertson and Wride, 1998) methods. The user may enter in a specific layer into the “Enter Layer Number” textbox to view that layer’s hazard curve, as seen in Figure 3-7. All data is easily copied and pasted into Microsoft Excel for additional plotting options. The “Export” tab also contains options for easily saving all calculated data into a tabulated format. An example of a completed liquefaction triggering hazard curve for a single soil layer is shown in Figure 3-8. For any return period of interest, the user can use this plot to estimate the performance-based factor of safety against liquefaction of the specific layer analyzed.

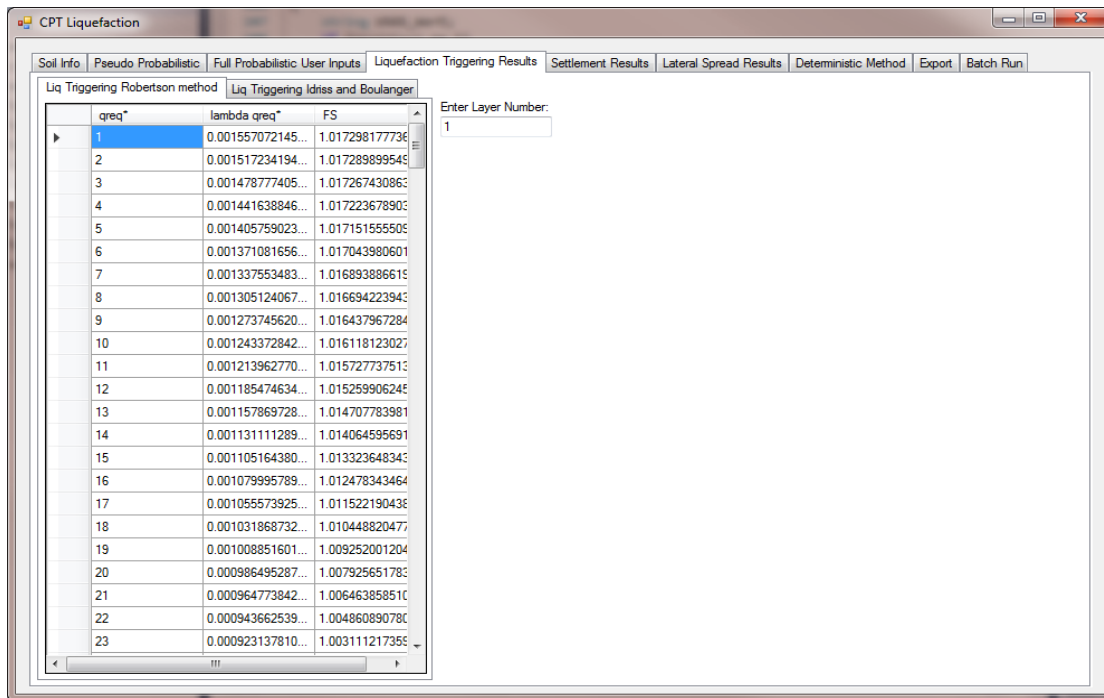


Figure 3-7: View of “Liquefaction Triggering Results” tab after analysis.

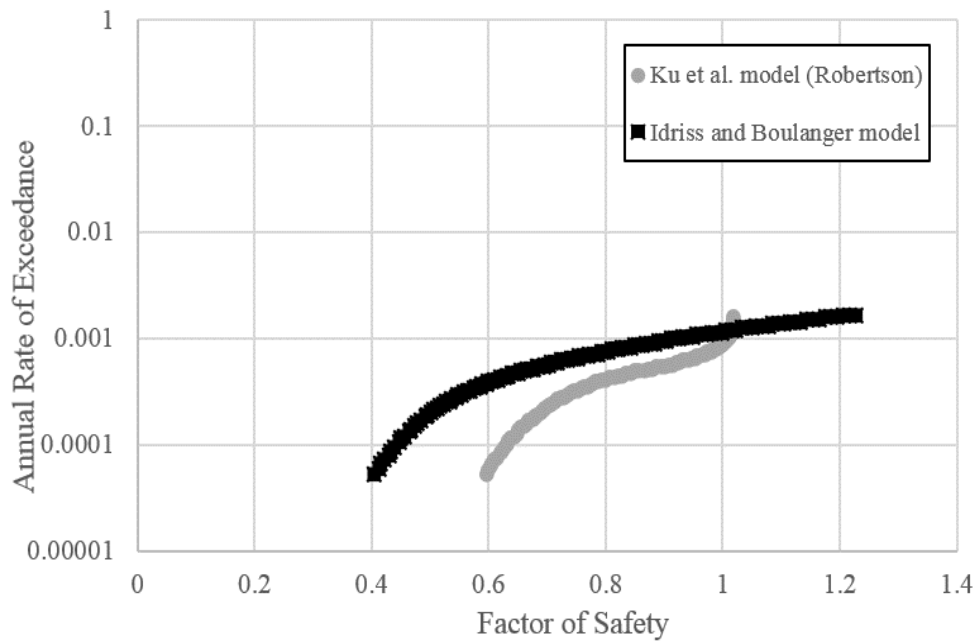


Figure 3-8: Example plot from “Liquefaction Triggering Results” tab.

3.2.5 Settlement Results Tab

After running the performance-based liquefaction triggering analysis, the user may navigate to the “Settlement Results” tab to view the free-field settlement results (Figure 3-9). This initial view contains the data for the PBEE total settlement hazard curve and the hazard curve for semi-probabilistic settlement. Examples of these hazard curves are shown in Figure 3-10.

Exceedance Rate	Return Period	Robertson Total Ground Settlement (cm)	Total Strain (%) Robertson	Idriss Total Ground Settlement (cm)	Total Strain (%) I&B	Total Ground Settlement (cm) Semi-Prob (Robertson)	Total Strain Semi-Prob (%) Robertson	Total Ground Settlement (cm) Semi-Prob (I&B)	Total Strain Semi-Prob (%) I&B
0.01	100.00	0.0000	0.0000	0.0000	0.0000	1.87594	37.67570	2.33156	46.82638
0.004484304...	223.00	0.0947	1.8752	0.2155	4.2687	2.31545	46.50275	2.81383	56.51213
0.002890173...	346.00	0.4418	8.7501	0.9479	18.7751	2.69254	54.07610	3.09179	62.09447
0.002132196...	469.00	0.7683	15.2164	1.5582	30.8629	2.99917	60.23444	3.25034	65.27877
0.001689189...	592.00	1.0534	20.8642	2.0380	40.3655	3.27114	65.69648	3.37862	67.85506
0.001398601...	715.00	1.3019	25.7861	2.3921	47.3786	3.50241	70.34135	3.49507	70.19385
0.001193317...	838.00	1.5188	30.0819	2.6624	52.7318	3.69129	74.13463	3.65711	73.44822
0.001040582...	961.00	1.7083	33.8345	2.8854	57.1494	3.79652	76.24814	3.78273	75.97109
0.000922509...	1,084.00	1.8724	37.0845	3.0833	61.0687	3.88868	78.09911	3.88116	77.94795
0.000828500...	1,207.00	2.0164	39.9371	3.2605	64.5780	3.97420	79.81650	3.97597	79.85206
0.000751879...	1,330.00	2.1414	42.4139	3.4206	67.7501	4.03059	80.94914	4.06342	81.60844
0.000688231...	1,453.00	2.2508	44.5809	3.5656	70.6226	4.09035	82.14932	4.15012	83.34961
0.000634517...	1,576.00	2.3487	46.5197	3.6981	73.2465	4.15127	83.37283	4.22525	84.85865
0.000588581...	1,699.00	2.4360	48.2490	3.8195	75.6503	4.19903	84.33198	4.29934	86.34660
0.000548847...	1,822.00	2.5162	49.8360	3.9317	77.8730	4.24011	85.15703	4.34369	87.23735
0.000514138...	1,945.00	2.5885	51.2679	4.0363	79.9448	4.28122	85.98260	4.42008	88.77152
0.000483558...	2,068.00	2.6554	52.5934	4.1339	81.8779	4.32254	86.81243	4.46647	89.70326
0.000456412...	2,191.00	2.7173	53.8200	4.2251	83.6849	4.35716	87.50773	4.50480	90.47302
0.000432152...	2,314.00	2.7749	54.9604	4.3107	85.3789	4.38072	87.98105	4.56004	91.58230
0.000410340...	2,437.00	2.8283	56.0184	4.3908	86.9655	4.41440	88.65749	4.59832	92.35122

Figure 3-9: View of “Settlement Results” tab after analysis is complete.

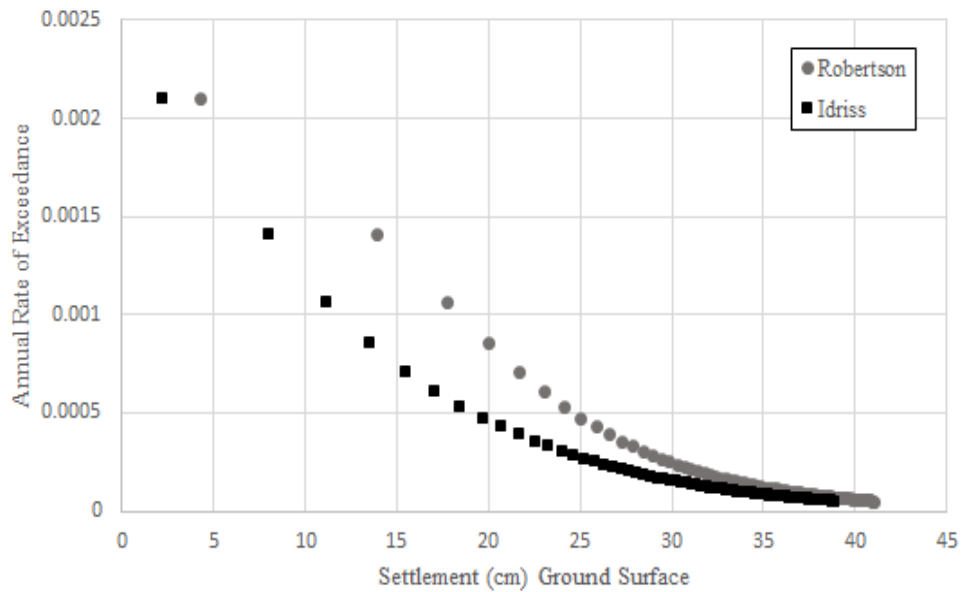


Figure 3-10: View of hazard curves for total ground surface settlement.

If the user selects the “Strain Hazard Curves by Layer” the data for each layer’s strain hazard curve is shown. The user may view a specific soil layer’s strain hazard curve by entering in the layer number they would like to view, as shown in Figure 3-11.

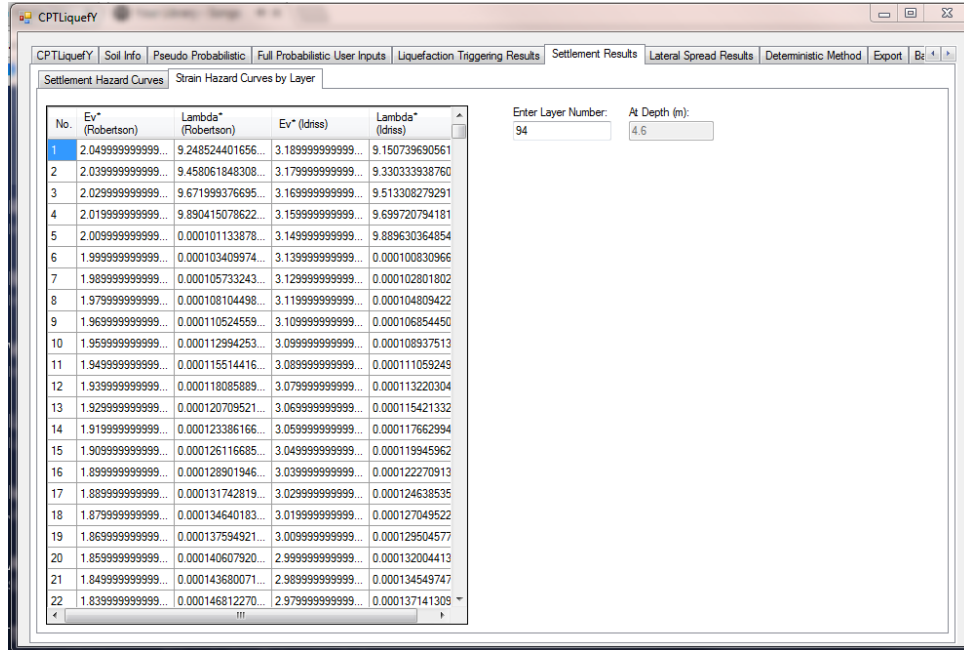


Figure 3-11: Strain hazard curve data for soil layer 94, corresponding to a depth of 4.6m.

3.2.6 Lateral Spread Results Tab

Similar to the “Settlement Results” tab, once the full performance-based liquefaction triggering analysis is complete, the user may navigate to the “Lateral Spread Results” tab to see performance-based results of lateral spread displacement. This tab is shown in Figure 3-12. This initial view contains the data for the PBEE total lateral spread displacement hazard curve and the hazard curve for semi-probabilistic lateral spread displacement. If the user selects the “Horizontal Strain Hazard Curves by Layer” the data for each layer’s strain hazard curve is shown. The user may view a specific soil layer’s strain hazard curve by entering in the layer number they would like to view.

Exceedance Rate	Return Period	Robertson Total Lateral Spread (cm)	Idriss Total Lateral Spread (cm)	Robertson Total Lateral Spread (cm) (Semi-Prob)	Idriss Total Lateral Spread (cm) (Semi-Prob)
0.01	100.00	0.33830	0.00000	203.75684	306.28233
0.004484304932...	223.00	52.85976	68.21495	224.39341	318.79257
0.002890173410...	346.00	115.89755	186.45275	236.29417	323.44794
0.002132196162...	469.00	160.08214	255.80914	244.89752	326.24740
0.001689189189...	592.00	192.43166	302.21484	251.04755	327.57359
0.001398601398...	715.00	214.28383	333.22742	256.85255	328.32257
0.001193317422...	838.00	229.85576	351.57097	260.33409	329.11047
0.001040582726...	961.00	241.86723	362.24188	262.46866	329.36705
0.000922509225...	1,084.00	251.40422	370.19622	264.27877	329.88008
0.000828500414...	1,207.00	259.46818	376.70844	265.56992	330.16329
0.000751879699...	1,330.00	266.24377	382.18839	266.78869	330.65910
0.000688231245...	1,453.00	272.07214	386.89910	267.75252	330.82191
0.000634517766...	1,576.00	277.03151	390.80832	268.49437	330.91040
0.000588581518...	1,699.00	281.20176	394.14500	269.31348	330.98541
0.000548847420...	1,822.00	284.81074	397.16383	270.04831	330.94302
0.000514138817...	1,945.00	288.03298	399.78523	270.75043	331.08837
0.000483558994...	2,068.00	290.78372	402.20123	271.54599	331.24618
0.000456412596...	2,191.00	293.27479	404.42634	271.80852	331.16794
0.000432152117...	2,314.00	295.53434	406.52295	272.54045	331.35046
0.000410340582...	2,437.00	297.65385	408.50391	272.92010	331.40095
0.000390625	2,560.00	299.66100	410.35265	273.56554	331.48676

Figure 3-12: View of “Lateral Spread Results” tab after analysis.

3.3 Inclusion of New USGS Deaggregation Tool

Coinciding with the release of the 2014 deaggregation model, USGS has decided to transition from an online interactive deaggregation to a local deaggregation software tool called “NSHMP-haz”. A beta version of this new tool has been integrated into *CPTLiquefy*.

3.3.1 USGS Offline Deaggregation tool (NSHMP-haz)

NSHMP-haz is currently in beta mode, but will be available to the public soon. In cooperation with the USGS programmers, we have obtained access to the source code of NSHMP-haz through the website GitHub.com. An image of the NSHMP-haz code repository is shown in Figure 3-13. From GitHub, a download is available of the tool to a compatible system. Once downloaded, the computer can run ground motion deaggregations without accessing the USGS servers through the Internet. This is a major step forward for performance-based earthquake engineering research because a major obstacle to the development of earlier research tools has been the instability caused by performing and downloading thousands of USGS ground motion deaggregation files. This should no longer be a problem in the future, as a single system will be

capable of developing all ground motion deaggregations and performing all performance-based calculations.

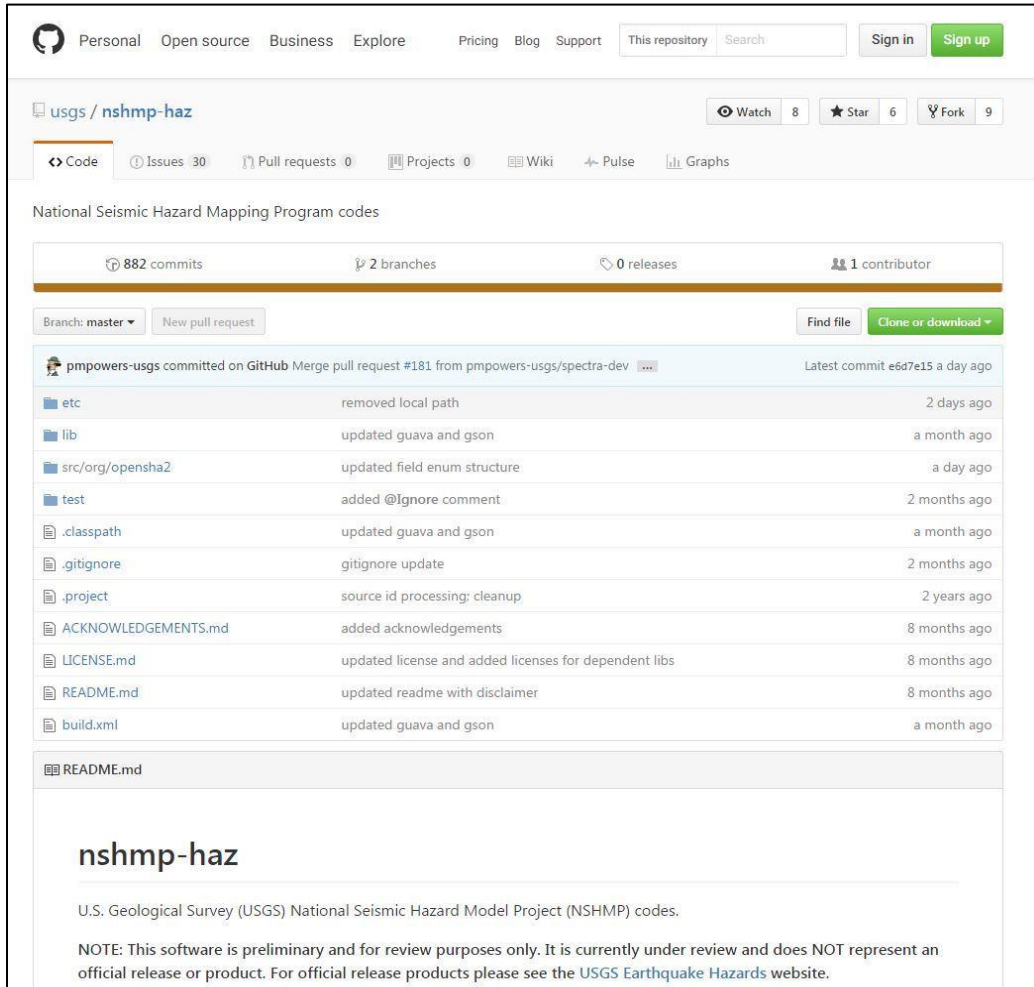


Figure 3-13: USGS NSHMP-haz code repository on GitHub.com.

The NSHMP-haz code uses the Java programming language, so installation of Java is required before running the tool. Setup of Java is a simple process and clear instructions have been developed by the USGS to guide users. Access to this new tool is crucial for the success of the liquefaction hazard analysis tool *CPTLiquefy*.

CPTLiquefy successfully runs and collects deaggregation data from the new tool for the 2008 and 2014 deaggregations for the western and eastern United States. As of now, all states are functional for the 2008 and 2014 deaggregations.

This NSHMP-haz code runs in a similar fashion to the old interactive deaggregation available online. The user chooses four parameters before running the analysis. These are a latitude, longitude, exceedance probability and a number of years to consider in the analysis. An image of the old online interactive deaggregation is shown with major parameters highlighted in Figure 3-14.

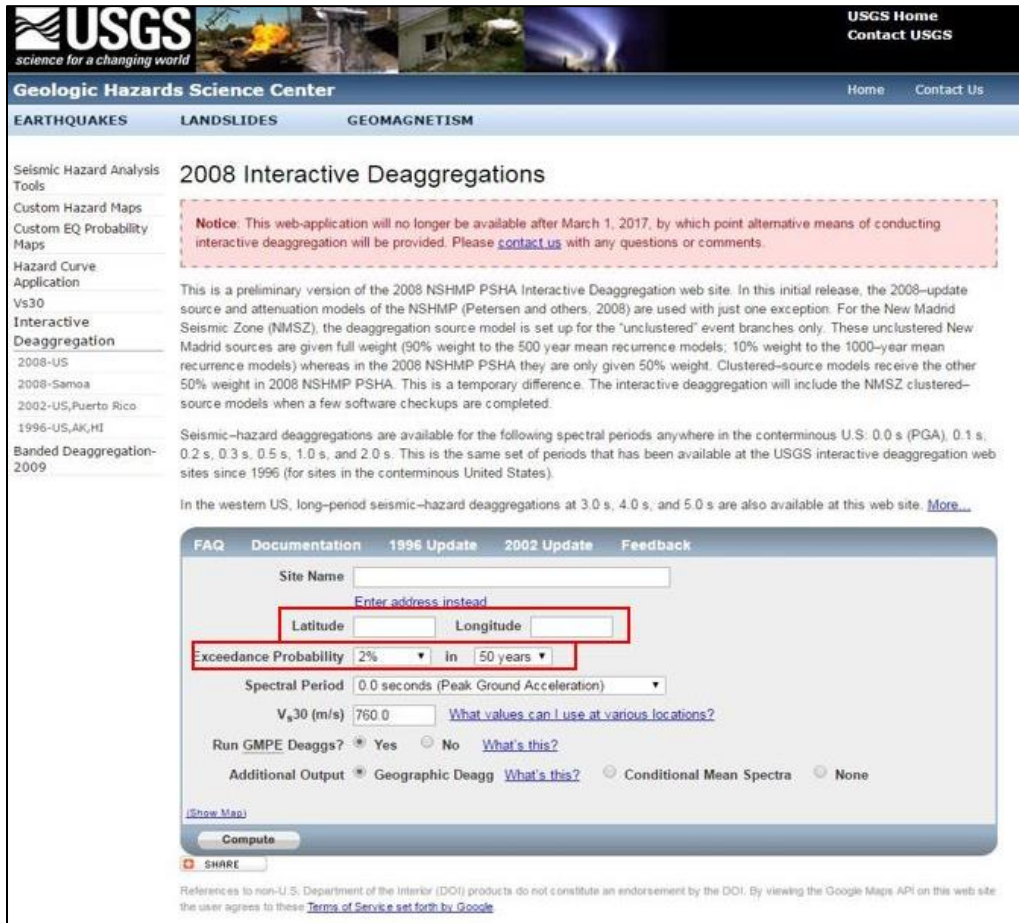


Figure 3-14: Image of the old USGS online deaggregation tool.

These options remain the same with the new NSHMP-haz tool. The user simply selects the same four parameters in the “Pseudo Probabilistic” tab in the program *CPTLiquefy* as highlighted in Figure 3-15. *CPTLiquefy* will then pass the parameters on to the USGS tool and display the results after completion of the deaggregation run. The new tool runs on the system

command prompt so when the tool is activated a command line window will briefly open as the tool runs. Figure 3-16 shows an example of the window launched by the application.

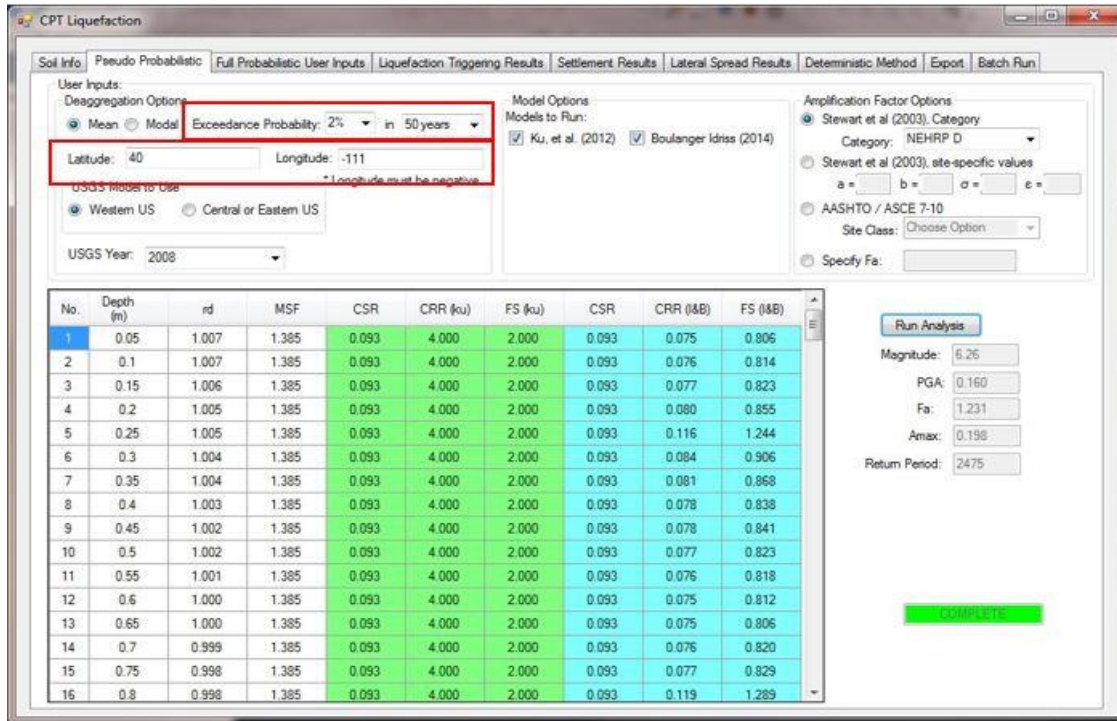


Figure 3-15: Input options for new USGS tool on the “Pseudo Probabilistic” tab.

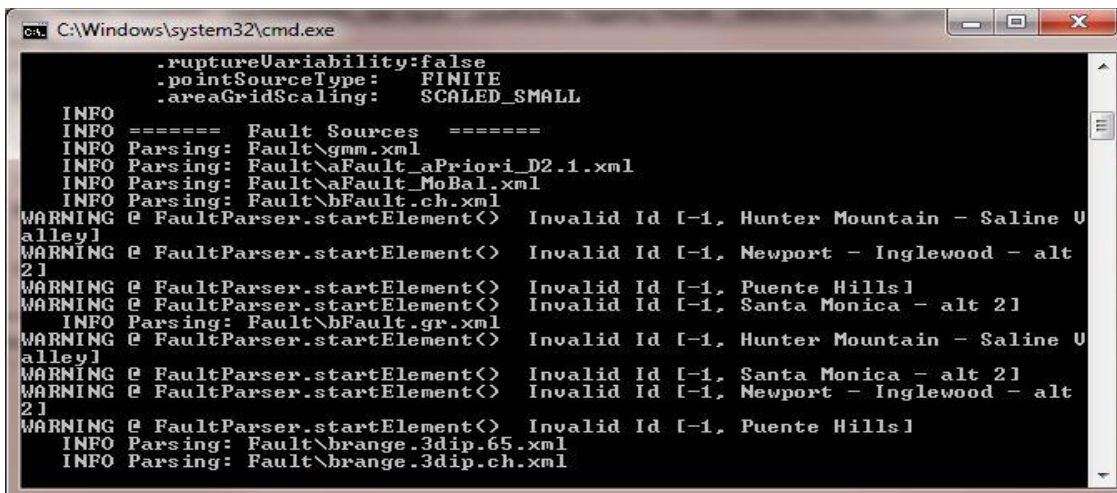


Figure 3-16: View of the window launched by NSHMP-haz.

There is one slight difference in the new USGS tool. Users are now required to select which region of the United States the location of interest is found. There are currently two options: option 1 is for the western US, and option 2 is for the central and eastern US. The division between western, central, and eastern states can be seen in Figure 3-17. If the wrong region is selected an error will occur and the user will be notified to use the other model.

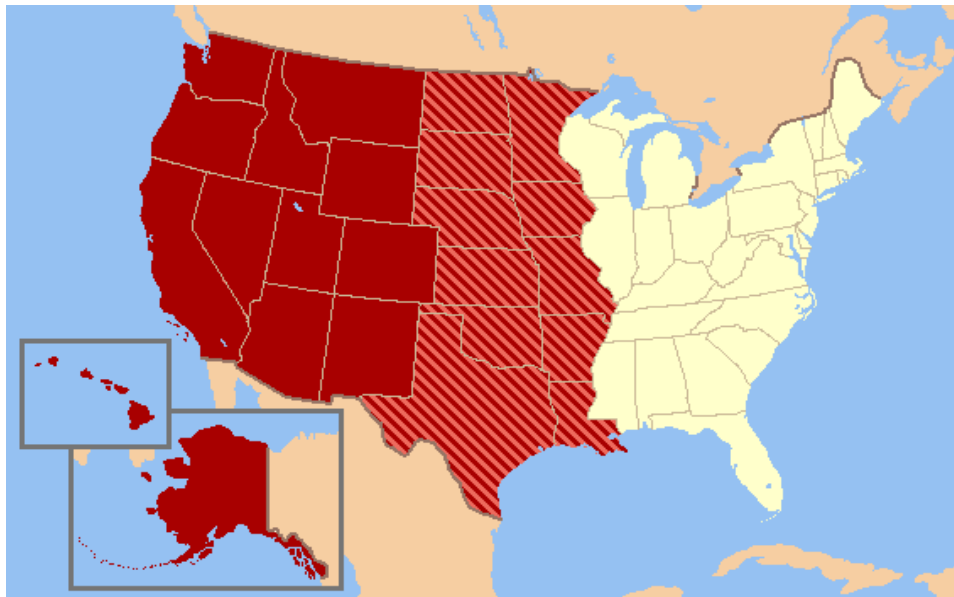


Figure 3-17: Map showing the division in USGS between western, central, and eastern states.

4.0 METHODOLOGY AND RESULTS

4.1 Methodology

To perform a thorough comparison of design methods, a comprehensive range of various soil conditions and site seismicity levels needed to be considered. The methods used to create a thorough comparative study are discussed below.

4.1.1 Soil Profiles

Twenty actual CPT soundings are selected, containing a comprehensive range of soil stiffness and type. These CPT soundings are collected from the United States Geologic Survey (USGS) database of CPT data (<https://earthquake.usgs.gov/research/cpt/data/table/>). The CPT profiles are selected with the intention to have a thorough range of soil type and relative density/stiffness. This range in relative density/stiffness is evident by investigating the plot of corrected cone tip resistance (Q_{mcs}) shown in Figure 4-1. Note the lack of “holes” (i.e., white space) in Figure 4-1.

Figure 4-1 shows how the chosen profiles adequately cover all potentially impactful Q_{mcs} , or stiffness, values across the depth. Only a few profiles are found with a Q_{mcs} value less than 50kPa, because there are very few soils that exist naturally that are soft enough to have such a low value of Q_{mcs} . Also, any soil with a Q_{mcs} value greater than 250kPa is automatically considered too dense to liquefy per the liquefaction triggering databases of Boulanger and Idriss (2014) and Robertson and Wride (1998, 2009). Therefore, it is not imperative to collect comprehensive Q_{mcs} data greater than 250kPa. All collected profiles are summarized in Table 4-1.

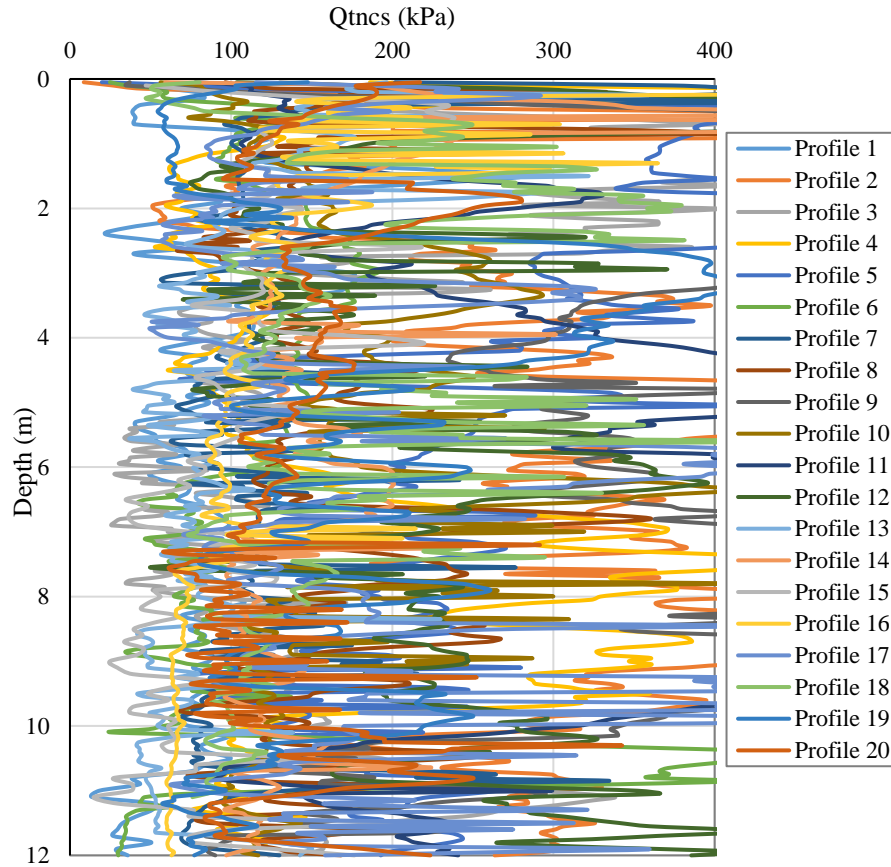


Figure 4-1: Stiffness of CPT profiles plotted at depth.

Table 4-1: Summary of Soil Profiles

Profile	Name	Location	Latitude	Longitude	Source	Sand Content	Stiffness	Full Depth (m)	Date Collected
1	SFO029	San Francisco	37.824	-122.364	USGS	Medium	soft/very soft	17	1/21/1994
2	LWE001	Lawrence(ville), Ill	38.747	-87.511	USGS	High	med to hard	12.5	10/6/2004
3	HNC005	Evansville, IN/ KT	37.872	-87.702	USGS	Medium	med	20	12/6/2003
4	BDY002	Arkansas	33.278	-92.333	USGS	Medium	med	12	12/14/2005
5	SBC030	Riverside,CA	34.070	-117.290	USGS	High	med/hard	19	3/24/2001
6	BKY006	Charleston, SC	32.905	-79.924	USGS	High	soft	20	11/6/2004
7	MGA003	Matagorda, TX	28.765	-95.787	USGS	Low	soft	18.15	1/5/2006
8	SCR001	East St. Louis, Ill	38.620	-90.162	USGS	High	med	24	10/6/2008
9	SOC024	Oceano, CA	35.104	-120.631	USGS	High	med/hard	15	3/2/2004
10	POR006	Chesterton, IN	41.660	-87.051	USGS	Medium	soft/med	15	9/24/2004
11	HTN003	Upper peninsula, MI	47.159	-88.245	USGS	High	soft to hard	17	9/15/2004
12	SYC001	Memphis, TN	35.195	-89.987	USGS	Medium	soft/med	20	10/29/2003
13	BZA001	Freeport, TX	28.979	-95.285	USGS	low(interbedded)	soft	30	1/3/2006
14	CMN002	Rio grande valley, TX	25.953	-97.560	USGS	Medium	soft	20	1/14/2005
15	LAC076	Northridge, CA	34.227	-118.560	USGS	Low	soft	14	6/18/1996
16	RCD052	Fargo, ND	46.471	-96.834	USGS	very low	very soft	18	9/8/2008
17	SCC097	Santa Clara, CA	37.427	-122.041	USGS	Low	soft	18	6/26/2000
18	Oak061	Oakland, CA	37.818	-122.281	USGS	very low	very soft	20	3/30/1999
19	SCS001	St. Charles, MO	38.856	-90.212	USGS	very high	medium	24	10/6/2008
20	BKY021	North Charleston, SC	33.036	-79.736	USGS	Low	medium	20	11/14/2004

To accurately demonstrate the differences between design methods, variables such as total depth and water table depth were standardized. For this study, all profiles were limited to 12 meters regardless of the full profile depth available from the database. This depth was chosen because after about 12m soil layers will have little to no effect on ground surface settlements or lateral spreading, and in part because 12m has been used in other performance-based (full-probabilistic) studies (Franke et al. 2014). The depth of the water table can have a considerable impact on the amount of liquefiable soil layers. For liquefaction to occur soils have to be saturated, therefore any soils above the water table cannot liquefy. For this study, the water table was assumed to be at the ground surface. Finally, none of the CPT profiles from the USGS database contained a cone pore water pressure reading. For this study, the cone pore water pressure was assumed to be zero for each soil layer.

Although altering the water table depth and assuming zero for the cone pore water pressure will produce inaccurate estimations of site-specific liquefaction hazard effects, the purpose of this study is to compare the calculations from different design methods. These changes would be problematic if the purpose was to accurately predict liquefaction effects at a specific site; but because the purpose of this study is to compare calculation methods, these alterations do not affect the accuracy of this study's results.

In order to perform an analysis of lateral spread, the site geometry had to be specified. Two different geometries were used to ensure consistency of results. The first geometry was for a gently sloping ground with the ground slope, S , of 3%. The second geometry was a level ground with a free face, where the free face height, H , is 6m, and the length of the level ground, L , is 50m. These geometries were chosen as they have been used in previous studies.

4.1.2 Site Locations

To address the potential variable levels of seismicity a site could have, ten different cities are examined in this study. Each city is chosen to represent a different level of seismicity and in part because they have been used in other PBEE studies (Kramer and Mayfield 2007, Franke et al. 2014). The chosen cities are distributed as such: four on the west coast near the San Andreas Fault, two in the Pacific north-west near the Cascadia Subduction zone and associated faults, two near the Wasatch fault and Rocky Mountain region, one near the New Madrid fault system, and one on

the east coast in Charleston, SC. A map of the cities are shown in Figure 4-2, and a list of the cities with their corresponding latitude, longitude, mean/modal magnitudes is presented in Table 4-2.



Figure 4-2 Map of all ten cities in this study.

Table 4-2: Selected Cities Used in Study

City	Latitude	Longitude	Mean Magnitude	Modal Magnitude	PGA (g)
			(475 T _R / 2475 T _R)	(475 T _R / 2475 T _R)	(475 T _R / 2475 T _R)
Butte, MT	46.0038	-112.535	6.03 / 6.05	5.20 / 6.20	0.08344 / 0.1785
Charleston, S.C.	32.7765	-79.9311	6.61 / 7.00	7.36 / 7.37	0.1513 / 0.7287
Eureka, CA	40.8021	-124.164	7.33 / 7.45	6.99 / 6.99	0.6154 / 1.4004
Memphis, TN	35.1495	-90.049	6.98 / 7.24	7.70 / 7.70	0.1604 / 0.5711
Portland, OR	45.5231	-122.677	7.24 / 7.31	9.00 / 9.00	0.199 / 0.4366
Salt Lake City, UT	40.7608	-111.891	6.75 / 6.90	6.99 / 6.99	0.2126 / 0.6717
San Fran, CA	37.7749	-122.419	7.31 / 7.44	7.99 / 7.98	0.4394 / 0.7254
San Jose, CA,	37.3382	-121.886	6.66 / 6.66	6.60 / 6.60	0.456 / 0.6911
Santa Monica, CA	34.0195	-118.491	6.74 / 6.84	7.21 / 7.22	0.3852 / 0.7415
Seattle, WA	47.6062	-122.332	6.75 / 6.88	6.60 / 6.80	0.311 / 0.6432

4.1.3 Return Periods

Every structure is designed for a different level of earthquake depending on either the importance of that structure (e.g., hospitals, fire stations, etc.) or the level of negative impact resulting from structural failure (e.g., nuclear facilities, football stadiums, etc.). Less critical structures are designed for seismic events with shorter return periods, in other words smaller seismic events, while more critical structures are designed for higher return periods. This study focuses on return periods 475 years, 1039 years, and 2475 years, which correspond to probabilities of exceedance of 10% in 50 years, 7% in 75 years, and 2% in 50 years, respectively. While the AASHTO standard uses a 1033 year return period, the USGS hazard tool does not use this return period. A return period of 1039 years was used as it is the closest to 1033 years used by the USGS hazard tool. These chosen return periods represent relatively low, medium, and high levels of seismic loading, respectively.

4.2 Liquefaction Triggering Results

At the completion of the liquefaction analysis, all liquefaction triggering results were compiled into one database. Comparisons were made between the results of both of the new full-probabilistic models based on Ku et al. (2012) and Boulanger and Idriss (2014). A comparison was also made between the full-probabilistic results and results from more conventional methods of liquefaction analysis, such as the Robertson and Wride (1998, 2009) and Boulanger and Idriss (2014) pseudo-probabilistic methods. General trends associated with these comparisons are presented.

4.2.1 Example of Results from *CPTLiquefY*

After completion of full-probabilistic calculations in *CPTLiquefY*, the liquefaction triggering results can be viewed on the “Triggering Results” tab. The data provided on this tab represents hazard curves for each individual soil layer analyzed in the input soil profile. When the results are plotted, a hazard curve like those shown in Figure 4-3 is produced. This curve relates design values for the factor of safety against liquefaction (FS_L) with corresponding rates of exceedance (inverse of return period). The curves in Figure 4-3 show the results from both the Ku

et al. and Boulanger and Idriss full-probabilistic methods along with a horizontal line that represents the mean annual rate of exceedance that correlates to a 475 year return period. In order to obtain design values from this curve, values should be interpolated from the hazard curve for a return period of interest. For example, the Boulanger and Idriss method has a value of about $FS_L = 0.35$ at the 475 year return period, while the Ku et al. method gives a value of $FS_L = 0.6$. Given that these values are less than $FS = 1$, both methods would in this case predict the initiation of liquefaction for the considered soil layer.

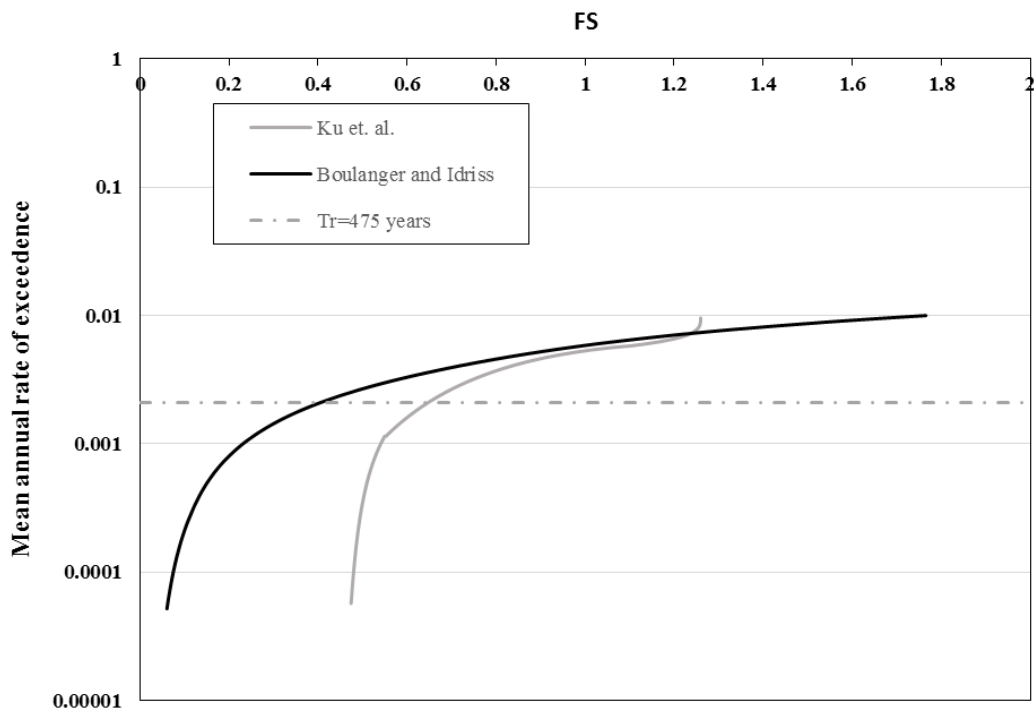


Figure 4-3: Example FS_L Hazard curve output from *CPTLiquefy*.

In order to consider the liquefaction triggering hazard for a full soil profile using the full-probabilistic results, FS_L values must be chosen from each layer in the soil profile at a selected return period. *CPTLiquefy* has the capability to select these values and then export a clean Excel file with the results from the analyzed soil profile. The results are then easily plotted as a profile. Figure 4-4 presents an example of a completed soil profile comparing FS_L with depth. With this

profile it is possible to analyze the liquefaction hazard at any depth, as well as compare the results from the different methods and results from different return periods of interest.

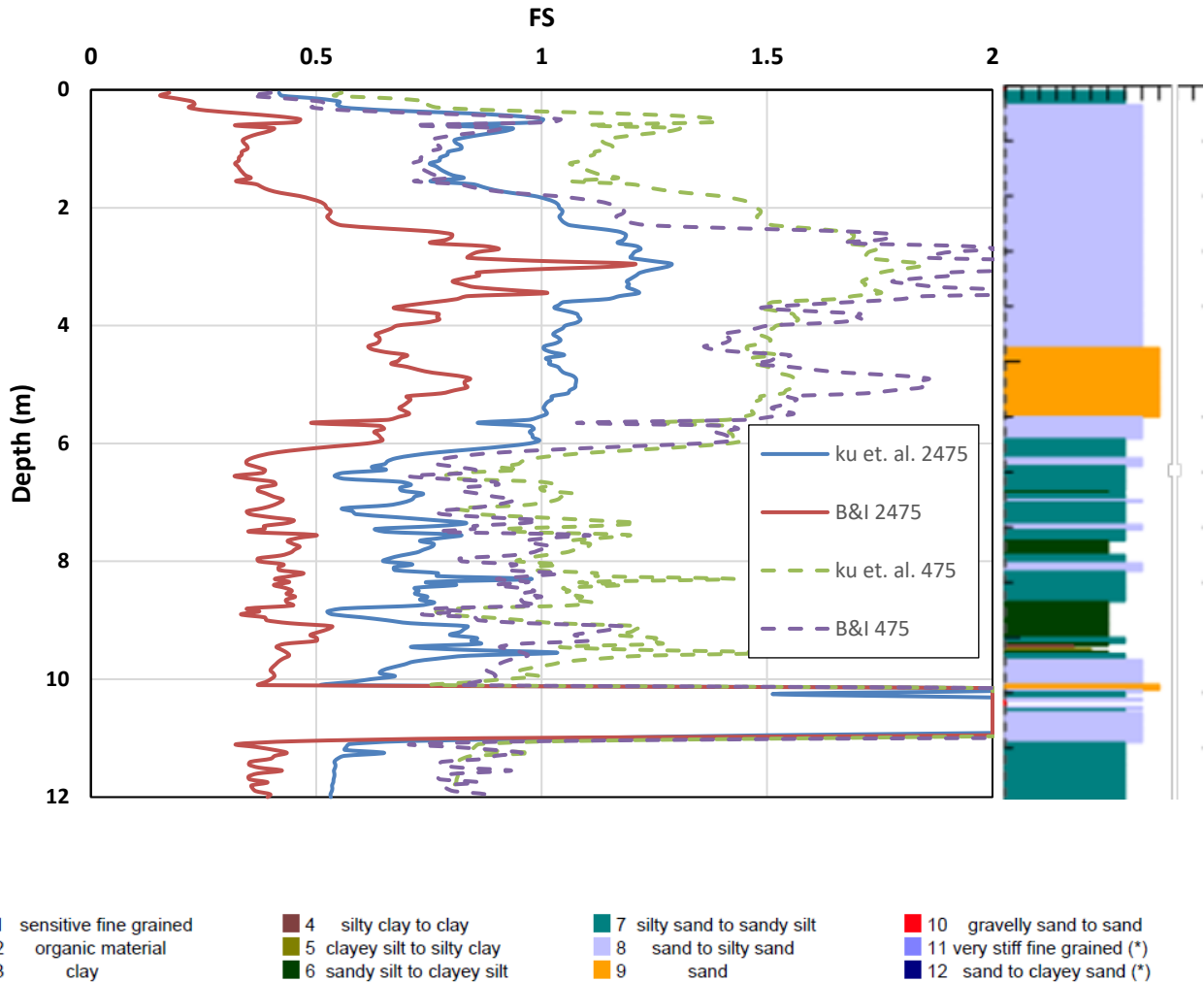


Figure 4-4: Comparison of results from the full-probabilistic liquefaction analysis of profile 6 at Butte, MT relating FS_L to depth in meters.

4.2.2 Comparison of Ku et al. and Boulanger and Idriss Full-Probabilistic Results.

Using the results from the analysis conducted with 20 soil profiles and 10 locations, a dataset of full-probabilistic results was formed for both methods. The comparison of these results with the Ku et al. full-probabilistic results on the x-axis and Boulanger and Idriss full-probabilistic

results on the y-axis can be seen in Figure 4-5. From the plot, the following trends were noted. First, the Ku et al. methods tend to predict higher values for FS_L if the computed FS_L is less than one. For values of FS_L greater than one, it becomes much more likely that the computed FS_L from each method could be similar, or the Boulanger and Idriss could predict larger values. Second, data scatter seems to increase when the FS approaches the range of 1 to 1.4. In this region the calculation of FS is highly varied depending on other factors than the full-probabilistic model (profile stiffness, location). It can be noted that a large number of points can be seen on the $FS_L = 2$ line on each axis. This is because a limit was placed at a value of $FS_L = 2$, which is a design value at which liquefaction will generally not be a concern. Without the application of this limit, the trends seen in Figure 4-5 simply continue beyond the shown values.

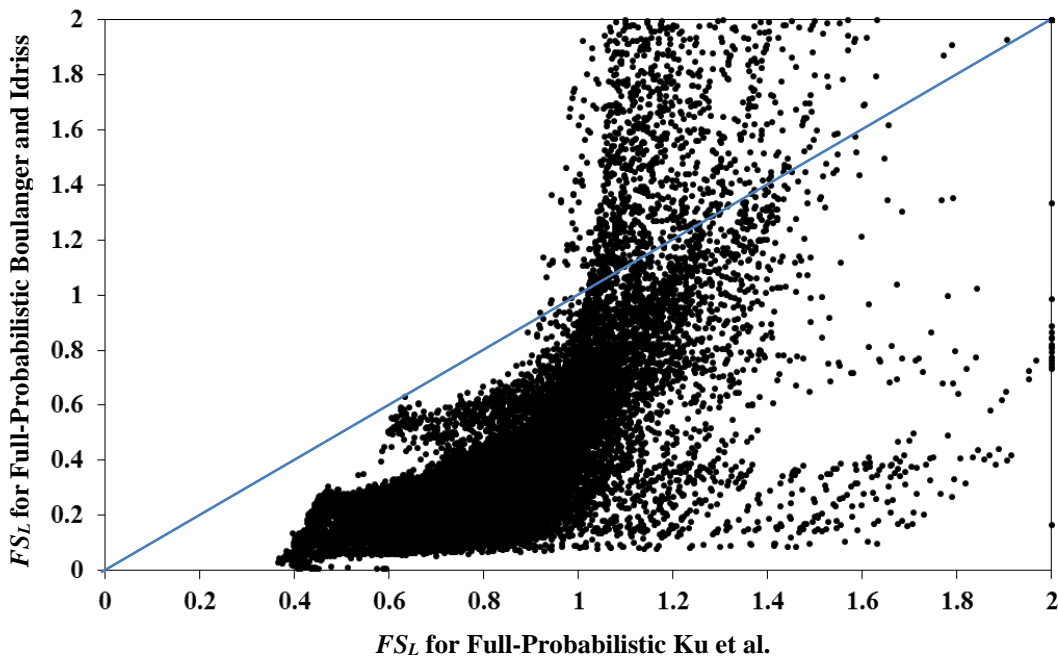


Figure 4-5: Comparison of FS_L for both full-probabilistic methods (Return Period = 1039 years).

4.2.3 Variation of FS_L between Sites

To see the effect of individual factors on the computed FS_L values, the results from the previous analysis were limited to one profile. To obtain a wide range of FS_L values, a moderately liquefiable soil profile (profile 14) was chosen as an example. The results shown in Figure 4-6 illustrate the effect of location on FS_L . The lowest seismicity site (Butte) has the most values above $FS_L = 1$ and the highest seismicity site (Eureka) has the most below $FS_L = 1$. Interestingly, the two methods on average seem to predict more consistent values at low seismicity locations, than high seismicity locations. Also, by looking at Figure 4-7 and Figure 4-8 which represent the same comparisons but at higher return periods, it becomes clear that the two methods produce more consistent values at lower return periods rather than higher ones.

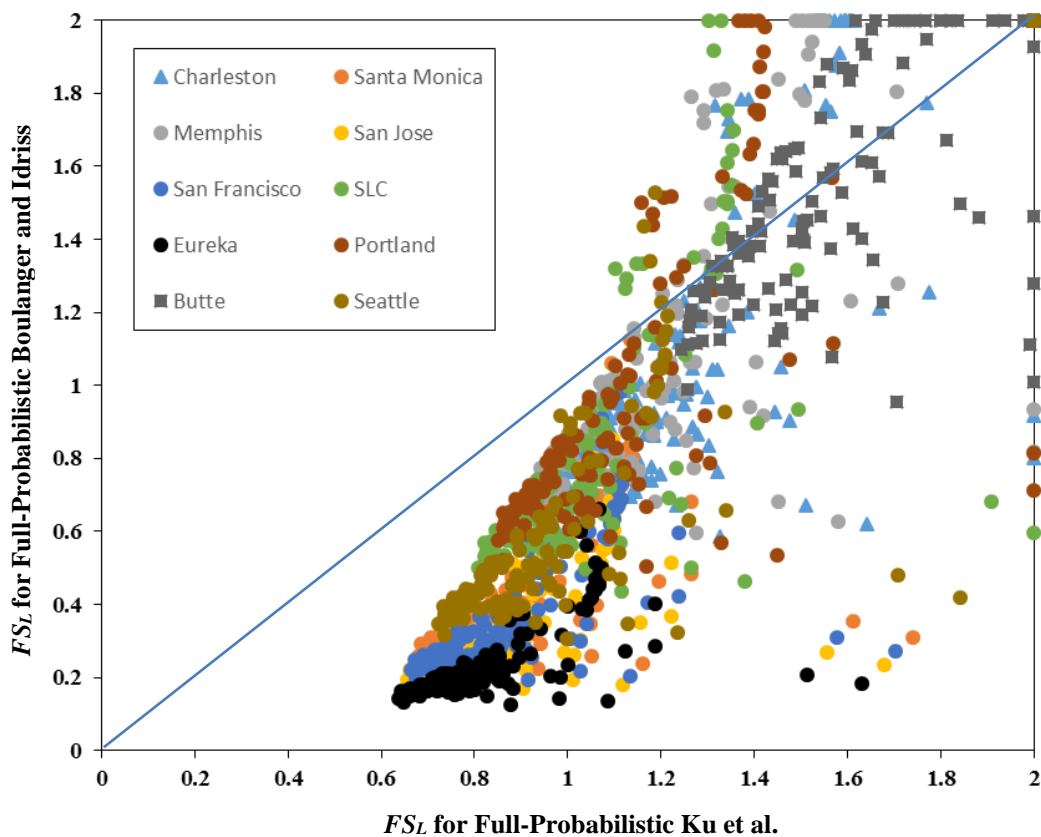


Figure 4-6: FS_L results for profile 14 at a return period of 475 years.

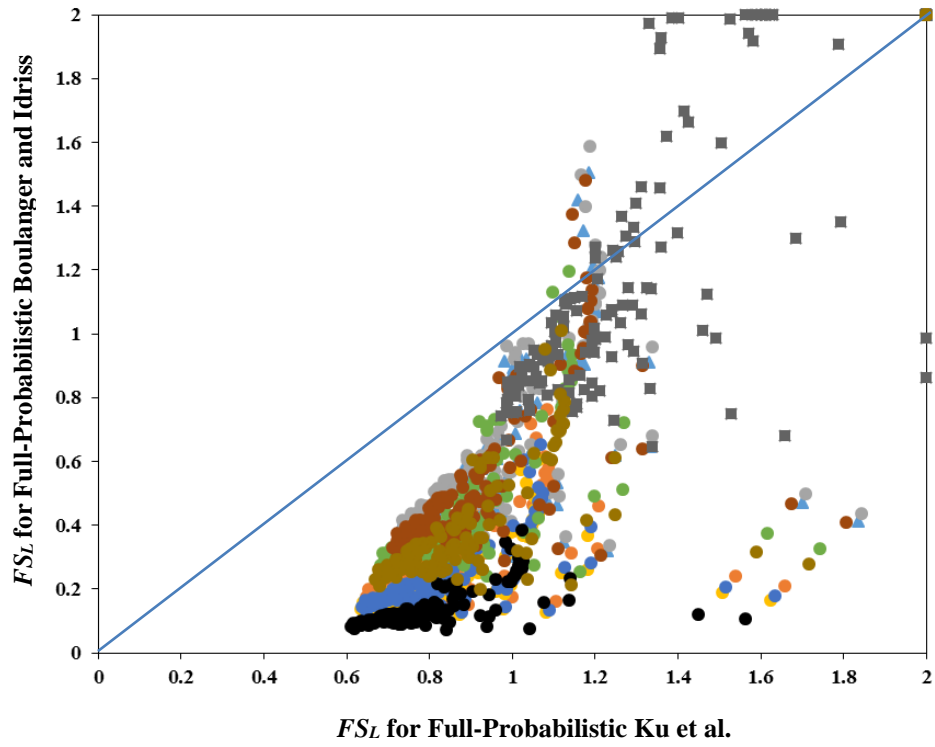


Figure 4-7: FS_L results for profile 14 at a return period of 1039 years.

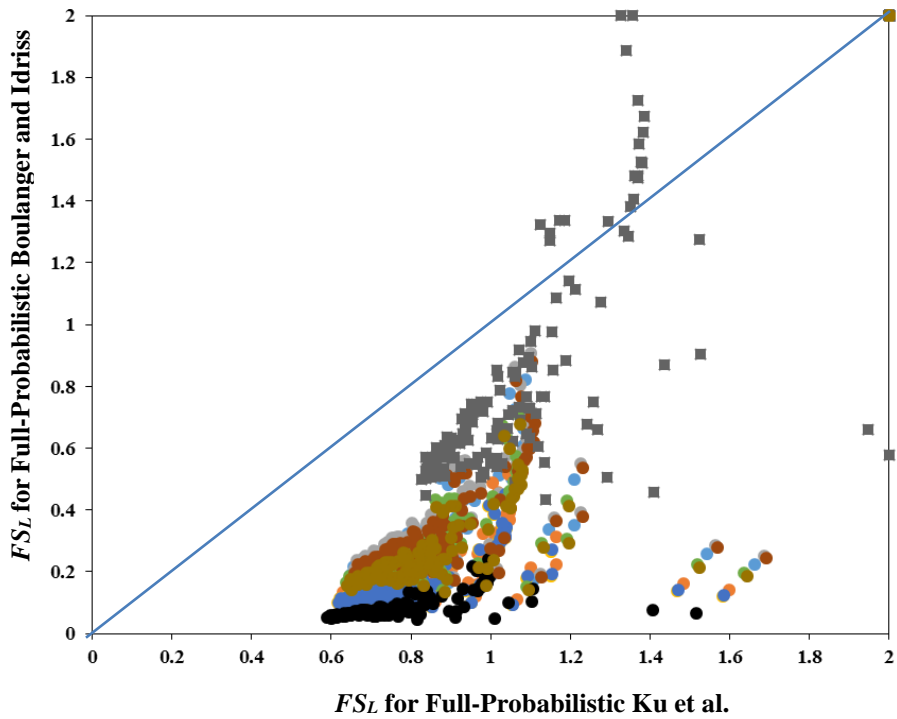


Figure 4-8: FS_L results for profile 14 at a return period of 2475 years.

4.2.4 Variation of FS_L between Return Periods

As suggested previously, the return period of the analysis appears to have a significant effect on the comparison of the two full-probabilistic methods. To more clearly show this effect, a plot of one soil profile at one location of moderate seismicity is shown in Figure 4-9. As the return period increases, the values drift farther from the one-to-one line which represents where the two methods would calculate identical results. This can be explained by the tendency of the Boulanger and Idriss method to predict significantly smaller values for FS_L if FS_L is less than 1, while predicting similar or even greater values if FS_L is greater than 1.

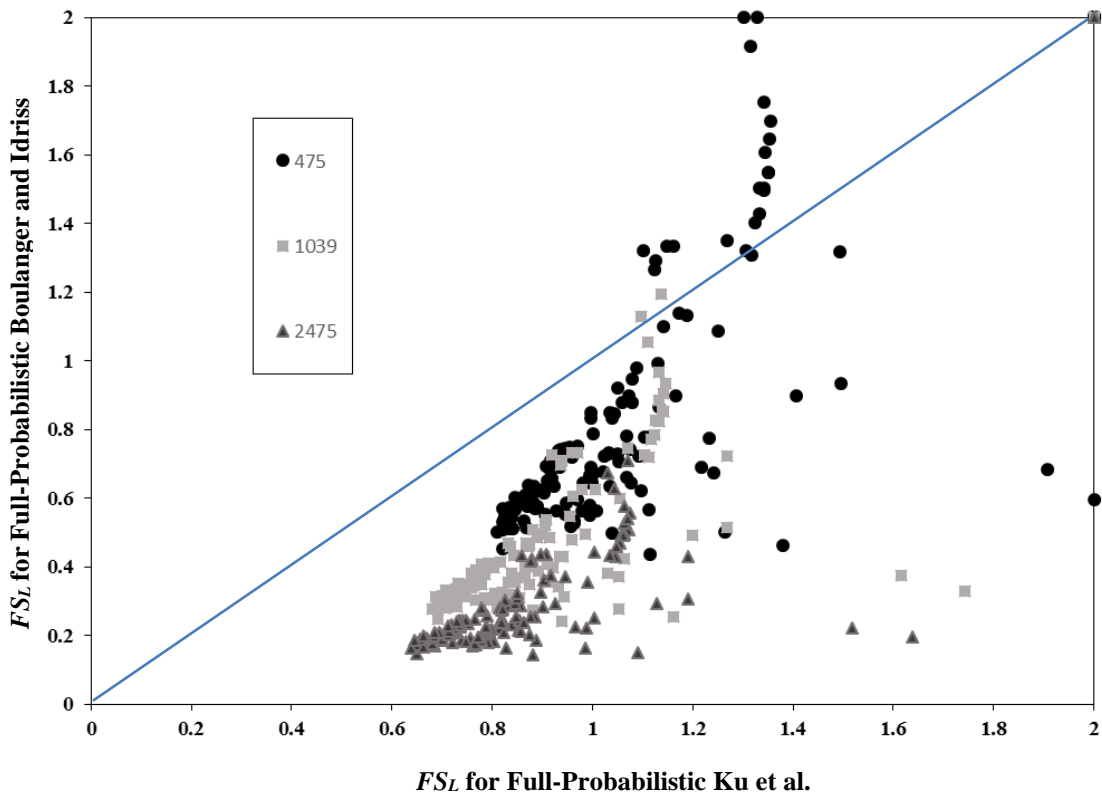


Figure 4-9: Comparison of FS_L for 3 return periods (profile 14, Salt Lake City).

4.2.5 Variation of FS with Soil Profile Stiffness

Before beginning the analysis, all 20 soil profiles were divided into three basic levels of stiffness; soft or very soft, moderate, and stiff. Figure 4-10 shows the general trends caused by the profile stiffness. Predictably, soft profiles tended to have lower values of FS_L , as well as the greatest discrepancy between the two methods. Stiff profiles, on the other hand generally had higher values of FS_L , but maintained the same trends between methods at low values of FS_L . Values above $FS_L > 1$ tended to give larger FS_L values for the Boulanger and Idriss method. Finally, moderately stiff profiles fit well between the soft and stiff profiles, and showed a good range of behavior seen in both the soft and stiff profiles. This likely takes place because many of the moderate profiles contain a mix of different soft and stiff layers along with layers with actual stiffness values that would be considered moderately stiff.

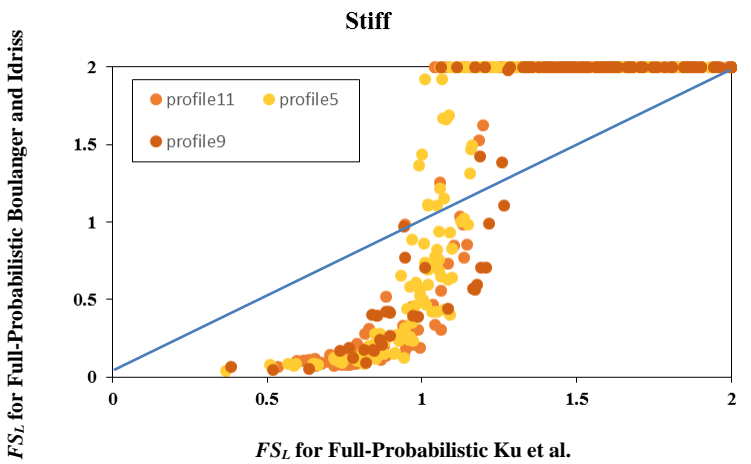
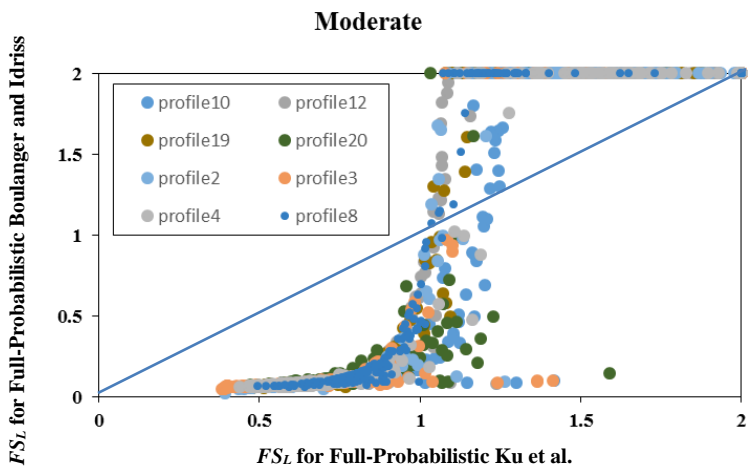
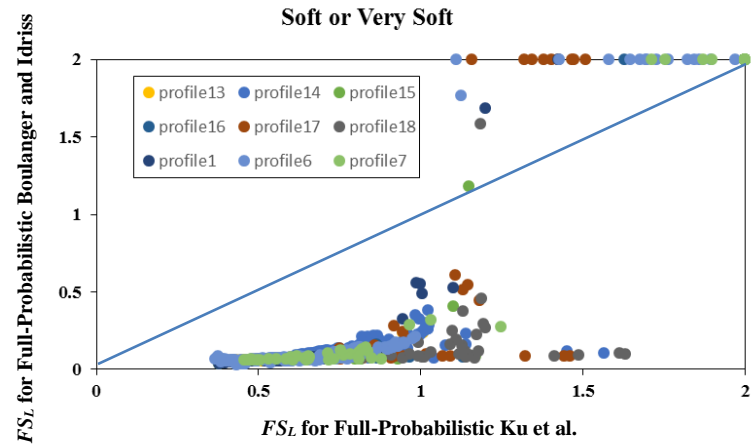


Figure 4-10: Comparison of FS_L results from different categories of profile stiffness.

4.2.6 Comparison of Full-Probabilistic Methods with Pseudo-Probabilistic Methods

A comparison of the full-probabilistic results with the results from the conventional method is helpful in comparing the difference between engineering design values currently calculated by practicing engineers, and engineering design values calculated from a performance-based (full-probabilistic) design method. The pseudo-probabilistic results in this section were computed from a PSHA using either mean or modal values. All 20 CPT profiles and all 10 sites discussed previously were included in the body of the data to show trends that correlate to a wide range of conditions.

The following results are displayed in a scatter plot format with conventional values on the y-axis and full-probabilistic values on the x-axis. If the two methods were to compute identical values, the data points would fall directly on the 1:1 line (blue) displayed in the following figures. Lines at the value which divide predicted liquefied and non-liquefied behavior ($FS_L = 1$) (red) are drawn from each axis on the plot to divide the plot into 4 quadrants (Figure 4-11). The four quadrants are defined as:

1. Top Left- The full-probabilistic method predicts liquefaction, the pseudo-probabilistic method does not
2. Top Right- The full-probabilistic method and pseudo-probabilistic method both predict no liquefaction.
3. Bottom Left- The full-probabilistic method and pseudo-probabilistic method both predict liquefaction.
4. Bottom Right- The full-probabilistic method predicts no liquefaction, while the pseudo-probabilistic method predicts liquefaction.

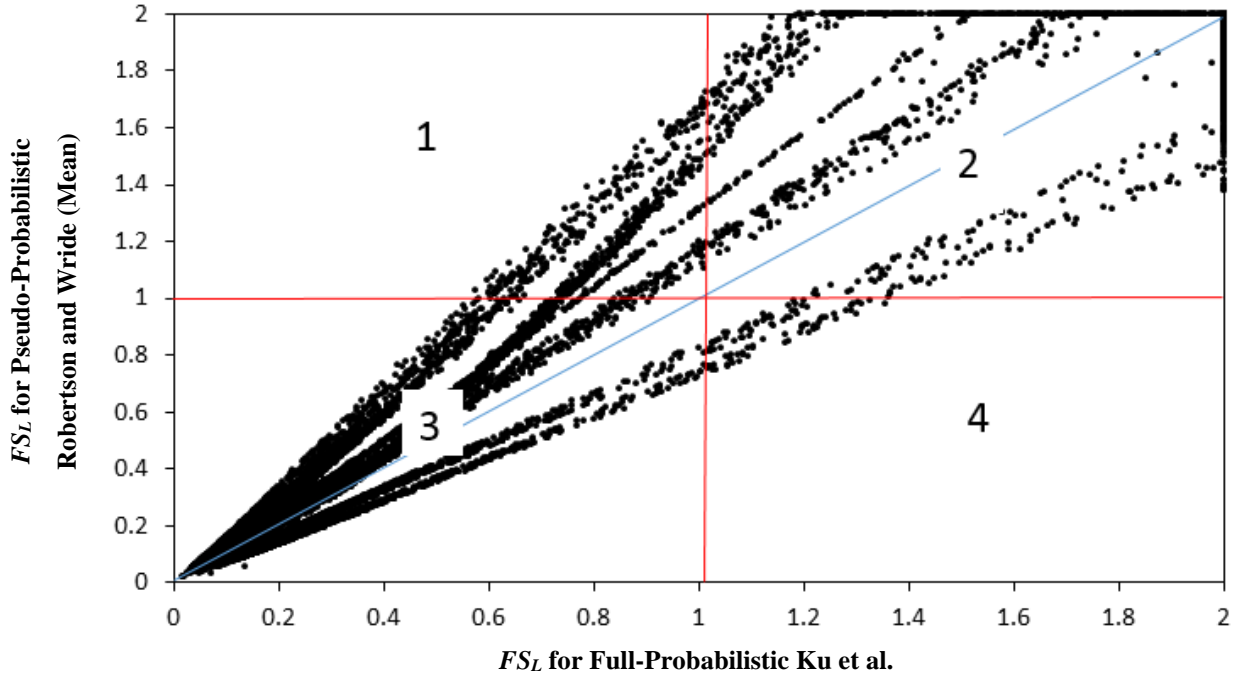


Figure 4-11: Location of four quadrants on an example plot.

4.2.7 Robertson and Wride Pseudo-probabilistic vs. Ku et al. Full-Probabilistic Method

The results of the four-quadrant comparison (see Figure 4-11) between the Robertson and Wride pseudo-probabilistic method and the Ku et al. full-probabilistic method are presented in Figure 4-12 to Figure 4-17. These figures illustrate that for FS_L values less than 1, the conventional method generally predicts smaller values of FS_L when compared to the full-probabilistic method. However, it appears that most of the plotted points from the full comparison lie in quadrants 2 and 3, indicating a common prediction on whether liquefaction is expected to occur. The statistical distribution of the points will be discussed later in this section.

These plots also appear to show that for values of FS_L greater than 1, the conventional method will generally give higher values for FS_L than the full-probabilistic method. This could be significant if a different value of FS_L is used as the boundary between liquefied and non-liquefied behavior (ex. $FS_L=1.2$). In that case, the distribution of data in each quadrant would

change. Differences between the mean and modal methods appears to be limited to small shifts of the trends to the left or right caused by values obtained from the PSHA (low seismicity shifts left for modal; high seismicity shifts right for modal). From observation of the figures, it also appears that the data tends to aggregate in bands based on the seismic loading at the different locations used in the analysis.

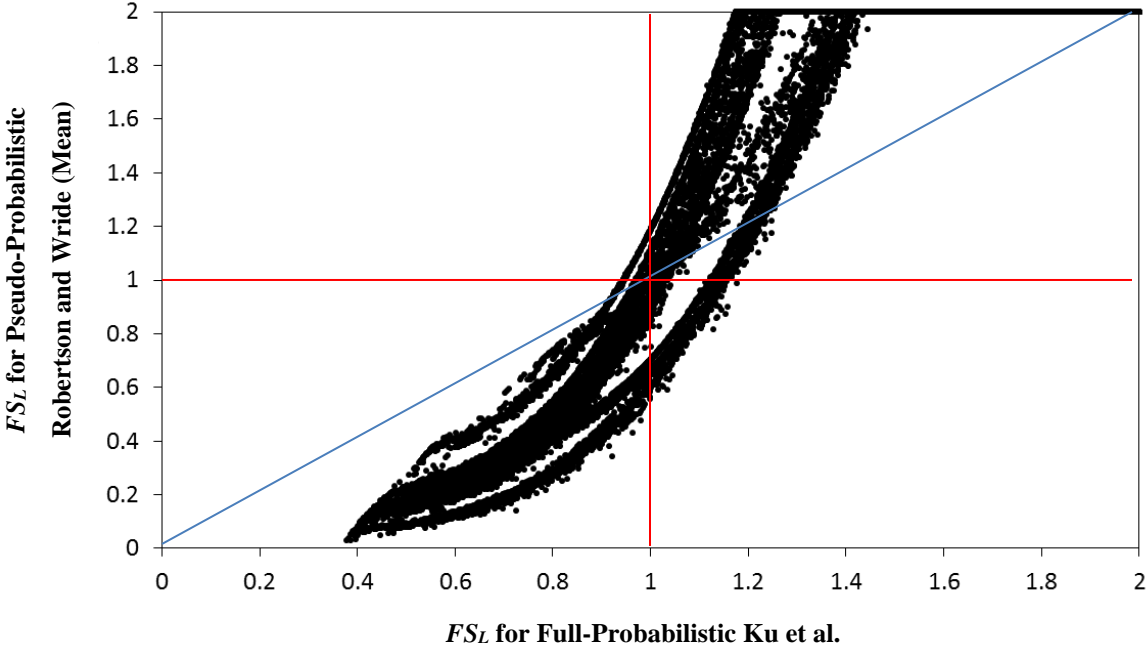


Figure 4-12: Comparison of FS_L from Robertson and Wride conventional (Mean) and Ku et al. full-probabilistic approaches, $T_r = 475$ years.

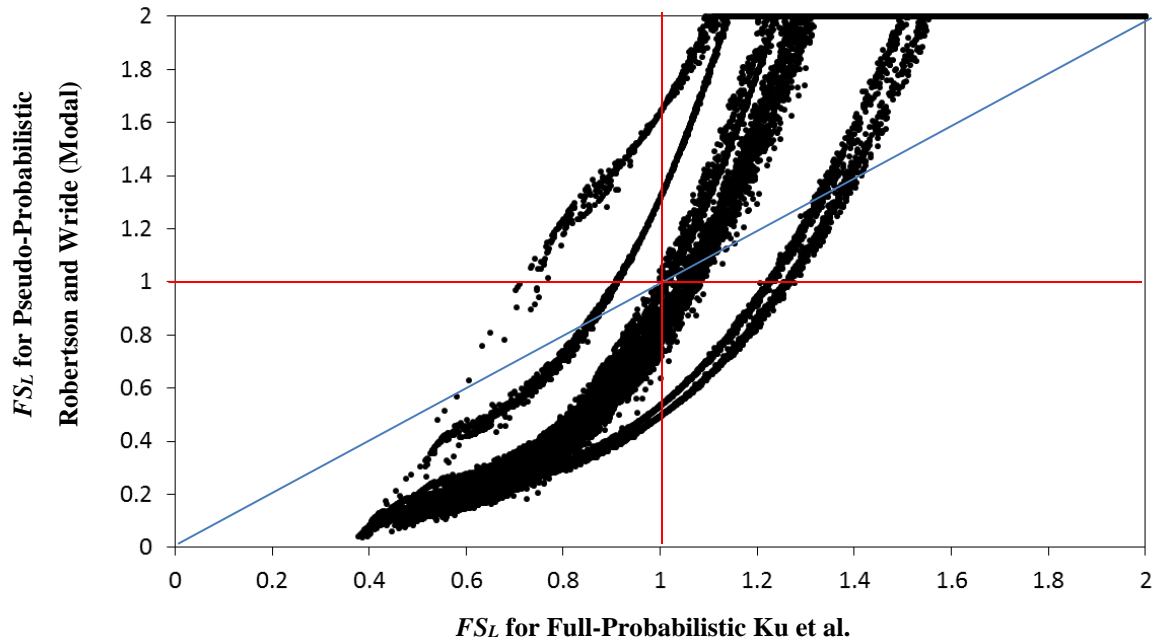


Figure 4-13: Comparison of FS_L from Robertson and Wride conventional (Modal) and Ku et al. full-probabilistic approaches, $T_r = 475$ years.

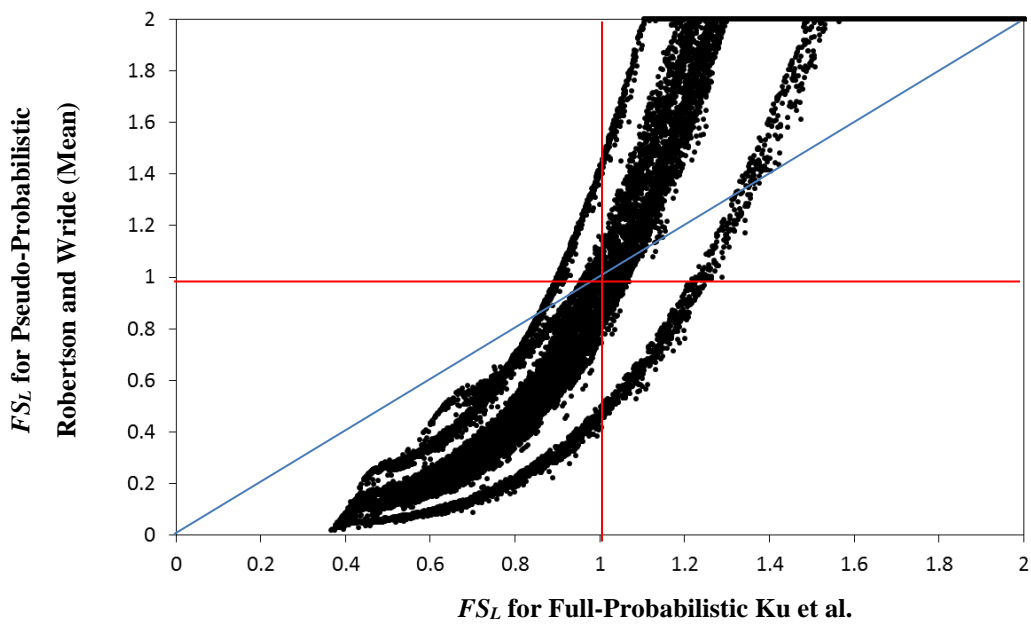


Figure 4-14: Comparison of FS_L from Robertson and Wride conventional (Mean) and Ku et al. full-probabilistic approaches, $T_r = 1039$ years.

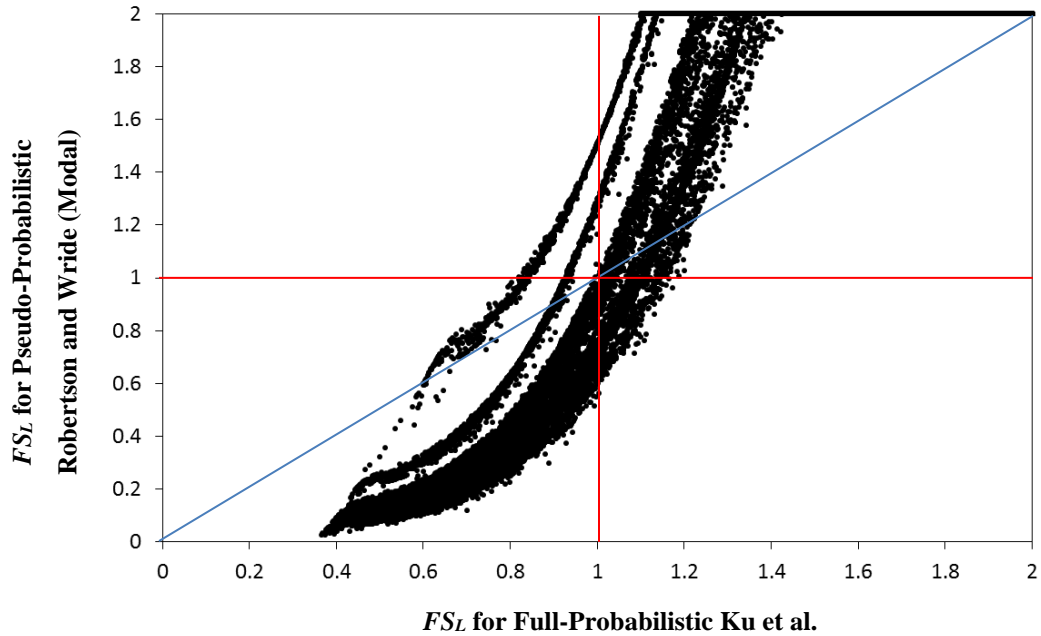


Figure 4-15: Comparison of FS_L from Robertson and Wride conventional (Modal) and Ku et al. full-probabilistic approaches, $T_r = 1039$ years.

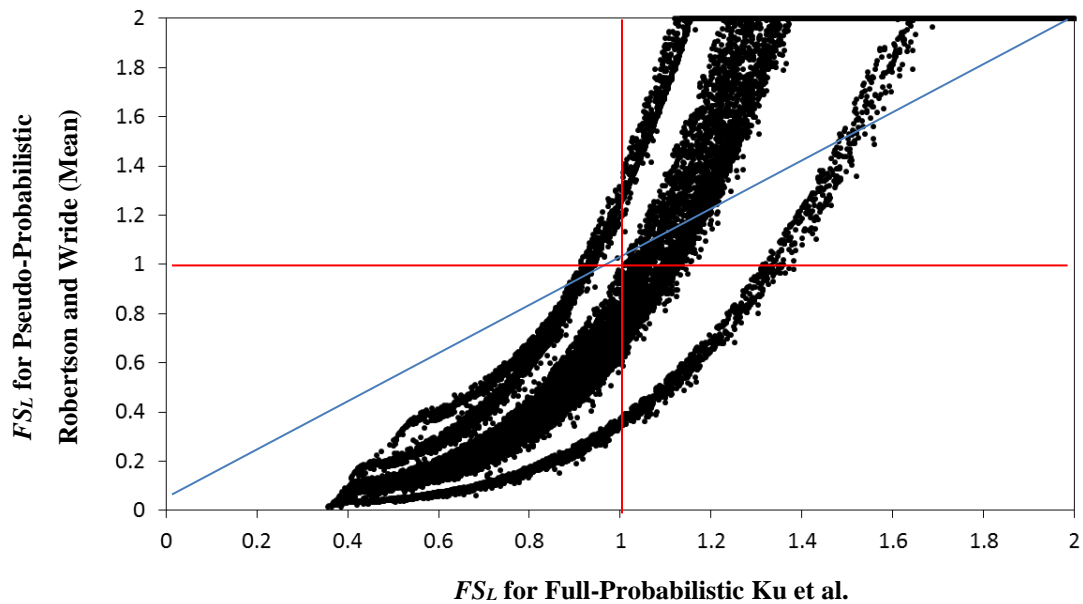


Figure 4-16: Comparison of FS_L from Robertson and Wride conventional (Mean) and Ku et al. full-probabilistic approaches, $T_r = 2475$ years.

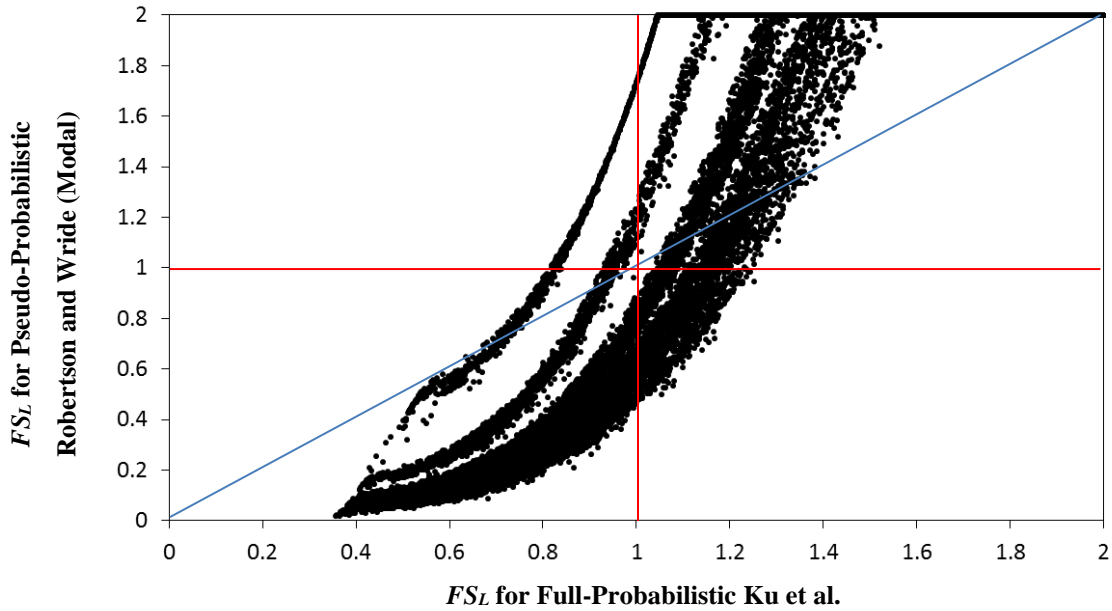


Figure 4-17: Comparison of FS_L from Robertson and Wride conventional (Modal) and Ku et al. full-probabilistic approaches, $T_r = 2475$ years.

4.2.8 Boulangier and Idriss Pseudo-probabilistic vs. Full-Probabilistic Methods

The trends noted in the comparison of the Boulangier and Idriss methods are somewhat different than those from the previous methods. While the previous comparisons showed a curved relationship, the results in Figure 4-18 to Figure 4-23 show a more linear relationship. Because of the general linearity of the relationship, the results from the conventional analysis will generally either predict higher values for FS_L for most possible values of FS_L , or predict lower values of FS_L for all possible values of FS_L . Although few of the predictions line up with the 1:1 line, relatively few data points seem to appear in quadrants 1 or 4, which represent a disagreement on the prediction of liquefaction triggering between the methods.

Similar to the previous comparison, the results are seen to be separated into bands relating to the location of each analysis. An interesting observation from this comparison is that data scatter seems to increase when using modal values instead of mean values for the pseudo-probabilistic analysis. Uniquely, this comparison showed divergent behavior, in that the comparison between

the conventional and full-probabilistic methods are very close at very low values of FS_L , but the predictions are farther apart at values of higher FS_L . Of particular interest are values close to $FS_L = 1$. It is at $FS_L = 1$ that the conventional and full-probabilistic methods would disagree in this analysis. It can be seen that at $FS_L = 1$ there is a significant difference between the methods, unlike at a lower value like $FS_L = 0.2$, where the methods are in almost total agreement. This trend signifies that there should be some degree of disagreement between the methods on the prediction of liquefaction initiation.

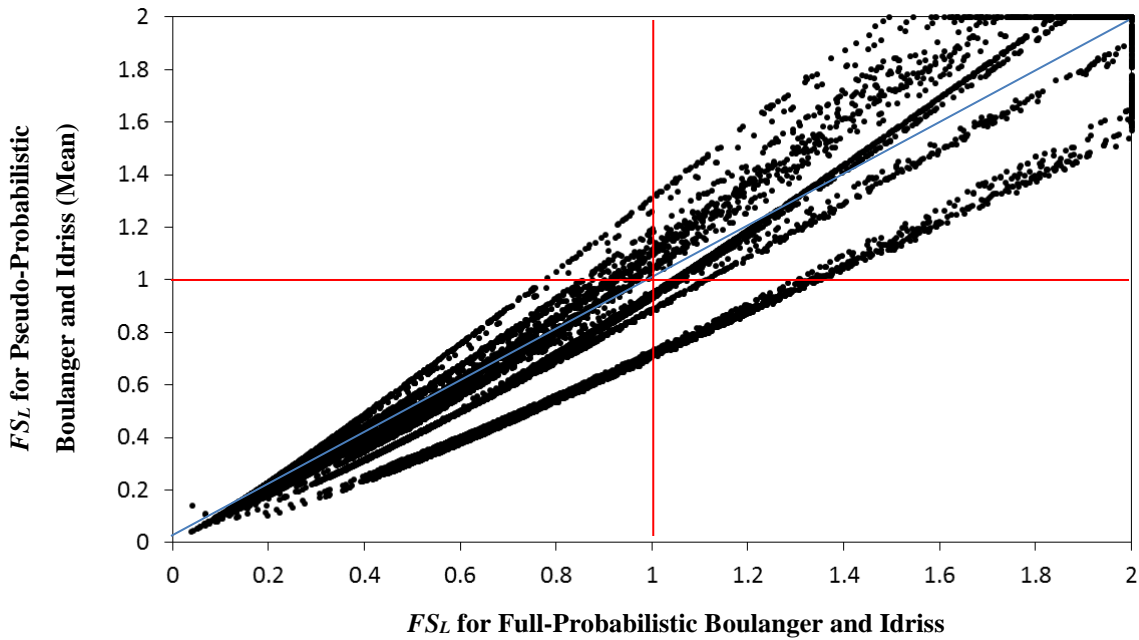


Figure 4-18: Comparison of FS_L for Boulanger and Idriss conventional (Mean) and full-probabilistic approaches, $T_r = 475$ years.

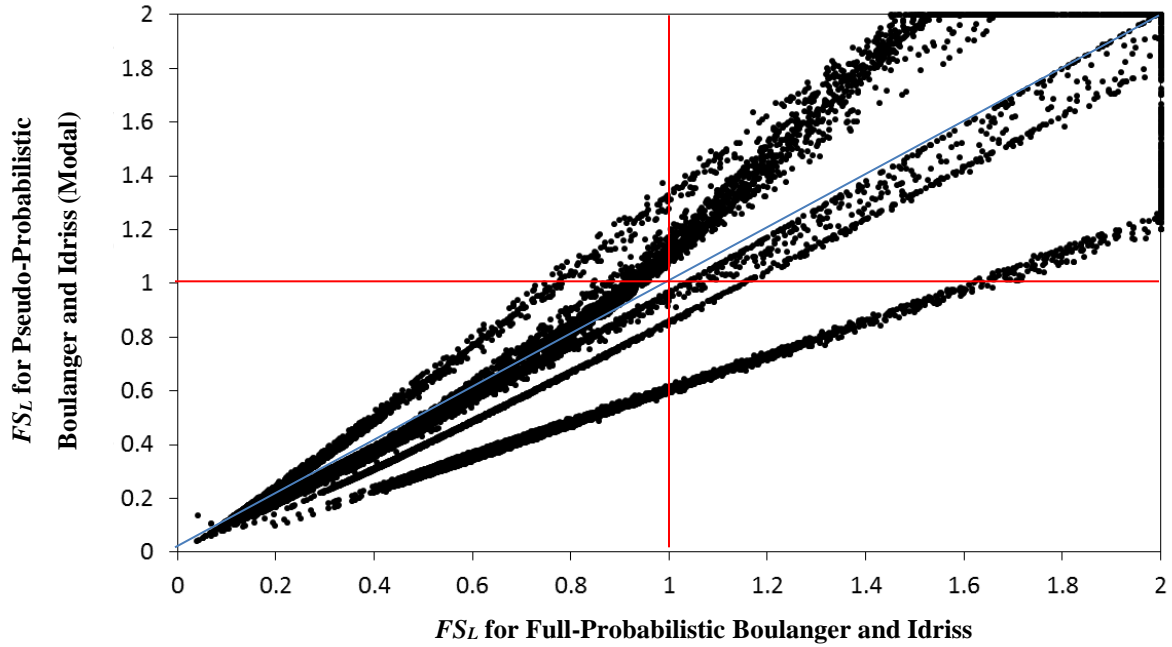


Figure 4-19: Comparison of FS_L for Boulanger and Idriss conventional (Modal) and full-probabilistic approaches, $T_r = 475$ years.

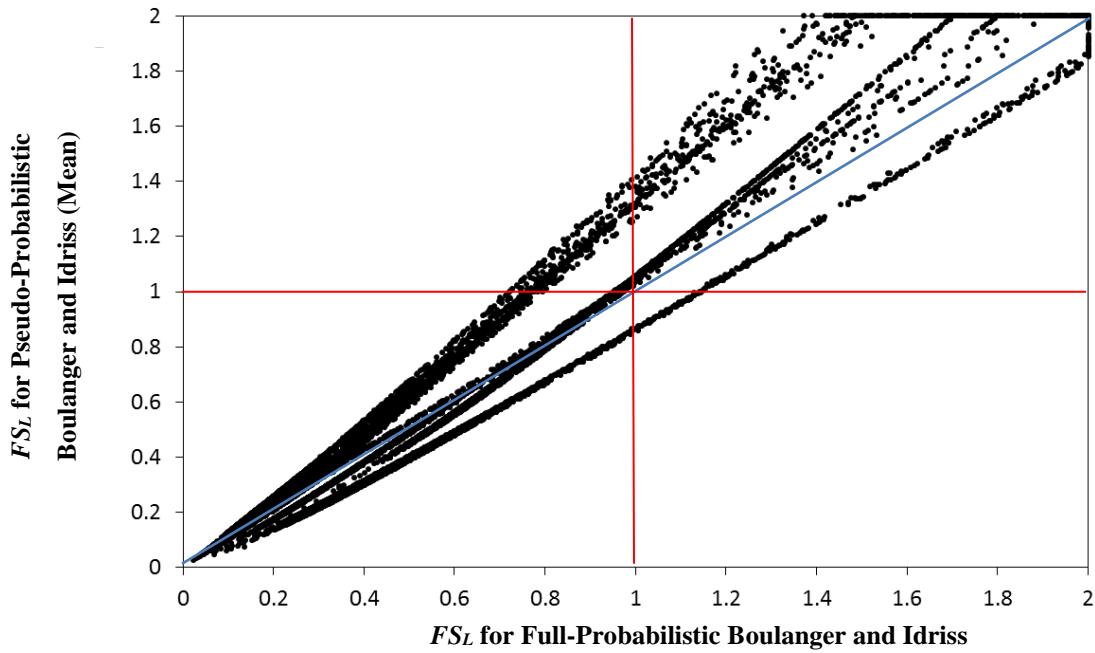


Figure 4-20: Comparison of FS_L for Boulanger and Idriss conventional (Mean) and full-probabilistic approaches, $T_r = 1039$ years.

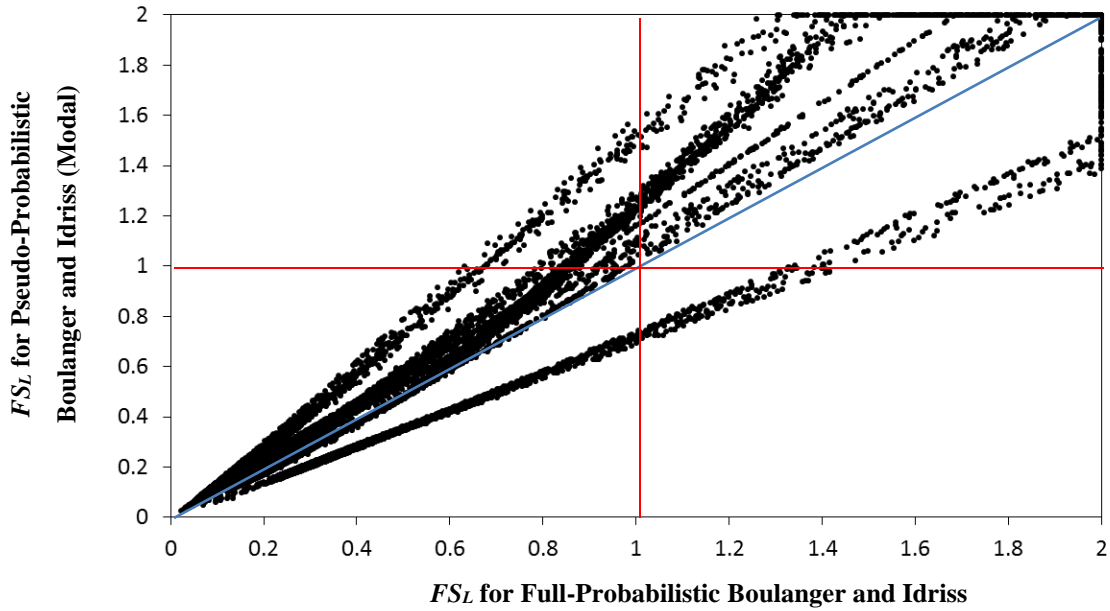


Figure 4-21: Comparison of FS_L for Boulanger and Idriss conventional (Modal) and full-probabilistic approaches, $T_r = 1039$.

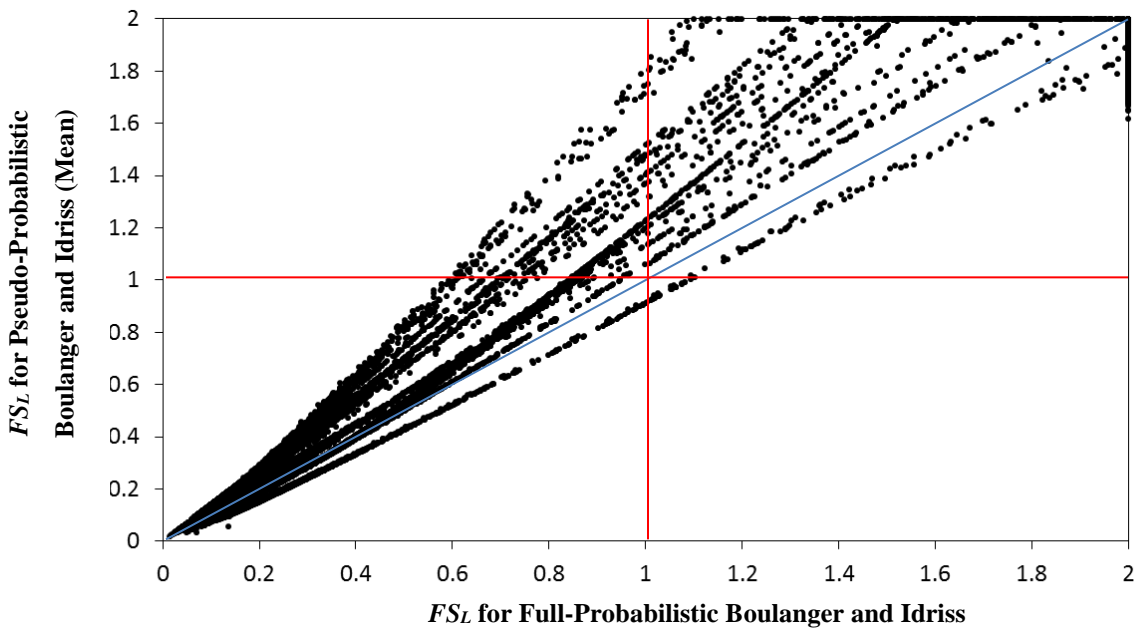


Figure 4-22: Comparison of FS_L for Boulanger and Idriss conventional (Mean) and full-probabilistic approaches, $T_r = 2475$.

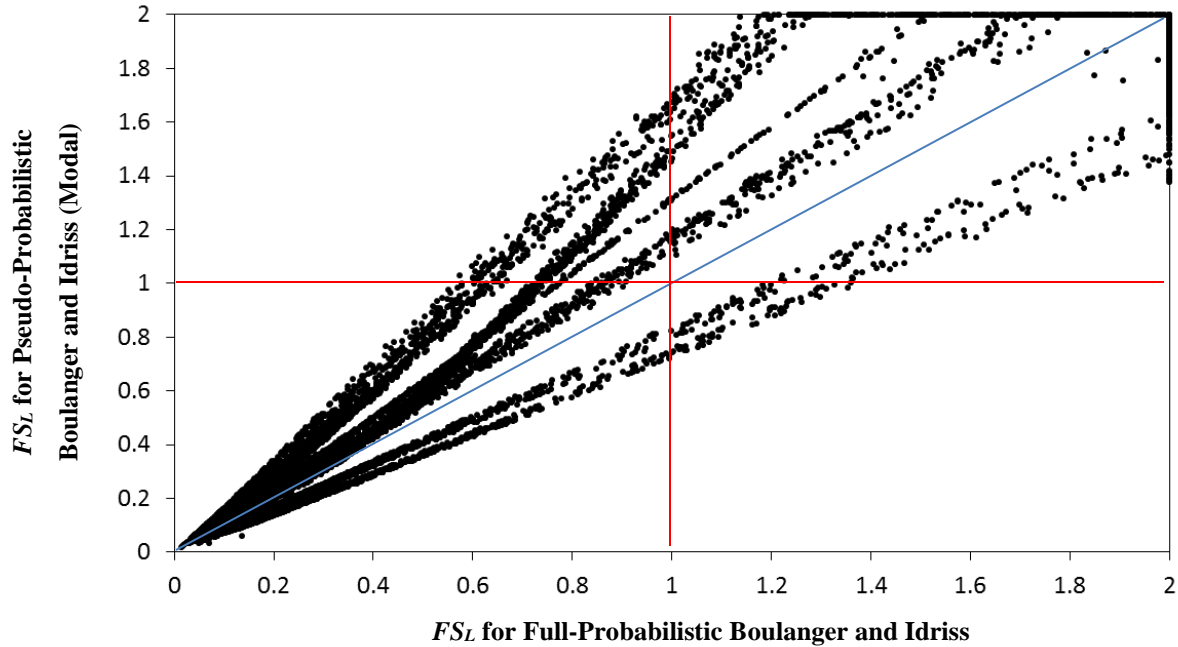


Figure 4-23: Comparison of FS_L for Boulanger and Idriss conventional (Modal) and full-probabilistic approaches, $T_r = 2475$.

4.2.9 Summary of Comparisons

A brief statistical analysis of the distribution of the liquefaction triggering data in each of the four defined quadrants was conducted. A total of 45,590 different liquefaction triggering predictions were analyzed from each of the plots in the previous sections. The results of this analysis can be viewed in Table 4-3 through Table 4-8.

These results suggest that the full-probabilistic and conventional liquefaction triggering analysis methods agree on the prediction of liquefaction triggering around 95% to 99% of the time. The comparison of the Robertson and Wride pseudo-probabilistic vs. the Ku et al. full-probabilistic method showed that about 2 to 4% of the time the performance-based method predicted the non-occurrence of liquefaction, while the pseudo-probabilistic predicted liquefaction to occur. Conversely, generally less than 1% of the cases represented predictions of non-liquefaction by the pseudo-probabilistic method and liquefaction by the full-probabilistic method. These values were

fairly constant across the different return periods analyzed as well as when mean or modal values were used in the pseudo-probabilistic analysis.

The Boulanger and Idriss comparison values had a smaller percentage of points in quadrants 1 and 4 (different liquefaction triggering predictions). At low return periods, the full-probabilistic method predicted non-liquefaction while the conventional method predicted liquefaction about 1.5 percent of the time. This value drops to well below 1 percent for higher return periods. Trends for the opposite prediction (pseudo-probabilistic predicts non-liquefaction and full-probabilistic predicting liquefaction), followed a similar trend but in the opposite direction (percentage increase from low to high return periods).

Table 4-3: Percentage Data in Each Quadrant: Robertson and Wride vs. Ku et al. $T_r = 475$ Years

Robertson and Wride vs. Ku et al.			
475			
Mean		Modal	
0.54%	71.08%	1.02%	69.52%
26.02%	2.36%	25.54%	3.92%

Table 4-4: Percentage Data in Each Quadrant: Robertson and Wride vs. Ku et al. $T_r = 1039$ Years

Robertson and Wride vs. Ku et al.			
1039			
Mean		Modal	
0.92%	63.88%	1.21%	63.25%
33.17%	2.03%	32.88%	2.65%

Table 4-5: Percentage Data in Each Quadrant: Robertson and Wride vs. Ku et al. $T_r = 2475$ Years

Robertson and Wride vs. Ku et al.			
2475			
Mean		Modal	
0.79%	59.17%	1.33%	58.61%
36.67%	3.37%	36.13%	3.93%

Table 4-6: Percentage Data in Each Quadrant: Boulanger and Idriss (Conventional) vs. Boulanger and Idriss (Full-Probabilistic) $T_r = 475$ Years

B&I pseudo-probabilistic vs. B&I full-probabilistic			
475			
Mean		Modal	
0.35%	63.16%	0.79%	62.99%
35.12%	1.38%	34.68%	1.55%

Table 4-7: Percentage Data in Each Quadrant: Boulanger and Idriss (Conventional) vs. Boulanger and Idriss (Full-Probabilistic) $T_r = 1039$ Years

B&I pseudo-probabilistic vs. B&I full-probabilistic			
1039			
Mean		Modal	
0.83%	59.57%	1.04%	59.37%
39.42%	0.18%	39.21%	0.38%

Table 4-8: Percentage Data in Each Quadrant: Boulanger and Idriss (Conventional) vs. Boulanger and Idriss (Full-Probabilistic) $T_r = 2475$ Years

B&I pseudo-probabilistic vs. B&I full-probabilistic			
2475			
Mean		Modal	
1.03%	57.39%	1.28%	57.22%
41.52%	0.05%	41.28%	0.22%

The significance of these results is that potentially, in 1 to 4 percent of cases, the conventional liquefaction triggering methods are clearly over predicting the initiation of liquefaction. Although this would make it appear that in 95% or greater of cases that the prediction of liquefaction hazard would be the same with both the pseudo-probabilistic and performance-based methods, this is not necessarily the case. Because of the trends noted in the figures above, on average, it appears that the performance-based method will still give lower values of FS_L than the pseudo-probabilistic method. To explain how the methods do not necessarily compute equivalent values for liquefaction hazard, an example is provided.

Consider the hypothetical case of a prediction of $FS_L = 0.9$ from the full-probabilistic method, and a prediction of $FS_L = 0.3$ from the pseudo-probabilistic method. In this case, both predictions would indicate liquefaction, and would thus plot in quadrant 3. Although these values both represent the same liquefaction initiation prediction, they do not represent the same liquefaction initiation hazard. In terms of FS_L , it is somewhat difficult to compare the actual liquefaction initiation hazard of these predictions. In order to compare the liquefaction triggering hazard in a more precise manner, a simple conversion to the probability of liquefaction (P_L) can be made. This conversion can be done using either the Ku et al. or Boulanger and Idriss methods by using equations (15) and (34), respectively. By using these equations, the results of the value of $FS_L = 0.9$ gives: $P_L = 50.4\%$ and $P_L = 58.2\%$, while the value $FS_L = 0.3$ gives: $P_L = 99.9\%$ and $P_L = 99.1\%$. From these P_L values, the actual liquefaction initiation hazard can more accurately be analyzed, as the $FS_L = 0.9$ prediction indicated that the soil will be about as likely to liquefy as to

not liquefy, while the $FS_L = 0.3$ prediction indicates that liquefaction is almost guaranteed. These results represent how the actual liquefaction hazard can vary significantly even though predictions of liquefaction initiation using different FS_L methods appear to agree.

To see the full effect of the conversion to the realm of P_L , Figure 4-24 and Figure 4-25 show examples of the comparison of P_L at a return period of 475 years. In the Ku et al. comparison, out of the 45,590 predictions, 42 percent of the performance-based values predicted a lower liquefaction hazard compared to the conventional method, while 26% percent predicted a lower hazard for the conventional method. The remainder of the values computed an equivalent hazard with both methods. For the Boulanger and Idriss methods, the performance-based method predicted a lower liquefaction hazard 23% of the time compared to the conventional method which predicted a lower liquefaction hazard 18% of the time. The remainder of predictions gave equivalent values for the predicted liquefaction hazard regardless of the method used. This paints a significantly different picture than the FS_L comparisons, as a much larger percentage of the analysis could potentially calculate a reduced liquefaction hazard with use of the performance-based method.

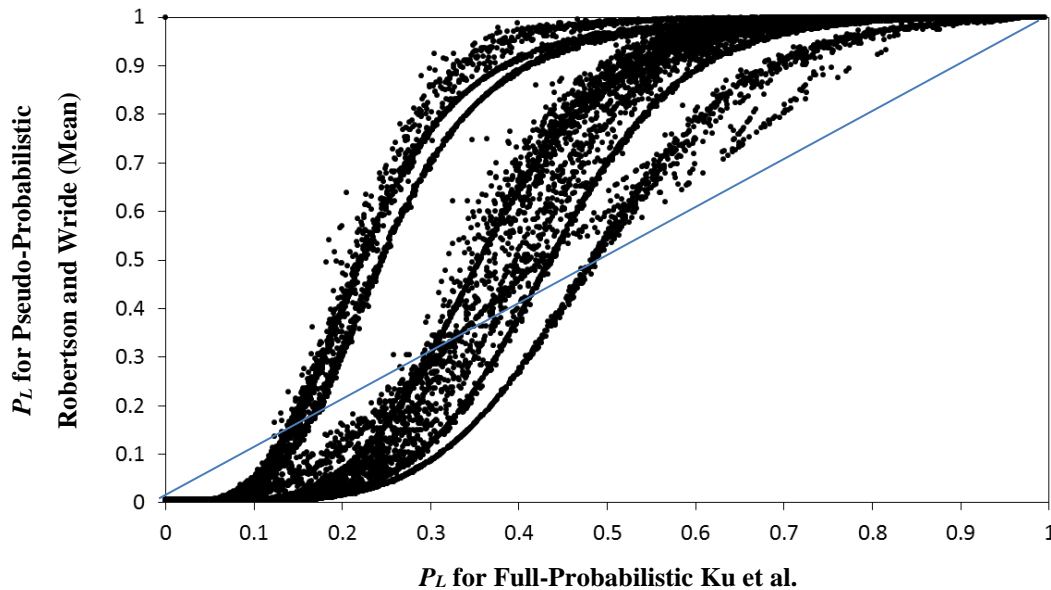


Figure 4-24: Probability of liquefaction values from study (using Ku et al. equation) $T_r = 475$.

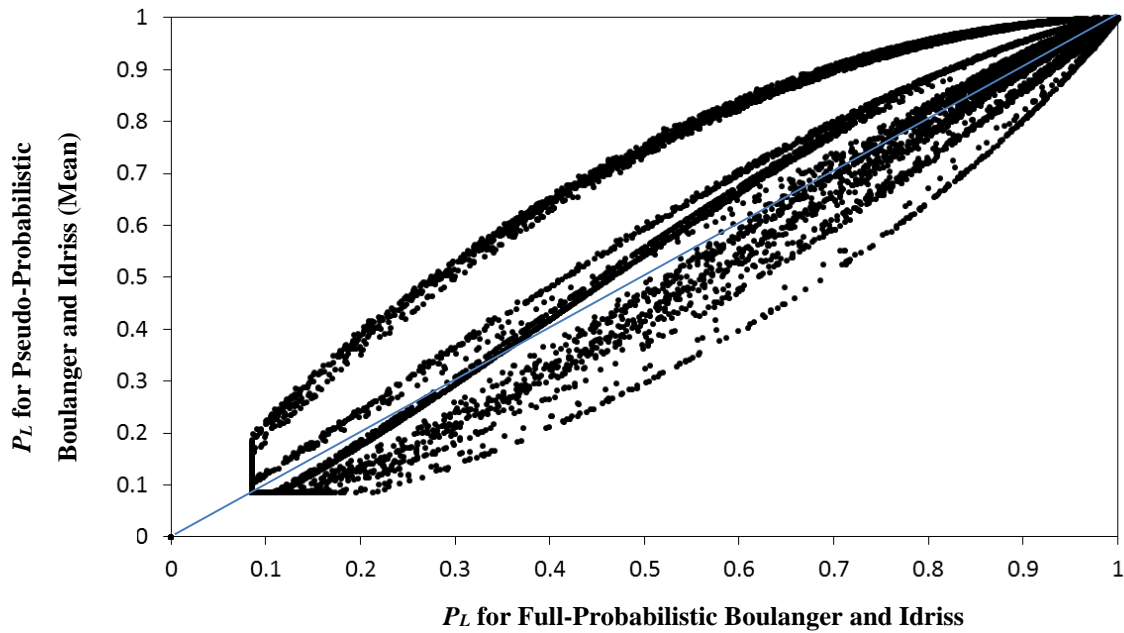


Figure 4-25: Probability of liquefaction values from study (using Boulanger and Idriss equation) $T_r = 475$.

Even though only a relatively small percentage of cases disagree in the prediction of liquefaction when considering FS_L , by looking at the P_L , which is facilitated by a probabilistic framework, the conventional analysis on average will predict a slightly greater liquefaction hazard. This means that in many cases the conventional analysis would require a larger amount of ground improvement to bring the soil to a satisfactory state to resist liquefaction and related hazards. This also signifies the possibility that the use of a performance-based method could provide cost savings in a potential design.

4.3 Settlement Results

This section presents all results from the study for calculated liquefaction-induced settlement estimates. Included is a discussion of the results of the comparative study between the fully-probabilistic method and the pseudo- and semi-probabilistic methods.

4.3.1 Example of Results Calculated by CPTLiquefY

After *CPTLiquefY* has completed a full-probabilistic analysis, the settlement results can be viewed. Under the “Settlement Results” tab, the data for the total ground surface settlement hazard curve is shown. This hazard curve represents the expected settlement values, at that site, for return periods ranging from the 475 year to the 10,000 year return period. This data is easily copied and pasted into Excel for plotting. An example of a full-probabilistic settlement hazard curve is shown in Figure 4-26.

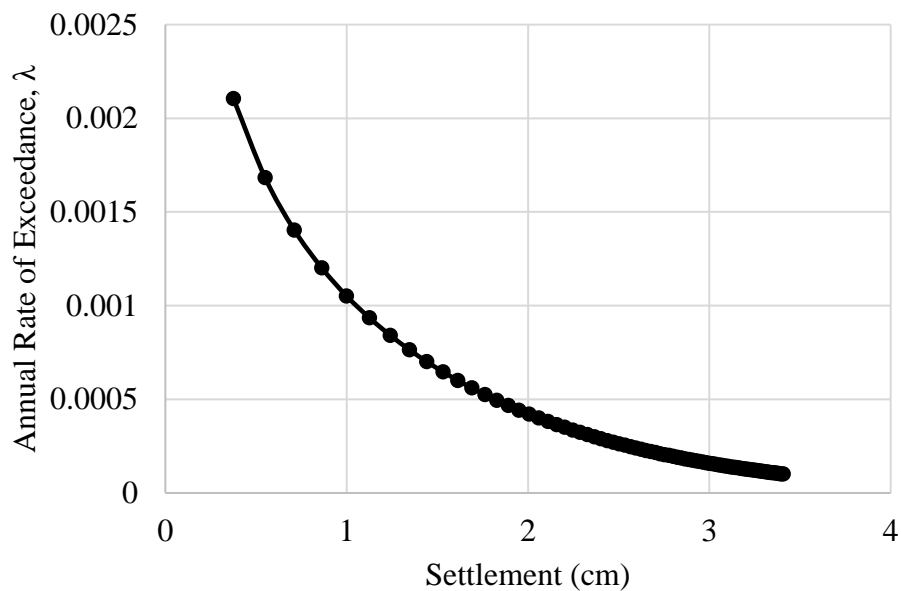


Figure 4-26: Example settlement hazard curve.

4.3.2 Comparison of Full-Probabilistic, Pseudo-Probabilistic, and Semi-Probabilistic

First, in areas of low seismicity the pseudo-probabilistic methods calculated about 10-50% higher settlement values than the PBEE method. This relationship is logical because the pseudo-probabilistic method does not take into account the low probability of large earthquakes occurring. However, with higher return periods, the PBEE method predicted about 5-50% more settlement than pseudo-probabilistic procedures. Second, in areas of medium to high seismicity the pseudo-probabilistic method predicts similar settlement values to the full-probabilistic method for lower

return periods, but about 30-100% less settlement values at higher return periods. The higher the return period and the seismicity of a city, the more the pseudo-probabilistic method under-predicts settlements. These trends reflect those found in the SPT study. Finally, by comparing the liquefaction triggering methods, both methods generally calculate similar settlement values, but the Boulanger and Idriss method proves to be more conservative than the Robertson and Wride method.

A comparative study is also performed for the semi-probabilistic settlement approach and the PBEE settlement approach. Similar trends observed from the pseudo-probabilistic comparative study are observed from the semi-probabilistic approach. However, at the higher return periods, the semi-probabilistic approach tends to under-predict settlements marginally more than the pseudo-probabilistic approach. Also, across all return periods, the data scatter for the semi-probabilistic approach is tighter than the pseudo-probabilistic results. This trend indicates a slightly higher level of consistency and efficiency as compared to the pseudo-probabilistic approach.

To see these trends visually, comparison plots were created to compare the pseudo-probabilistic and semi-probabilistic results to the full-probabilistic results. These plots are presented in Figure 4-27 through Figure 4-44. Figure 4-27 through Figure 4-35 represent all cities and profiles using the Robertson and Wride (2009) method, with the best fit line shown in blue. Figure 4-36 through Figure 4-44 represent all cities and profiles using the Boulanger and Idriss (2014) method, with the best fit line shown in red. Also included on each comparison plot is a one-to-one line, shown in black. If the pseudo-probabilistic or semi-probabilistic methods correlated perfectly with the full-probabilistic methods the data would fall directly on the one-to-one line. However, a data trend line that falls above the one-to-one line indicates an over-prediction of settlement by the pseudo-probabilistic and semi-probabilistic methods and, conversely, when the data trend line plots below the one-to-one line pseudo-probabilistic and semi-probabilistic methods are under predicting settlement.

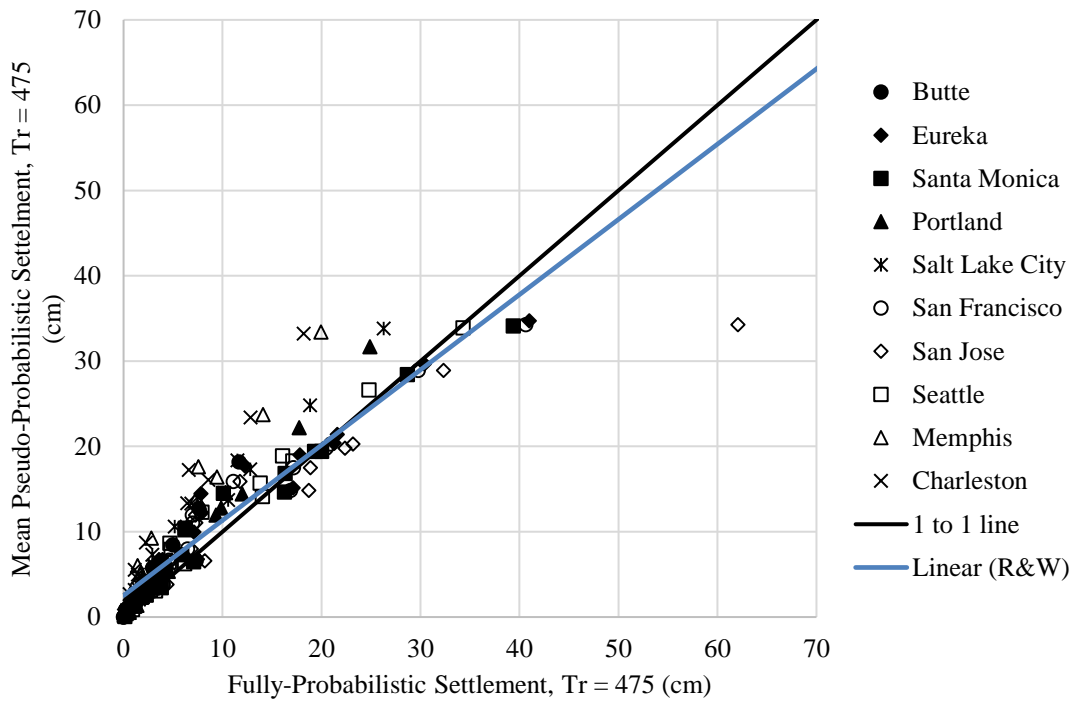


Figure 4-27: Mean magnitude pseudo-probabilistic versus fully-probabilistic for the 475 year return period using the Robertson and Wride liquefaction triggering procedure.

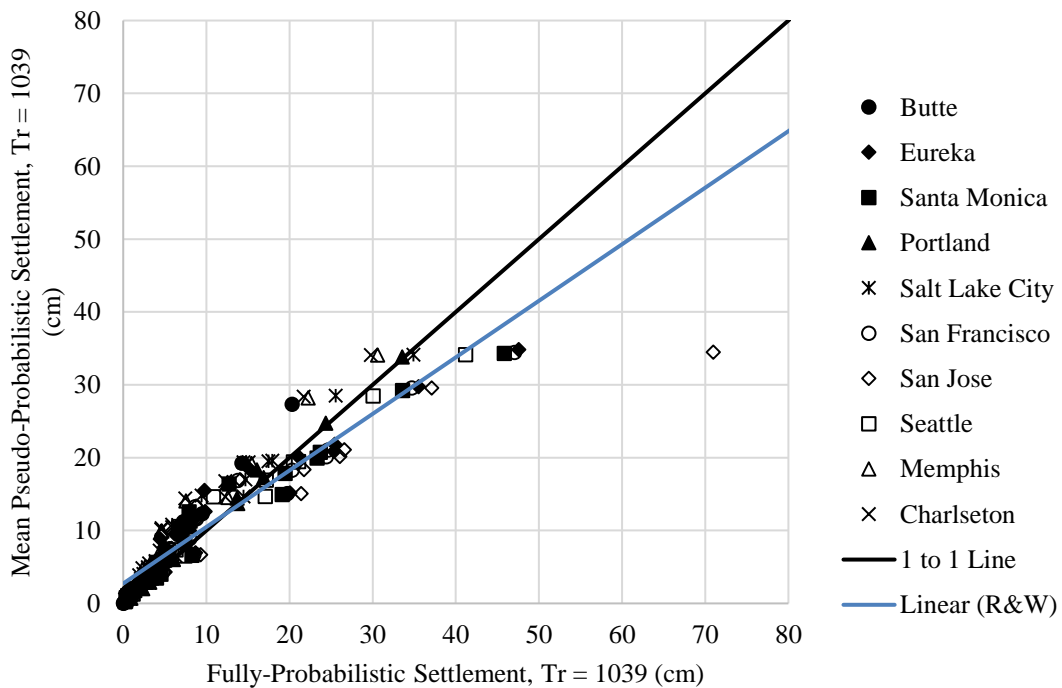


Figure 4-28: Mean magnitude pseudo-probabilistic versus fully-probabilistic for the 1039 year return period using the Robertson and Wride liquefaction triggering procedure.

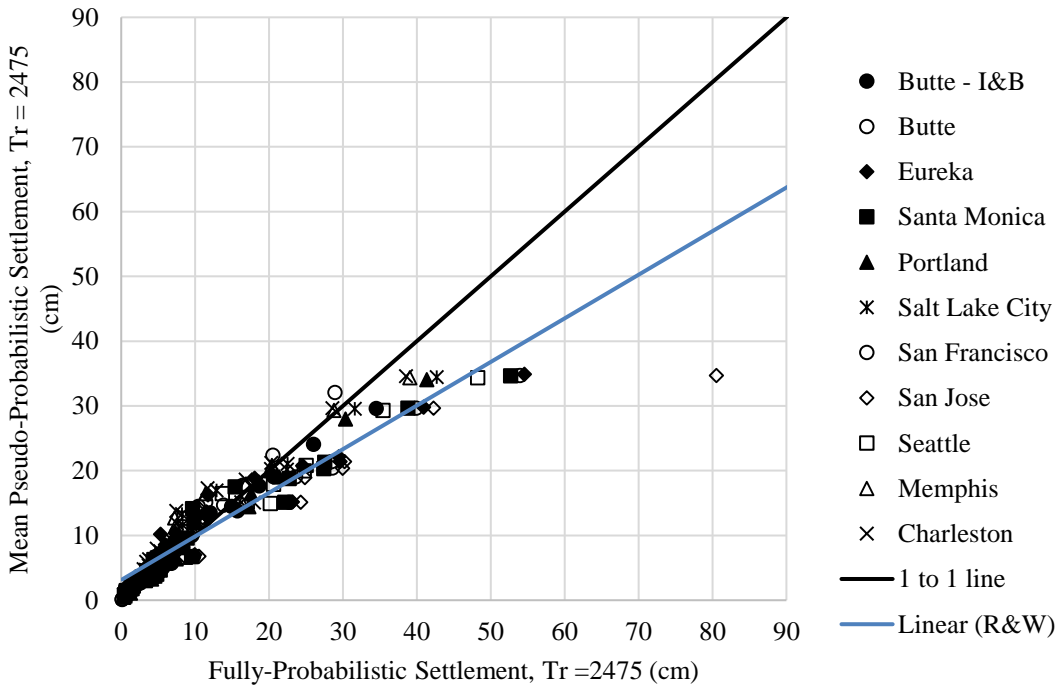


Figure 4-29: Mean magnitude pseudo-probabilistic versus fully-probabilistic for the 2475 year return period using the Robertson and Wride liquefaction triggering procedure.

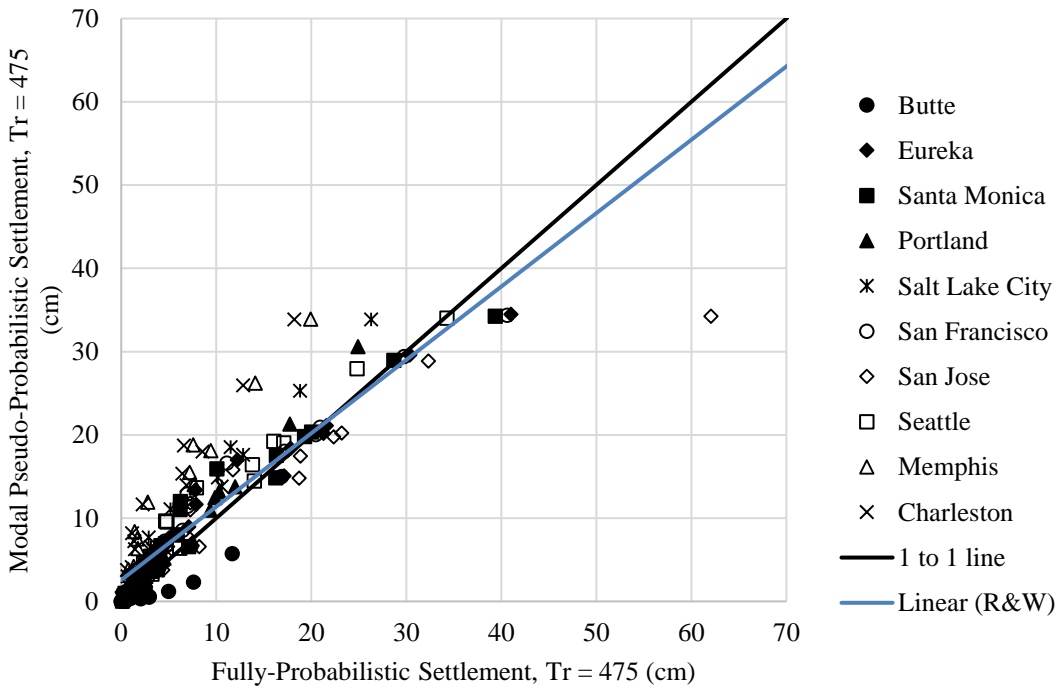


Figure 4-30: Modal magnitude pseudo-probabilistic versus fully-probabilistic for the 475 year return period using the Robertson and Wride liquefaction triggering procedure.

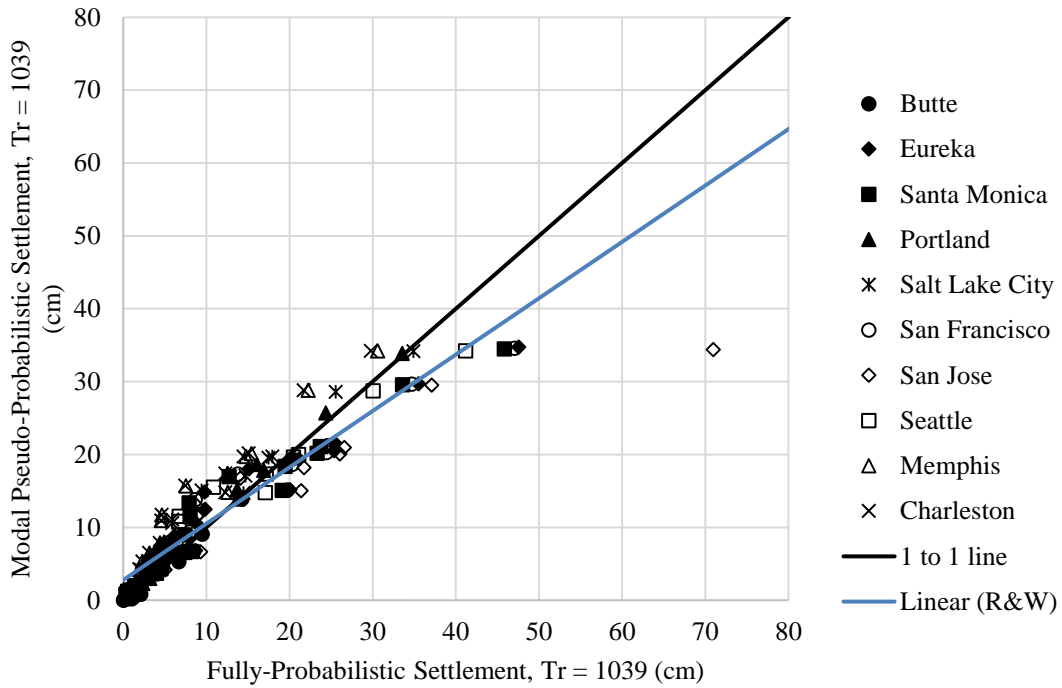


Figure 4-31: Modal magnitude pseudo-probabilistic versus fully-probabilistic for the 1039 year return period using the Robertson and Wride liquefaction triggering procedure.

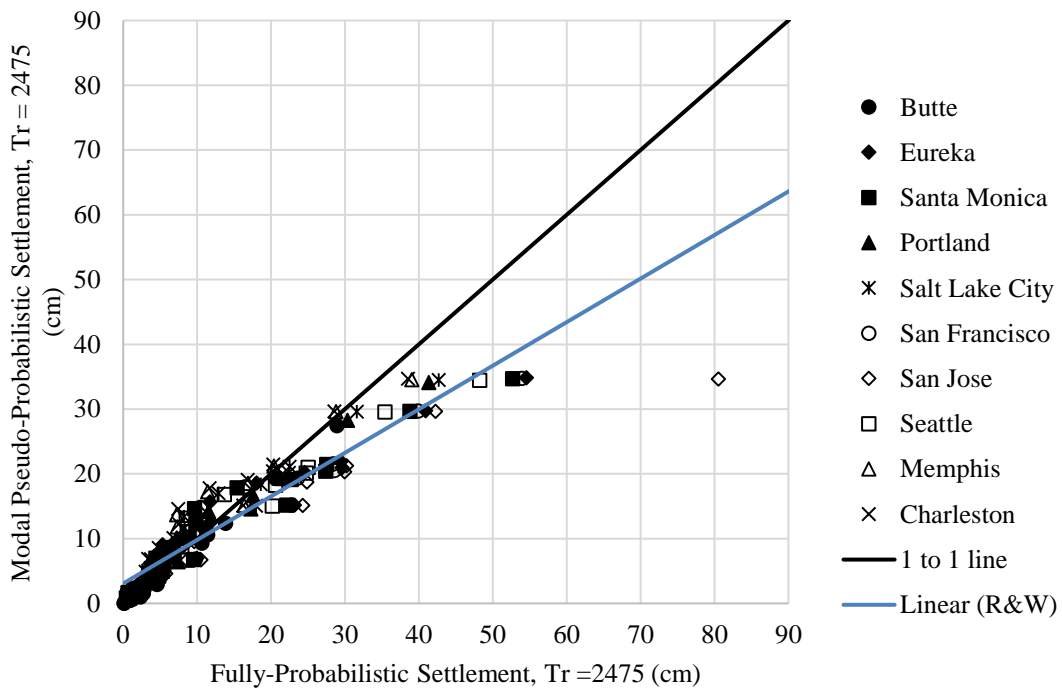


Figure 4-32: Modal magnitude pseudo-probabilistic versus fully-probabilistic for the 2475 year return period using the Robertson and Wride liquefaction triggering procedure.

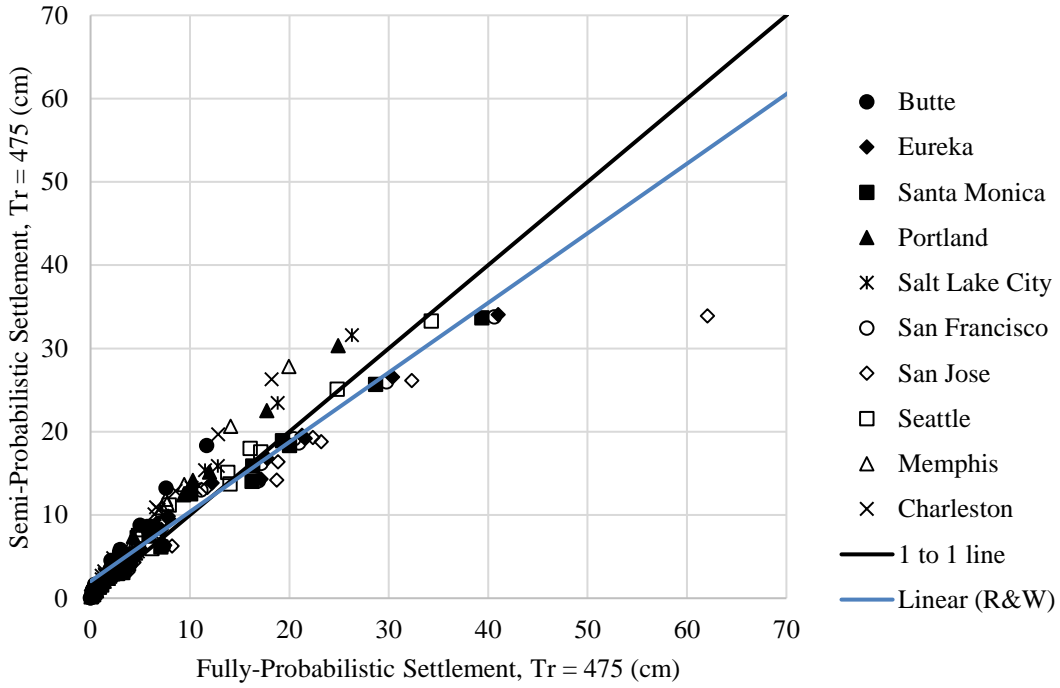


Figure 4-33: Semi-probabilistic versus fully-probabilistic for the 475 year return period using the Robertson and Wride liquefaction triggering procedure.

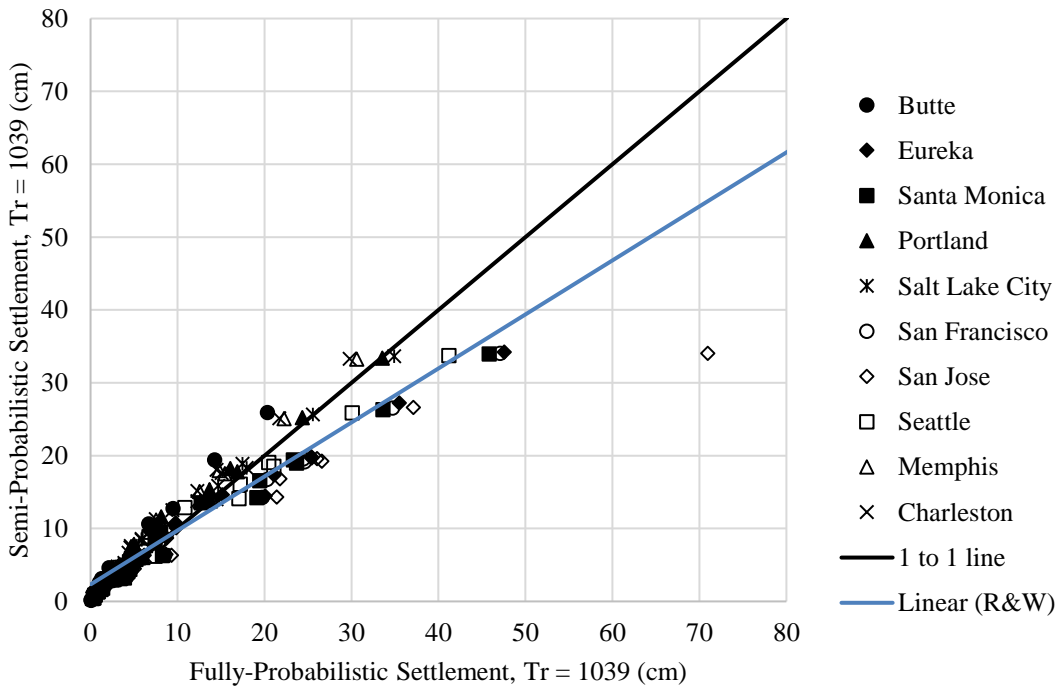


Figure 4-34: Semi-probabilistic versus fully-probabilistic for the 1039 year return period using the Robertson and Wride liquefaction triggering procedure.

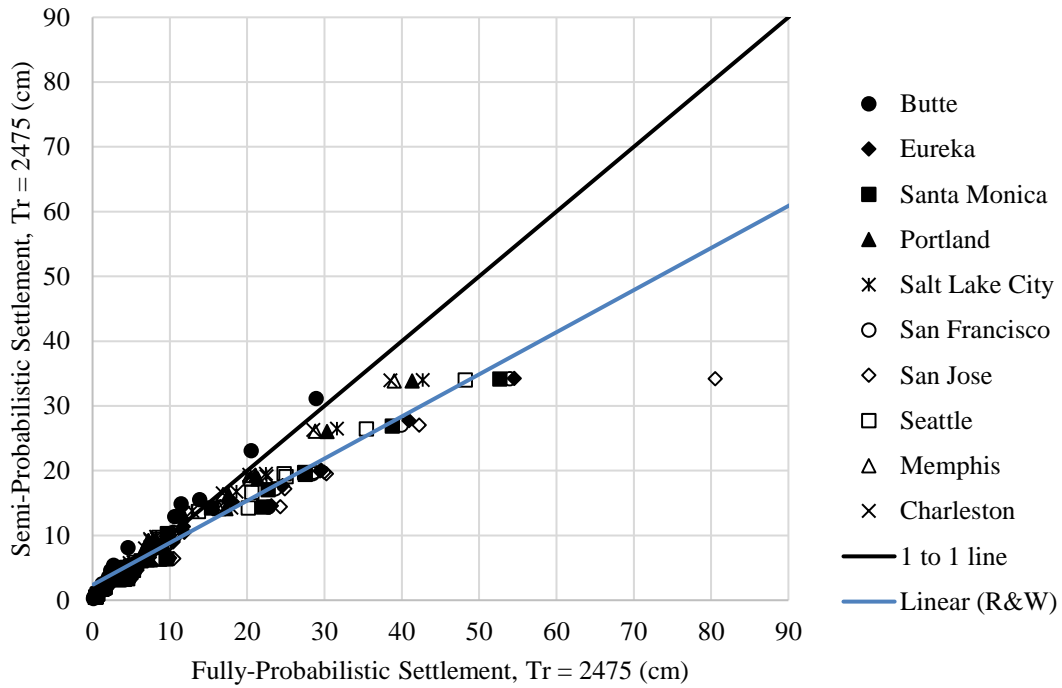


Figure 4-35: Semi-probabilistic versus fully-probabilistic for the 2475 year return period using the Robertson and Wride liquefaction triggering procedure.

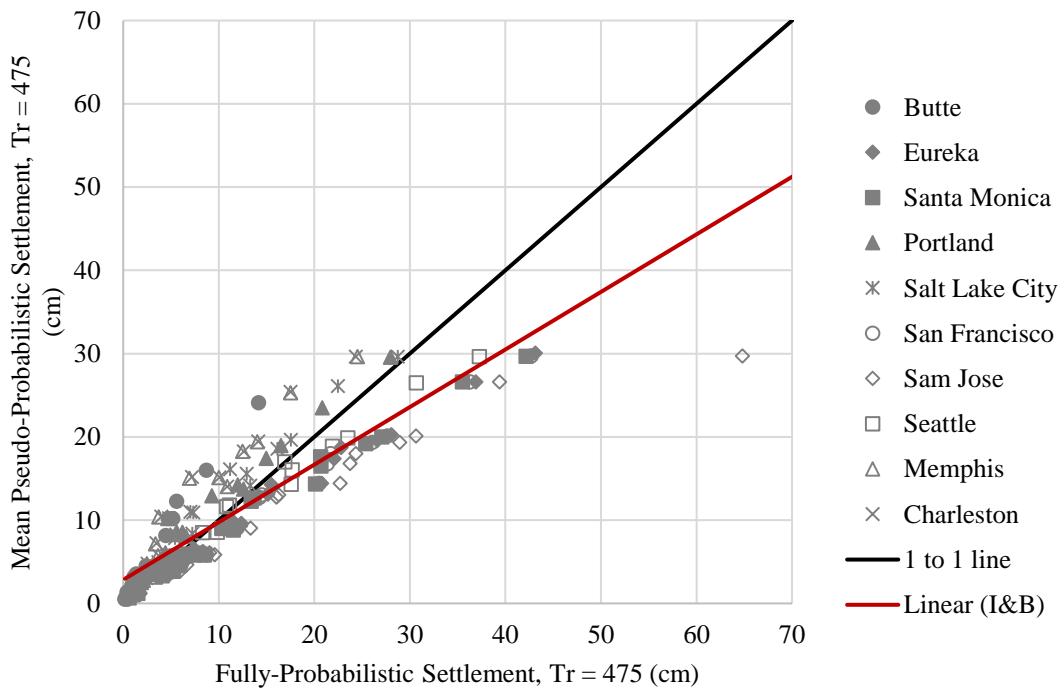


Figure 4-36: Mean magnitude pseudo-probabilistic versus fully-probabilistic for the 475 year return period using the Boulanger and Idriss liquefaction triggering procedure.

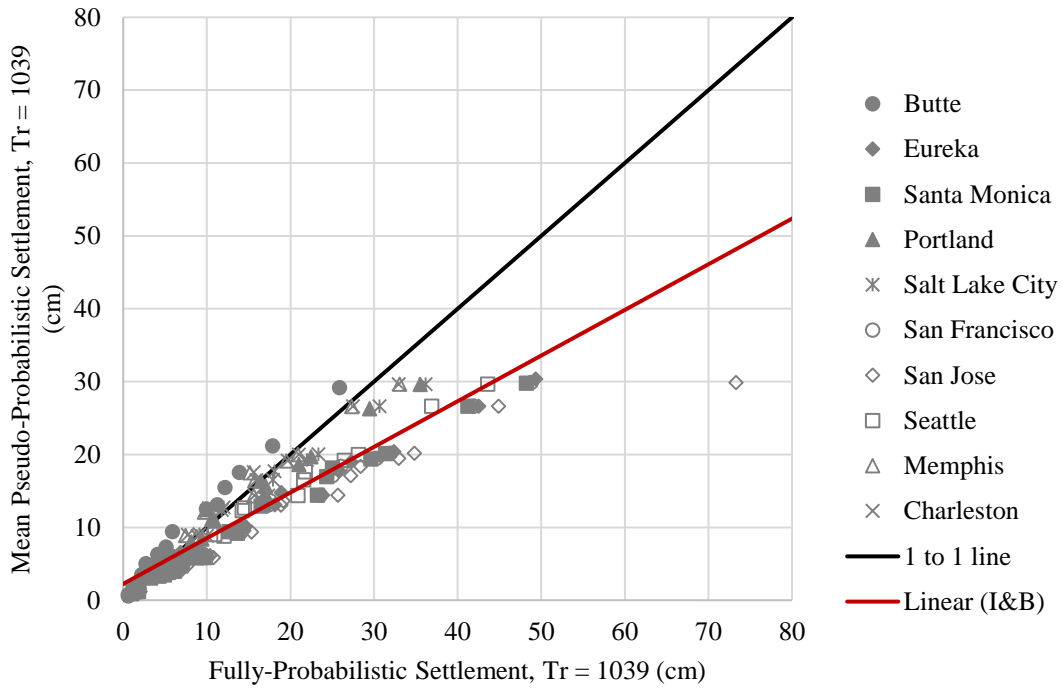


Figure 4-37: Mean magnitude pseudo-probabilistic versus fully-probabilistic for the 1039 year return period using the Boulanger and Idriss liquefaction triggering procedure.

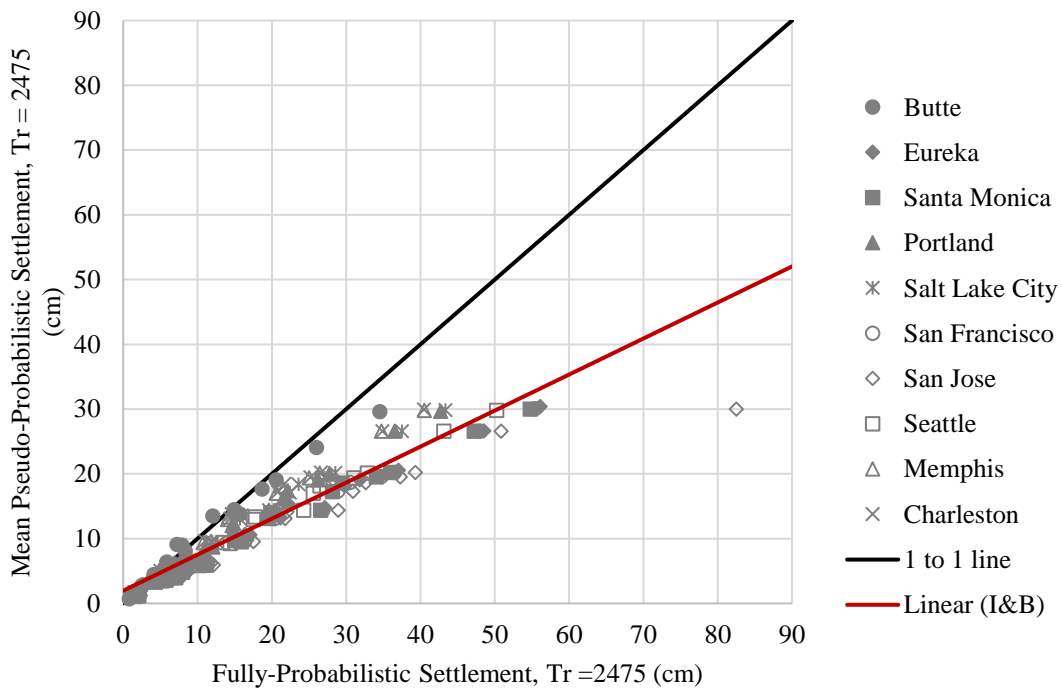


Figure 4-38: Mean magnitude pseudo-probabilistic versus fully-probabilistic for the 2475 year return period using the Boulanger and Idriss liquefaction triggering procedure.

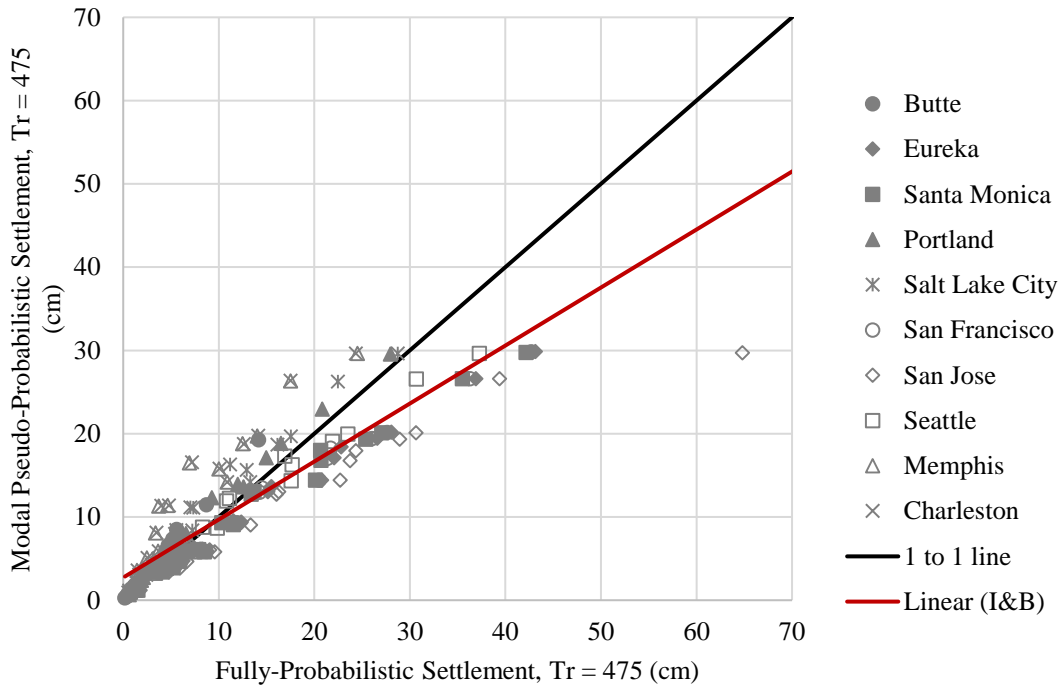


Figure 4-39: Modal magnitude pseudo-probabilistic versus fully-probabilistic for the 475 year return period using the Boulanger and Idriss liquefaction triggering procedure.

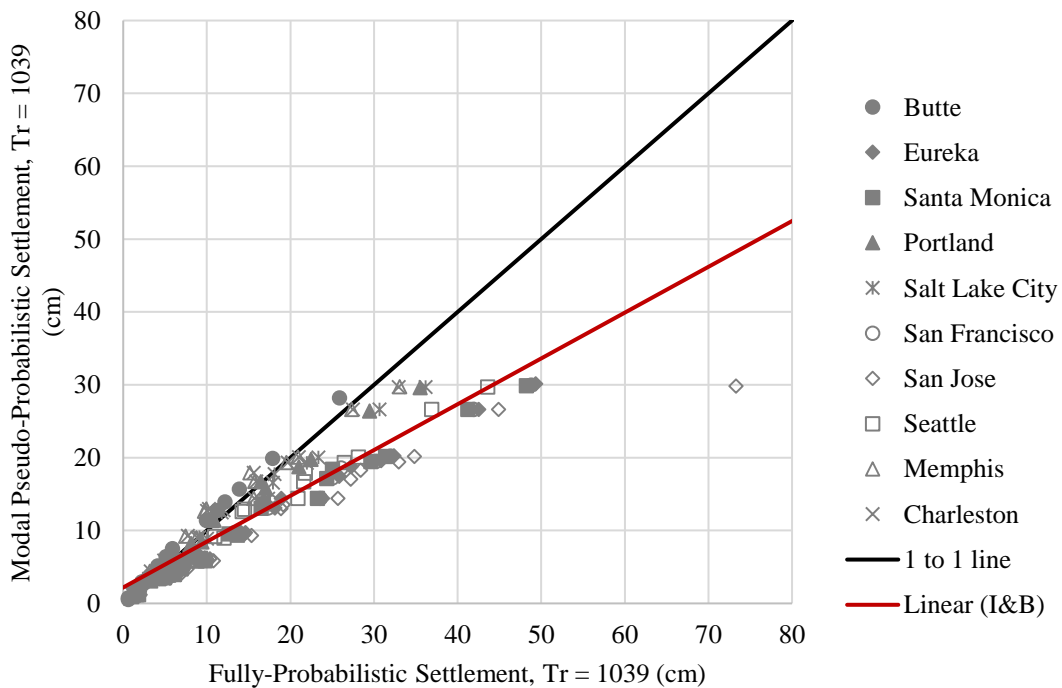


Figure 4-40: Modal magnitude pseudo-probabilistic versus fully-probabilistic for the 1039 year return period using the Boulanger and Idriss liquefaction triggering procedure.

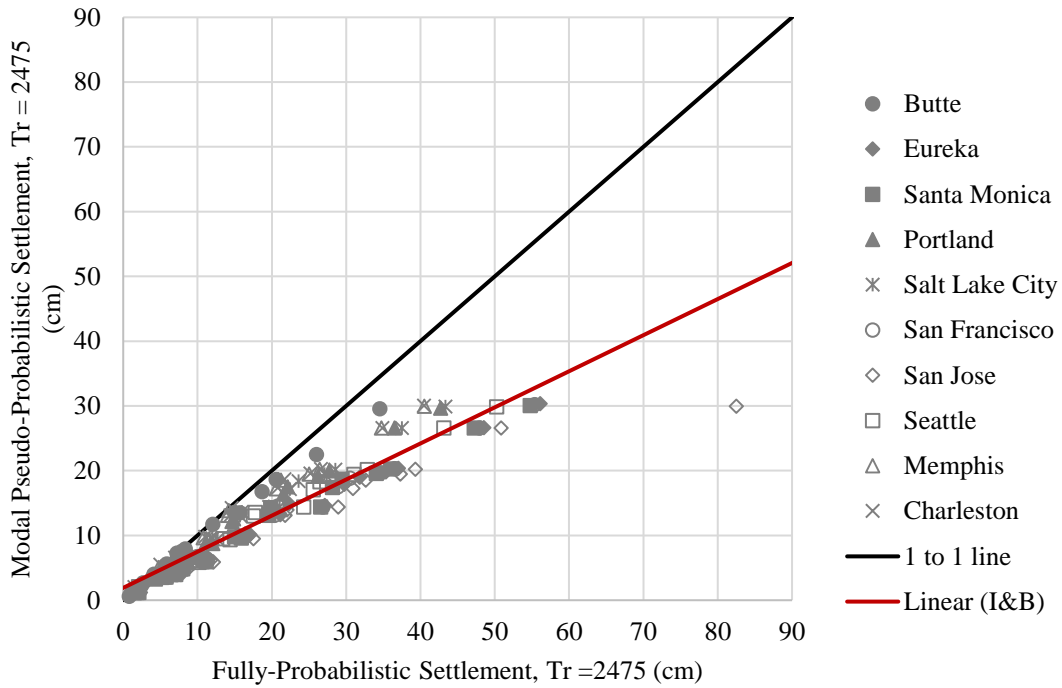


Figure 4-41: Modal magnitude pseudo-probabilistic versus fully-probabilistic for the 2475 year return period using the Boulanger and Idriss liquefaction triggering procedure.

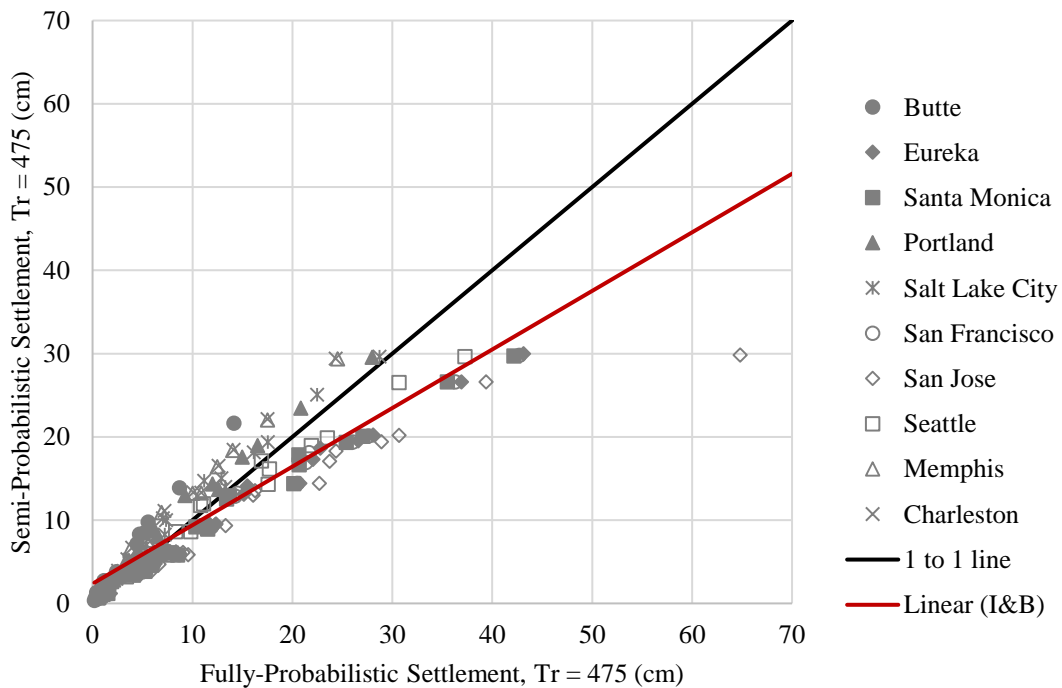


Figure 4-42: Semi-probabilistic versus fully-probabilistic for the 475 year return period using the Boulanger and Idriss liquefaction triggering procedure.

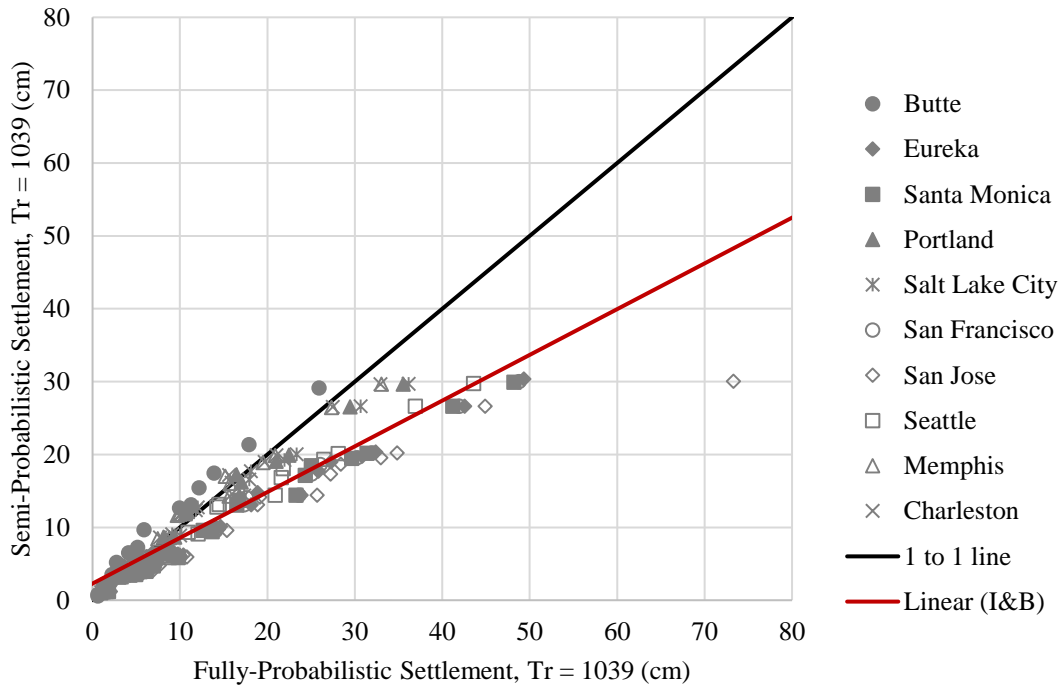


Figure 4-43: Semi-probabilistic versus fully-probabilistic for the 1039 year return period using the Boulanger and Idriss liquefaction triggering procedure.

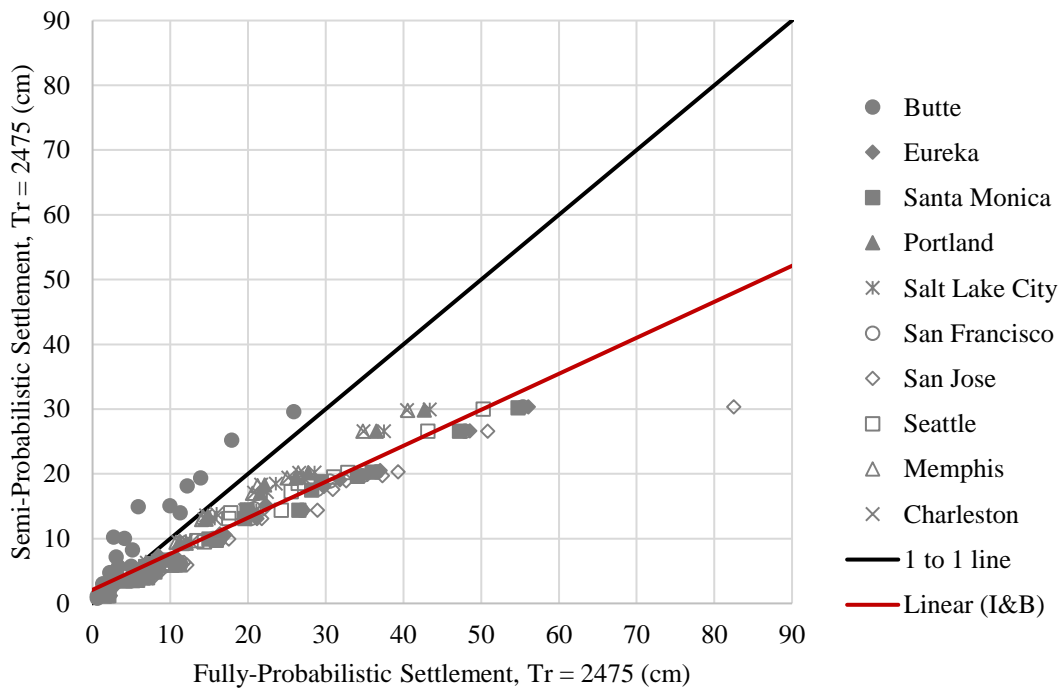


Figure 4-44: Semi-probabilistic versus fully-probabilistic for the 2475 year return period using the Boulanger and Idriss liquefaction triggering procedure.

The data trend lines tend to correlate with the one-to-one line fairly well up to a certain level of settlement for each return period when comparing the full-probabilistic approach to the pseudo-probabilistic (mean magnitude) approach. The Robertson and Wride data, from the two settlement approaches, tend to match up well until about 20cm, 15cm, and 10cm of settlement for the 475 year, 1039 year, and 2475 year return periods, respectively. While the Boulanger and Idriss data, from the two settlement approaches, tend to line up fairly well until about 10cm, 5cm, and 3cm for the 475 year, 1039 year, and 2475 year return periods, respectively. The modal magnitude pseudo-probabilistic approach follows similar trends, but digress from the one-to-one line at lower values. The Robertson and Wride modal magnitude pseudo-probabilistic data lines up with the PBEE data fairly well until about 13cm, 10cm, and 6cm for the 475 year, 1039 year, and 2475 year return periods, respectively. While the Boulanger and Idriss data averages line up fairly well until about 8cm, 6cm, and 5cm for the 475 year, 1039 year, and 2475 year return periods, respectively.

To further examine the source of the trends mentioned above, the settlement values computed from pseudo and semi-probabilistic methods, for the 1039 year and 2475 year return periods, were entered into the probabilistic hazard curve to back-calculate the actual return period associated with that settlement value. The results of this process are summarized as box and whisker plots in Figure 4-45 and Figure 4-46.

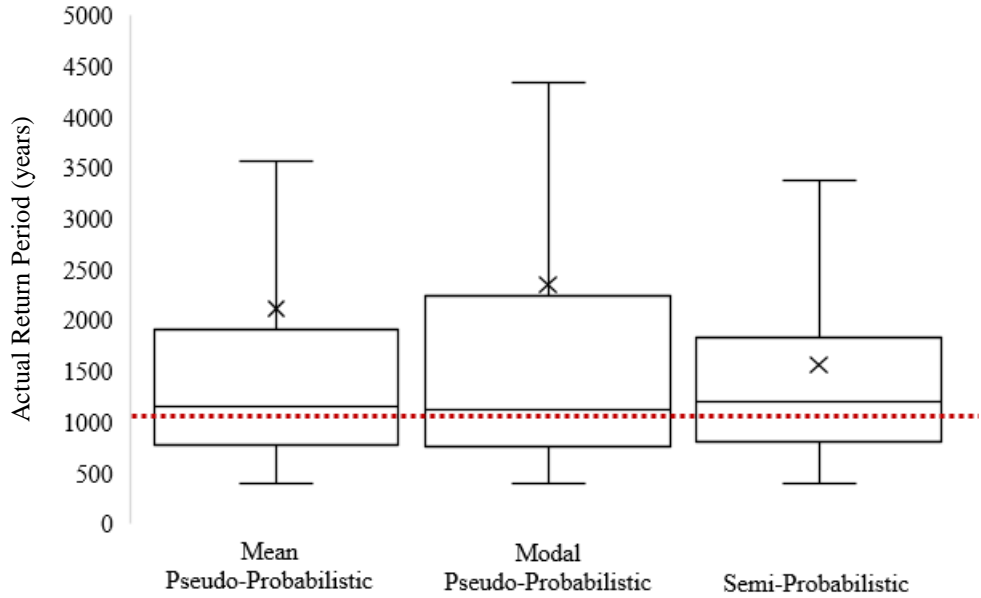


Figure 4-57: Box and whisker plots of actual return periods versus assumed 1039 year return period in the settlement analysis.

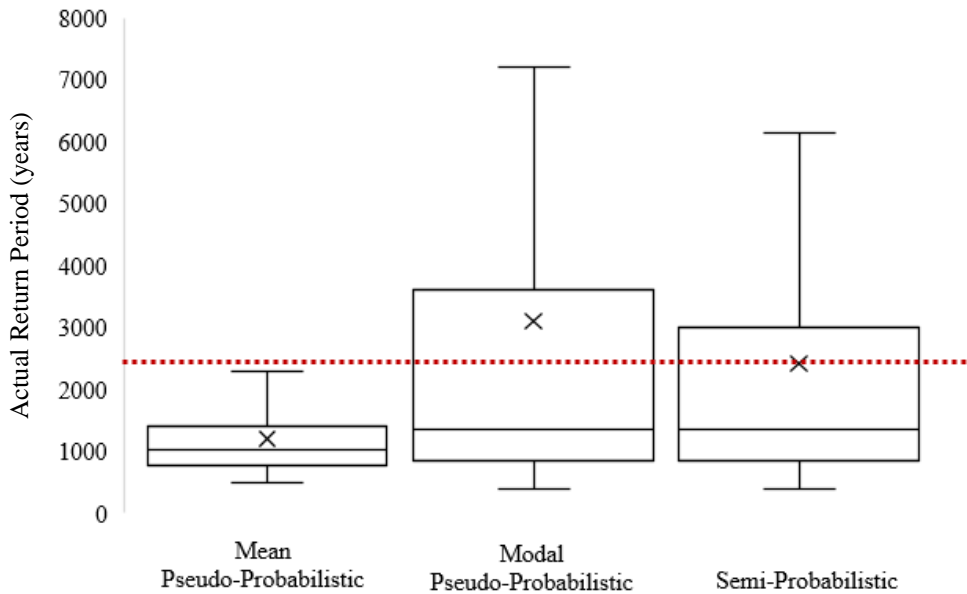


Figure 4-76: Box and whisker plots of actual return periods versus assumed 2475 year return period in the settlement analysis.

The box and whisker plots shown in Figure 4-45 and Figure 4-46 illustrate the median, first and third quartiles, maximum and minimum values, and the average (marked by an “x”) values of the return periods. As noted previously, these values represent actual return periods because they

are generated from the full-probabilistic settlement hazard curve. The assumed return period is presented as a red dashed line for reference.

The results for the 1039 return period box plots (Figure 4-45) seem to match the results from Figure 4-27 through Figure 4-44 fairly well. The one-to-one plots and the box and whisker plots both indicated a fairly good match between approaches for the 1039 return period. The results from the 2475 return period (Figure 4-46) also line up with the results from the one-to-one plots, by indicating an under-prediction of post-liquefaction settlements from conventional standards. The data suggest that, on average the deterministic analyses underestimate the seismic hazard by 50% when considering a larger seismic event.

To examine these trends even further, a heat map was generated (Figure 4-47). Each number in the map represents the number of CPT soundings, out of the total 20, in which the pseudo-probabilistic approach predicted less settlement than the full-probabilistic approach. These values are presented for both triggering procedures, each return period, and both magnitudes (mean and modal) at each city. The cities are ordered from the lowest seismicity to the highest from top down.

	Robertson & Wride (2009)						Idriss & Boulanger (2014)					
	475		1039		2475		475		1039		2475	
	Mean	Modal	Mean	Modal	Mean	Modal	Mean	Modal	Mean	Modal	Mean	Modal
Butte, MT	2	20	4	20	3	19	0	0	1	1	12	18
Portland, OR	2	8	7	3	11	11	0	0	18	15	20	20
Memphis, TN	0	0	0	0	4	4	0	0	9	7	19	18
Seattle, WA	3	1	8	7	9	9	15	13	20	20	20	20
Salt Lake City, UT	0	0	1	1	9	8	0	0	15	14	20	20
San Francisco, CA	7	6	9	9	9	9	20	19	20	20	20	20
Charleston, S.C.	0	0	0	0	4	3	0	0	10	9	18	18
Santa Monica, CA	6	3	9	9	9	9	20	19	20	20	20	19
San Jose, CA,	9	9	9	9	9	10	20	20	20	20	20	20
Eureka, CA	6	6	8	8	8	8	18	20	19	20	20	20

Figure 4-77: A heat map representing the number of CPT soundings, out of 20 soundings, in which the pseudo-probabilistic method under predicted settlement compared to the full-probabilistic procedure.

The heat map reinforces the trends observed above. The heat map illustrates that the Boulanger and Idriss triggering procedure is under predicting settlement at a higher percentage than the Robertson and Wride method. This trend can also demonstrate how the Boulanger and Idriss method produces larger PBEE settlement values than the Robertson and Wride method. The

heat map reinforces the trend indicating that the under prediction of settlement increases with an increasing level of site seismicity and return period. The Robertson and Wride procedure shows about 50% of the CPT soundings under predicting settlement at the 2475 year return period. While the Boulanger and Idriss procedure shows under predicted settlements for almost 90% of the CPT soundings at the 2475 return period.

The heat map points out 3 outliers at Butte, MT for the modal magnitude pseudo-probabilistic values where all 20 profiles under predicted settlement for all three return periods. This discrepancy is likely due to a large difference in the MSF due to a significant difference in the mean and modal magnitudes at Butte, MT (Table 4-2). This discrepancy does not manifest in the Boulanger and Idriss procedure because of the differing MSF calculation methods. The Boulanger and Idriss procedure does not depend solely on the magnitude to calculate the MSF like the Robertson and Wride method.

At the 475-year return period the pseudo-probabilistic method generally over-predicted or the methods predicted similar settlement values. This trend is logical because the pseudo-probabilistic procedure uses a deterministic method of predicting settlements. Deterministic methods are considered to be a conservative approach because they typically consider the controlling scenario earthquake.

However, this idea is concerning after reviewing the results from the higher return periods. The data suggests, as the return period increased, the pseudo-probabilistic analyses under-predicted the level of liquefaction-induced settlement hazard by up to 90%. This trend is likely caused by the fact that the pseudo-probabilistic and semi-probabilistic methods compute post-liquefaction volumetric strains deterministically. Deterministic strain calculations ignore the inherent uncertainty associated with calculating strain values. The full-probabilistic procedure, however, accounts for this uncertainty, resulting in higher settlement estimations.

Results from the semi-probabilistic approach had less scatter but underestimated settlements at about the same percentage as the pseudo-probabilistic approach. The trends depicted in the semi-probabilistic results are very similar to the trends from the pseudo-probabilistic results. These similarities in the two methods' results suggest the uncertainty in the liquefaction triggering is less significant than the uncertainty in the strain calculations. These results also prove the semi-probabilistic method is not an improvement to the current pseudo-probabilistic methods. Significant calculations are required to perform the calculations necessary for the semi-

probabilistic approach and, therefore, may not be worth it for engineers to use this approach as a replacement to the pseudo-probabilistic approach. Engineers should either continue using the easier and equally accurate pseudo-probabilistic approach, or go all the way to the full-probabilistic approach for more accuracy.

By comparing the results, a comparison can be made between the Robertson and Wride and Boulanger and Idriss triggering methods. The two methods consistently predicted similar full-probabilistic settlements for the varying CPT soundings and cities. However, the Boulanger and Idriss procedure consistently produced larger settlement values. This trend indicates the Boulanger and Idriss method is a more conservative option than the Robertson and Wride method.

Pseudo-probabilistic methods are widely accepted in industry because they are considered to be a simple way to incorporate probabilistic ground motions into the liquefaction analysis. If, in fact, these methods are under-predicting liquefaction-induced settlements, then relying on pseudo-probabilistic methods for design presents a dangerous risk. This data suggests that pseudo-probabilistic design methods are a conservative option for areas of lower seismicity and lower return periods. However, according to this data, fully-probabilistic methods should be used for regions of higher seismicity and when designing for medium to large seismic events.

4.4 Lateral Spread Results

Presented in this section is the discussion of results of the lateral spread analysis. The general trends remain consistent with those found in the settlement results. However, as a different model is used in calculating lateral spread displacements there are some differences from the trends found in the settlement results. These differences will be emphasized in this section. As mentioned in the methodology section, two lateral spread geometries were analyzed. The first geometry was that of a gently sloping ground with a ground slope of 3% (referred to as lateral spread geometry 1). The second geometry was a level ground with a free face, with the height of the free face, H , set to 6m, and the length to the toe, L , set to 50m (referred to as lateral spread geometry 2).

4.4.1 Example of Results Calculated by *CPTLiquefY*

After *CPTLiquefY* has completed a full-probabilistic analysis, the lateral spread results can also be viewed under the “Lateral Spread Results” tab. Similar to the settlement results, the data

for a hazard curve is then displayed, showing estimated lateral spread results for return periods of 475 to 10,000 years. An example hazard curve for lateral spread is shown in Figure 4-48.

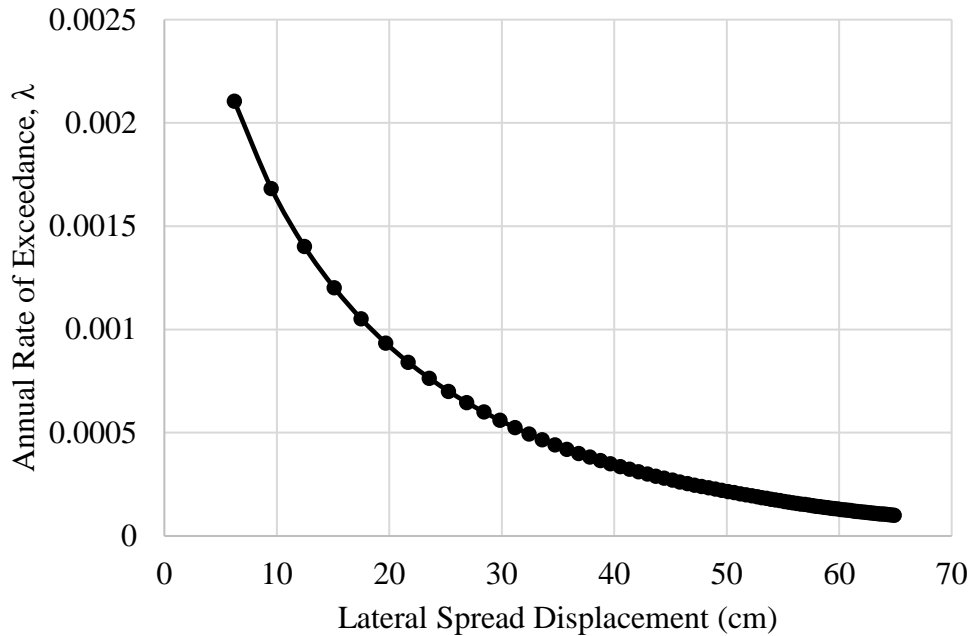


Figure 4-48 Example of lateral spread hazard curve.

4.4.2 Comparison of Full-Probabilistic, Pseudo-Probabilistic, and Semi-Probabilistic

Just as in the settlement analysis, the pseudo-probabilistic and full-probabilistic results were compared and trends were identified. The general trends were similar to those found in the settlement results. In areas of higher seismicity, the pseudo-probabilistic method calculated lower lateral spread displacements than the full-probabilistic method, especially at higher return periods. In areas of lower seismicity, both the pseudo-probabilistic and full-probabilistic calculated similar values at higher return periods, but the full-probabilistic method resulted in lower values at lower return periods. In general, the higher the seismicity of a site and the higher the return period, the more the pseudo-probabilistic method under-predicted the lateral spread, for both mean and modal magnitude calculations.

The two liquefaction triggering methods followed consistent trends to those seen in the settlement results. Lateral spread displacements calculated using the Boulanger and Idriss

procedure consistently showed more conservative values (for any method) than the Robertson and Wride procedure.

When comparing the semi-probabilistic and full-probabilistic results for lateral spread, the same trends found in the settlement results remain true. That is, the semi-probabilistic results show similar trends found in the pseudo-probabilistic comparison, but tend to show slightly lower values of lateral spread than the pseudo-probabilistic results. Also, there is much less scatter in this data, indicating more consistent results in the semi-probabilistic method. However, when compared to the full-probabilistic method, the semi-probabilistic approach has similar levels of accuracy as the pseudo-probabilistic approach. Therefore, the semi-probabilistic approach is not an improvement to the pseudo-probabilistic approach.

Comparison plots for lateral spread are shown in Figure 4-49 through Figure 4-66, showing the relationship between full-probabilistic results and the pseudo-probabilistic or semi-probabilistic results. One thing to note is that the trend line for the Robertson and Wride values in the pseudo-probabilistic comparisons lies slightly above the one-to-one line for the 475-year return period. This indicates that at low return periods, the full-probabilistic method under-predicts lateral spread displacements. While this is different than what was found in the settlement results, it is still consistent with the general trends seen. The “Robertson Data” trend line in this instance for settlement is below the one-to-one line due to a single value (soil profile 1 at San Jose). If this value were removed, the trend line for settlement would look identical to the trend line for lateral spread. That point was not as far from the general trend for lateral spread, and therefore did not have as big of an effect.

The comparison plots in Figure 4-49 through Figure 4-66 are only for lateral spread geometry 1. Lateral spread geometry 2 showed the exact same trends, only the values were scaled down. The comparison plots for lateral spread geometry 2 can be found in the Appendix.

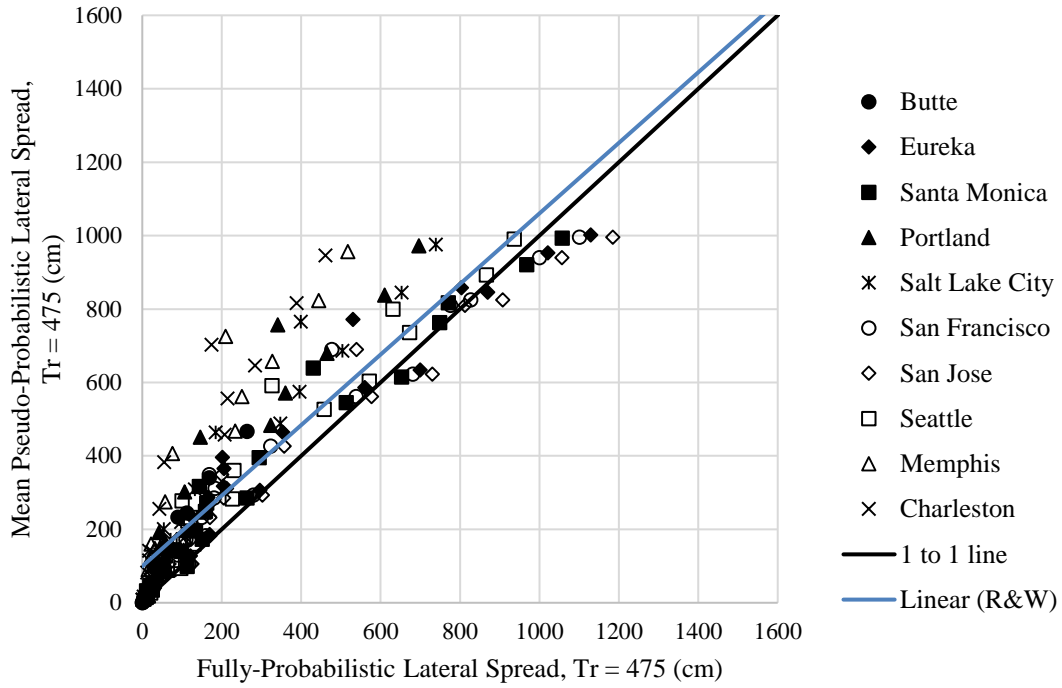


Figure 4-49: Mean magnitude pseudo-probabilistic versus fully-probabilistic for the 475 year return period using the Robertson and Wride liquefaction triggering procedure.

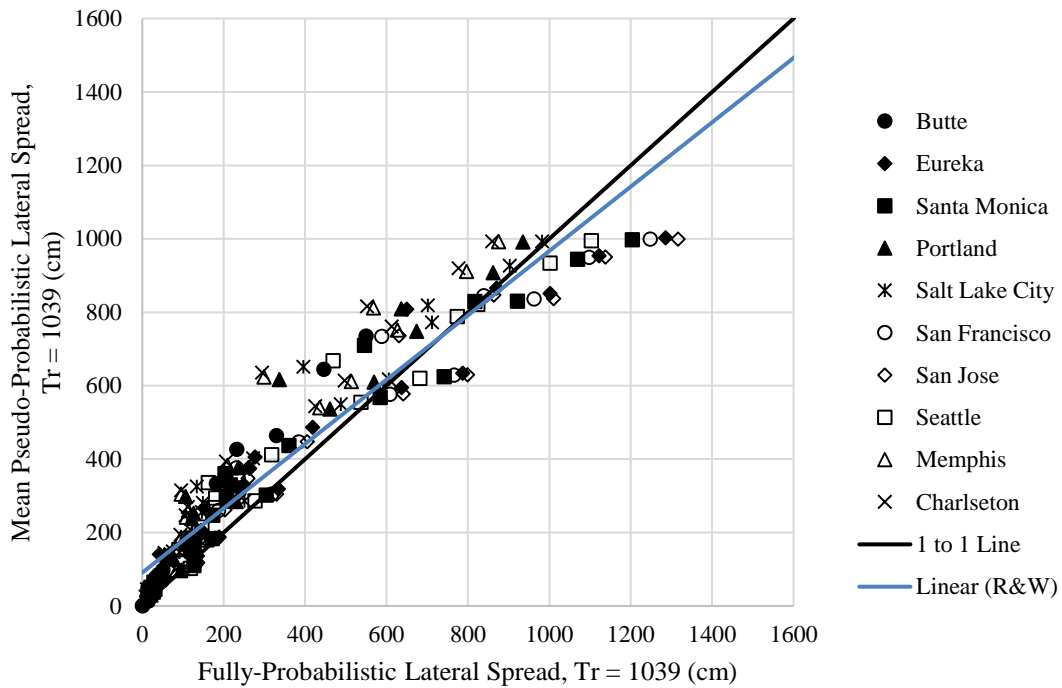


Figure 4-50: Mean magnitude pseudo-probabilistic versus fully-probabilistic for the 1039 year return period using the Robertson and Wride liquefaction triggering procedure.

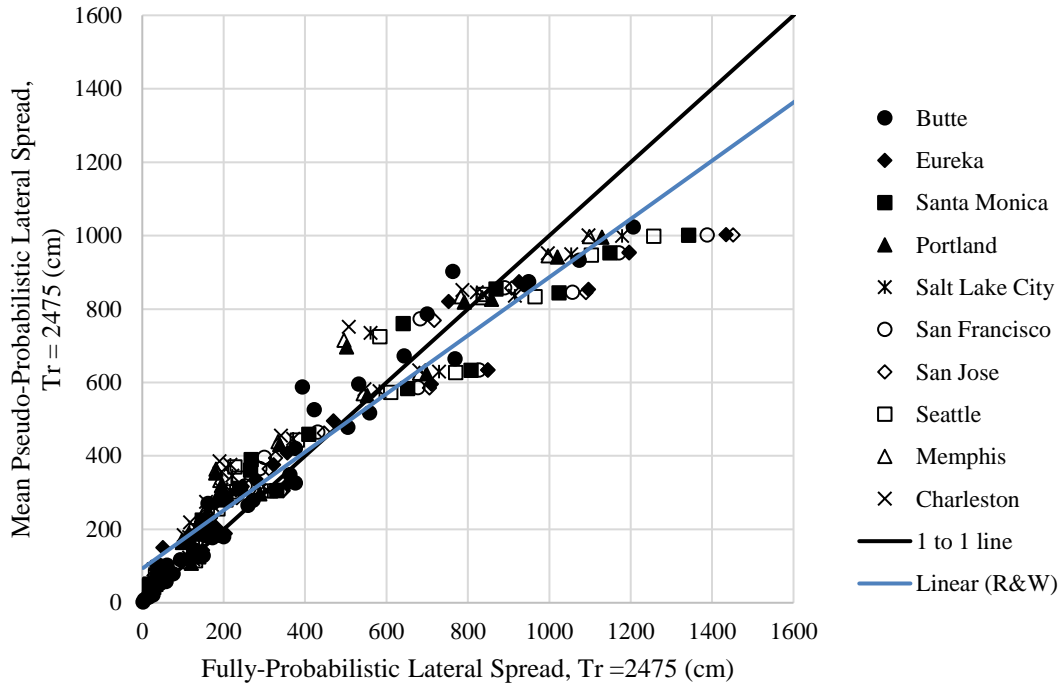


Figure 4-51: Mean magnitude pseudo-probabilistic versus fully-probabilistic for the 2475 year return period using the Robertson and Wride liquefaction triggering procedure.

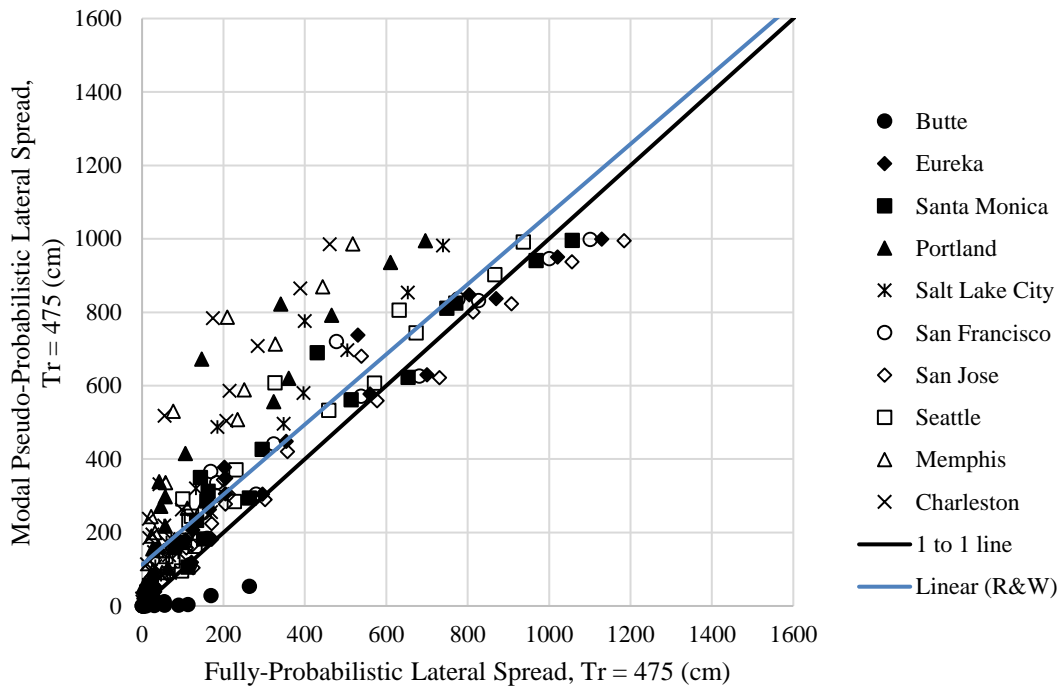


Figure 4-52: Modal magnitude pseudo-probabilistic versus fully-probabilistic for the 475 year return period using the Robertson and Wride liquefaction triggering procedure.

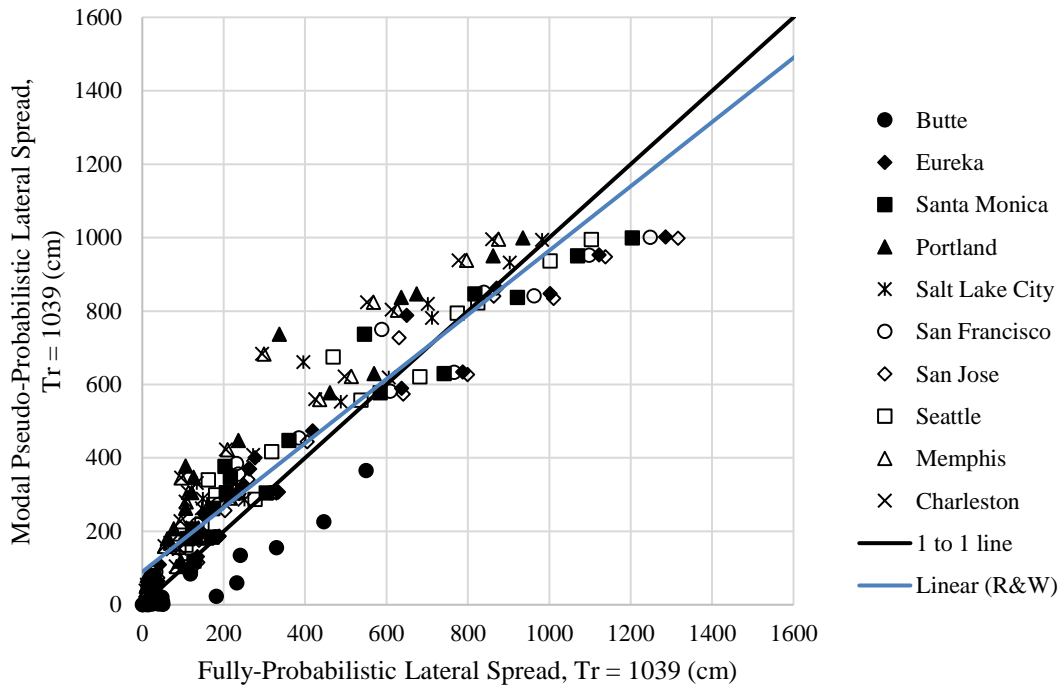


Figure 4-53: Modal magnitude pseudo-probabilistic versus fully-probabilistic for the 1039 year return period using the Robertson and Wride liquefaction triggering procedure.

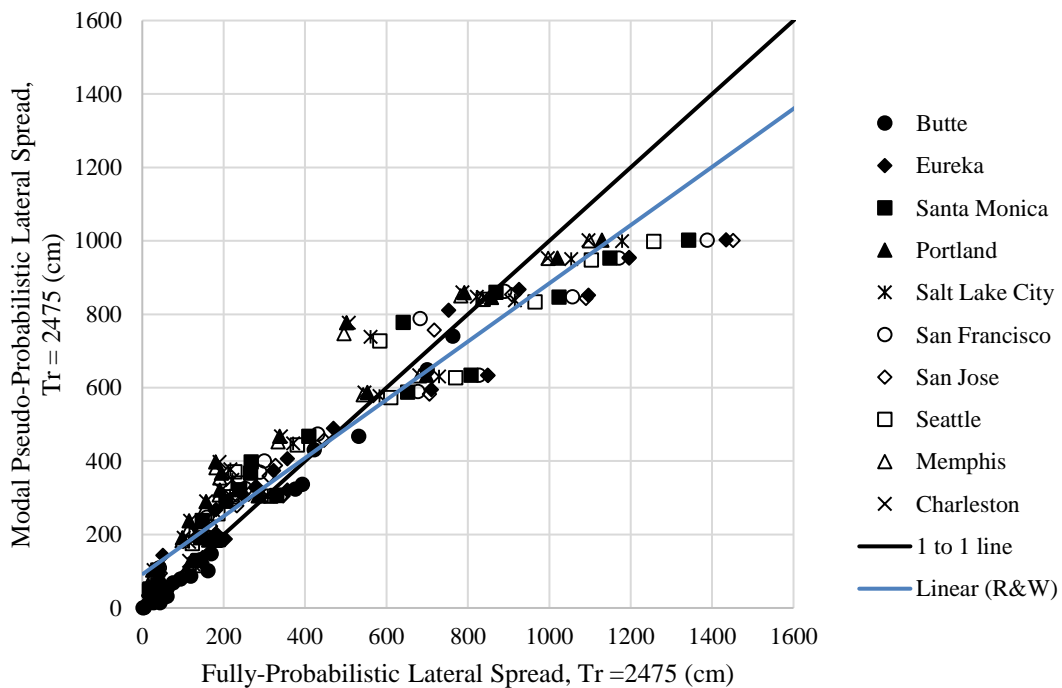


Figure 4-54: Modal magnitude pseudo-probabilistic versus fully-probabilistic for the 2475 year return period using the Robertson and Wride liquefaction triggering procedure.

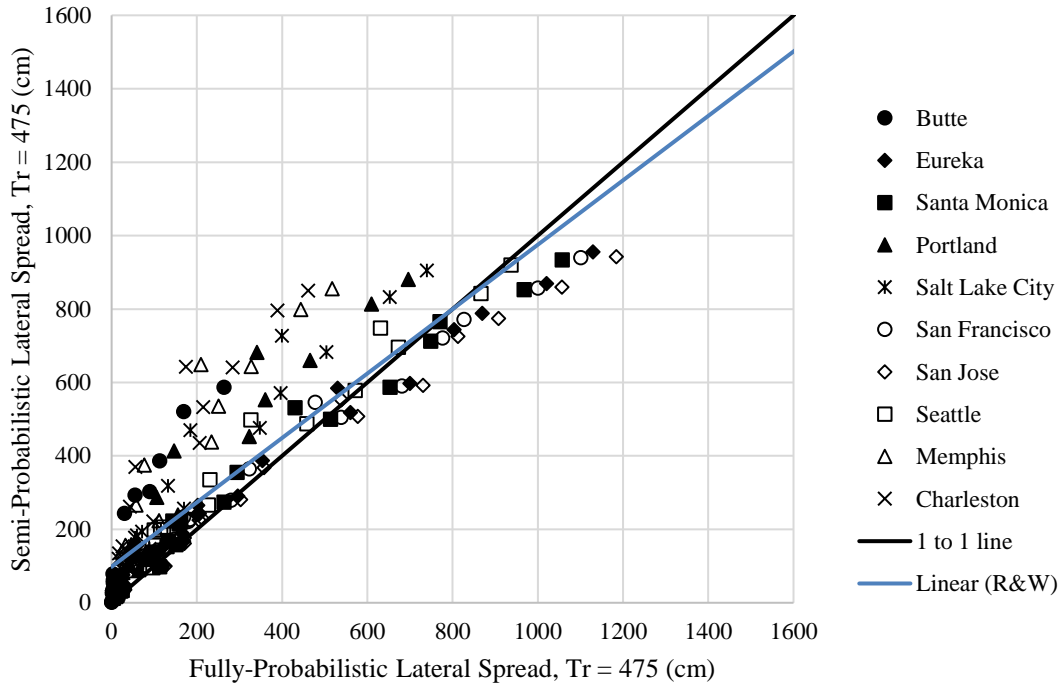


Figure 4-55: Semi-probabilistic versus fully-probabilistic for the 475 year return period using the Robertson and Wride liquefaction triggering procedure.

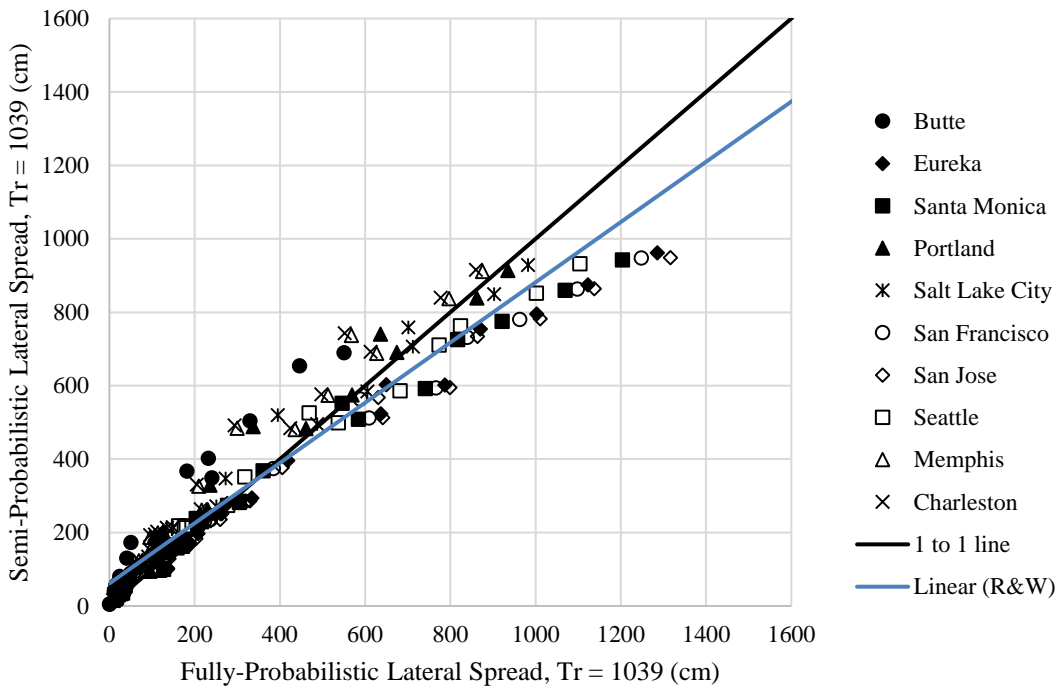


Figure 4-56: Semi-probabilistic versus fully-probabilistic for the 1039 year return period using the Robertson and Wride liquefaction triggering procedure.

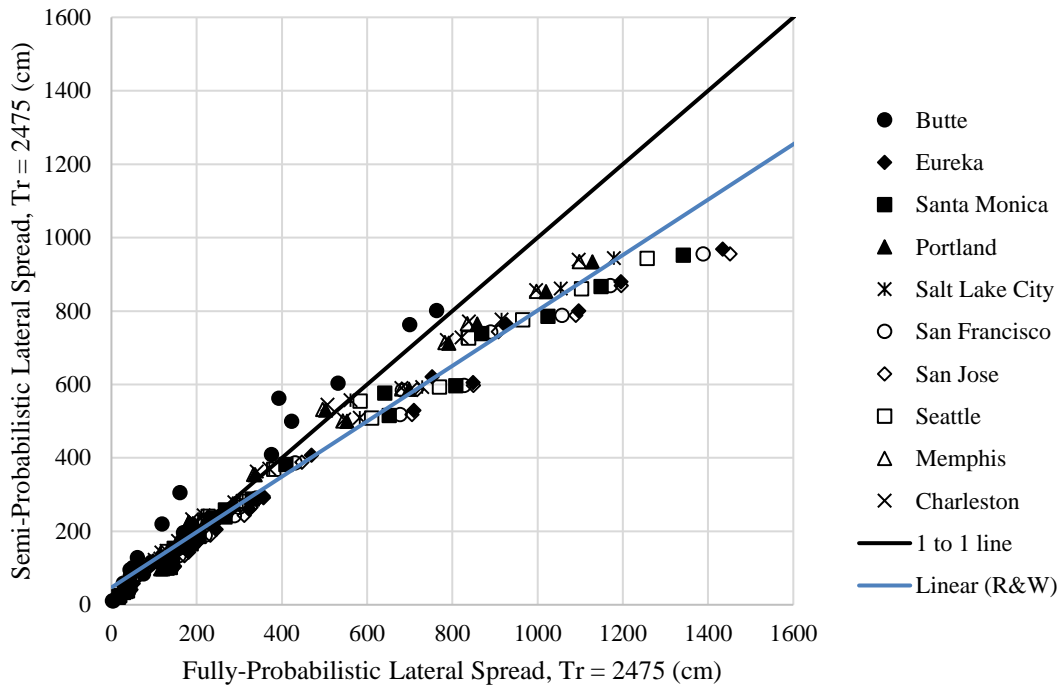


Figure 4-57: Semi-probabilistic versus fully-probabilistic for the 2475 year return period using the Robertson and Wride liquefaction triggering procedure.

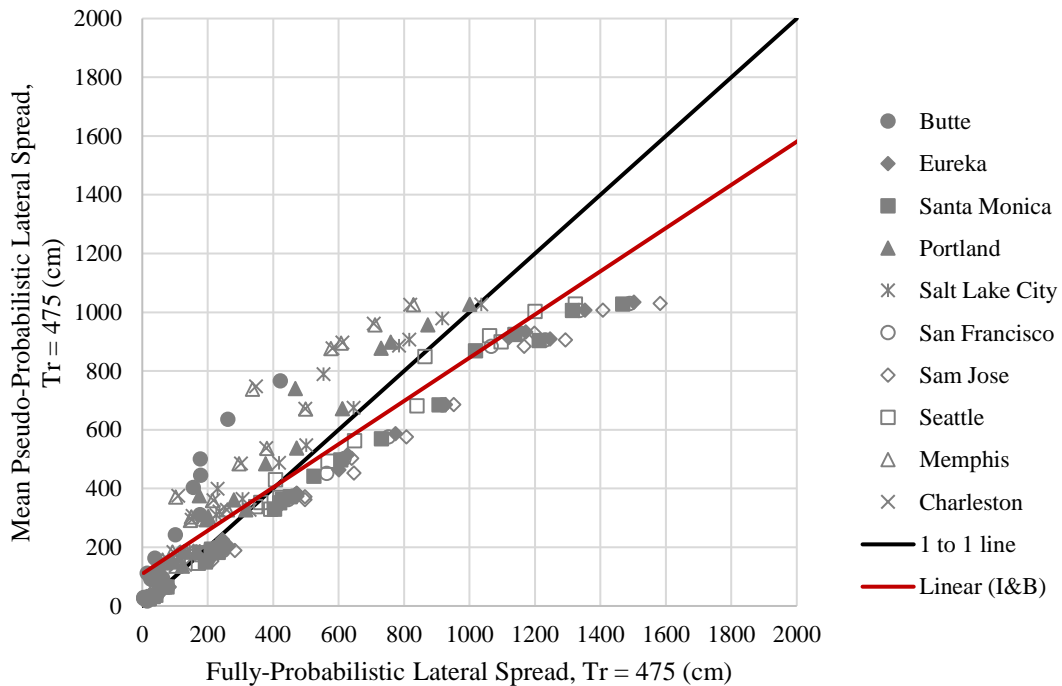


Figure 4-58: Mean magnitude pseudo-probabilistic versus fully-probabilistic for the 475 year return period using the Boulanger and Idriss liquefaction triggering procedure.

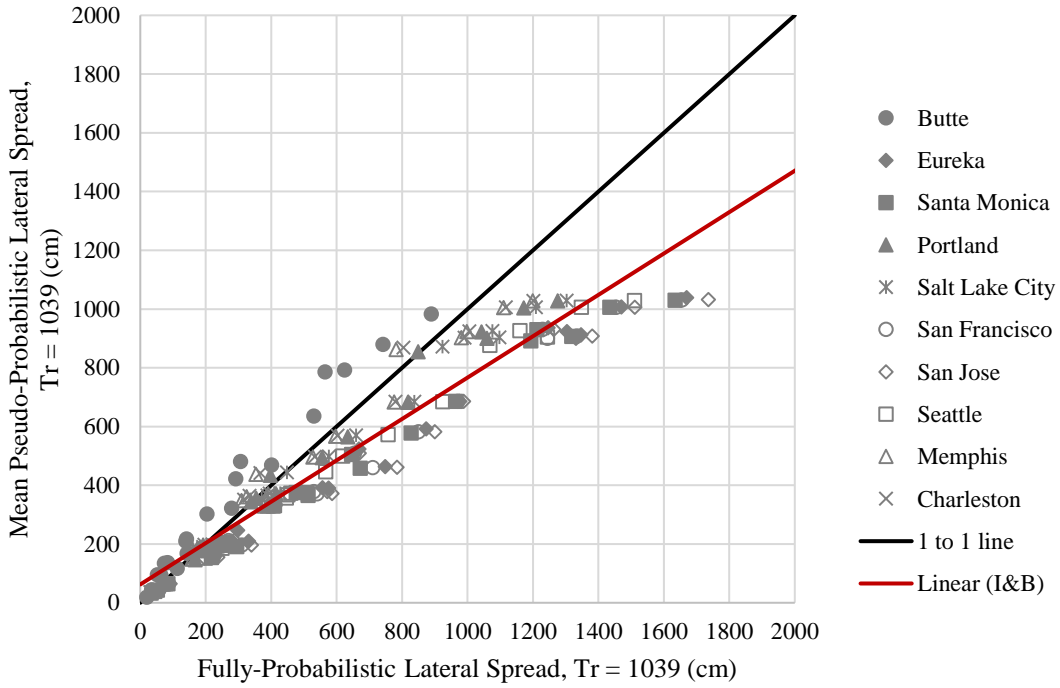


Figure 4-59: Mean magnitude pseudo-probabilistic versus fully-probabilistic for the 1039 year return period using the Boulanger and Idriss liquefaction triggering procedure.

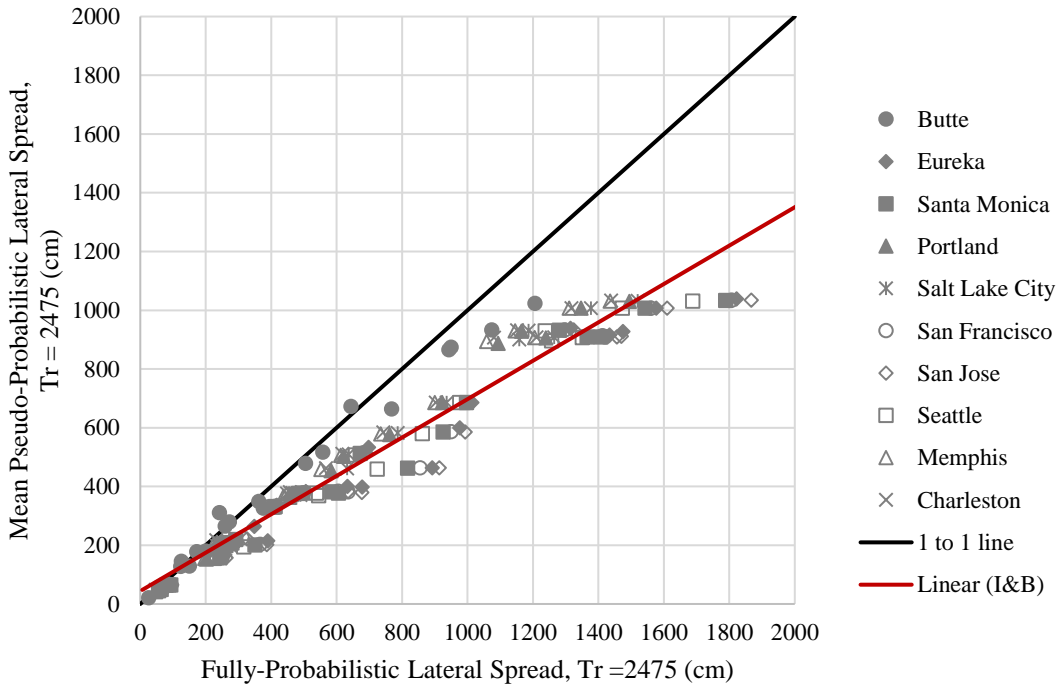


Figure 4-60: Mean magnitude pseudo-probabilistic versus fully-probabilistic for the 2475 year return period using the Boulanger and Idriss liquefaction triggering procedure.

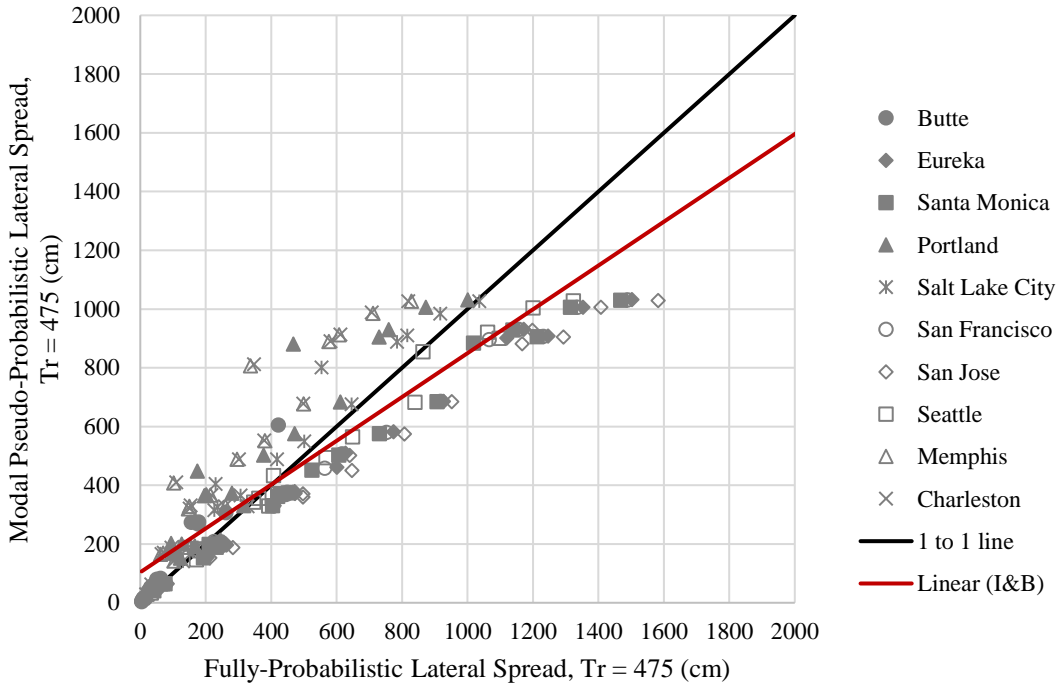


Figure 4-61: Modal magnitude pseudo-probabilistic versus fully-probabilistic for the 475 year return period using the Boulanger and Idriss liquefaction triggering procedure.

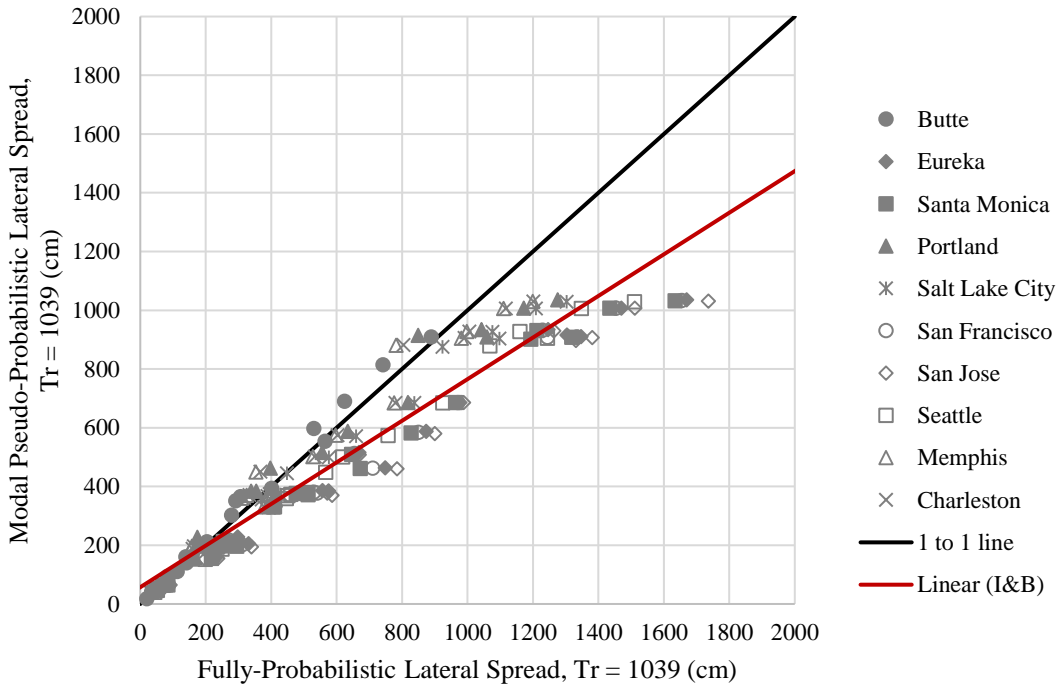


Figure 4-62: Modal magnitude pseudo-probabilistic versus fully-probabilistic for the 1039 year return period using the Boulanger and Idriss liquefaction triggering procedure.

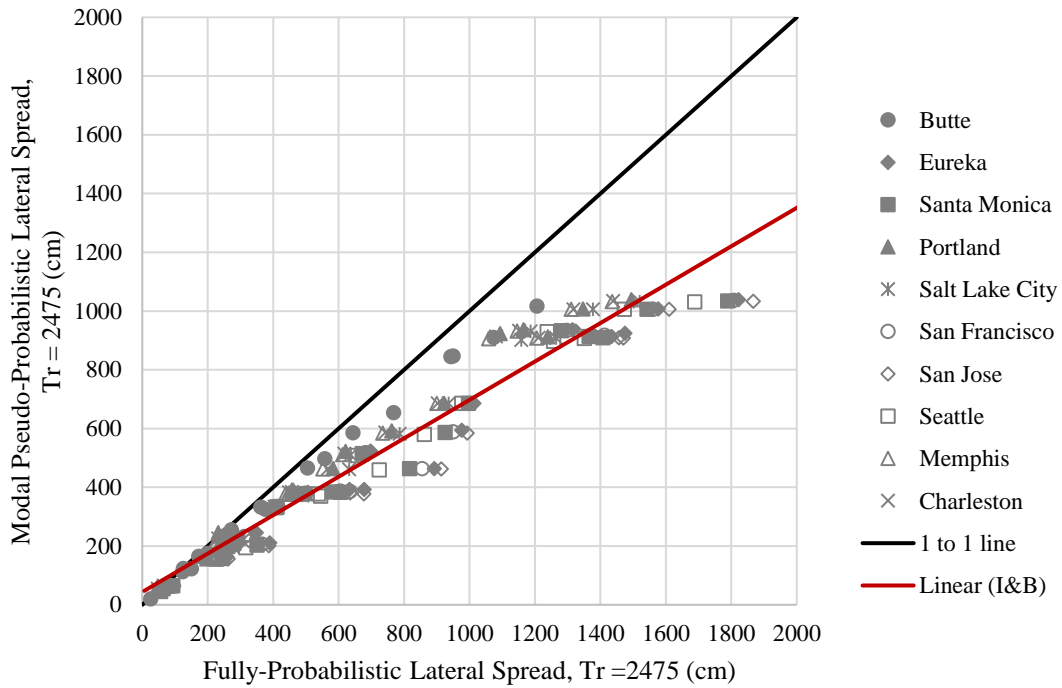


Figure 4-63: Modal magnitude pseudo-probabilistic versus fully-probabilistic for the 2475 year return period using the Boulanger and Idriss liquefaction triggering procedure.

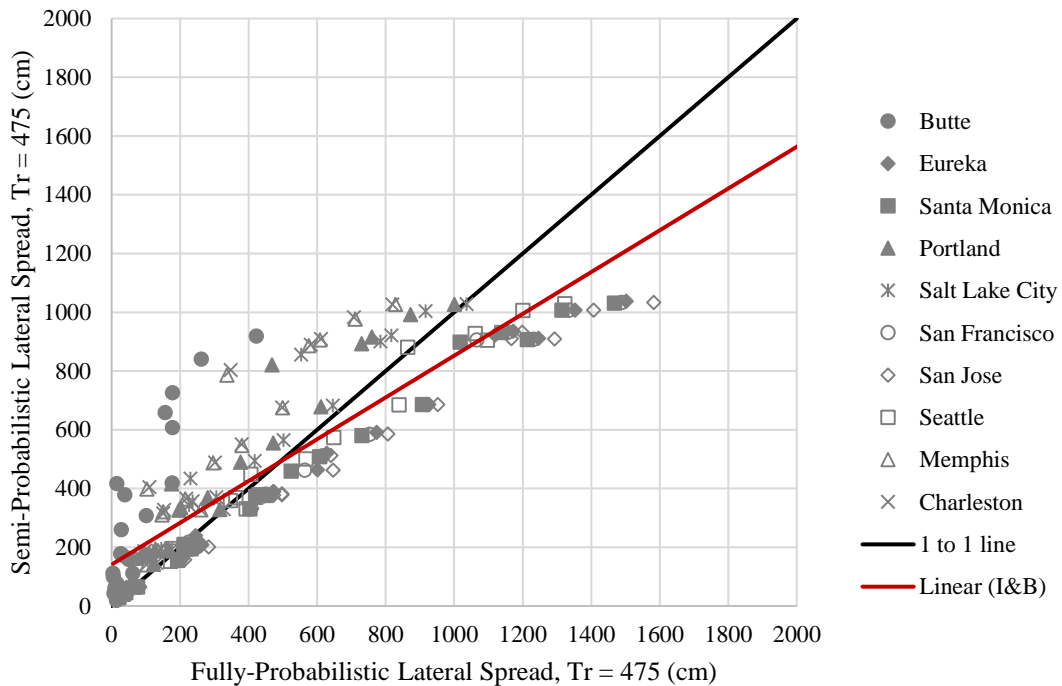


Figure 4-64: Semi-probabilistic versus fully-probabilistic for the 475 year return period using the Boulanger and Idriss liquefaction triggering procedure.

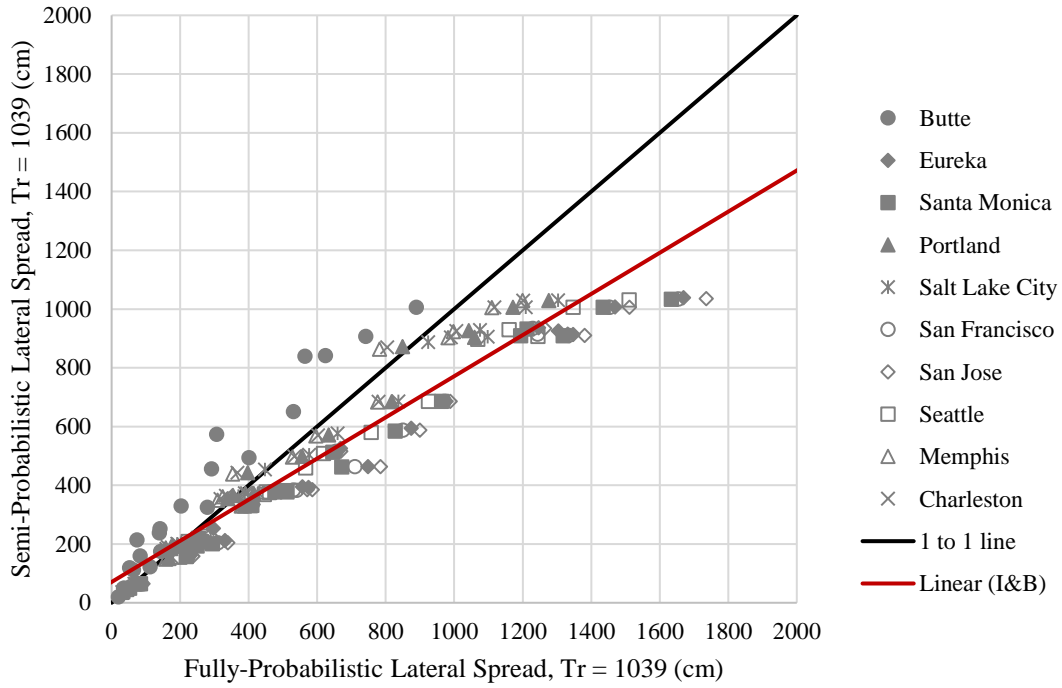


Figure 4-65: Semi-probabilistic versus fully-probabilistic for the 1039 year return period using the Boulanger and Idriss liquefaction triggering procedure.

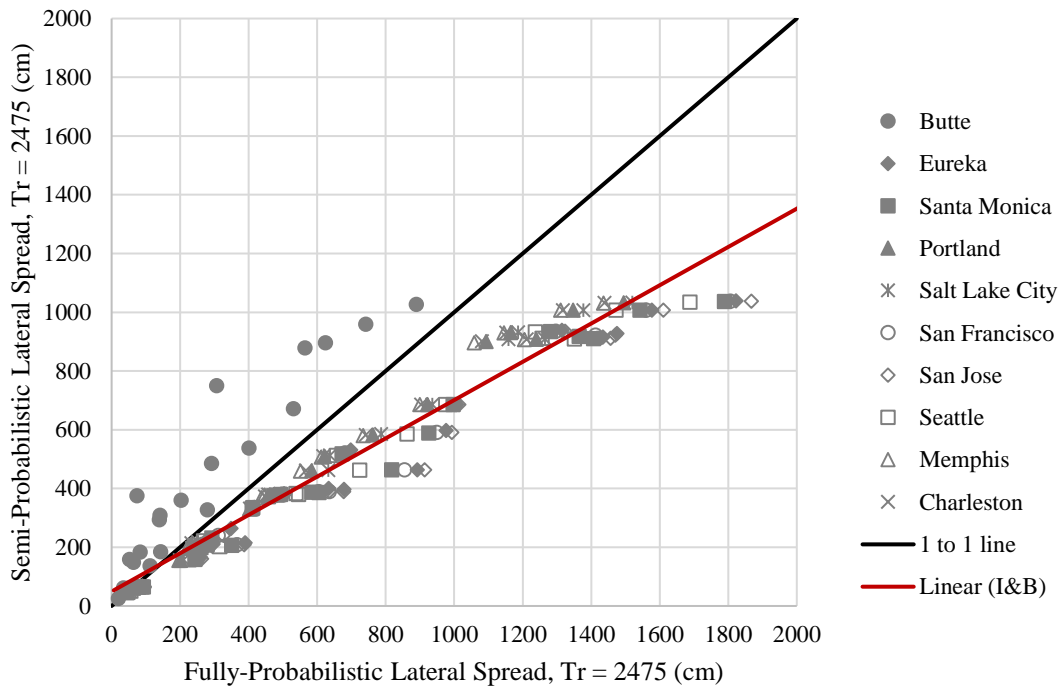


Figure 4-66: Semi-probabilistic versus fully-probabilistic for the 2475 year return period using the Boulanger and Idriss liquefaction triggering procedure.

Figure 4-49 through Figure 4-66 clearly show the difference in the results when using a full-probabilistic analysis of lateral spread. The results seen in the lateral spread analysis are very similar to those seen in the settlement analysis previously discussed, however while the plots of the results may look similar there are some key differences to note. In general there is more scatter in the data when compared to the results from the settlement analysis. Because of this scatter there seems to be very few times when the data follows the one-to-one line and matches the conventional approach to the full-probabilistic approach. For all return periods and each different conventional approach, it is seen that the Boulanger and Idriss data plots below the Robertson and Wride data. This indicates that the Boulanger and Idriss method produces more values that fall below the one-to-one line, or in other words are being under-predicted by the conventional approach.

When looking at the comparison between the pseudo-probabilistic and full-probabilistic approaches it can be seen that the trend for both methods begins above the one-to-one line, and at times does not even cross below it. The Robertson and Wride approach crosses below the one-to-one line at 200cm, and 100cm for the 1039 year, and 2475 year return periods, respectively (for the 475 year return period it stays consistently above the one-to-one line). The Boulanger and Idriss approach crosses below the one-to-one line at 400cm, 800cm, and 500cm for the 475 year, 1039 year, and 2475 year return periods, respectively. These trends were consistent between mean and modal magnitude pseudo-probabilistic analyses. The semi-probabilistic analysis provided very similar results, with trends beginning above the one-to-one line and eventually going below it.

As with the analysis of settlement, to further examine the trends and results from the lateral spread analysis, the values for the 1039 year and 2475 year return periods were entered into the probabilistic hazard curve to back-calculate the actual return period associated with that lateral spread displacement. The results of this process are summarized as box and whisker plots in Figure 4-67 and Figure 4-68.

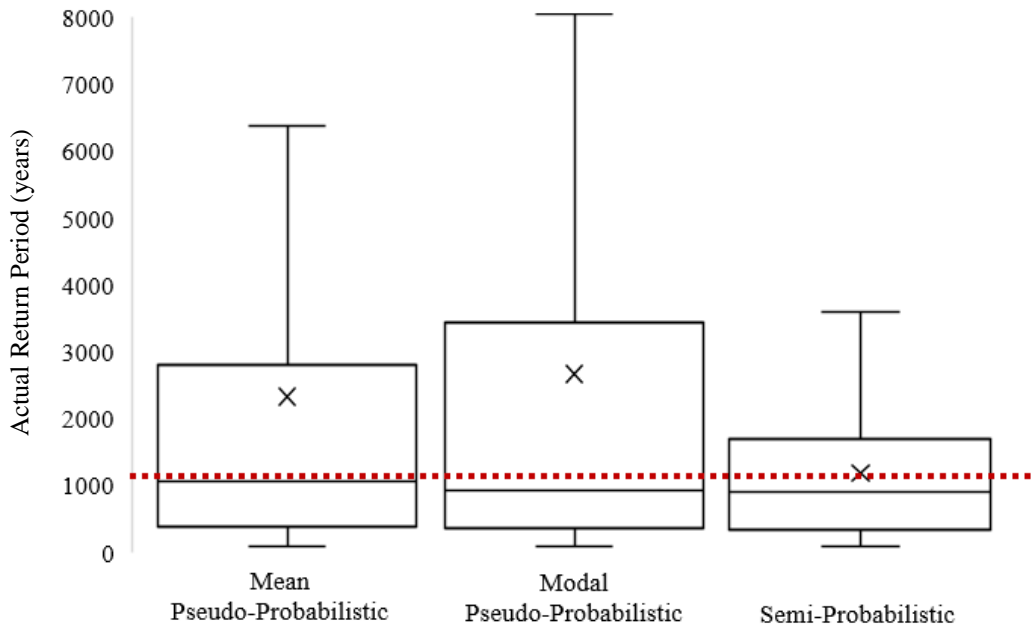


Figure 4-67: Box and whisker plots of actual return periods versus assumed 1039 year return period in the lateral spread analysis.

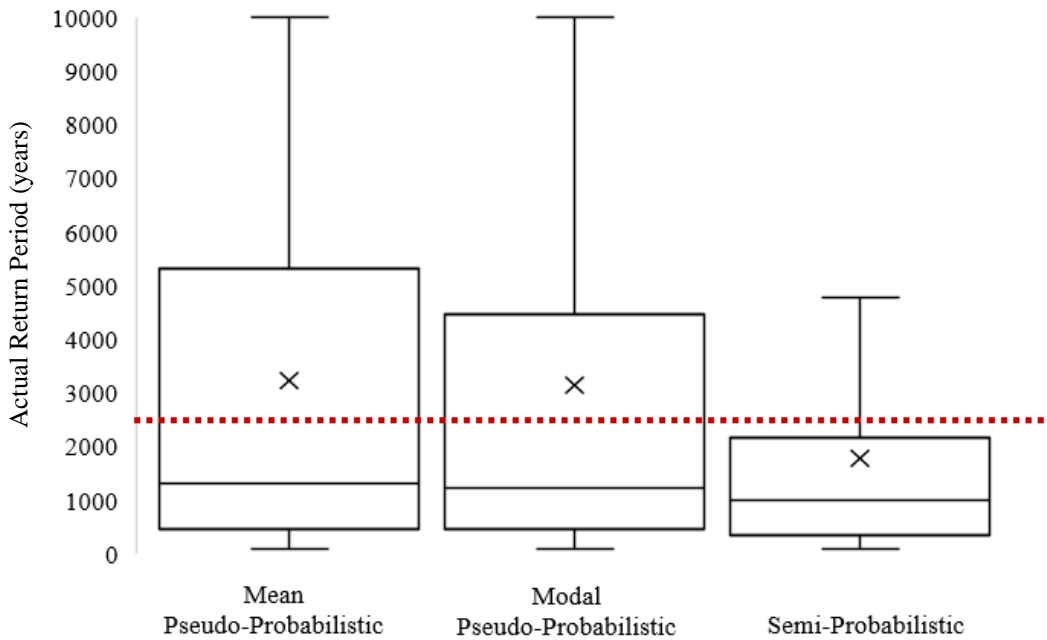


Figure 4-68: Box and whisker plots of actual return periods versus assumed 2475 year return period in the lateral spread analysis.

The box and whisker plots shown in Figure 4-67 and Figure 4-68 illustrate the median, first and third quartiles, maximum and minimum values, and the average (marked by an “x”) values of the return periods. As noted previously, these values represent actual return periods because they are generated from the full-probabilistic settlement hazard curve. The assumed return period is presented as a red dashed line for reference.

In Figure 4-67, while there is still significant scatter, it can be seen that the median actual return periods are fairly close to the assumed return period of 1039 years. While there is significant scatter in the box plots, the median value of calculated return period falls right along with the assumed return period of 1039 years. This is true for all three different analysis methods. For the 2475 year return period shown in Figure 4-68 it can be seen that the median assumed return period is closer to 1200 years, indicating that there is significant under-prediction of lateral spread displacements when using the conventional analysis methods. These results are fairly consistent with what was found in the one-to-one plots, showing that as the return period increases the amount of under-prediction of lateral spread displacements using conventional methods also increases.

Further examination of the trends in the lateral spread analysis can be done by generating a heat map as was created in Figure 4-47 for the settlement analysis. This heat map was created, but not included in this report as the trends observed were identical to that created for settlement. For an explanation of these trends please refer to Section 4.3.2.

In general, it was found that the pseudo-probabilistic approach of predicting lateral spread displacements typically over-predicted compared to the full-probabilistic approach for lower return periods (475 years) and lower seismic areas. Conversely, the pseudo-probabilistic approach typically under-predicted compared to the full-probabilistic approach for higher return periods (2475 years) and higher seismic areas. The trends show that Robertson and Wride procedure consistently had lower displacements than the Boulanger and Idriss procedure when looking at the full-probabilistic approach. This indicates that while the Robertson and Wride procedure may be a closer fit to more conventional methods, the Boulanger and Idriss procedure is a more conservative full-probabilistic approach when comparing the two together. The semi-probabilistic approach showed these similar trends as mentioned for the pseudo-probabilistic approach, with less scatter in the data, and is not a significant improvement on the pseudo-probabilistic method.

Based on these results it can be seen that while the pseudo-probabilistic method may be accepted in industry, it has its shortcomings when compared to the full-probabilistic approach. For

areas of lower seismicity and lower return periods, the pseudo-probabilistic approach may be adequate. But for areas of higher seismicity and higher return periods the use of the pseudo-probabilistic approach poses a risk as the lateral spread displacements could possibly be under-predicted. In these cases it is recommended that the full-probabilistic method be used.

5.0 SENSITIVITY ANALYSIS

In addition to the comparative study, a sensitivity analysis was performed to test the effect of correction factors on the full-probabilistic procedure for settlement and lateral spread. This analysis was performed for the thin layer correction and depth weighting factor correction. These results can show the impact and importance these factors can have on the newly developed full-probabilistic procedure.

5.1 Thin Layer Correction and Depth Weighting Factor

When dealing with all levels of probability, some unrealistic or impossible strain values can be computed. Various correction methods have been developed to address and correct unrealistic strain values.

5.1.1 Depth Weighting Factor Correction

The likelihood of a soil to liquefy decreases with depth (Iwasaki et al., 1982). A depth weighting factor (DF) was developed to account for this phenomenon. This depth factor aids in producing a better fit between models and case studies and is based on the following: (1) the triggering of void ratio redistribution, resulting in unfavorably higher void ratios for shallower layers from upward seepage; (2) reduced induced shear stresses and number of shear stress cycles transmitted to deeper soil layers due to initial liquefaction of surficial layers; and (3) possible arching effects due to nonliquefied soil layers (Cetin et al., 2009). For these reasons, it is assumed that the contribution of layers to ground surface settlement and lateral spread diminishes with depth. After statistical assessments by Cetin et al. (2009), 18m is the critical depth at which the soil layers past this point will not affect the ground surface settlement. This depth factor can be computed as

$$DF_i = 1 - \frac{d_i}{18m} \quad (58)$$

where d_i is the depth of the specific soil layer.

For settlement and lateral spread displacement of gently sloping ground, DF is then multiplied by the individual strain at each layer. This scales down the strain, resulting in more realistic settlement and lateral spread values. However, for lateral spread of a level ground with free face, a depth factor is not calculated. If the depth of the layer is greater than 2 times the height of the free face, the strain from that layer is considered to not contribute to the lateral spread (personal communication from T.L. Youd, June 2017).

5.1.2 Thin Layer Correction

When a thin sand layer is embedded within a soft clay, the cone from the CPT will read the sand layer's cone tip resistance as much lower than the actual stiffness of the thin layer because it has started to pick up the soft clay layer's resistance early (Ahmadi & Robertson, 2005). This discrepancy results in an over-prediction of post-liquefaction settlements and lateral spread displacements because the cone is reading the soil as softer than its actual stiffness. A correction factor is suggested to correct the cone tip resistance in the thin sand layers. As shown in Figure 5-1, as the cone enters deposit A (thin sand layer), the soil resistance is significantly reduced before the cone reaches deposit B (soft clay layer). This phenomena occurs because the cone is picking up the softness of deposit B before it reaches deposit B. The higher the stiffness and thinner the layer of sand interbedded within soft clay, the larger the thin layer correction factor will be.

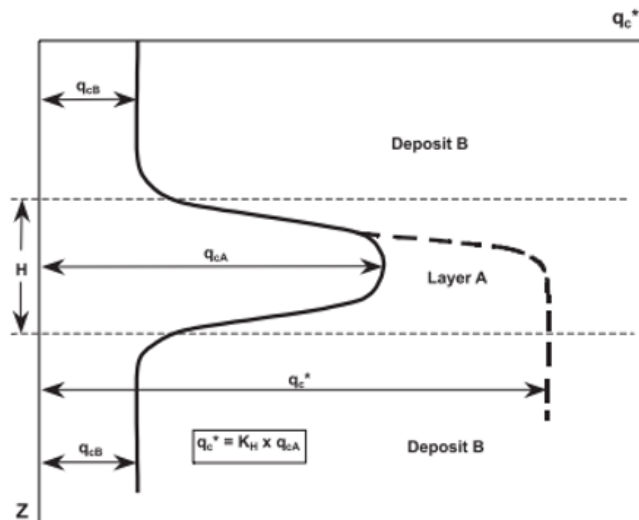


Figure 5-1: Tip resistance analysis for thin sand layer (deposit A) interbedded within soft clay layer (deposit B). (Ahmadi & Robertson, 2005).

Once a layer has been identified as needing the thin layer correction, the tip resistance can be adjusted with a correction factor. A layer is identified as a thin layer if there is a steep change in the soil behavior index (I_c), usually a change of 0.01 or greater, for multiple soil sublayer increments, usually 4 (Robertson, 2011). Once identified, these layer's tip resistance can be corrected using

$$q_c^* = K_H q_c \quad (59)$$

where q_c^* is the corrected cone tip resistance and K_H is the correction factor (Youd, 2001). This factor can be calculated by

$$K_H = 0.25 \left[\frac{\left(\frac{H}{d_c}\right)}{17} - 1.77 \right]^2 + 1.0 \quad (60)$$

where d_c is the diameter of the cone, and H is the layer thickness.

5.2 Sensitivity Analysis of Settlement

Four separate full-probabilistic settlement calculations were performed, for each city and CPT profile used previously, to test the sensitivity of the full-probabilistic procedure to different correction factors. These four calculations included a baseline (i.e., no corrections applied), a run with the depth weighting factor, a run with the thin layer correction, and a run with both the thin layer and depth factor correction applied. All 20 soil profiles, at all of the cities, and for all three return periods were run for each of these options. The data was combined and is presented in box and whisker plots below (Figure 5-2 through Figure 5-4).

To create these box and whisker plots, a ratio (R) was created, which represents the ratio of each of the separate options' calculated settlement values to the baseline corrected settlement values. This means that if R is equal to 1, the specific correction factor had no impact on the

settlement calculation. Therefore, the further away R is from 1, the more sensitive the probabilistic procedure is to that particular option.

The box and whisker plots show the impact each correction factor has on the full-probabilistic procedure. The box and whisker plots prove the importance and impact of correction factors. Based on the plots, it is apparent the full-probabilistic procedure is more sensitive to the depth weighting factor than the thin layer correction factor. However, the depth factor correction experienced a larger spread than the thin layer correction. It is logical that the thin layer correction had a smaller impact on the calculated settlement values. For the thin layer correction to even be applied the soil profile needed to contain thin sand layers interbedded within soft clay layers. A few of the 20 profiles did not have this criteria and therefore did not experience any thin layer correction. However, because the depth weighting factor is independent of soil type, the depth weighting factor was always applied.

The data suggests that return period does not affect the sensitivity significantly. Across all three return periods, the median value and general trends are about the same. This is logical because the degree of sensitivity is dependent on soil type for thin layer correction, and the depth factor correction will be constant because it is only dependent on depth, which was kept constant for each settlement calculation. However, as the return period increased, the scatter decreased.

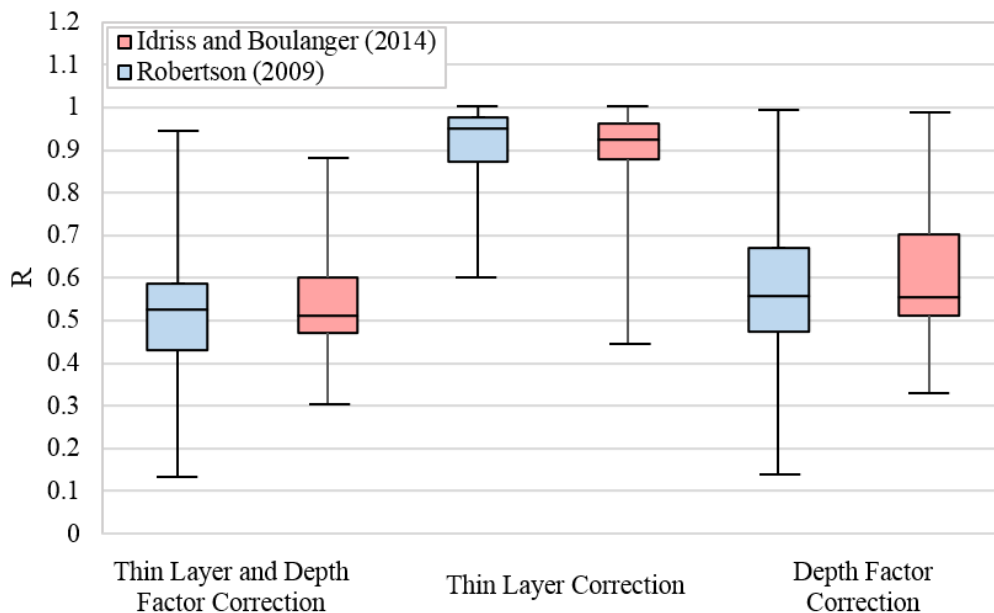


Figure 5-2: Box and whisker plots for R (settlement) at a return period of 475 years.

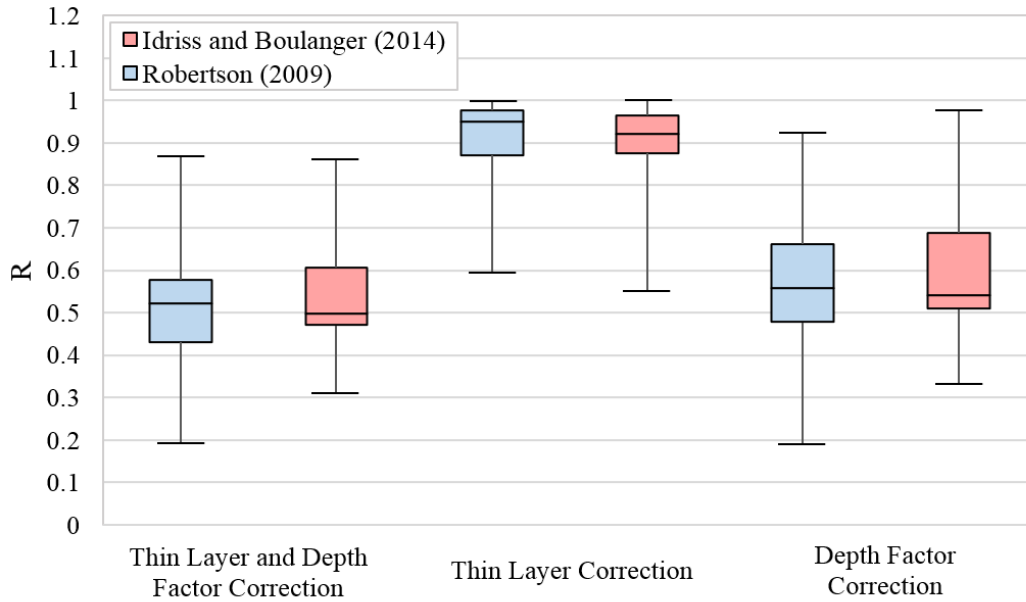


Figure 5-3: Box and whisker plots for R (settlement) at a return period of 1039 years.

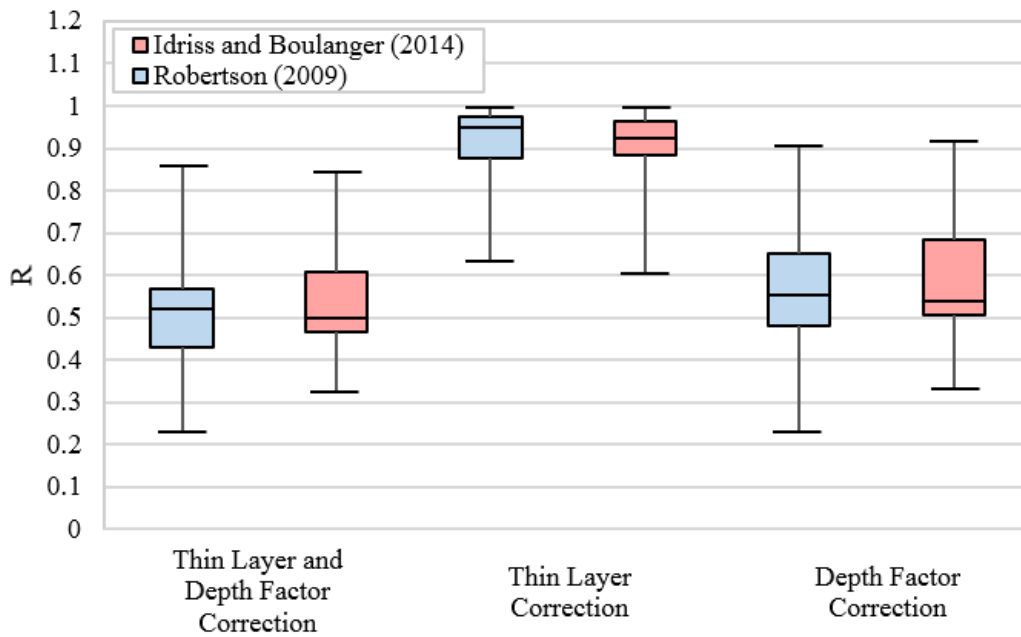


Figure 5-4: Box and whisker plots for R (settlement) at a return period of 2475 years.

5.3 Sensitivity Analysis of Lateral Spread

As in the sensitivity analysis of settlement, the sensitivity analysis of lateral spread was performed comparing the results of the baseline probabilistic method (i.e. no corrections applied), depth weighting factor, thin layer correction, and both thin layer and depth factor correction. This was also done for all 20 CPT profiles, 10 cities and 3 return periods. Box and whisker plots were created to illustrate this comparison. The box and whisker plots for lateral spread geometry 1 are displayed in Figure 5-5 through Figure 5-7. R is the ratio of the indicated correction option of lateral spread to the baseline lateral spread.

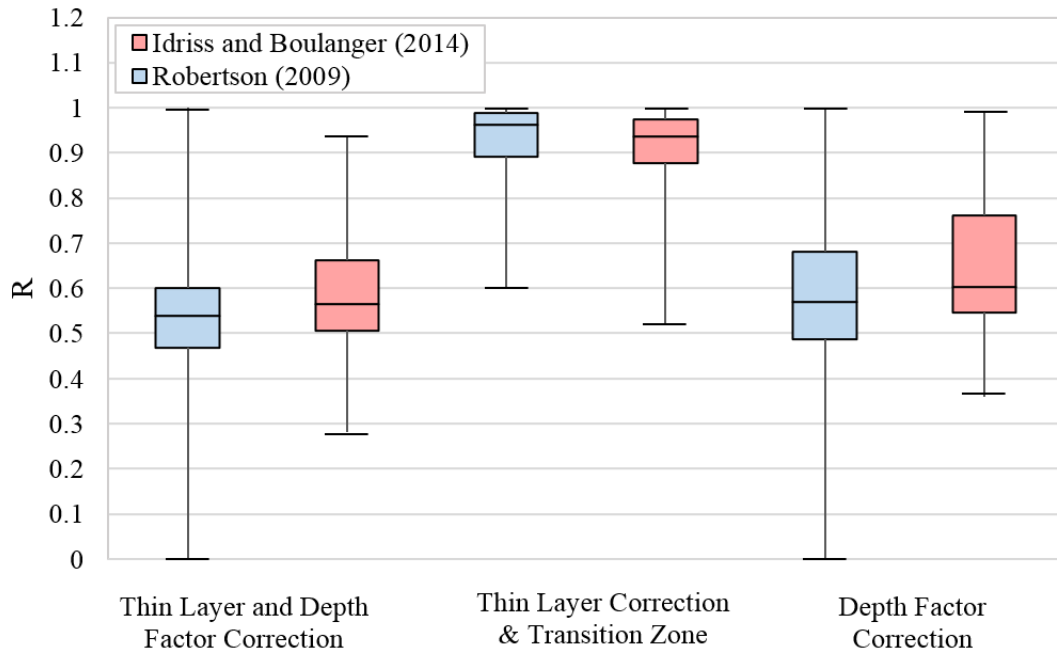


Figure 5-5: Box and whisker plots for R (lateral spread geometry 1) at a return period of 475 years.

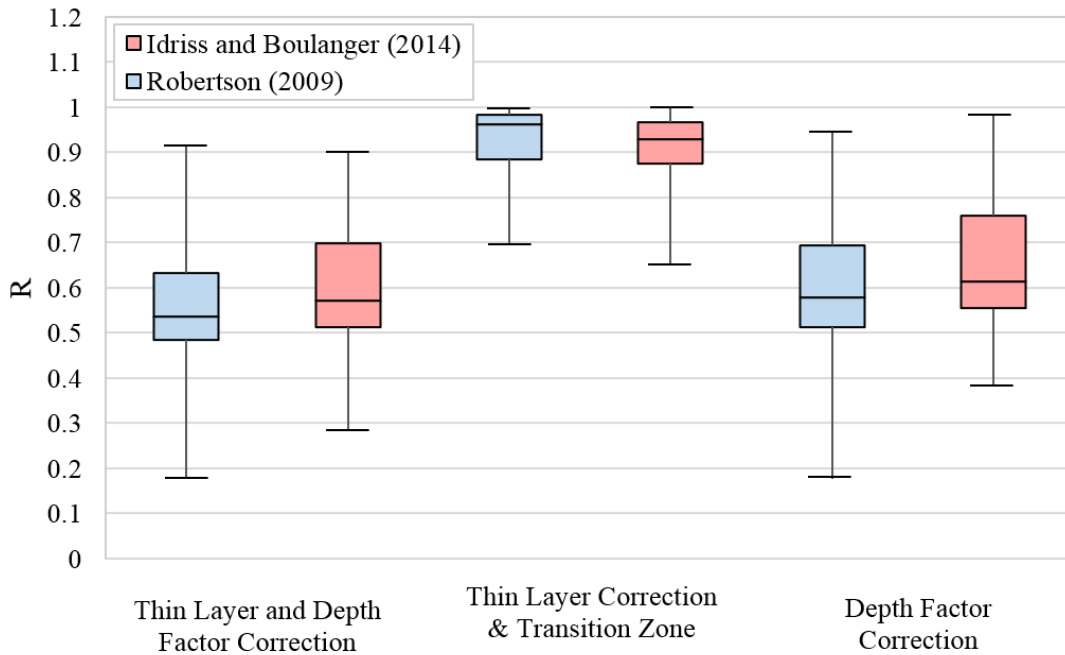


Figure 5-6: Box and whisker plots for R (lateral spread geometry 1) at a return period of 1039 years.

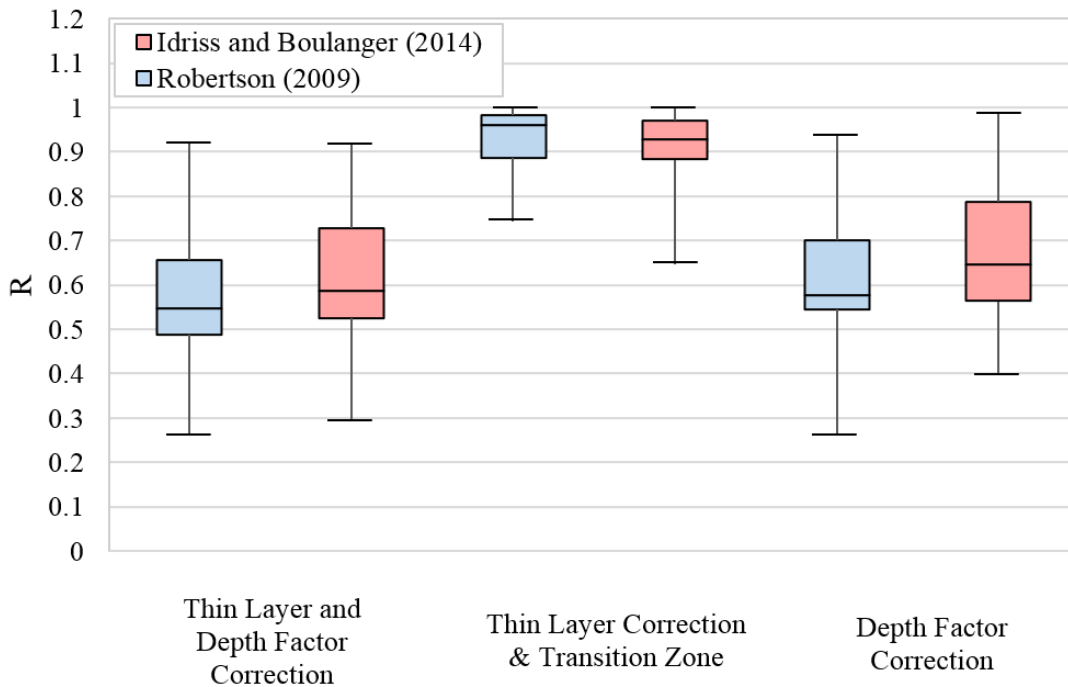


Figure 5-7: Box and whisker plots for R (lateral spread geometry 1) at a return period of 2475 years.

From the box and whisker plots in Figure 5-5 through Figure 5-7, it can be seen that the depth factor has more of an impact on the lateral spread displacements than the thin layer correction. For both procedures and all three return periods, the median R value for depth factor is approximately 0.55, while the median R value for thin layer correction is approximately 0.93 to 0.95. As the return period increased, the main change seen is that the spread of the R values decreases slightly. This is consistent with the results of the settlement sensitivity analysis.

It was desired that the same analysis be done for lateral spread geometry 2. Since geometry 2 is for level ground with a free face and not a gently sloping ground the depth correction is calculated differently. For level ground with a free face (geometry 2), a depth weighting factor is not calculated, simply if the depth of the layer in question is at a depth more than 2 times the height of the free face, H, it does not contribute to lateral spread. The height of the free face for geometry 2 was 6m. The maximum depth of all CPT profiles was 12m. Since none of the CPT profiles had layers at a depth beyond 2H, there was no depth factor correction for lateral spread geometry 2. Because of this it was decided to do the sensitivity analysis with a third geometry (referred to as lateral spread geometry 3).

Lateral spread geometry 3 has a free face height, H, of 3m, and a distance from the toe, L, of 25m. These values were chosen because the value of H needed to be smaller, and also the L/H ratio for lateral spread geometry 3 is the same as that of lateral spread geometry 2. With the same L/H ratio, the same result of lateral spread displacement is calculated. The only difference was that the depth correction calculated as 2H for geometry 3 is not equal to or greater than the depth of the CPT profiles. The box and whisker plots for lateral spread geometry 3 are displayed in Figure 5-8 through Figure 5-10. R is again the ratio of the indicated correction option of lateral spread to the baseline lateral spread.

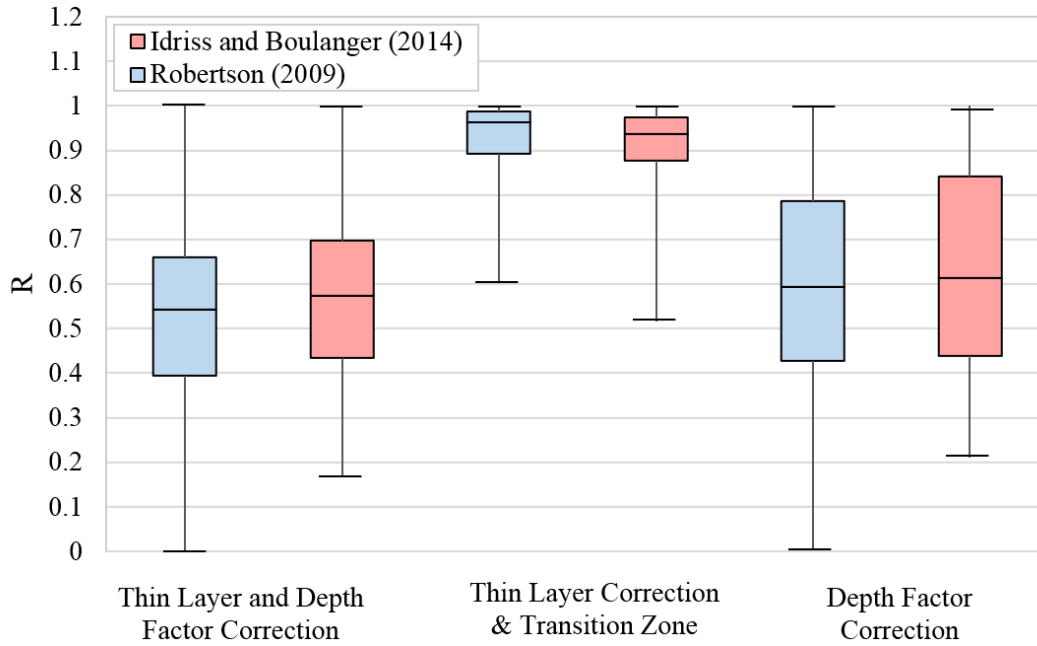


Figure 5-8: Box and whisker plots for R (lateral spread geometry 3) at a return period of 475 years.

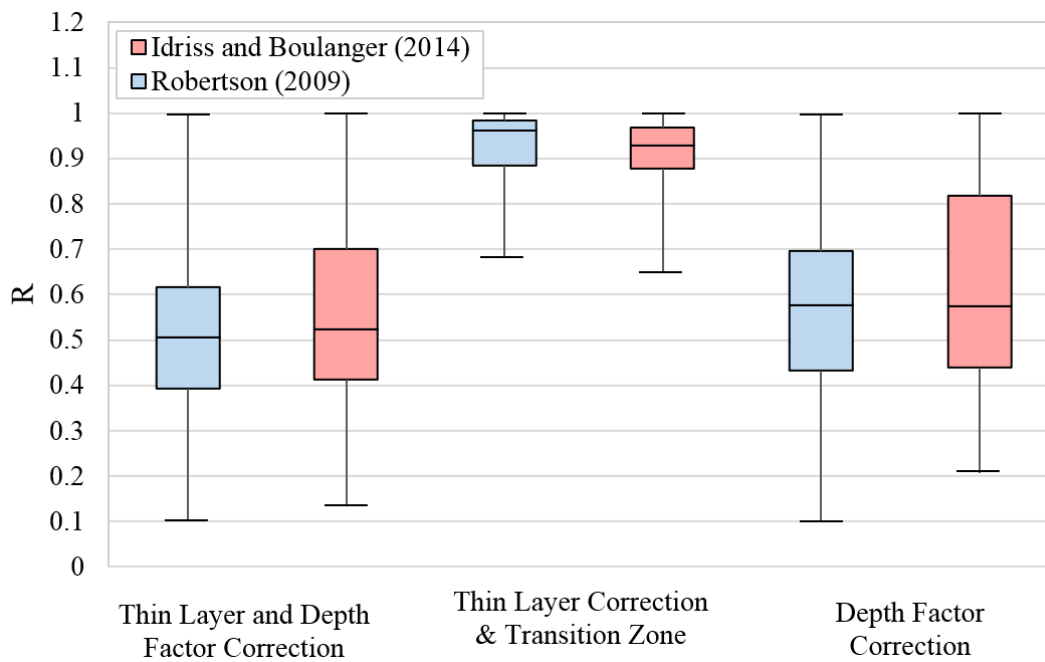


Figure 5-9: Box and whisker plots for R (lateral spread geometry 3) at a return period of 1039 years.

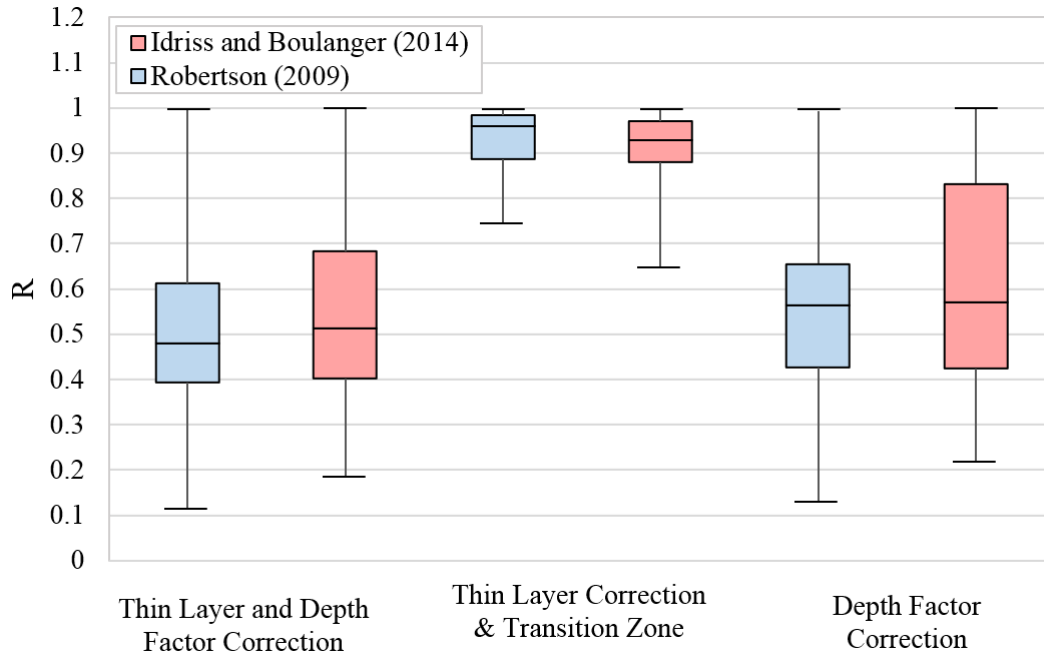


Figure 5-10: Box and whisker plots for R (lateral spread geometry 3) at a return period of 2475 years.

Just as with lateral spread geometry 1, in Figure 5-8 through Figure 5-10, it can be seen that the depth factor has more of an impact on the lateral spread displacements than the thin layer correction. For both procedures and all three return periods, the median R value for depth factor is approximately 0.55 to 0.60, while the median R value for thin layer correction is approximately 0.95. As the return period increased, the main change seen is that the spread of the R values decreases slightly. This is consistent with the results of the settlement sensitivity analysis.

6.0 CONCLUSIONS

6.1 Summary

This report marks the end of year one of this research project. At this point, a new PBEE liquefaction hazard analysis procedure has been developed for the CPT. The analysis tool, *CPTLiquefY*, has been created to perform pseudo-probabilistic, deterministic, semi-probabilistic, and fully-probabilistic (i.e. PBEE) liquefaction hazard analysis calculations. This report provides a review of all work completed throughout Phase 1, addressing Tasks 1 through 4 of the pooled fund study TPF-5(338) research contract.

The new PBEE liquefaction hazard analysis procedure was created by applying current design methods to the PBEE framework. Two PBEE liquefaction triggering analysis procedures were developed by using the Robertson and Wride (1998, 2009) and Idriss and Boulanger (2014) CPT liquefaction triggering models. Liquefaction-induced settlements and lateral spread displacement PBEE procedures were developed using the Juang et al. (2013) and Zhang et al. (2004) CPT methods, respectively.

These new PBEE procedures were tested and compared to conventional methods by performing liquefaction hazard analyses for 20 CPT profiles at 10 cities of varying levels of seismicity. The analysis of liquefaction triggering models appears to show that in general the Boulanger and Idriss fully-probabilistic procedure will give more conservative results than the Ku et al. fully-probabilistic procedure. The results indicated similar trends between the liquefaction-induced settlements and lateral spreading. The data suggests for a low return period, the pseudo-probabilistic settlement and lateral spread values correlated fairly well with full-probabilistic values. However, at medium to high return periods, this correlation deteriorated and showed pseudo-probabilistic methods under-predicting settlements and lateral spreading significantly.

In addition to the comparative study, a sensitivity analysis was performed to test the effect of correction factors on the full-probabilistic estimation procedure for settlement and lateral spread displacement calculations. This analysis was performed for the thin layer correction and depth weighting factor correction. The results proved the full-probabilistic procedure is more sensitive to the depth weighting factor than the thin layer correction.

The second phase of this research uses *CPTLiquefY* to develop simplified procedures, as well as generate probabilistic seismic hazard maps for liquefaction triggering, post-liquefaction settlement, and lateral spreading. This work is discussed in the Phase 2 final report volume.

REFERENCES

- Ahmadi, M. M., and Robertson, P. K. (2005). "Thin-layer effects on the CPT qc measurement." *Canadian Geotechnical Journal*, 42(5), 1302-1317.
- Boulanger, R., and Idriss, I. (2014). "CPT and SPT based liquefaction triggering procedures." *Center for Geotechnical Modeling, Department of Civil and Environmental Engineering, University of California, Davis, CA. Report No. UCD/CGM-14/01.*
- Cetin, K., Bilge, H., Wu, J., Kammerer, A., & Seed, R. (2009). Probabilistic Model for the Assessment of Cyclically Induced Reconsolidation (Volumetric) Settlements. *Journal of Geotechnical and Geoenvironmental Engineering*, 3(135), 387-393.
- Cornell, C. A., and Krawinkler, H. (2000). "Progress and challenges in seismic performance assessment." *PEER Center News*, 3(2), 1-3.
- Deierlein, G., Krawinkler, H., and Cornell, C. "A framework for performance-based earthquake engineering." *Proc., Pacific conference on earthquake engineering*, Citeseer, 1-8.
- Franke, K. W., Lingwall, B. N., and Youd, T. L. "Sensitivity of empirical liquefaction assessment to seismic loading in areas of low seismicity and its implications for sustainability." *Proc., Geo-Congress 2014 Technical Papers: Geo-characterization and Modeling for Sustainability*, ASCE, 1284-1293.
- Franke, K. W., Wright, A. D., & Hatch, C. K. (2014). *PBLiquefY: A New Analysis tool for the performance-based evaluation of liquefaction triggering*. Paper presented at the 10th National Conference on Earthquake Engineering.
- Huang, Y.M. (2008) "Performance-based design and evaluation for liquefaction-related seismic hazards." *Ph.D. Dissertation*, University of Washington, Seattle, WA.
- Ishihara, K., and Yoshimine, M. (1992). "Evaluation of settlements in sand deposits following liquefaction during earthquakes." *SOILS AND FOUNDATIONS*, 32(1), 173-188.
- Iwasaki, T., Tokida, K., Tatsuka, F., Wantabe, S., Yasuda, S., & Sato, H. (1982). *Microzonation for soil liquefaction potential using the simplified methods*. Paper presented at the 3rd International Conference on Microzonation, Seattle.
- Jefferies, M.G., and Davies, M.P., 1993. Use of CPTU to estimate equivalent SPT N60. *Geotechnical Testing Journal*, ASTM, 16(4): 458-468.

- Juang, C. H., Ching, J., Wang, L., Khoshnevisan, S., and Ku, C.-S. (2013). "Simplified procedure for estimation of liquefaction-induced settlement and site-specific probabilistic settlement exceedance curve using cone penetration test (CPT)." *Canadian Geotechnical Journal*, 50(10), 1055-1066.
- Kramer, S.L., (2008). "Evaluation of liquefaction hazards in Washington State." WSDOT Report WA-RD 668.1, 152 pp.
- Kramer, S.L., Huang, Y.M., and Greenfield, M.W. (2014). Performance-based assessment of liquefaction hazards. *Geotechnics for Catastrophic Flooding Events*, Iai ed., ISBN 978-1-138-02709-1, Taylor and Francis Group, London, 17-26.
- Kramer, S. L., and Mayfield, R. T. (2007). "Return period of soil liquefaction." *Journal of Geotechnical and Geoenvironmental Engineering*, 133(7), 802-813.
- Krawinkler, H. "A general approach to seismic performance assessment." *Proc., Proceedings*, 173-180.
- Ku, C.-S., Juang, C. H., Chang, C.-W., and Ching, J. (2011). "Probabilistic version of the Robertson and Wride method for liquefaction evaluation: development and application." *Canadian Geotechnical Journal*, 49(1), 27-44.
- Mayfield, R. T., Kramer, S. L., and Huang, Y.-M. (2009). "Simplified approximation procedure for performance-based evaluation of liquefaction potential." *Journal of geotechnical and geoenvironmental engineering*, 136(1), 140-150.
- Rathje, E.M. and Saygili, G. (2008). Probabilistic seismic hazard analysis for the sliding displacement of slopes: scalar and vector approaches. *J. Geotech. Geoenviron. Eng.* 134(6), 804-814.
- Robertson, P. "Performance based earthquake design using the CPT." *Proc., Proceedings of IS-Tokyo 2009: international conference on performance-based design in earthquake geotechnical engineering—from case history to practice, Tokyo, Japan*, 15-18.
- Robertson, P. (2009). *Performance based earthquake design using the CPT*. Paper presented at the Proceedings of IS-Tokyo 2009: international conference on performance-based design in earthquake geotechnical engineering—from case history to practice, Tokyo, Japan.
- Robertson, P. (2011). "Computing in Geotechnical Engineering-Automatic Software Detection of CPT Transition Zones." *Geotechnical News*, 29(2), 33.

- Robertson, P., and Cabal, K. "Estimating soil unit weight from CPT." *Proc., 2nd International Symposium on Cone Penetration Testing*, 2-40.
- Robertson, P., and Wride, C. (1998). "Evaluating cyclic liquefaction potential using the cone penetration test." *Canadian Geotechnical Journal*, 35(3), 442-459.
- Seed, H. B. (1979). "SOIL LIQUEFACTION AND CYCLIC MOBILITY EVALUTION FOR LEVEL GROUND DURING EARTHQUAKES." *Journal of Geotechnical and Geoenvironmental Engineering*, 105(ASCE 14380).
- Seed, H. B., and Idriss, I. M. (1971). "Simplified procedure for evaluating soil liquefaction potential." *Journal of Soil Mechanics & Foundations Div.*
- Seed, H. B., and Idriss, I. M. (1982). *Ground motions and soil liquefaction during earthquakes*, Earthquake Engineering Research Institute.
- Seed, H. B., Tokimatsu, K., Harder, L., and Chung, R. M. (1985). "Influence of SPT procedures in soil liquefaction resistance evaluations." *Journal of Geotechnical Engineering*, 111(12), 1425-1445.
- Stewart, J. P., Liu, A. H., and Choi, Y. (2003). "Amplification factors for spectral acceleration in tectonically active regions." *Bulletin of the Seismological Society of America*, 93(1), 332-352.
- Shamoto, Y., Zhang, J.-M., and Tokimatsu, K. (1998). "Methods for evaluating residual post-liquefaction ground settlement and horizontal displacement," *Soils and Foundations*, Special Issue No. 2, 69-83.
- Tatsuoka, F., Zhou, S., Sato, T., and Shibuya, S. (1990). "Evaluation method of liquefaction potential and its application." *Report on seismic hazards on the ground in urban areas. Ministry of Education of Japan, Tokyo*, 75-109.
- Tokimatsu, K. and Seed, H.B. (1987). "Evaluation of settlements in sand due to earthquake shaking," *Journal of Geotechnical Engineering*, ASCE, Vol. 113, No. 8, pp. 861-878.
- U.S.G.S. Earthquake Hazards Program. *Table of CPT Data, All Regions*. Retrieved from <https://earthquake.usgs.gov/research/cpt/data/table/>
- Wu, J. and Seed, R.B. (2004). "Estimation of liquefaction-induced ground settlement (case studies)," *Proceedings, Fifth International Conference on Case Histories in Geotechnical Engineering*, New York, pp. 1-8.

- Youd, L. (2001). Liquefaction Resistance of Soils: Summary Report from the 1996 NCEER and 1998/NSF Workshops on Evaluation of Liquefaction Resistance of Soils. *Journal of Geotechnical and Geoenvironmental Engineering*, 127(4).
- Zhang, G., Robertson, P. K., and Brachman, R. (2004). "Estimating liquefaction-induced lateral displacements using the standard penetration test or cone penetration test." *Journal of Geotechnical and Geoenvironmental Engineering*, 130(8), 861-871.

APPENDIX A: LATERAL SPREAD COMPARISONS

The following figures show the comparison of the fully-probabilistic method to the pseudo-probabilistic method or semi-probabilistic method for lateral spread geometry 2.

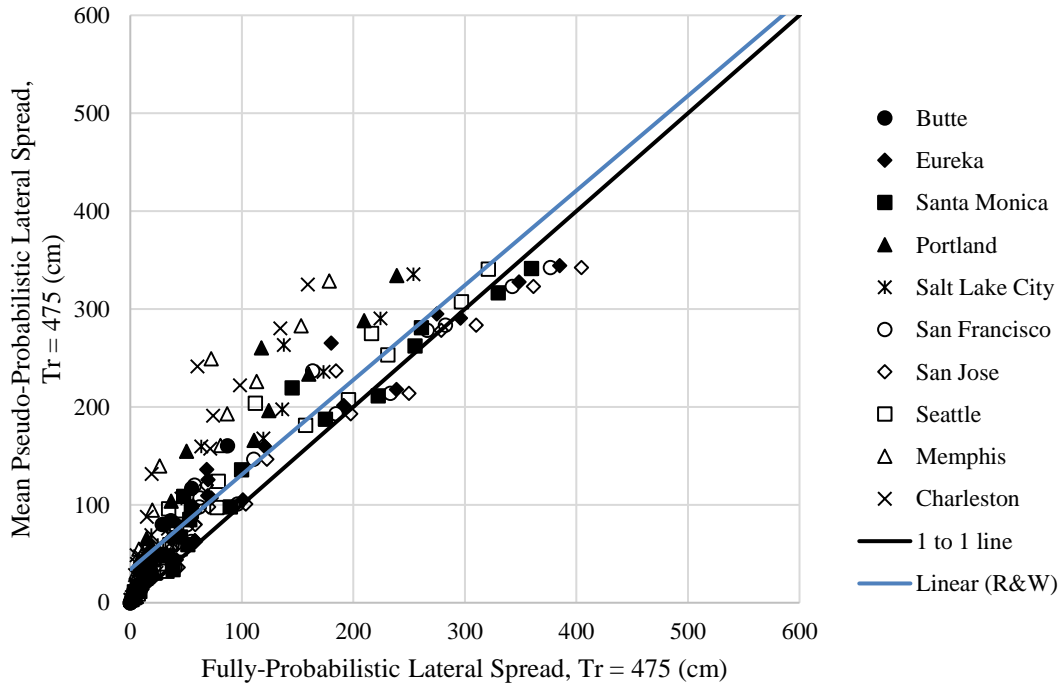


Figure A-1: Mean magnitude pseudo-probabilistic versus fully-probabilistic for the 475 year return period using the Robertson and Wride liquefaction triggering procedure.

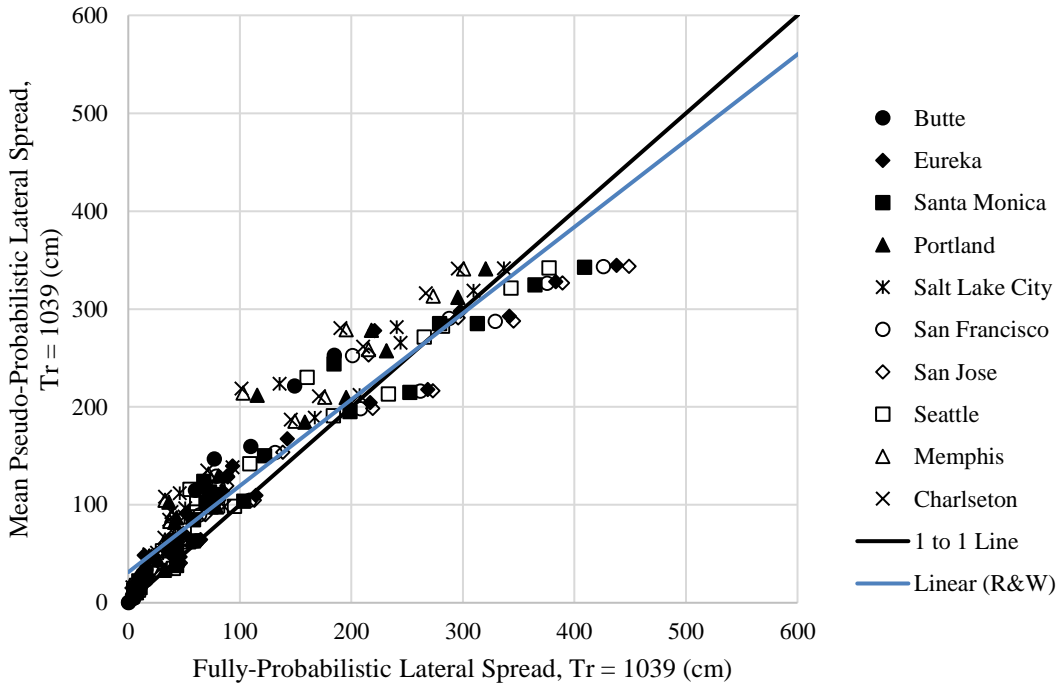


Figure A-2: Mean magnitude pseudo-probabilistic versus fully-probabilistic for the 1039 year return period using the Robertson and Wride liquefaction triggering procedure.

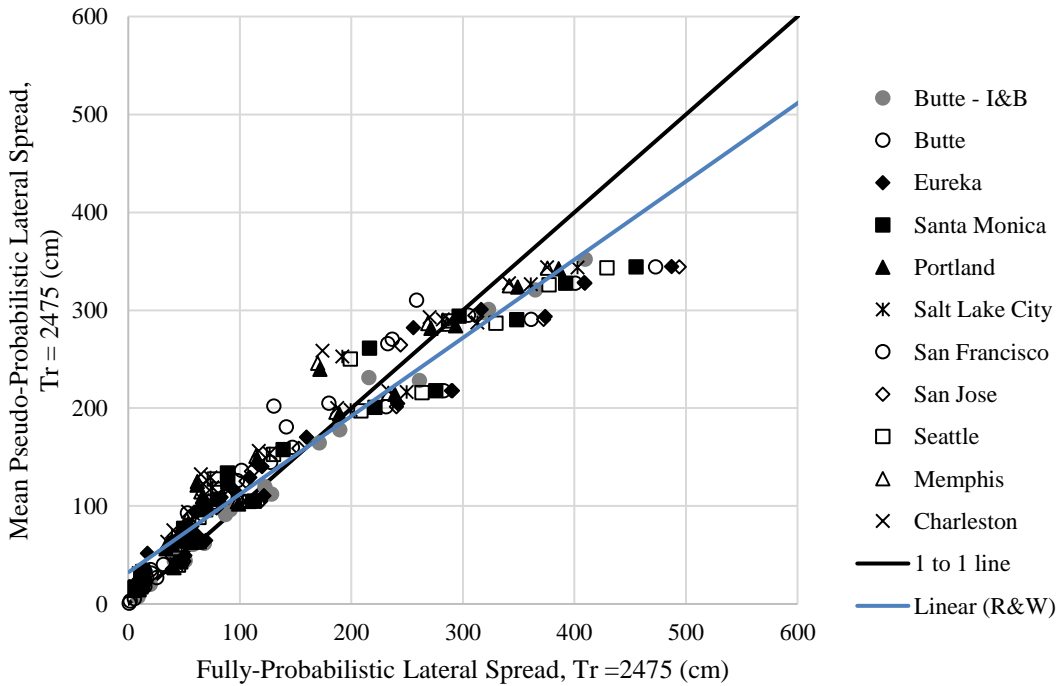


Figure A-3: Mean magnitude pseudo-probabilistic versus fully-probabilistic for the 2475 year return period using the Robertson and Wride liquefaction triggering procedure.

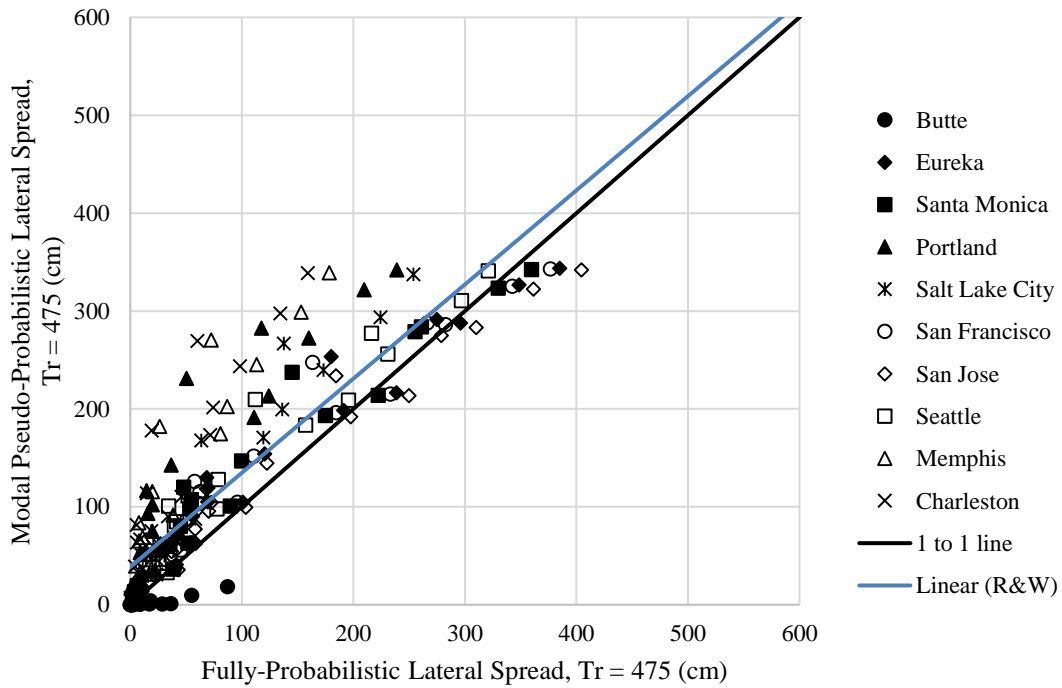


Figure A-4: Modal magnitude pseudo-probabilistic versus fully-probabilistic for the 475 year return period using the Robertson and Wride liquefaction triggering procedure.

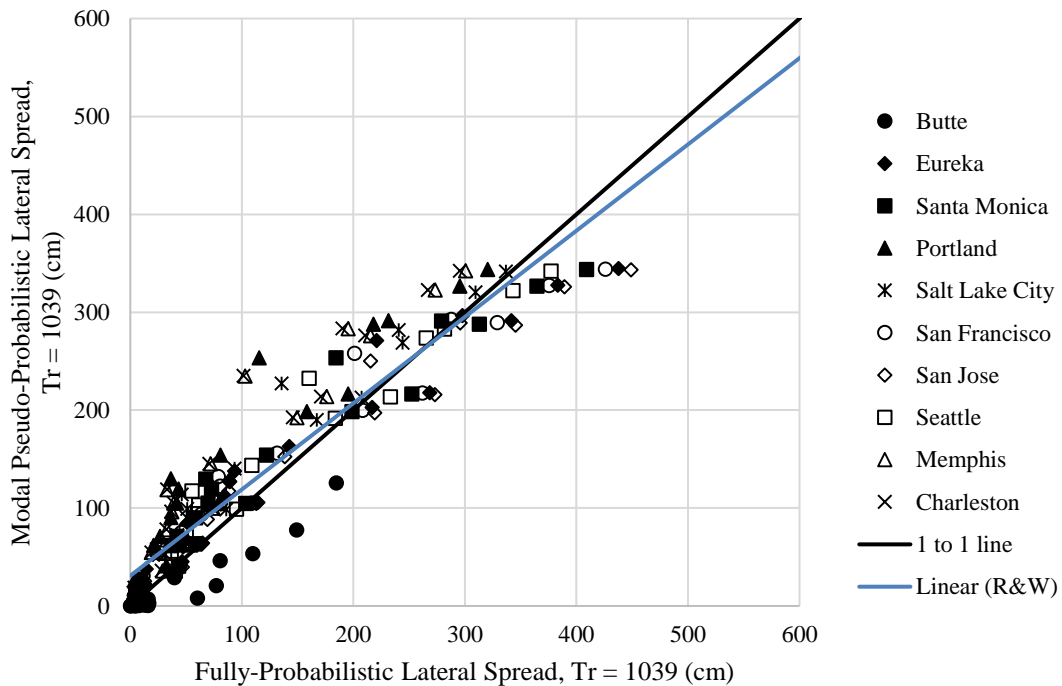


Figure A-5: Modal magnitude pseudo-probabilistic versus fully-probabilistic for the 1039 year return period using the Robertson and Wride liquefaction triggering procedure.

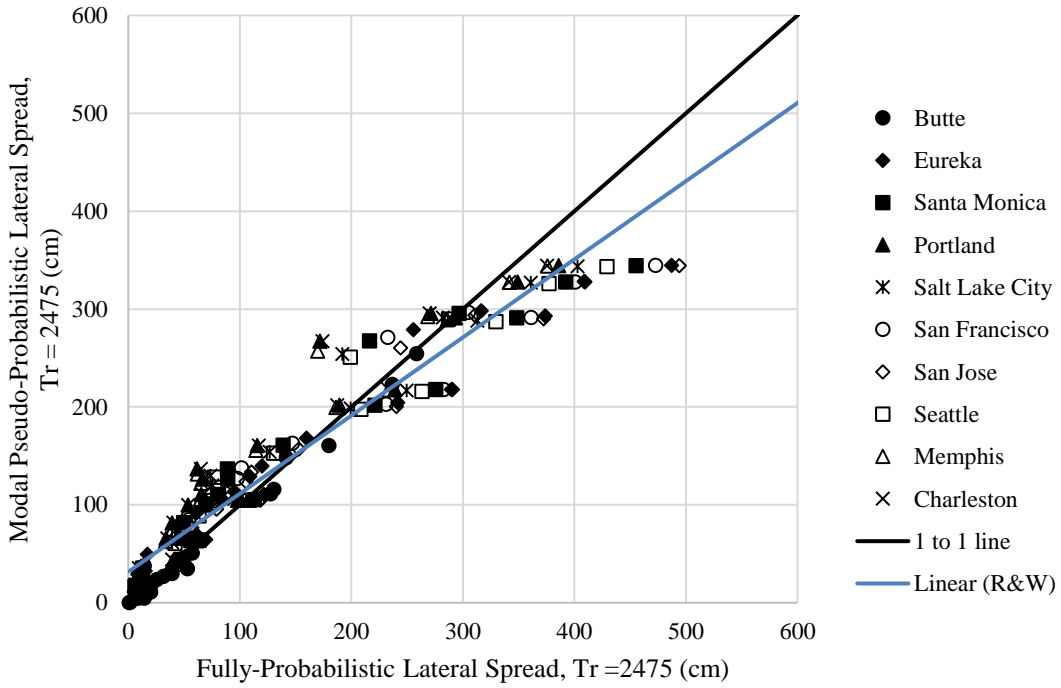


Figure A-6: Modal magnitude pseudo-probabilistic versus fully-probabilistic for the 2475 year return period using the Robertson and Wride liquefaction triggering procedure.

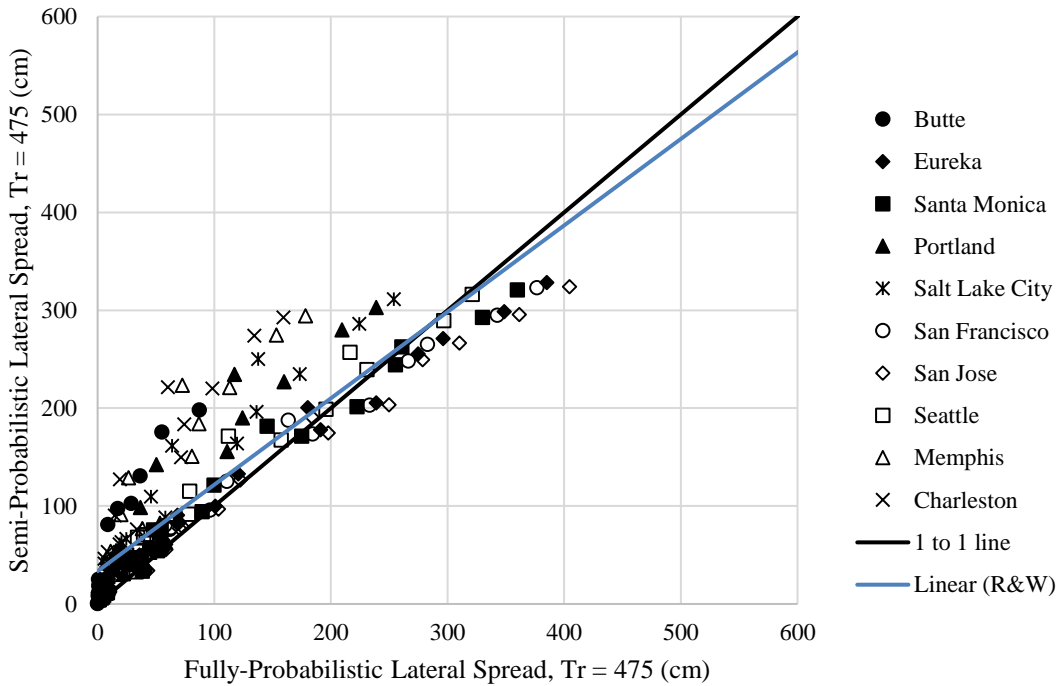


Figure A-7: Semi-probabilistic versus fully-probabilistic for the 475 year return period using the Robertson and Wride liquefaction triggering procedure.

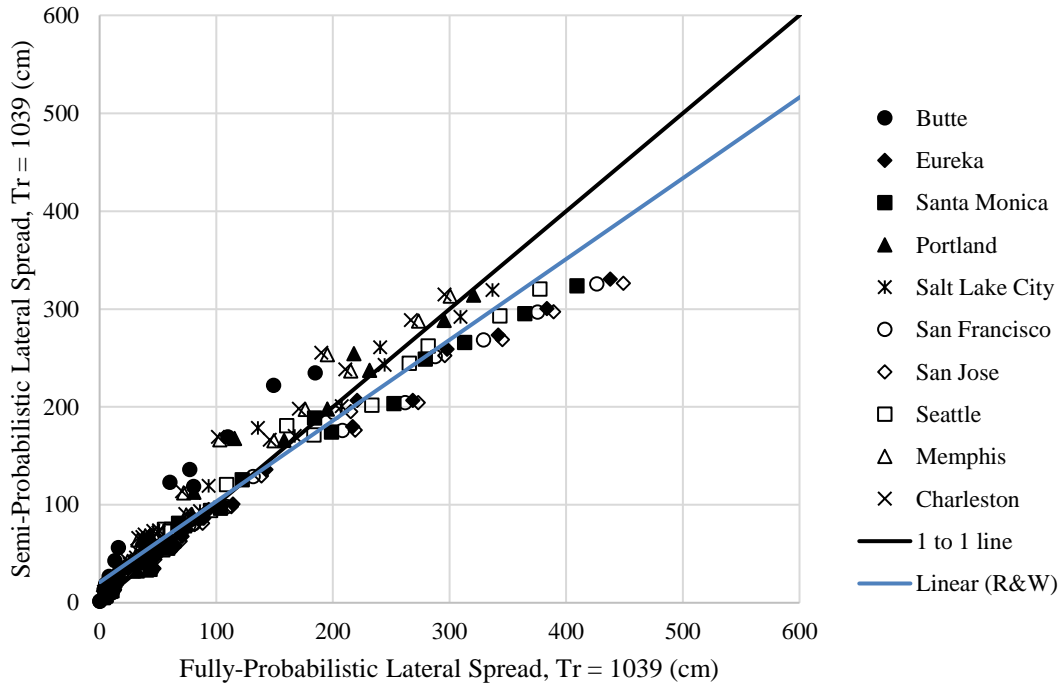


Figure A-8: Semi-probabilistic versus fully-probabilistic for the 1039 year return period using the Robertson and Wride liquefaction triggering procedure.

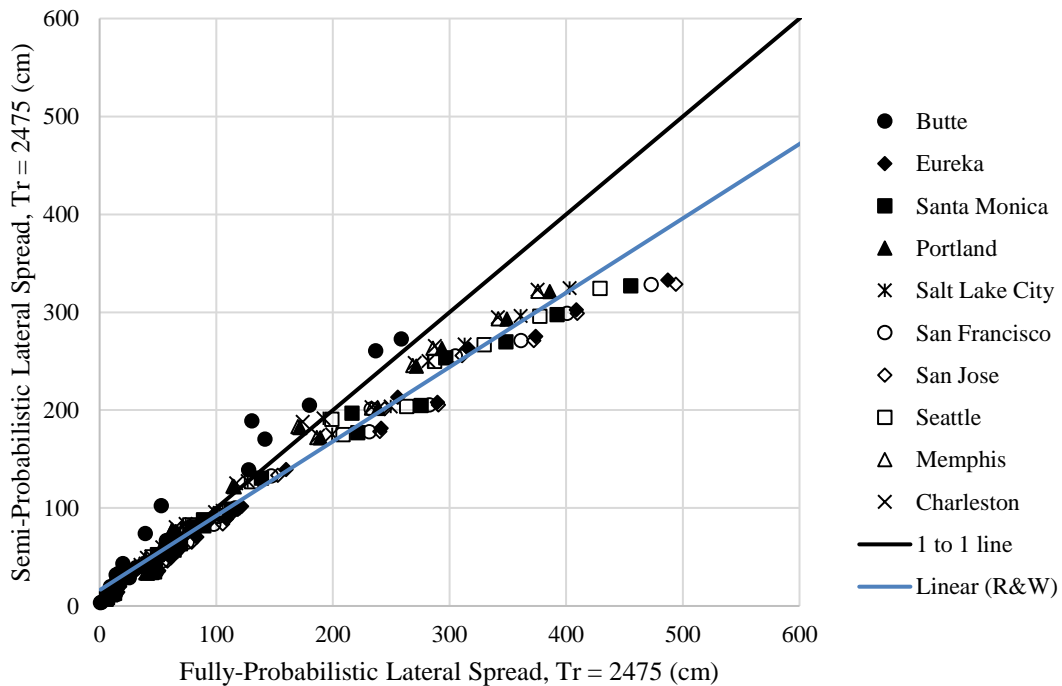


Figure A-9: Semi-probabilistic versus fully-probabilistic for the 2475 year return period using the Robertson and Wride liquefaction triggering procedure.

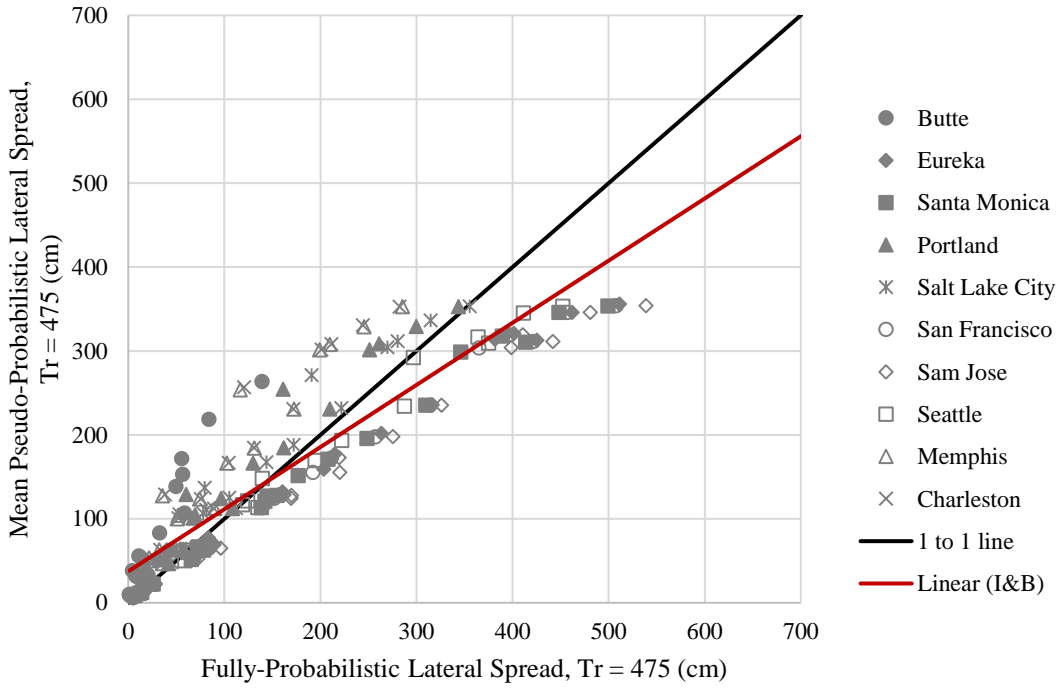


Figure A-10: Mean magnitude pseudo-probabilistic versus fully-probabilistic for the 475 year return period using the Boulanger and Idriss liquefaction triggering procedure.

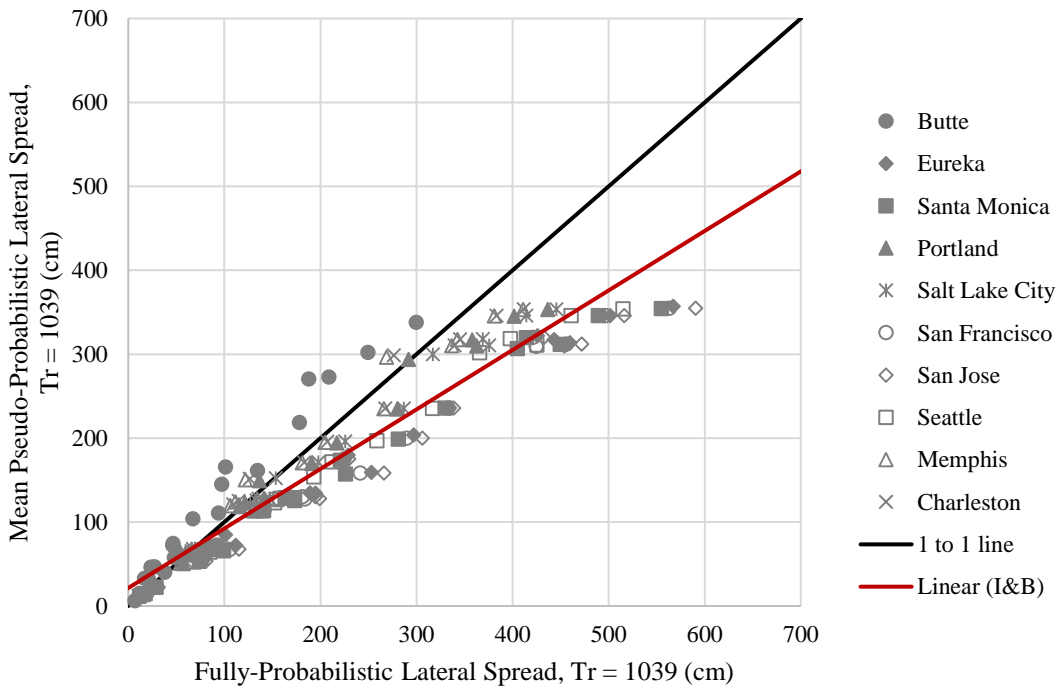


Figure A-11: Mean magnitude pseudo-probabilistic versus fully-probabilistic for the 1039 year return period using the Boulanger and Idriss liquefaction triggering procedure.

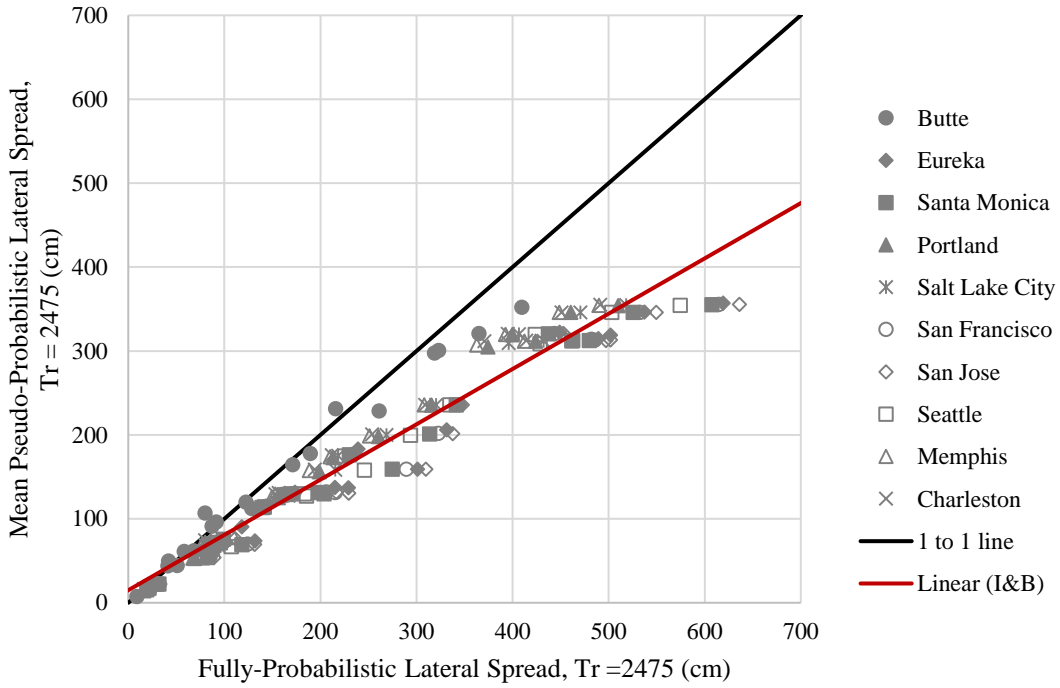


Figure A-12: Mean magnitude pseudo-probabilistic versus fully-probabilistic for the 2475 year return period using the Boulanger and Idriss liquefaction triggering procedure.

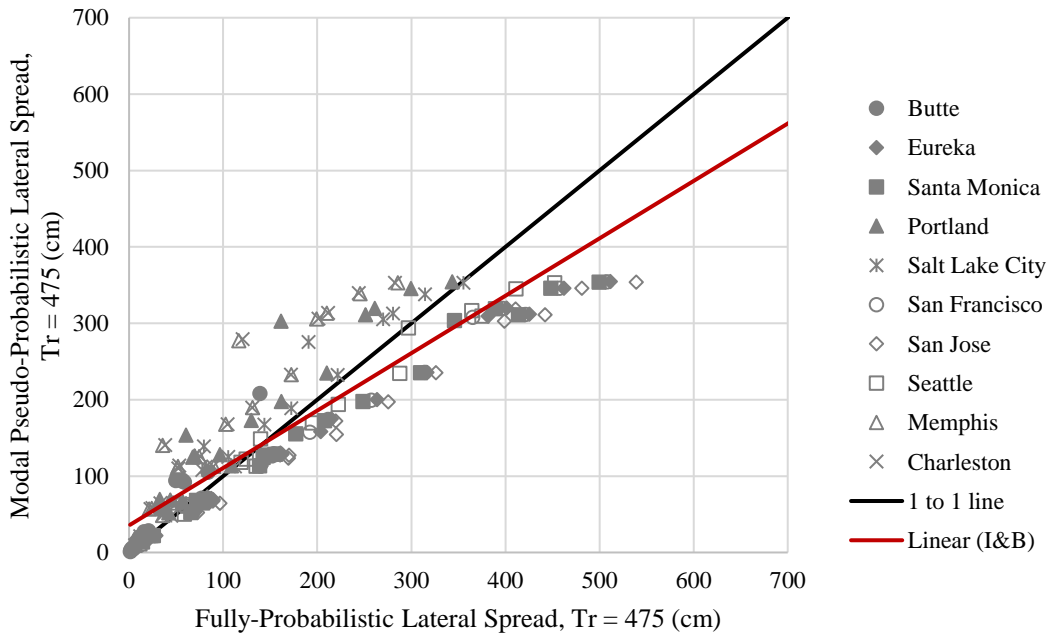


Figure A-13: Modal magnitude pseudo-probabilistic versus fully-probabilistic for the 475 year return period using the Boulanger and Idriss liquefaction triggering procedure.

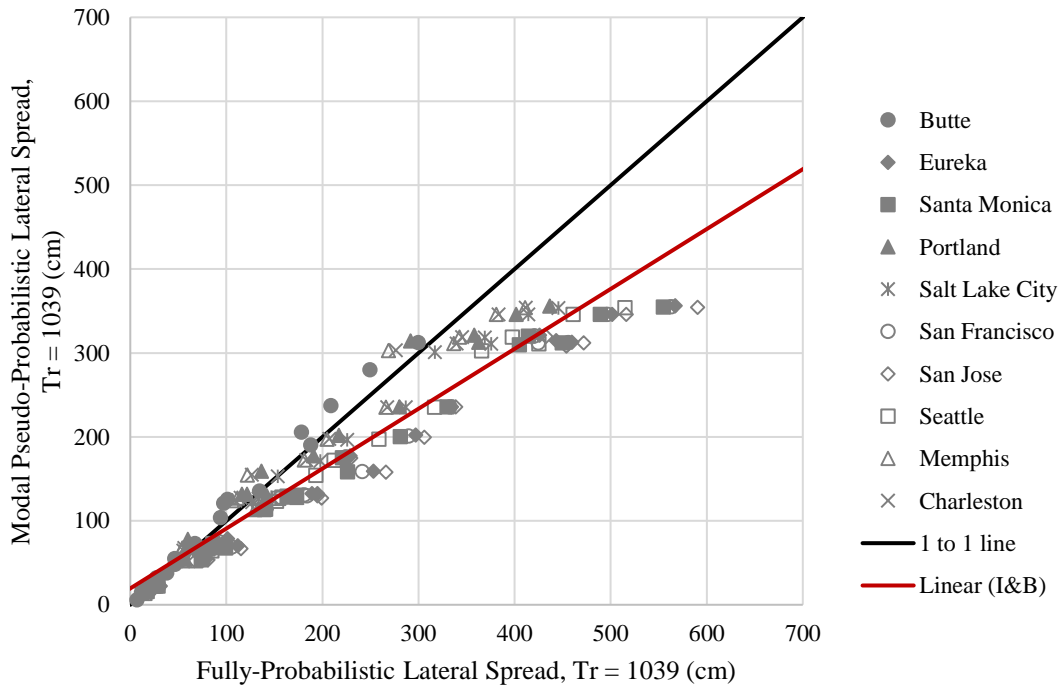


Figure A-14: Modal magnitude pseudo-probabilistic versus fully-probabilistic for the 1039 year return period using the Boulanger and Idriss liquefaction triggering procedure.

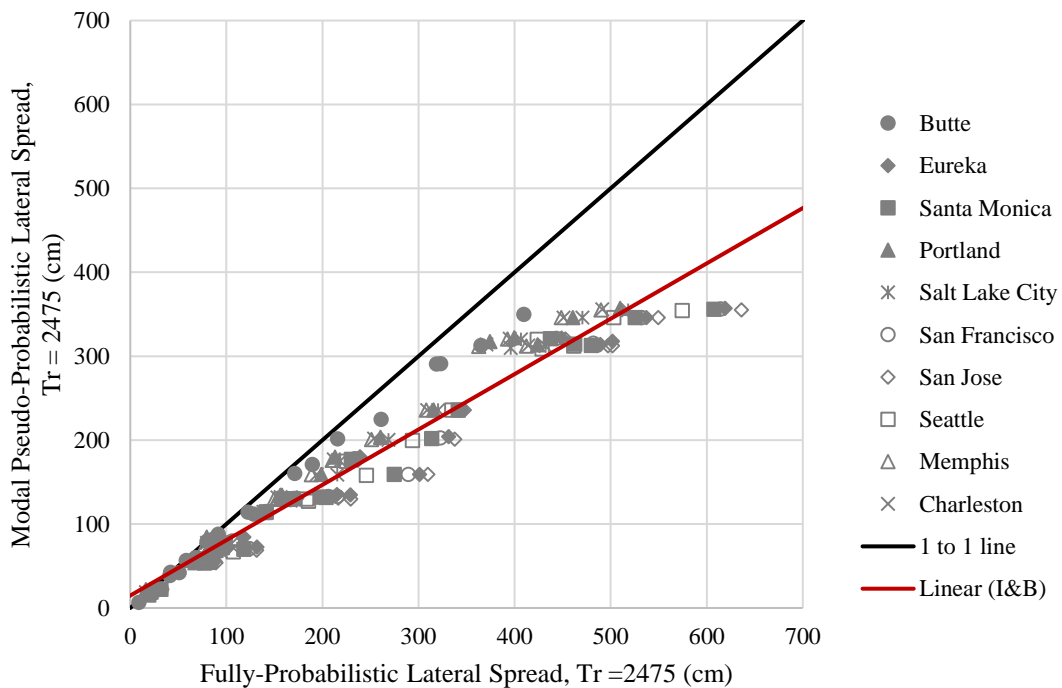


Figure A-15: Modal magnitude pseudo-probabilistic versus fully-probabilistic for the 2475 year return period using the Boulanger and Idriss liquefaction triggering procedure.

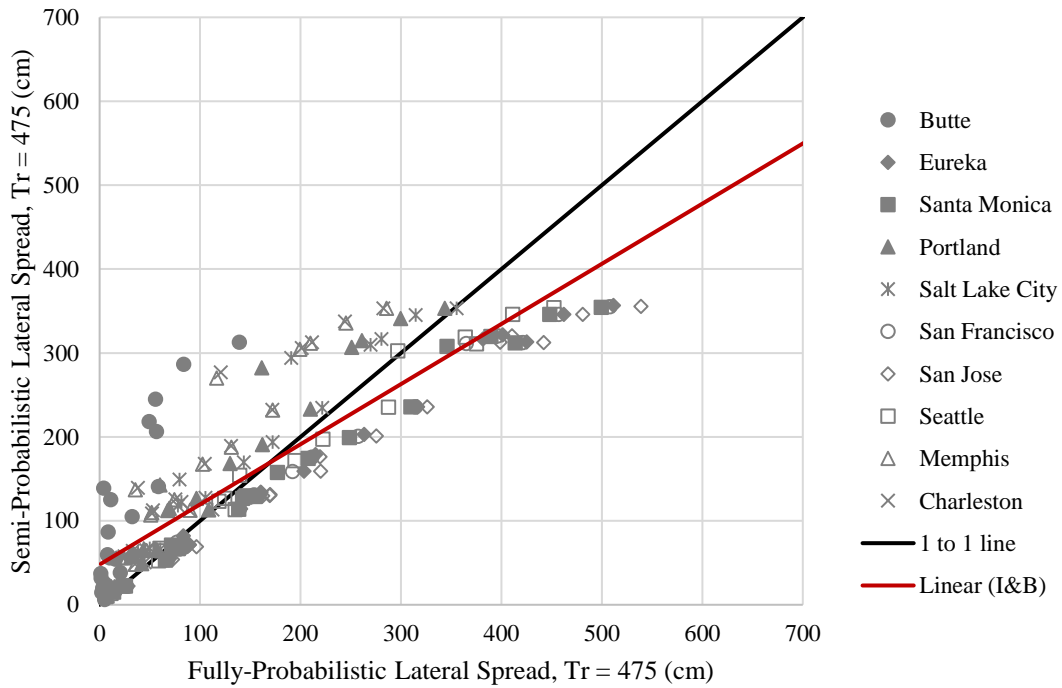


Figure A-16: Semi-probabilistic versus fully-probabilistic for the 475 year return period using the Boulanger and Idriss liquefaction triggering procedure.

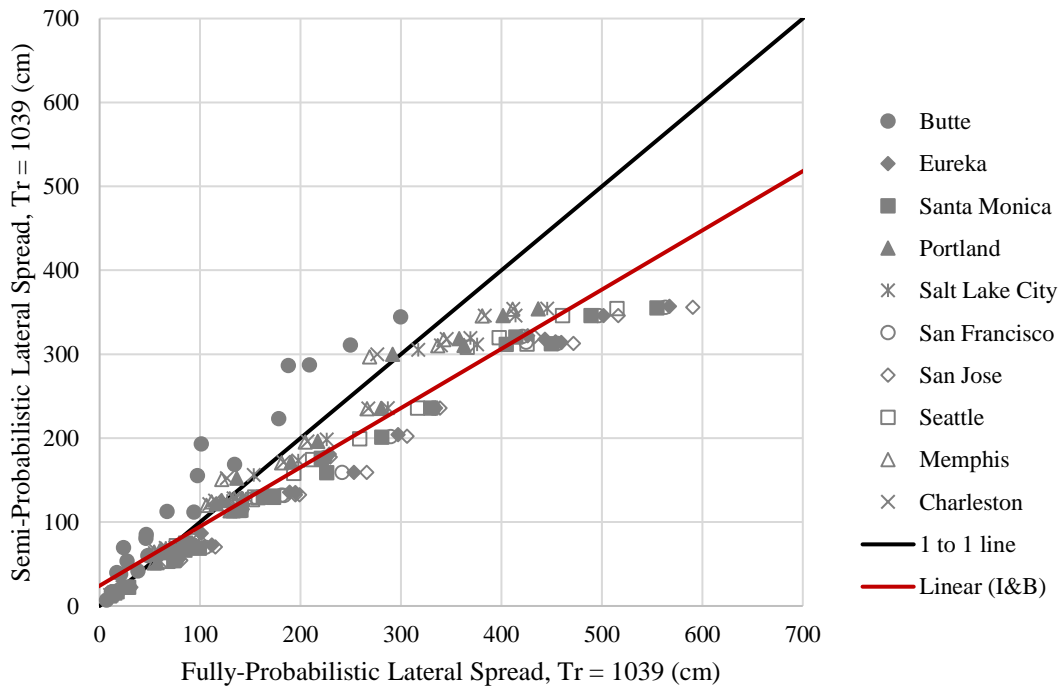


Figure A-17: Semi-probabilistic versus fully-probabilistic for the 1039 year return period using the Boulanger and Idriss liquefaction triggering procedure.

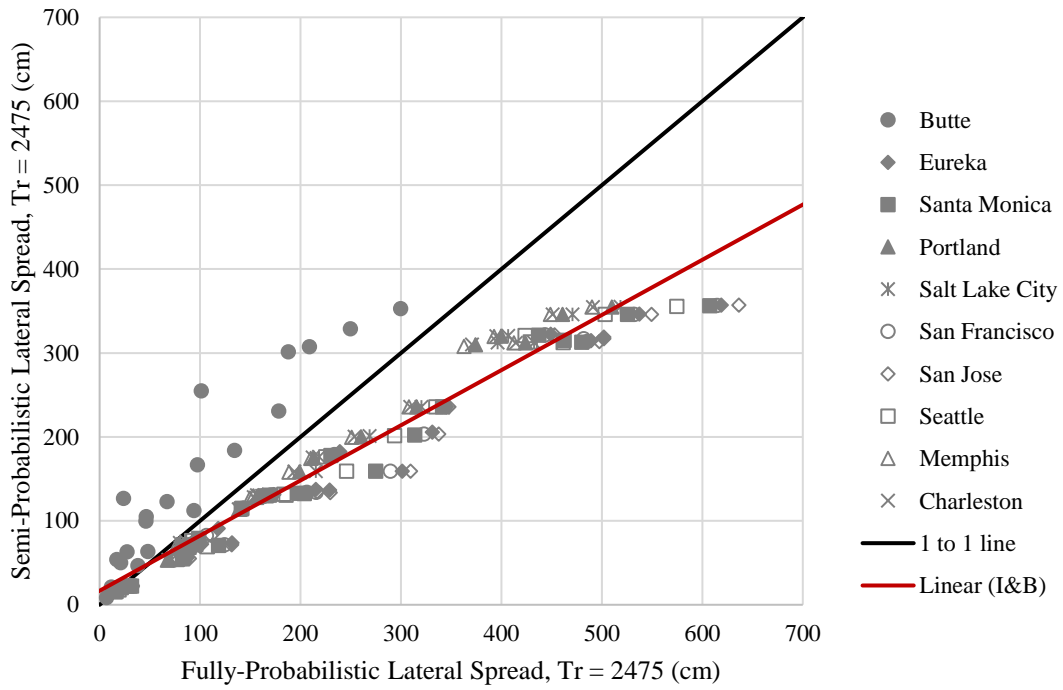


Figure A-18: Semi-probabilistic versus fully-probabilistic for the 2475 year return period using the Boulanger and Idriss liquefaction triggering procedure.